

In-vitro, ex-vivo and in-vivo modeling to assess continuous flow cardiac assist physiology and end-organ interactions

Citation for published version (APA):

Tuzun, E. (2014). *In-vitro, ex-vivo and in-vivo modeling to assess continuous flow cardiac assist physiology and end-organ interactions*. [Phd Thesis 1 (Research TU/e / Graduation TU/e), Biomedical Engineering]. Technische Universiteit Eindhoven. <https://doi.org/10.6100/IR781404>

DOI:

[10.6100/IR781404](https://doi.org/10.6100/IR781404)

Document status and date:

Published: 19/11/2014

Document Version:

Publisher's PDF, also known as Version of Record (includes final page, issue and volume numbers)

Please check the document version of this publication:

- A submitted manuscript is the version of the article upon submission and before peer-review. There can be important differences between the submitted version and the official published version of record. People interested in the research are advised to contact the author for the final version of the publication, or visit the DOI to the publisher's website.
- The final author version and the galley proof are versions of the publication after peer review.
- The final published version features the final layout of the paper including the volume, issue and page numbers.

[Link to publication](#)

General rights

Copyright and moral rights for the publications made accessible in the public portal are retained by the authors and/or other copyright owners and it is a condition of accessing publications that users recognise and abide by the legal requirements associated with these rights.

- Users may download and print one copy of any publication from the public portal for the purpose of private study or research.
- You may not further distribute the material or use it for any profit-making activity or commercial gain
- You may freely distribute the URL identifying the publication in the public portal.

If the publication is distributed under the terms of Article 25fa of the Dutch Copyright Act, indicated by the "Taverne" license above, please follow below link for the End User Agreement:

www.tue.nl/taverne

Take down policy

If you believe that this document breaches copyright please contact us at:

openaccess@tue.nl

providing details and we will investigate your claim.

**In-vitro, ex-vivo and in-vivo
modeling to assess continuous flow
cardiac assist physiology and end-
organ interactions**

A catalogue record is available from the Eindhoven University of Technology Library

ISBN: 978-90-386-3719-8

Copyright © 2014 by E. Tuzun

All rights reserved. No part of this book may be reproduced, stored in a database or retrieval system, or published, in any form or in any way, electronically, mechanically, by print, photo print, microfilm or any other means without prior written permission by the author.

Printed by Ipskamp Drukkers, Enschede, The Netherlands.

In-vitro, ex-vivo and in-vivo modeling to assess continuous flow cardiac assist physiology and end-organ interactions

PROEFSCHRIFT

ter verkrijging van de graad van doctor aan de Technische Universiteit Eindhoven,
op gezag van de rector magnificus prof.dr.ir. C.J. van Duijn,
voor een commissie aangewezen door het College voor Promoties, in het openbaar
te verdedigen op woensdag 19 november 2014 om 14:00 uur

door

Egemen Tuzun

geboren te Izmir, Turkije

Dit proefschrift is goedgekeurd door de promotoren en de samenstelling van de promotiecommissie is als volgt:

Voorzitter:	prof.dr. P.A.J. Hilbers
1e promotor:	prof.dr.mr.dr. B.A.J.M de Mol
2e promotor:	prof.dr.ir.F.N. van de Vosse
copromotor(en):	dr.ir.M.C.M. Rutten
leden:	prof.dr. B. Meyns (KU Leuven)
	prof.dr. J.R.Lahpor (UU)
	prof.dr.ir. H.E.H. Meijer
	prof.dr.ir. J.W.M. Bergmans

Contents

Summary	v
Chapter 1: General introduction	1
1.1 Introduction	2
1.2 Outline	5
Chapter 2: Effects of Continuous-Flow Cardiac Assist Device on Aortic Valve Function in a Mock Loop	9
2.1 Abstract	10
2.2 Introduction	10
2.3 Materials and methods	11
2.4 Results	14
2.5 Discussion	16
2.6 Conclusion	19
Chapter 3: Assessment of aortic valve pressure overload and leaflet functions in an ex-vivo beating heart loaded with a continuous flow cardiac assist device	21
3.1 Abstract	22
3.2 Introduction	22
3.3 Materials and methods	23
3.4 Results	27
3.5 Discussion	33
3.6 Conclusion	36
Chapter 4: The Effect of Intermittent Low Speed Mode on Aortic Valve Opening in Calves Supported With a Jarvik 2000 Axial-Flow Device	37
4.1 Abstract	38
4.2 Introduction	38
4.3 Materials and methods	39
4.4 Results	41
4.5 Discussion	43
4.6 Conclusion	45
Chapter 5: Continuous flow cardiac assist and regional myocardial	

perfusion interaction: An ex-vivo heart study	47
5.1 Abstract	48
5.2 Introduction	48
5.3 Materials and methods	49
5.4 Results	52
5.5 Discussion	61
5.6 Conclusion	64
 Chapter 6: Myocardial Hemodynamics, Physiology, and Perfusion with an Axial-Flow Left Ventricular Assist Device in the Calf	 65
6.1 Abstract	66
6.2 Introduction	66
6.3 Materials and methods	67
6.4 Results	72
6.5 Discussion	79
6.6 Conclusion	81
 Chapter 7: Effect of Pump-Flow Mode of Novel Left Ventricular Assist Device on End-Organ Perfusion in Dogs with Doxorubicin-Induced Heart Failure	 83
7.1 Abstract	84
7.2 Introduction	84
7.3 Materials and methods	85
7.4 Results	88
7.5 Discussion	95
7.6 Conclusion	100
 Chapter 8: Ventricular Assist Device Outflow-Graft Site: Effect on Myocardial Blood Flow	 101
8.1 Abstract	102
8.2 Introduction	102
8.3 Materials and methods	103
8.4 Results	106
8.5 Discussion	110
8.6 Limitations	111
8.6 Conclusion	111

Chapter 9: Modification of a volume-overload heart failure model to track myocardial remodeling and device-related reverse remodeling	113
9.1 Abstract	114
9.2 Introduction	114
9.3 Materials and methods	115
9.4 Results	119
9.5 Discussion	122
9.6 Conclusion	123
Chapter 10: The Effects of Continuous and Intermittent Reduced Speed Modes on Renal and Intestinal Perfusion in an Ovine Model	125
10.1 Abstract	126
10.2 Introduction	126
10.3 Materials and methods	127
10.4 Results	130
10.5 Discussion	135
10.6 Conclusion	137
Chapter 11: Discussion	139
11.1 Main finding	140
11.2 Wrap-up and conclusions	144
References	145
Dankwoord	159
Curriculum vitae	161

Summary

In-vitro, ex-vivo and in-vivo modeling to assess continuous flow cardiac assist physiology and end-organ interactions

Continuous flow left ventricular assist devices (CFVADs) are implantable pumps that support the heart when it is no longer capable of sustaining sufficient blood flow through the body. CFVADs available today are being used to bridge patients with end-stage heart failure to heart transplantation, by enhancing myocardial and systemic end-organ perfusion. It has been demonstrated that in the lack of a donor heart, they can provide adequate systemic flow to a heart failure patient for up to 8+ years. Nevertheless, the (patho-) physiological effects of the continuous and/or reduced pulsatile flow conditions on aortic valve functions, myocardial-renal-cerebral and gastrointestinal perfusion are not well understood. Therefore, there is substantial need for research of the new devices prior to the clinical use to assess efficacy and safety or during use to understand adverse outcome due to interactions between the device and the end-organs. The main objective of the research described in this thesis is to investigate the complex interaction between continuous flow cardiac assist devices, aortic valve functions, myocardial-renal-cerebral and gastrointestinal regional blood flow in in-vitro, ex-vivo and in-vivo experimental models.

An in-vitro experimental beating heart model has been developed to calculate the aortic valve's average mechanical load, open time and transvalvular flow at different CFVAD device flow settings and to determine the correlation between CFVAD flow and aortic valve function in healthy and failing heart conditions. In this mock circulation study, we demonstrated that the mean aortic pressure load on the aortic valve gradually increases with increasing LVAD speeds and flows, while the aortic duty cycle decreases sharply.

To better simulate the real clinical scenario and dynamic tissue properties, we developed a porcine model of ex-vivo beating heart implanted with a CFVAD and assessed the aortic valve functions and left-right ventricular myocardial perfusion changes in healthy and failing heart conditions. This study confirmed the increased pressure overload above the aortic valve and impaired valve opening at increasing CFVAD flows as observed in in-vitro studies. Increasing CFVAD support resulted in increased right and left ventricular coronary blood flow but unchanged or slightly decreased regional myocardial perfusion and cell metabolism in healthy and failing heart conditions. Increased coronary artery flow along with unchanged regional blood flow and cell metabolism, and coronary sinus hyperoxia supported occurrence of intramyocardial arteriovenous shunts at increasing CFVAD supports.

To further understand this complex interaction, the effects of reduced pulsatile flow on myocardial perfusion is investigated under continuous vs induced pulse modes with microsphere studies, as well as under ascending and descending aortic outflow graft anastomosis locations in healthy bovine (n=21) and failing canine (n=7) models implanted with CFVAD. In all in-vivo scenarios, myocardial perfusion decreased at increasing CFVAD supports along with a stable or increased total coronary blood flow independent from the outflow graft anastomosis location or flow mode, either continuous or induced pulse modes. Renal and cerebral regional blood perfusions were not adversely affected by CFVAD support level and flow modes.

And finally, we did investigate the effects of the continuous and induced pulse modes on the renal and gastrointestinal regional blood perfusion in a healthy in-vivo sheep model implanted with a CFVAD using microsphere and PET/CT techniques. Our data suggested that renal and intestinal tissue perfusion is not adversely and differentially affected by a cardiac assist device loaded with continuous and intermittent reduced speed modes. Immediate mesenteric venous hyperoxia and increased CO₂ production occurred during all pump modes and may be evidence of gastrointestinal arteriovenous shunting.

In this thesis, it has been observed that increasing CFVAD flow increases pressure overload above the aortic valve and interferes with the aortic valve opening which may lead to aortic valve fusion, regurgitation or thrombus formation during CFVAD support. In addition, higher CFVAD flows resulted in decreased myocardial perfusion and intramyocardial arteriovenous shunting which may be particularly important in patients supported for bridge to recovery. Although renal and cerebral regional blood flows were not affected at increasing CFVAD supports, evidence of immediate arteriovenous shunt occurrence at the gastrointestinal system may be an important preliminary finding to explain gastrointestinal arteriovenous malformation development.

1

General introduction

1.1 Introduction

Heart failure is one of the leading causes of death and hospitalization in the United States and more than 5 million Americans are currently living with congestive heart failure (CHF) [46]. Treatment of advanced heart failure often requires frequent hospitalization and prolonged intensive care, accounts for more hospitalizations annually than all forms of cancer combined, and is a major contributor to health care costs. Fifty percent of the patients with CHF either do not respond to medical therapy or become unresponsive to medical therapy within 5 years of diagnosis. While heart transplantation is the best treatment for heart failure, mechanical circulatory support has become an important alternative because only a limited number of donor hearts are available each year [162]. In addition, a growing number of people need cardiac support but are ineligible for heart transplantation. The clinical success of ventricular assist devices (VADs) offers an innovative strategy for increasing the life expectancy of patients with CHF. The landmark REMATCH trial established the left ventricular assist device (LVAD) as a successful alternative to medical therapy. LVAD recipients had 1- and 2-year survivals that were 2 times greater than patients treated with medical therapy alone [100] (**Figure 1.1**).

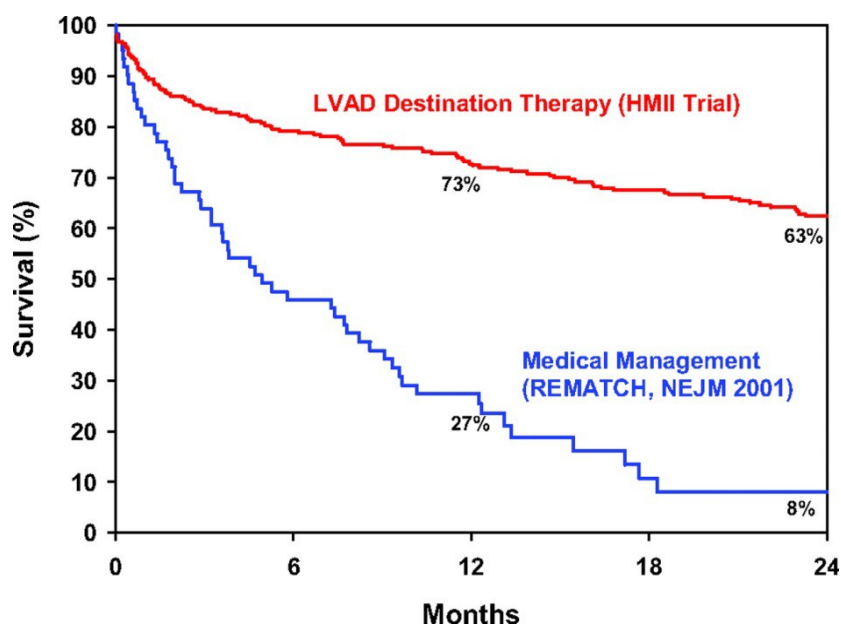


Figure 1.1: Inference of the survival benefit of current destination therapy with current continuous-flow left ventricular assist device (LVAD) compared with medical management from the REMATCH trial. HMII indicates HeartMate II.

Additional studies have demonstrated similar efficacy for LVAD use as a bridge-to-transplant in patients awaiting a donor heart [137] (**Figure 1.2**).

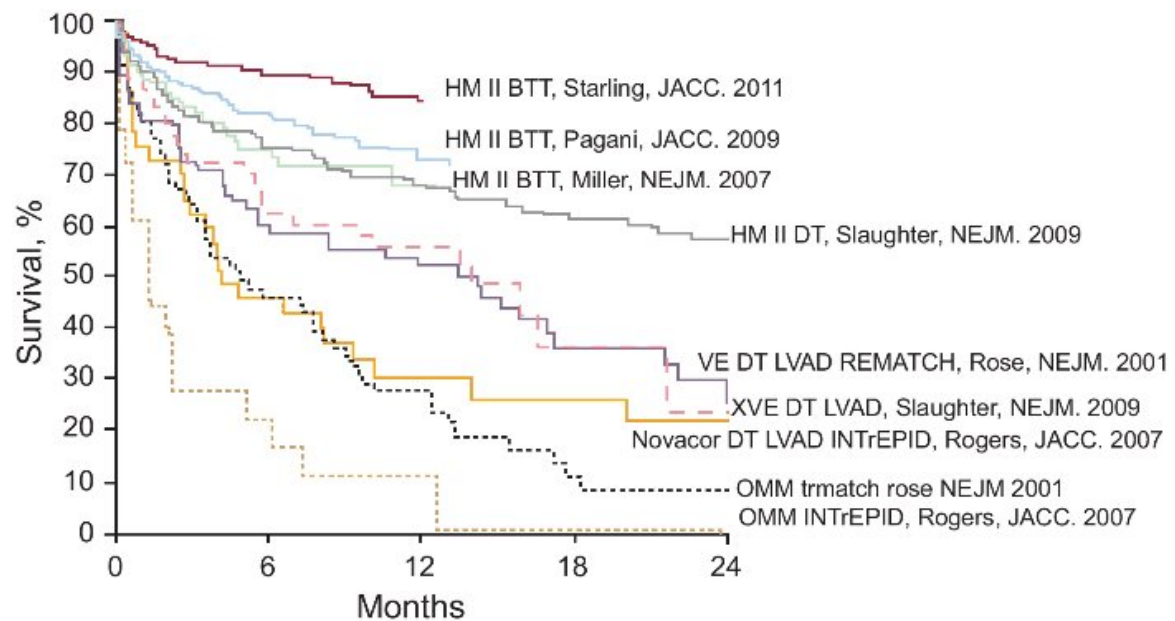


Figure 1.2: Improved survival in left ventricular assist device trials.

While pulsatile flow conditions are considered the most physiologic, continuous-flow (non-pulsatile) pumps (CFVADS) are also being developed to reduce some of the complications associated with pulsatile technology, such as infection, surgical bleeding, and mechanical device failure, and to address the needs of patients who are too small to be fitted with the current pulsatile devices. Early follow-up of CFVAD recipients demonstrated improved functional status and quality of life 3 months after implantation, with a 6-month survival of 90% [144].

When continuous flow pumps are used as left ventricular assist devices (LVADs), the resulting aortic pressure waveform has reduced pulse amplitude and a rounded shape. Therefore, continuous flow pumps are not really “nonpulsatile” pumps, although they do provide reduced pulse perfusion. The pressure and flow waveforms in the aorta have residual pulsatility because the flow output from a continuous flow LVAD is proportional to the pressure gradient across the pump. As long as the left ventricle is generating some pressure during each contraction, then the pressure gradient also will be pulsatile, and the resultant cyclic increase in pump flow will impart some degree of pulsatility to the arterial wave form [28] (**Figure 1.3**).

Recently, however, we have seen patients with advanced heart failure who because of poor unloading and severely impaired ventricular function have a weak or no detectable pulse, despite the absence of heart failure symptoms. As the worldwide experience with CFVADS, there is now considerable evidence that chronic support with continuous flow, reduced-pulse circulatory assistance is clinically viable. Previous studies have demonstrated that nonpulsatile circulation can lead to certain vasomotor, metabolic, hemodynamic, hormonal, functional, and morphologic

changes however the topic remains controversial [142]. The clinical relevance of pulsatility for VADs is unclear, especially since most evidence is largely confined to the context of cardiopulmonary bypass (CPB). To further confound matters, a uniform definition of what constitutes a physiologically meaningful pulse has hampered comparisons among studies. Indeed, unlike the CPB setting, wherein the heart is arrested, CFVAD circulation generally reflects a component of the native pulse generated in proportion to the patient's native ventricular function and in inverse proportion to the degree of mechanical circulatory support (MCS). The importance of pulsatility in long-term MCS is a relatively new topic. At the very least, it remains possible that in certain circumstances it may be desirable to either temporarily or occasionally produce or enhance native pulsatility in LVAD patients by production of an artificial pulse [143].

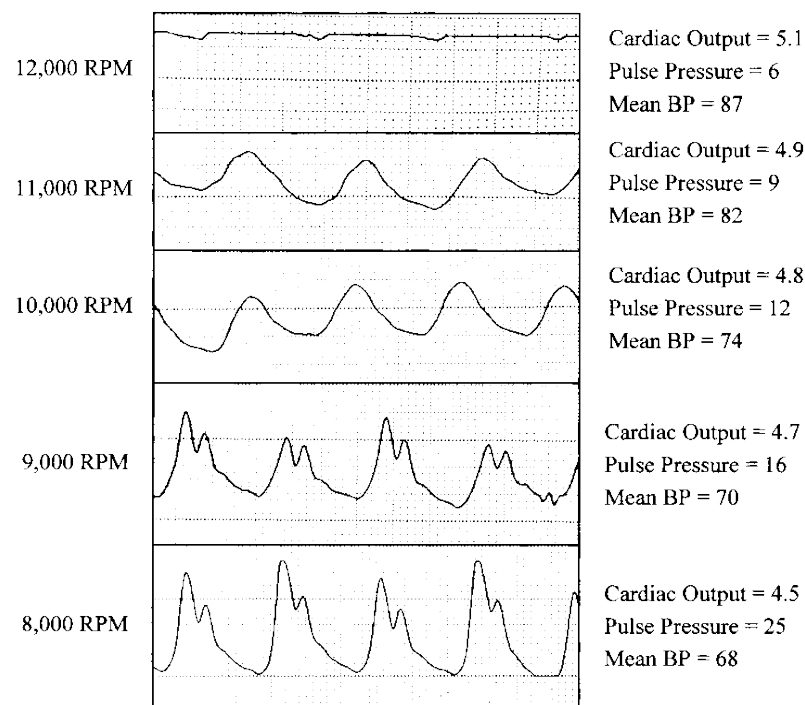


Figure 1.3: Arterial pressure waveform observed when the pump speed was increased by 1000-rpm increments over the entire operating range (8000 to 12 000 rpm). The dicrotic notch is present at 8000 and 9000 rpm but is absent at 10 000 rpm. In this case, the pump speed was set at 9000 rpm, so was some aortic outflow. BP indicates blood pressure.

Despite technologic advances, prolonged use of LVADs has raised concerns about their long-term effects upon flow properties and end-organ physiology, such as aortic valve leaflet fusion, increased cerebral and gastrointestinal bleeding complications and lack of myocardial reverse remodeling. For this reason, surgeon's skill and expertise, which are obviously basic requirements to ensure a satisfactory long-term success rate of a procedure, should be supported by innovative predictive

approaches provided by in-vitro, ex-vivo and in-vivo models. In this concept patient specific simulations are performed to evaluate continuous flow cardiac assist physiology, the efficacy of various possible treatments and to plan and design the optimal surgical or device solution based on predictions of outcomes provided by these models. In order to achieve the above-mentioned goal, cardiac surgeons, cardiologists, engineers, basic scientists, radiologists and veterinarians forming basic teams of academia and industry, need to strictly collaborate to create accurate models for realistic simulations and solutions. During the evolution and formation of our thesis, we aimed to create this multidisciplinary collaboration for a better problem analysis (leading to understanding the pathophysiological mechanisms) and solving (leading to device design or medical/surgical treatment improvements) in continuous flow cardiac assist related complications. We planned to start our workflow from mock-loop models in order to create a link between bench to bed-side translational medicine and to reduce the use of the experimental animal resources. Then, eventually we moved to ex-vivo and in-vivo studies to evaluate our preliminary data in more sophisticated and relevant animal models to better simulate the clinical scenarios which requires a combination of surgical, medical and engineering expertise, strong knowledge on developing reproducible healthy and failing heart animal models, and significant amount of financial support and time dedication.

1.2 Outline

In order to assess the complex interaction between continuous flow or reduced pulse physiology and the end-organs, different objectives have been raised which were discussed in the following chapters of this thesis:

Chapter 2: The effects of the continuous flow cardiac assist device on aortic valve functions were assessed under in-vitro conditions with the use of a mock loop circulation.

Given the aim of predicting the aortic valve functions following a CFLVAD implantation by means of realistic simulations, we aim to develop and/or modify a reliable mock-loop circuit loaded with a CFLVAD. Then we will run the circuit in normal and low output modes to simulate low and normal cardiac output scenarios and assess the effects of the continuous flow physiology on aortic valve functions and pressure load. This initial study will start a close collaboration and knowledge exchange between engineers, cardiovascular surgeons and cardiologists.

Chapter 3: Changes in aortic valve pressure overload and leaflet functions were investigated in an ex-vivo beating heart loaded with a continuous flow cardiac assist device.

In this chapter, we plan to validate our data collected from the mock-loop study in a more physiological model which will allow us to understand not only functional and hemodynamic changes of the aortic valve under continuous flow conditions, but structural changes of the leaflets and aortic root as well. We will develop an ex-vivo beating heart model loaded with a CFLVAD and assess the device and aortic leaflet interactions on healthy and failing swine hearts with a multidisciplinary approach which requires combination of engineering, medical and surgical skills. The data collected from this study will potentially help us to understand the mechanisms of aortic leaflet fusion or aortic regurgitations complications after CFLVAD implantations.

Chapter 4: The Effect of Intermittent Low Speed Mode on Aortic Valve Opening in Calves Supported With a Jarvik 2000 Axial-Flow Device

Giving the data collected from our previous in-vitro and in-vivo studies, we observed that CFLVAD support may cause reduction of forward ejection across the aortic valve and increase of aortic diastolic pressure due to increased pump outflow and/or severely impaired ventricular contractions which may end-up impairment of aortic valve opening and aortic flow stagnation. This may in turn cause thrombosis, fusion or regurgitation of the aortic valve during long-term support as reported in clinical trials. In this study we propose that intermittently lowering the speed of the pump rotational speed will reduce LV unloading and allow for some degree of valve opening to wash out the aortic root. Therefore, we have tested the chronic effects of a CFLVAD loaded with a custom made intermittent reduced pump speed mode on aortic leaflet structure and functions in a healthy bovine model (n=6). Moreover, at the study termination, we planned an acute heart failure scenario to investigate the effect of this mode on aortic valve opening and aortic wash-out in extremely depressed ventricular functions. This study required a close collaboration of engineers, cardiovascular surgeons, cardiologists and industry. Our team aimed to provide a valuable data to the cardiac assist community in order to improve the device design to prevent aortic valve dysfunction in patients implanted with CFLVADs.

Chapter 5: Continuous flow cardiac assist and regional myocardial perfusion interaction was assessed in an ex-vivo heart study.

Chapter 6: Changes in myocardial hemodynamics, physiology, and perfusion will be investigated in an acute bovine model implanted with an axial-flow left ventricular assist device.

Chapter 7: Effects of the continuous flow and induced pulse modes on end-organ perfusion will be compared in a canine doxorubicin-induced heart failure model.

Chapter 8: The effects ventricular assist device outflow-graft site (ascending vs descending aorta) on myocardial perfusion will be assessed in a bovine model.

Chapter 9: Myocardial remodeling and device related reverse remodeling will be investigated in chronic ovine volume-overload heart failure models supported with continuous flow pumps.

Chapter 10: The effects of the continuous vs intermittent reduced speed modes on renal and gastrointestinal perfusion will be assessed by microsphere and PET/CT techniques.

Meeting these objectives will lead to more knowledge regarding CFLVAD related physiology and end-organ interaction.

In **Chapter 11**, the overall study results will be discussed and the implications and ideas for future research will be outlined.

2

Effects of Continuous-Flow Cardiac Assist Device on Aortic Valve Function in a Mock Loop

The contents of this chapter are based on: Tuzun E, Rutten M, Dat M, Van de Vosse F, Kadipasaoglu C, de Mol B. Continuous Flow Cardiac Assistance: Effects on Aortic Valve Function in a Mock Loop. J Surg Res. 2011 Dec;171(2):443-7.

2.1 Abstract

Background: As the use of left ventricular assist devices (LVADs) to treat end-stage heart failure has become more widespread, leaflet fusion—with resultant aortic regurgitation—has been observed more frequently. To quantitatively assess the effects of nonpulsatile flow on aortic valve function, we tested a continuous-flow LVAD in a mock circulatory system (MCS) with an interposed valve.

Materials and Methods. To mimic the hemodynamic characteristics of LVAD patients, we utilized an MCS in which a Jarvik 2000 LVAD was positioned at the base of a servomotor-operated piston pump (left ventricular chamber). We operated the LVAD at 8000 to 12,000 rpm, changing the speed in 1000-rpm increments. At each speed, we first varied the outflow resistance at a constant stroke volume, then varied the stroke volume at a constant outflow resistance. We measured the left ventricular pressure, aortic pressure, pump flow, and total flow, and used these values to compute the change, if any, in the aortic duty cycle (aortic valve open time) and transvalvular aortic pressure loads.

Results. Validation of the MCS was demonstrated by the simulation of physiologic pressure and flow waveforms. At increasing LVAD speeds, the mean aortic pressure load steadily increased, while the aortic duty cycle steadily decreased. Changes were consistent for each MCS experimental setting, despite variations in stroke volume and outflow resistance.

Conclusions. Increased LVAD flow results in an impaired aortic valve-open time due to a pressure overload above the aortic valve. Such an overload may initiate structural changes, causing aortic leaflet fusion and/or regurgitation.

2.2 Introduction

Aortic valve commissural fusion and resultant insufficiency have recently begun to be considered complications of the prolonged use of left ventricular assist devices (LVADs), whether they produce pulsatile or nonpulsatile flow [7,67]. Previous reporters have suggested that these complications result from certain local hemodynamic forces that affect aortic valve function during LVAD support [7,67,178]. To date, no detailed flow analyses or hemodynamic assessments have been available concerning the effects of reduced or nonpulsatile flow on aortic valve function during the cardiac cycle. We believe that the increased pressure load above the aortic valve due to increased LVAD flow may result in reduced aortic valve-open times and, consequently, may lead to aortic valve complications. The objective of the present study was to quantitatively assess the complex interaction between reduced

or nonpulsatile aortic flow and aortic valve function in a mock-loop circulation using a nonpulsatile LVAD. The assessment was undertaken to calculate the aortic valve's average mechanical load, open time, and transvalvular flow at different pump-flow settings and to determine the correlation between LVAD flow and aortic valve function.

2.3 Materials and methods

2.3.1 Mock Circulation Setup

The “systemic” mock circulation (**Figure 2.1A**) comprised a left ventricle, an aortic valve, an aortic tube model, and a Windkessel system that provided peripheral impedance (HemoLab BV, Eindhoven, The Netherlands). The system was primed with water and 0.5 g/L of xanthan gum solution, which has a viscosity of 3.71 mPa, equal to the viscosity of blood with a hematocrit of 34%. The left ventricle was a servomotor-operated piston pump that could be programmed to deliver a cardiac output of 10 L/min at a heart rate of 120 bpm. The shape of the output-flow curve was freely programmable. For this study, we used a symmetric systolic output flow that lasted for 35% of a heartbeat. The left ventricle ejected the test solution through a 21-mm standard bileaflet mechanical aortic valve (CarboMedics Inc., Austin, TX) into a flexible polyurethane tube that had the mechanical characteristics of the human aorta, ensuring proper pressure-wave propagation and reflection. The aortic tube terminated in a three-element hydraulic Windkessel system that mimicked total arterial resistance and compliance. The

Windkessel's resistance was adjustable with a clamp. From the Windkessel, the test solution returned to an open storage container mounted directly onto the left ventricle. The liquid returned to the left ventricle via a second mechanical heart valve. The following properties were measured simultaneously at a 1-kHz data rate with pressure transducers (Gould Instrument Systems, Valley View, OH) and flow probes (Transonic Systems Inc., Ithaca, NY): left ventricular pressure, aortic pressure, aortic flow, and pump flow.

To mimic the hemodynamic properties of an ejecting left ventricle as closely as possible (thereby ensuring minimal deviation from physiologic hemodynamic conditions in an LVAD recipient), we used the above-mentioned 21-mm Carbomedics standard bileaflet mechanical aortic valve. To ensure proper filling of the left ventricle, we used a 25-mm Carbomedics prosthesis as a mitral valve substitute.

The LVAD used in this study was the Jarvik 2000 intraventricular assist device (Jarvik Heart, Inc., New York, NY) [177], which features five constant speeds of operation, ranging from 8000 to 12,000 rpm.

The data measured by the pressure and flow sensors were received and recorded in the HemoLab software program. **Figure 2.1B** is a schematic representation of the above-described system components.

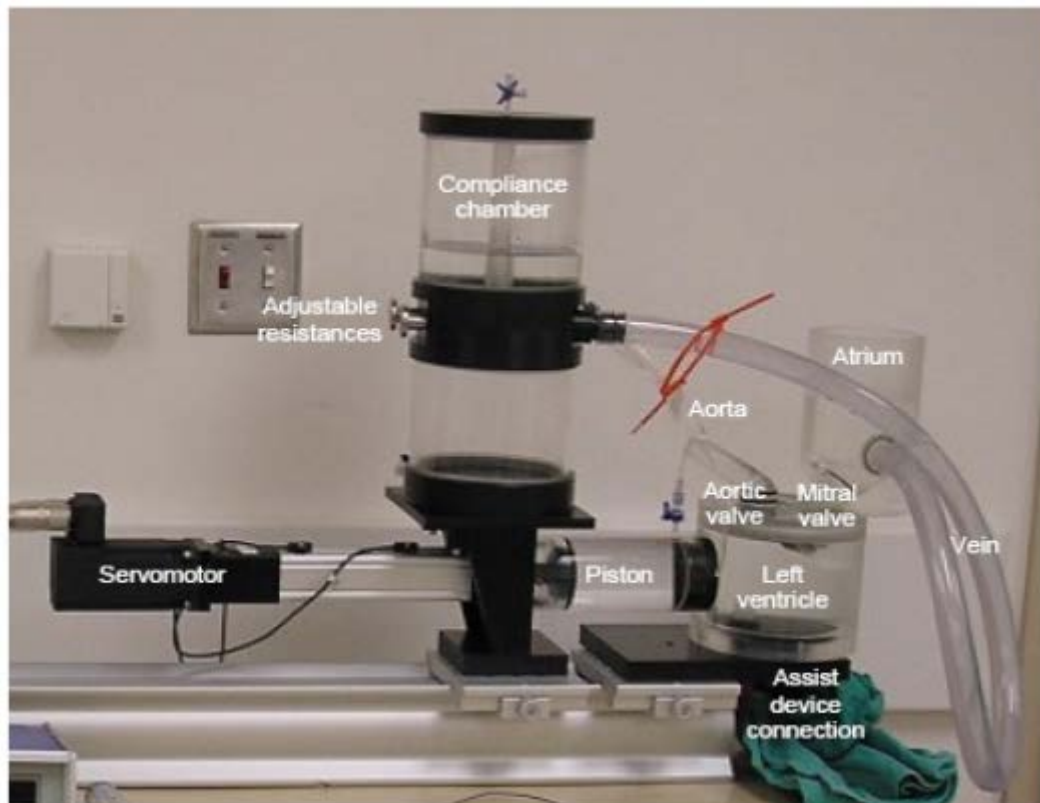


Figure 2.1A. Photograph of the cardiovascular mock circulation system

2.3.2 Study Design

At each LVAD speed, the mock loop simulated a different clinical hemodynamic state. Initially, we used a stroke volume of 60 mL and adjusted the clamp to vary the aortic pressure from 80/50 to 120/80 and then 140/100 mmHg. Without changing the Windkessel settings, we lowered the stroke volume to 40 mL at each setting, resulting in lower aortic pressures. Subsequently, with the Windkessel set to an aortic pressure of 120/80 mmHg and a stroke volume of 60 mL, we changed the stroke volume to 32 and then 48 mL. Finally, with the Windkessel adjusted to yield an aortic pressure of 120/80 mmHg, we tested the mock loop again at stroke volumes of 32 and 48 mL. All experiments were conducted at a heart rate of 60 bpm. **Table 2.1** summarizes the settings used. At each combined LVAD setting (speed, heart rate, cardiac output, and afterload), the total and pump flows were measured along with the left ventricular and aortic pressures. Measurements were taken during 50 consecutive heartbeats at a data rate of 1 kHz.

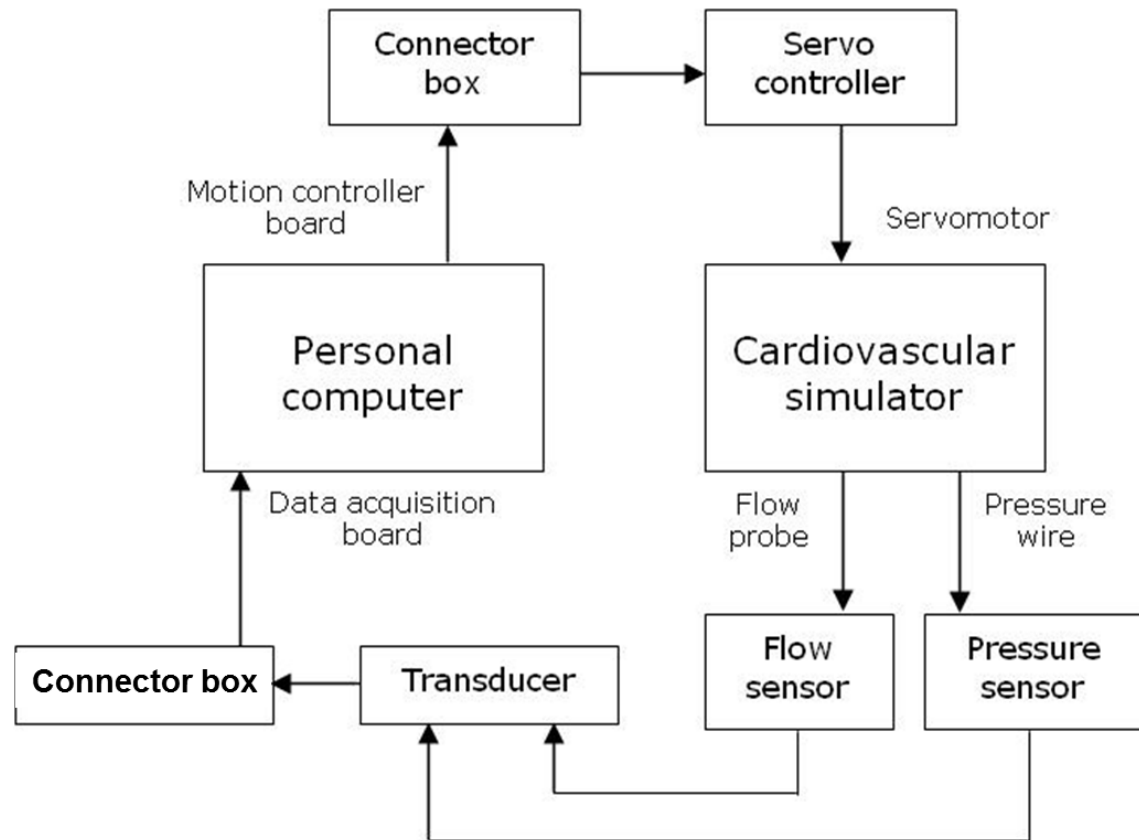


Figure 2.1B. Schematic representation of the data-acquisition system components.

Table 2.1

Summary of Test Settings

Experiment	SV (mL)	BP (mmHg)
1	40	60/40
2	60	120/80
3	40	80/60
4	60	140/100
5	40	50/25
6	60	80/50
7	40	75/40
8	60	140/90
9	32	40/25
10	48	80/50
11	32	120/80
12	48	120/80

SV=stroke volume; BP=blood pressure.

The aortic valve-open time was defined as the time in which the left ventricular pressure was higher than the aortic pressure. The duty cycle (d) of the aortic valve was the ratio between the open time (t_o) of the valve and the cycle time (t_c), of the heartbeat: $d = t_o/t_c$. To assess the aortic pressure load (L) on the aortic valve, we determined the average pressure difference over the aortic valve for all of the combined LVAD settings and mock loop settings by measuring the difference between the aortic pressure (AoP) and left ventricular pressure (LVP): $L = \text{AoP} - \text{LVP}$. For reference, the aortic valve flow was determined by subtracting the pump flow from the total flow.

All statistical tests were performed by using Microsoft Office Excel software (Microsoft Corp., Redmond, WA) on a personal computer. Analysis of variance (ANOVA) was used to compare continuous variables. P values of < 0.05 were considered significant.

2.4 Results

Twelve sets of experiments were performed, each at all five possible pump settings for the Jarvik 2000 LVAD. In each of the twelve experiments, despite different pressure and stroke volume settings, the trends for the changes in the pump flow, pressure difference over the aortic valve, and valve duty cycle were all uniform. Therefore, at each of the five pump settings, we averaged the data for the twelve experiments, and then graphed the resulting five data points to easily visualize these changes. **Figure 2.2** shows the mean pump flow at increasing pump speeds. **Figure 2.3** shows typical pressure (**A**) and flow waveforms (**B**), which indicate the functionality of the mock loop and the validity of the acquired data. The data in **Figure 2.3** were taken from the 120/80-mmHg experiments involving a normal ventricular stroke volume. The mock circulatory system was operating under these settings with the LVAD outlet clamped just below the ventricle-pump connection, so that normal blood flow patterns could be simulated. Correlation of these waveforms with standard physiologic pressure and flow waveforms indicated the functionality of the mock loop and LVAD and the validity of the acquired data. **Figure 2.4** shows the pressure difference over the aortic valve, which was averaged for each experiment. In all cases, the average pressure load on the aortic valve increased with increasing pump speeds in comparison to baseline. Only with the pump connected and switched off was the transvalvular pressure lower. The increase in the pressure load directly affected the aortic valve's duty cycle (**Figure 2.5**). In all cases, the duty cycle decreased at increasing pump speeds, reflecting a shorter valve-open time during each heartbeat. In half of the cases (experiments 2, 7, 8, 10, 11, and 12), the duty cycle was reduced to almost zero at higher pump speeds; in the rest of the cases, it

stayed at 15%. Under normal conditions, the duty cycle is around 30%, but the valve remained closed most of the time at high pump speeds. In this set of experiments, the duty cycle was a function of pump speed. The reduced open time (**Figure 2.5**) was also reflected in the reduced aortic flow (**Figure 2.6**).

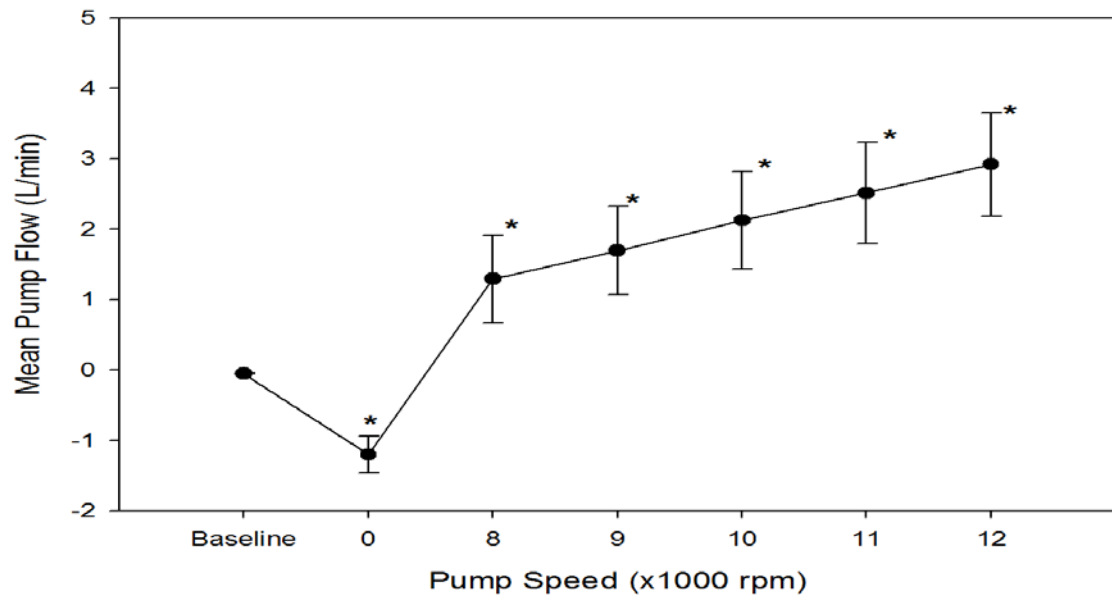


Figure 2.2: Mean pump flow at increasing pump speeds *P < 0.05 versus baseline). Baseline=pump off and outflow graft clamped; 0=pump off and outflow graft unclamped.

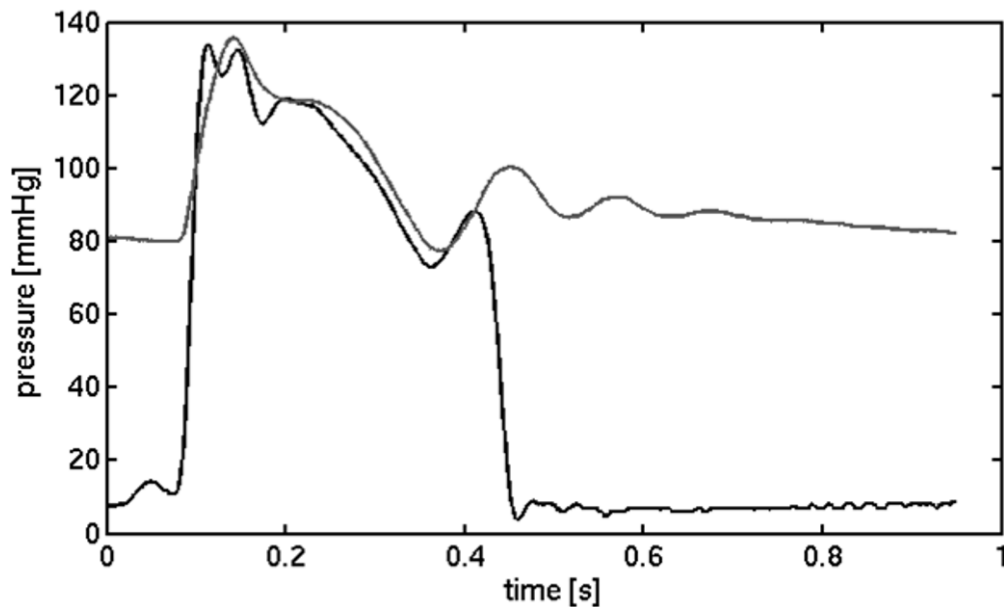


Figure 2.3A: Typical aortic (gray) and left ventricular (black) pressure waveforms

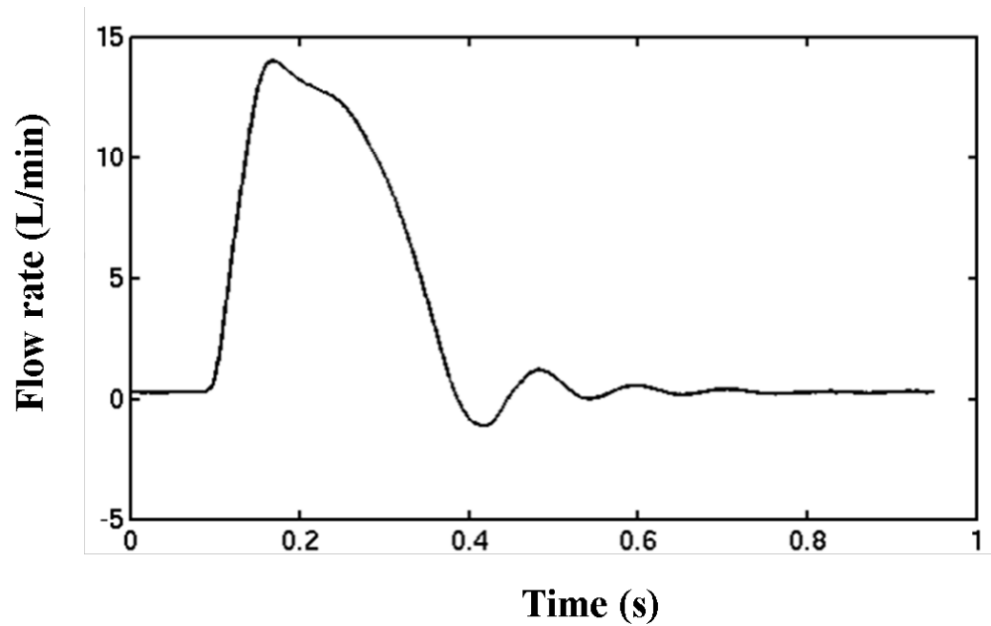


Figure 2.3B: Typical aortic (gray) and left ventricular (black) pressure waveforms

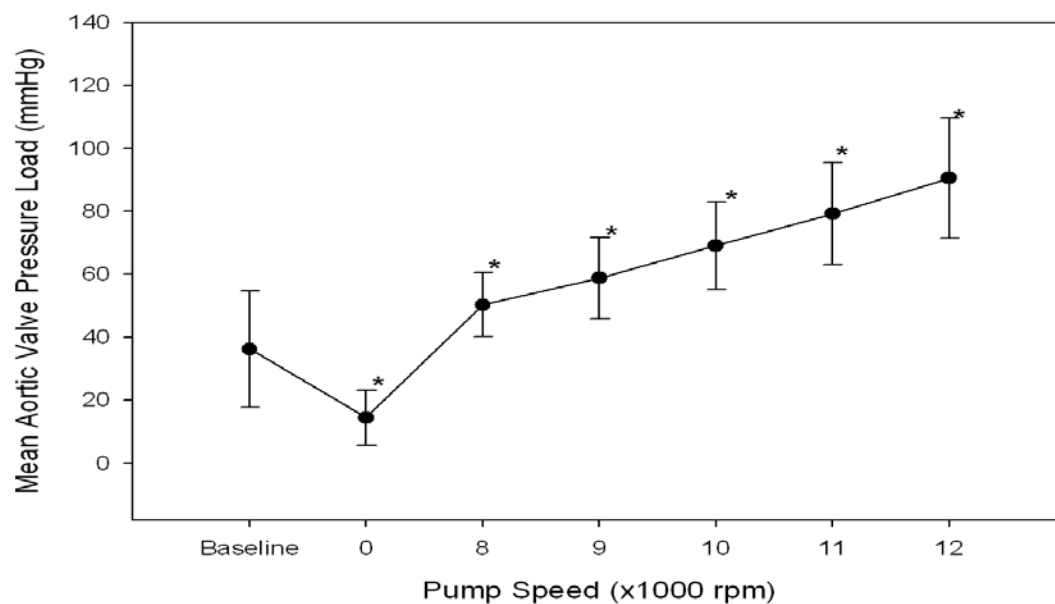


Figure 2.4: Mean aortic valve pressure load (*P < 0.05 versus baseline). Baseline=pump off and outflow graft clamped; 0=pump off and outflow graft unclamped

2.5 Discussion

In this mock circulation study, we demonstrated that the mean aortic pressure load on the aortic valve gradually increases with increasing LVAD speeds and flows, while the aortic duty cycle decreases sharply. The validity of the mock circulatory system was initially confirmed by our ability to produce physiologic pressure and flow waveforms for normal heart function with no functioning LVAD support. Once the

system was validated, we incorporated LVAD function into the model at increasing pump speeds, which correlated with clinically used pump settings. We were able to demonstrate that as the pump speed increased, the flow through the pump also increased, reflecting greater flow through the aorta. At the same time, flow through the aortic valve decreased, especially when the cardiac stroke volume was low, as in a failing ventricle. The failure-mode experiments (numbers 1, 3, 5, 7, and 9–12) also resulted in higher pump flows than the non-failure-mode experiments, likely due to the lower pressure increase needed to generate net forward flow. Whereas most of the test fluid continued “downstream” to the Windkessel compliance system, which represented systemic compliance in our model, there was also a small amount of retrograde flow towards the aortic valve. The augmentation of total flow at increasingly high pump speeds increased the aortic pressure load on the aortic valve, as characterized by elevated pressure differences across the valve.

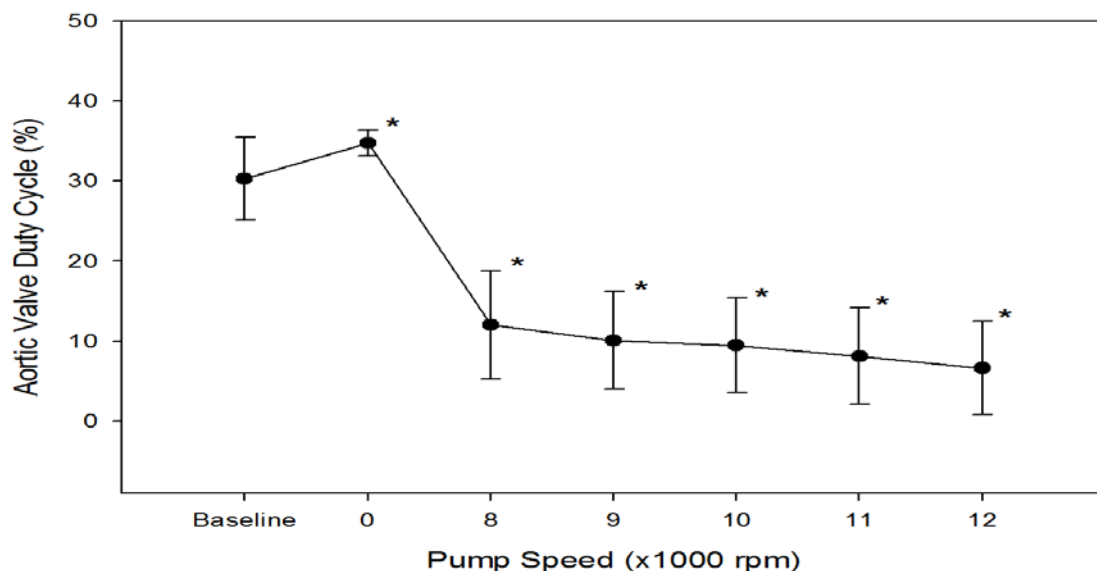


Figure 2.5: Aortic valve duty cycle (*P < 0.05 versus baseline). Baseline=pump off and outflow graft clamped; 0=pump off and outflow graft unclamped

With the growing aortic pressure load on the aortic valve, the total valve-open time was reduced, because an increasingly smaller portion of left ventricular systole involved a pressure that surpassed the aortic pressure—a necessary condition for valve opening. Furthermore, total flow through the valve was reduced with increasing LVAD support. This resulted not only in shorter valve-open times but also in a less than fully open valve configuration at peak systole. The aortic valve used in this study was a mechanical one. Although the deformation of such a valve is not comparable to that of a natural valve, the varying pressure-flow relationship and its resultant impact on aortic valve opening should reflect the same physiologic phenomena observed in natural valves [177]. Because the valve’s hemodynamic

boundary conditions were kept as physiologic as possible, the valve itself was not expected to significantly influence the total aortic flow and pressure in the mock system.

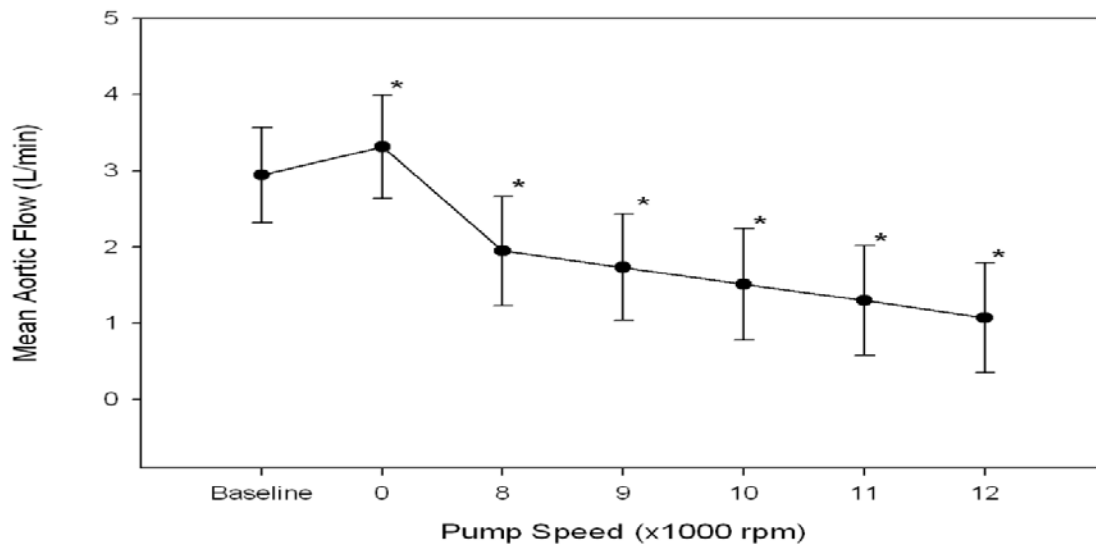


Figure 2.6: Reduced aortic flow (*P < 0.05 versus baseline). Baseline=pump off and outflow graft clamped; 0=pump off and outflow graft unclamped

Over their lifetime, aortic valve leaflets are exposed to considerable cyclical stresses. The leaflets are subjected to flexural deformations during valve opening (systole) and closing (diastole), shear stress while open, and planar tension while closed [148]. During diastole, the aortic valve withstands a transvalvular pressure of around 80 mmHg, causing the aortic leaflet tissue to undergo an average stress of nearly 250–400 kPa. Under physiologic conditions, the loading time is so brief that the effects of viscoelasticity on leaflet interstitial cell deformation are negligible and no cellular strain-rate effects occur. On the other hand, experimentally increasing the diastolic time results in time-dependent deformation of the interstitial cells when the aortic valve is closed [5]. Zamarripa-Garcia and coworkers [178] have shown that the aortic valve load increases in the presence of a continuous-flow LVAD. While the valve is closed, it can bear a pressure load, so the average transvalvular pressure may be higher at low duty cycles. Our data indicate not only that the absolute value of the average load increases by almost 25% but also (possibly of equal importance) that the time span in which the load is applied is approximately 20% longer than it would be under normal, physiologic conditions. Thubrikar and associates [149] have reported that the radial length of the aortic leaflets does not change significantly during systolic aortic flow; however, when the leaflets close and coapt under increasing pressure, the radial length increases during diastole. Moreover, Weston and Yoganathan [172] have reported that porcine aortic leaflets exposed to either

constant shear stress or a constant static pressure do not maintain the aortic valve interstitial cells' contractile phenotype after 48 h. The function of these cells is believed to be crucial for the long-term integrity of the aortic valve's surrounding extracellular matrix and for its continual renewal and repair.

In case of a continuous pressure overload above the aortic valve, as seen in our study, the radial length of the aortic leaflets is likely to increase further over time and result in a remodeled aortic valve, leading to regurgitation and annular deformation. Accordingly, the impaired opening time and concomitant regurgitation may result in further altered flow conditions, including longer leaflet exposure to blood components due to blood stagnation above the aortic valve. These changes may increase the likelihood of hemolysis, thrombosis, and/ or fusion of the aortic valve leaflets [74,99].

In the light of previous reports regarding an increasing rate of aortic valve regurgitation and fusion after LVAD implantation [7,67,178], our results may suggest the impact of impaired aortic valve mechanics on the development of this complication.

2.6 Conclusion

Continuous-flow LVAD support results in an increased average pressure load on the aortic valve, not only because of an increased diastolic blood pressure but also because of an increased valve-closure time. In a clinical situation, it is likely that the reduced valve open time and, more importantly, reduced forward flow through the valve would lead to incomplete opening of the valve during peak systolic flow, causing permanent deformation of the aortic leaflets and, thus, insufficiency of the valve. Additional in vivo and in vitro studies are ongoing at our institutions to further investigate the mechanisms of aortic valve regurgitation after LVAD implantation.

3

Assessment of aortic valve pressure overload and leaflet functions in an ex-vivo beating heart loaded with a continuous flow cardiac assist device

The contents of this chapter are based on: Tuzun E, Pennings K, van Tuijl S, de Hart J, Stijnen M, van de Vosse F, de Mol B, Rutten M. Assessment of aortic valve pressure overload and leaflet functions in an ex-vivo beating heart loaded with a continuous flow cardiac assist device. Eur J Cardiothorac Surg. 2013 Jun 30.

3.1 Abstract

Background:The aortic valve regurgitation, fusion or thrombosis are commonly reported clinical complications after continuous flow ventricular assist device implantations, however the complex interaction between reduced pulsatile flow physiology and aortic valve functions has not been studied experimentally. To address this, a continuous flow left ventricular assist device was implanted in four swine ex-vivo beating hearts and then operated at baseline (device off, no flow) and at device speeds ranging between 8500 to 11500 rpm under healthy and experimentally created failing heart conditions.

Materials and Methods. At baseline and after each speed increase aortic, left ventricular, left atrial and pulse pressure signals were monitored to assess the hemodynamic status of the ex-vivo heart, aortic valve opening time and the transvalvular pressure changes. Aortic root and device flows were recorded with flow probes. Left ventricular pressure-volume loops were measured with a conductance catheter. Changes in aortic leaflet motion and end-diastolic aortic root diameter were recorded with epicardial echocardiography.

Results: A 2-chamber healthy and failing ex-vivo beating heart model was successfully created. At increasing device flows, aortic valve open time steadily decreased from $36\pm 7\%$ of the baseline cardiac cycle to 0% at 11500 rpm in healthy heart and from $18\pm 16\%$ to 0% in failing heart mode ($p<0.05$). Aortic transvalvular pressure increased from 25 ± 5 mmHg (baseline) to 67 ± 7 mmHg (11500 rpm) in healthy heart and from 10 ± 9 mmHg (baseline) to 73 ± 8 mmHg (11500 rpm) in failing heart mode ($p<0.05$). Aortic root diameters were significantly increased at speeds exceeding 10500 rpm in healthy heart mode ($p<0.05$ vs baseline) and approached statistical significance in failing hearts.

Conclusions: Increasing assist device flows resulted in pressure overload above the aortic leaflets, impaired leaflet functions, caused aortic root dilation and altered leaflet coaptation at the central portion of the aortic valve in both modes. We conclude that the deleterious effect of the reduced pulsatile flow on the aortic valve functions and hemodynamics is immediate and such an insult, may explain the structural changes of the aortic valve causing leaflet fusion and/or regurgitation in chronic phase.

3.2 Introduction

Mechanical circulatory support with ventricular assist devices (VAD), either pulsatile or continuous flow, is an accepted therapeutic option for the patients who are not candidates for heart transplantation due to immediate need for cardiac support and/or donor shortage [31,33]. After the introduction of continuous flow VADs into the clinic, major complications such as infection and/or thromboembolic events significantly decreased in patients implanted with those devices [55]. However, the aortic valve regurgitation, fusion or stenosis are still common complications reported with an incidence of 11% at 6 months and 51% at 18 months after continuous flow VAD implantations [18,90]. Yet, little is known about the association of those complications with continuous or reduced flow physiology, nevertheless it is likely that the altered hemodynamics are leading to dysfunctional remodeling of the aortic valve, as reported by several investigators [56,83,160]. Unfortunately, previous in-vitro or postmortem studies performed with artificial valves and ventricles are not precise enough to simulate the real clinical scenario and dynamic tissue properties under continuous flow VAD support. On the other hand, the clinical reports lack of describing the mechanisms of the aortic valve-continuous flow VAD interaction due to unquestionable ethical restrictions for avoiding unnecessary invasive interventions in humans for research purposes. In order to overcome the above mentioned problems and better simulate the real clinical scenario, we used a porcine ex-vivo beating heart model (PhysioHeart, HemoLab) [20] loaded with a continuous flow VAD and assessed the hemodynamics during the aortic valve-continuous flow VAD interaction in healthy and failing heart conditions.

3.3 Materials and Methods

3.3.1 Animals

Four domestic Dutch landrace hybrid adult pig hearts were obtained from pigs that were slaughtered for human consumption. The protocols at the slaughterhouse and laboratory follow EC regulations 1774/2002 regarding the use of slaughterhouse animal material for diagnosis and research, supervised by the Dutch Government (Dutch Ministry of Agriculture, Nature and Food Quality) and are approved by the associated legal authorities of animal welfare (Food and Consumer Product Safety Authority). These protocols prevent additional animal suffering and sacrifice in performing the experiments. The slaughterhouse procedures were carried out under supervision of representatives (veterinary officers) of the regulatory authorities.

3.3.2 Preparation of Isolated Hearts

A detailed description of the preparation has been published previously [20]. Briefly, following stunning the pigs (weighing 100 ± 10 Kg) with an electroshock and hanging them on one hind leg and incising the carotid artery for exsanguination till death, the thorax was opened by a parasternal incision. The hearts (weighing 420 ± 30 gr) were then removed en bloc, usually still beating and preparation was started at the slaughterhouse. After opening the pericardial sack the heart was immediately cooled topologically in ice slush. The pulmonary artery was cut just before the bifurcation while the aorta was cut at the level of the first supra-aortic vessels and subsequently cannulated for administration of 1 liter of cold cardioplegic solution (4°C Modified StThomas2 added with 5000IU of Heparin) to the coronary arteries at a pressure of 80 mmHg. This procedure was optimized such that warm ischemic time never exceeded 5 minutes and was generally kept below 3 minutes. Meanwhile, 5 liters of fresh blood for reperfusion was collected from subsequently slaughtered pigs, since pigs lack the antibodies against different blood group factors. The heart and blood (heparinized with 5000IU/L) were then stored cold during transportation to the laboratory.

Each heart was placed in an insulated container filled with ice-cold saline solution to reduce damage to the heart tissue due to ischemia. The aorta and the left atrium were cannulated using $\frac{3}{4}$ -inch cannulas to connect the left side of the heart to an ex vivo circuit. The pulmonary artery was cannulated to measure coronary sinus outflow. Epicardial pacing wires (Ethicon, Inc.; Somerville, NJ) were placed on the aorta, left atrium, and left ventricle to monitor electrical activity and to pace the heart (if necessary).

A Micromed DeBakey continuous flow ventricular assist device which was described in details elsewhere [98] was used for all experiments. The inflow cannula was inserted into the left ventricle via ventricular apex and the sewing ring was attached to the ventricle using 2/0 ti-cron teflon pledgeted sutures. Once the implantation procedure was completed the outflow graft was mounted 15 cm distal to the aortic valve with a 90 degree angle.

3.3.3 Connection of Isolated Hearts to the Circuit

The perfusion circuit (**Figure 3.1**) was assembled and primed with a normothermic (38°C) 1:1 mixture of Krebs-Henseleit buffer (4.0 ± 0.5 L) (Sigma-Aldrich, Inc.; St. Louis, Mo) and heparinized autologous blood (4.0 ± 0.5 L) (final hematocrit, $15\% \pm 1\%$; pH, 7.40 ± 0.05) supplemented with insulin (0.32 units/L). At room temperature, each pig heart was suspended in an elastic sleeve, and the left side of the heart was connected to the circuit as follows. The aortic cannula was connected to the circuit to induce modified Langendorff mode. The heart was perfused retrogradely from the

aorta in order to keep the coronary perfusion pressure at 70 mmHg. Following five minutes of modified Langendorff mode perfusion, regular myocardial contractile activity was reestablished, and the left atrial cannula was connected to the circuit to induce beating-ejecting mode. If needed, the heart was defibrillated with 10J. The heart was then perfused anterogradely from the left ventricle into the coronary arteries through the aorta. The heights of the preload and afterload reservoirs were adjusted to create a preload of 10 to 20 mmHg and an afterload of 100 to 120 mmHg.

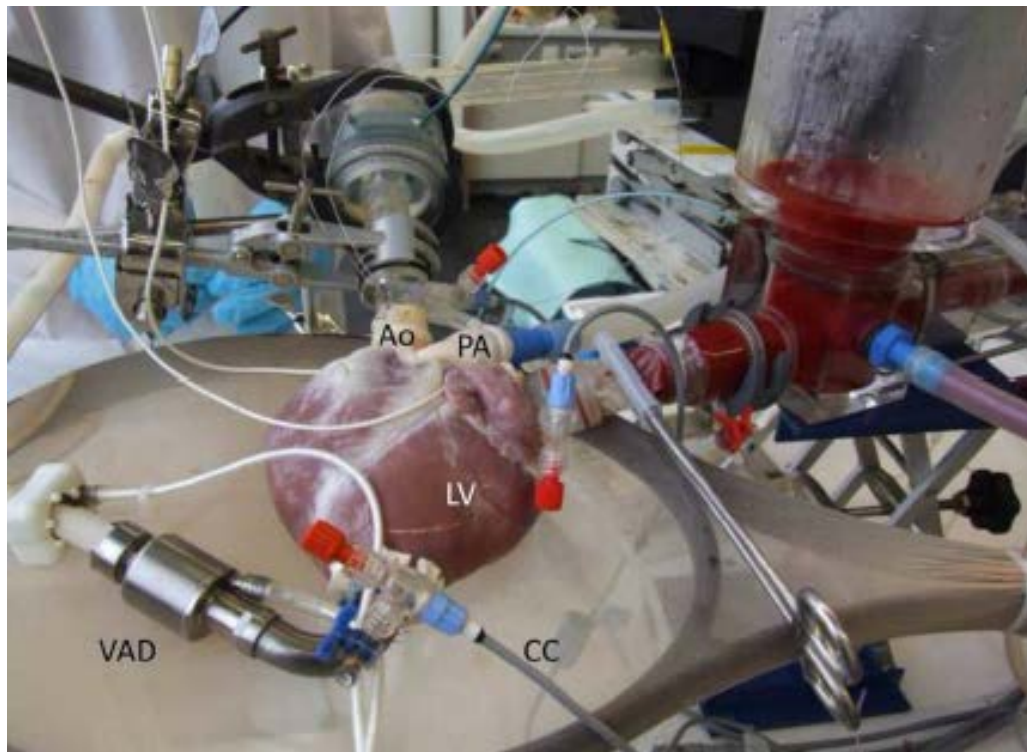


Figure 3.1: Ex-vivo beating heart perfusion circuit loaded with a left ventricular assist device. VAD: Ventricular assist device; CC: Conductance catheter; Ao: Aorta; PA: Pulmonary artery; LV: Left ventricle. .

3.3.4 Perfusion of Isolated Hearts on the Ex-Vivo Circuit

In this 2-chamber beating-ejecting mode, the left ventricle ejected the perfusate into the aortic cannula, where aortic pressure (AoP) was measured. The compliance chamber, placed in series between the aorta and the afterload reservoir, partially corrected cyclic fluctuations in pump pressure. Through an overflow tube in the afterload reservoir, the perfusate was collected into a reservoir and pumped by the first roller pump (Sarns 9000 Perfusion System, 3M) into the venous reservoir, where it then passed through an arterial filter (AFFINITY® Arterial 38µm blood filter, Medtronic). A centrifugal pump routed the perfusate into the oxygenator (AFFINITY® NT Oxygenator, Medtronic), which contained 95% oxygen and 5% carbon dioxide. The blood glucose level was maintained manually between 5 and 7 mmol/l by

addition of glucose-insulin-potassium (GIK). The oxygenator was connected to the heater-cooler, which kept the perfusate at 37 °C by recirculating heated water through the oxygenator. The heated and oxygenated perfusate was then pumped by the second roller pump back into the preload reservoir, where its temperature was measured. From the preload reservoir, the left atrium was supplied with oxygenated perfusate. Coronary venous perfusate was returned to the circuit through the cannula leading from the pulmonary artery to the reservoir. The mean coronary flow was measured with an ultrasound flow probe and the pressure was measured approximately 15 cm upstream from the coronary ostia with a pressure sensor (P10EZ-1, Becton Dickinson Medical). The third roller pump was used to fill the afterload reservoir initially for modified Langendorff-mode perfusion. The preload reservoir could be emptied into the reservoir through an overflow tube. Left atrial pressure (LAP) was measured with a pressure transducer connected to the left atrial cannula.

3.3.5 Data Collection

The following data is collected at the baseline (VAD is not running and outflow graft is clamped) and with the VAD running at speeds (outflow graft clamp is unclamped) from 8500, 9500, 10500 and 11500 rpm during measurements on healthy heart and failing heart, 2 minutes of interval between each speed change. Once hemodynamic steady state was reached in beating-ejecting mode, AoP, LAP, left ventricular pressure (LVP), pulse pressure (PP) electrocardiography, and heart rate (HR) were recorded continuously using a Labview-based data acquisition system (National Instruments, Austin, TX). Electrophysiological signals were monitored as ECG-derived signals epicardial pacing leads. The aortic and left atrial pressures were monitored with pressure sensors (P10EZ-1, Becton Dickinson Medical, Singapore). The left ventricular pressure-volume (PV) loops were measured with a conductance catheter (CD Leycom, The Netherlands) which was introduced into the ventricle trans-apically by means of a needle. The aortic flow (Q_a) was measured approximately 100 mm distal of the aortic valve annulus by an ultrasonic flow sensor (MA28PAX, Transonic Systems Inc.) VAD flow (Q_{vad}) is measured from the outflow graft with the Micromed flow probe. Total cardiac output (CO) was calculated (in L/min) as follows: $CO = Q_c + Q_a + Q_{vad}$, where Q_c is coronary blood flow.

Aortic leaflet motions and end-diastolic aortic root diameter (mm) were recorded with epicardial echocardiography with curved array probe (Picus Ultrasound Scanner, ESAOTE, Europe). Aortic valve open time (avot) was calculated with pressure signals. Transvalvular pressure (TP) was calculated with AoP and LVP measurements.

3.3.6 Induction of Ex-vivo Heart Failure

In 3 hearts, distal left anterior descending and circumflex obtuse margin coronary arteries were ligated and acute ischemic heart failure was successfully created as detected by PV loops. One heart failed without any ischemic induction probably due to insufficient myocardial protection during the harvesting, transportation or preparation. Each experiment state is repeated once.

3.3.7 Statistics

The results are expressed in mean \pm SD format. The reproducibility of the ex vivo measurements was determined using a paired t-test, comparing the two measurements done under the same conditions. A three-way ANOVA test is performed to calculate the significance of the hemodynamic parameters between healthy and failing conditions and different levels of LVAD support. Mean values of hemodynamic parameters were determined during measurements in four hearts at different pump speeds under either healthy or failing conditions. So for each measurement it is defined in which heart the measurement was done, in which condition this heart was and what level of LVAD support was performed. A p value smaller than 0.05 is considered statistically significant.

3.4 Results

A 2-chamber ex-vivo beating heart mode was used for all hearts. Data were collected at two time intervals (first healthy, then failing heart condition) for each ex-vivo experiment while the hearts were kept in a beating heart mode for up to 4 hours.

3.4.1 Baseline hemodynamic data in ex-vivo healthy and failing heart conditions

During the baseline data collection, the shunt created between the aorta and LV apex (through the VAD) was closed by an arterial clamp to the outflow graft. The mean AoP, LVP and PP achieved at the baseline healthy heart conditions were 84 ± 8 mmHg, 60 ± 7 mmHg and 38 ± 3 mmHg, respectively. These values were decreased to 64 ± 11 mmHg, 54 ± 8 mmHg and 32 ± 5 mmHg respectively, considering the failing heart ($p < 0.05$ for all parameters) (**Figure 3.2A and 3.2B**). The mean baseline LAP values significantly increased after the creation of heart failure compared to healthy heart values (18 ± 7 mmHg vs 23 ± 10 mmHg, $p < 0.05$). **Figures 3.3 and 3.4** show, respectively, the characteristic aortic and left ventricle pressure waveforms and PV loops generated by the healthy and failing heart conditions in one experiment prior to VAD support. The mean total cardiac output obtained at the baseline under

healthy heart conditions was 4.5 ± 0.9 L/min at a mean heart rate of 105 ± 3 bpm, with a corresponding mean stroke volume of 41.6 ± 8.3 mL. After the induction of heart failure, the mean cardiac output decreased to 3.8 ± 0.9 L/min with a mean heart rate of 103 ± 1 bpm and a stroke volume of 36.9 ± 8.7 mL ($p < 0.05$ for both parameters). The changes at the CO, Qa and Qvad before and after heart failure creation were summarized in **Figure 3.5**. Correlation of these parameters with standard healthy and failing heart conditions indicated the functionality of the ex-vivo beating heart platform and the validity of the acquired data.

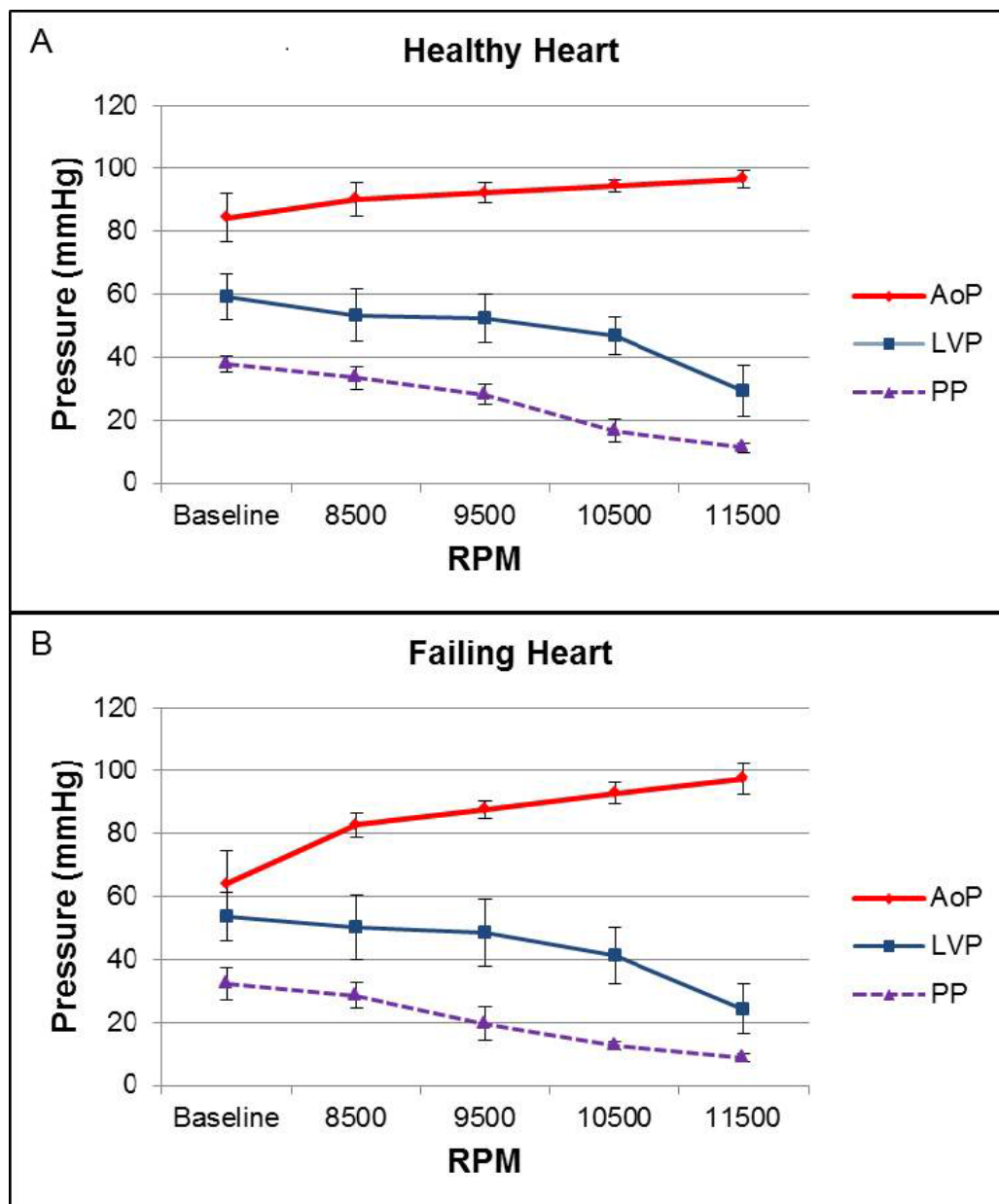


Figure 3.2: Figure 2. Mean aortic, left ventricular and pulse pressures at the baseline and increasing VAD supports in healthy (A) and failing (B) heart modes. ($p < 0.05$ vs baseline in all speeds). AoP: Mean aortic pressure; LVP: Left ventricular pressure; PP: Pulse pressure; VAD: Ventricular assist device; RPM: Rotation per minute

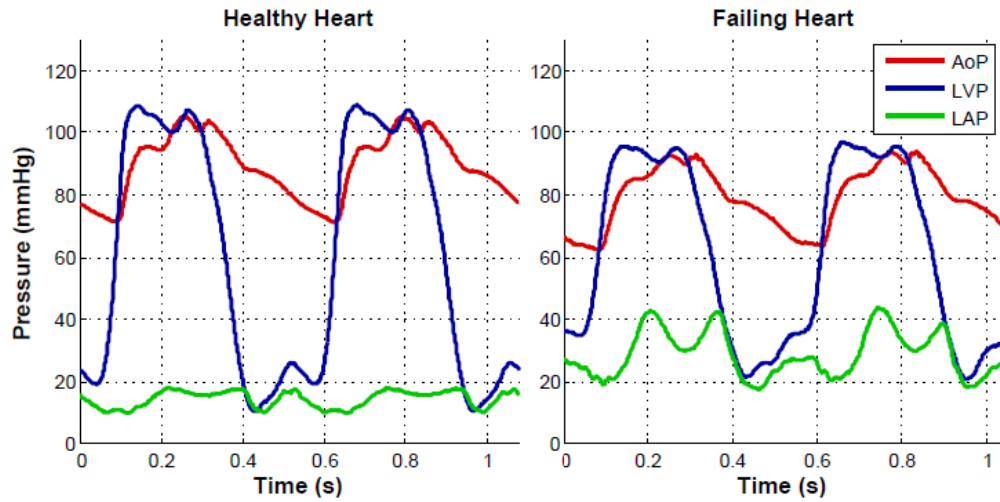


Figure 3.3: Typical left ventricular, aortic and left atrial pressure wave forms on healthy (left) and failing heart (right) modes. LVP: Left ventricular pressure; AoP: Aortic pressure; LAP: Left atrial pressure.

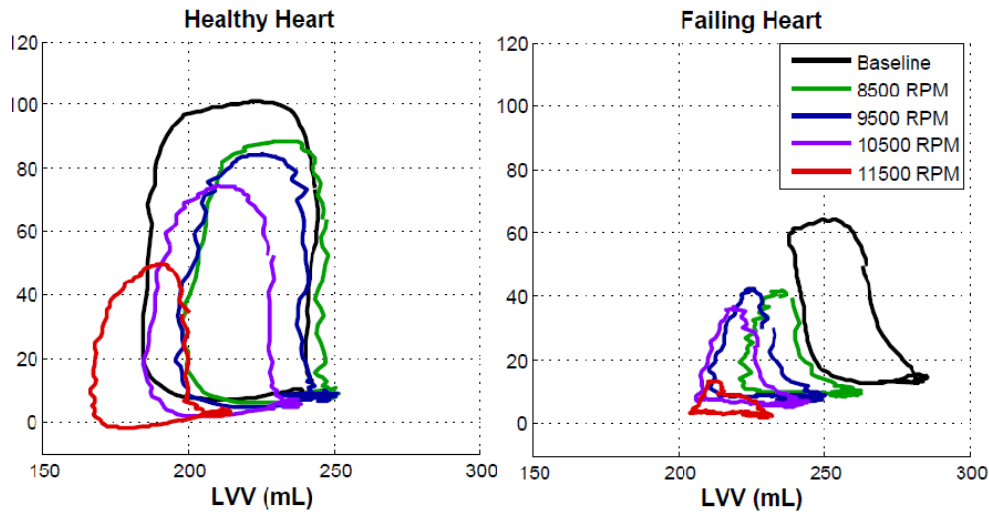


Figure 3.4: PV loops generated by the healthy (left) and failing (right) heart modes in one experiment before and after left VAD support. PV: Pressure-volume; VAD: Ventricular assist device; LVP: Left ventricular pressure; LVV: Left ventricular volume; RPM: rotation per minute.

Mean transvalvular pressure was 25 ± 5 mmHg and 10 ± 9 mmHg in healthy and failing heart conditions, respectively (**Figure 3.6**).

Aortic valve opening time was $36\% \pm 7\%$ of the cardiac cycle in healthy heart which increased to $18\% \pm 16\%$ in failing heart condition as calculated by pressure signals (**Figure 3.7**) Aortic leaflet function and coaptation was normal in healthy and failing

heart experiments. The baseline mean aortic root diameters were 28 mm and 23.7 ± 0.6 mm in healthy and failing hearts respectively ($p < 0.05$) (**Figure 3.8**).

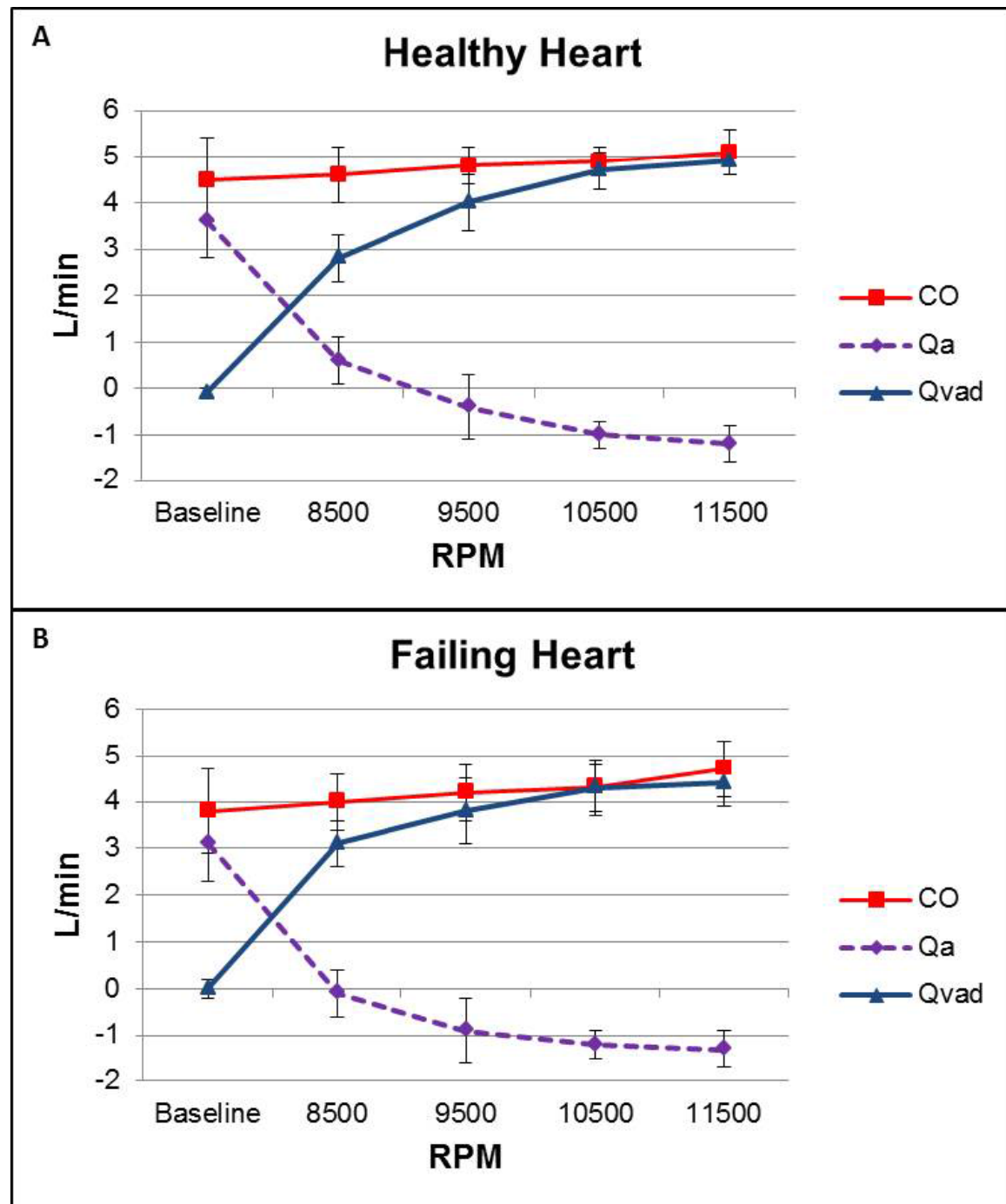


Figure 3.5: Total cardiac output, aortic and VAD flows at the baseline and increasing VAD supports in healthy (A) and failing (B) heart modes. ($p < 0.05$ vs baseline in all speeds). CO: Total cardiac output; Qa: Aortic flow; Qvad: Ventricular assist device flow; VAD: Ventricular assist device; RPM: Rotation per minute.

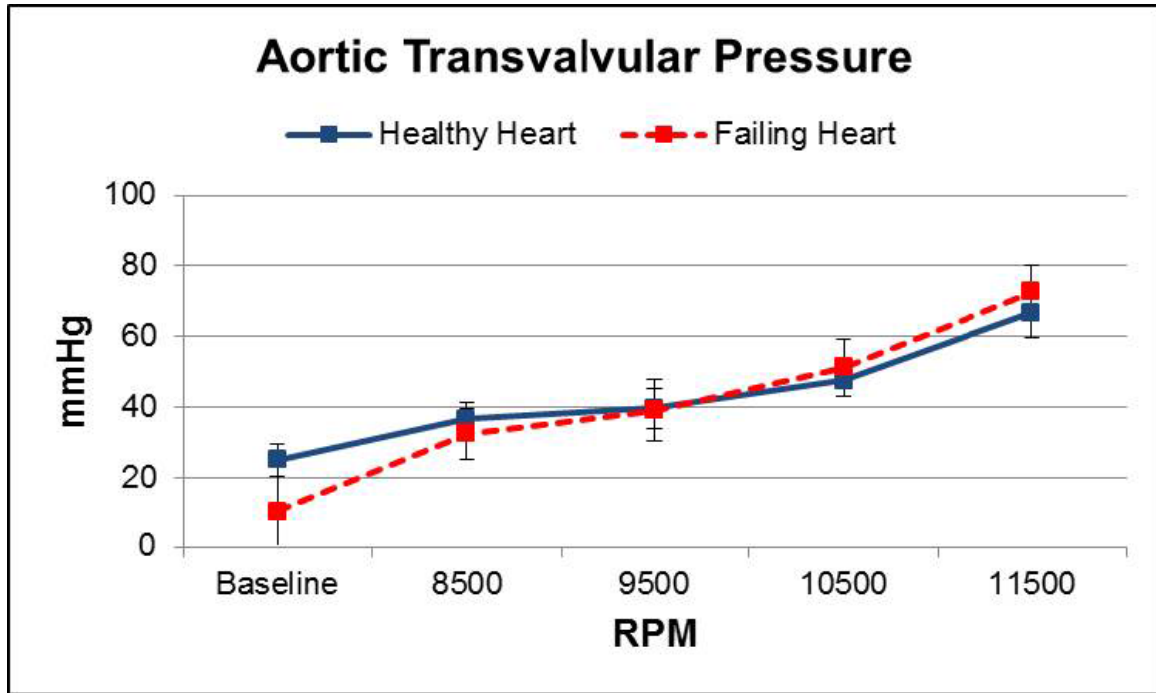


Figure 3.6: Aortic transvalvular pressures at the baseline and increasing VAD supports in healthy and failing heart modes. ($p < 0.05$ vs baseline in all speeds). VAD: Ventricular assist device; RPM: Rotation per minute.

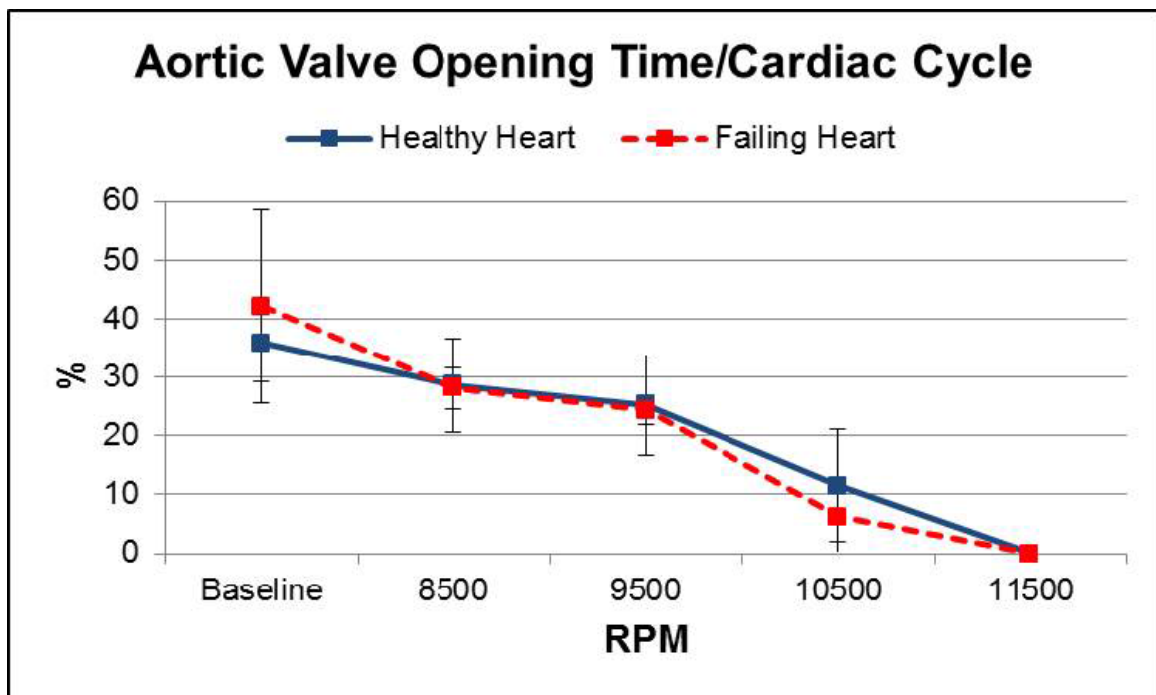


Figure 3.7: Aortic valve opening time per cardiac cycle at the baseline and increasing VAD supports in healthy and failing heart modes. ($p < 0.05$ vs baseline in all speeds). VAD: Ventricular assist device; RPM: Rotation per minute.

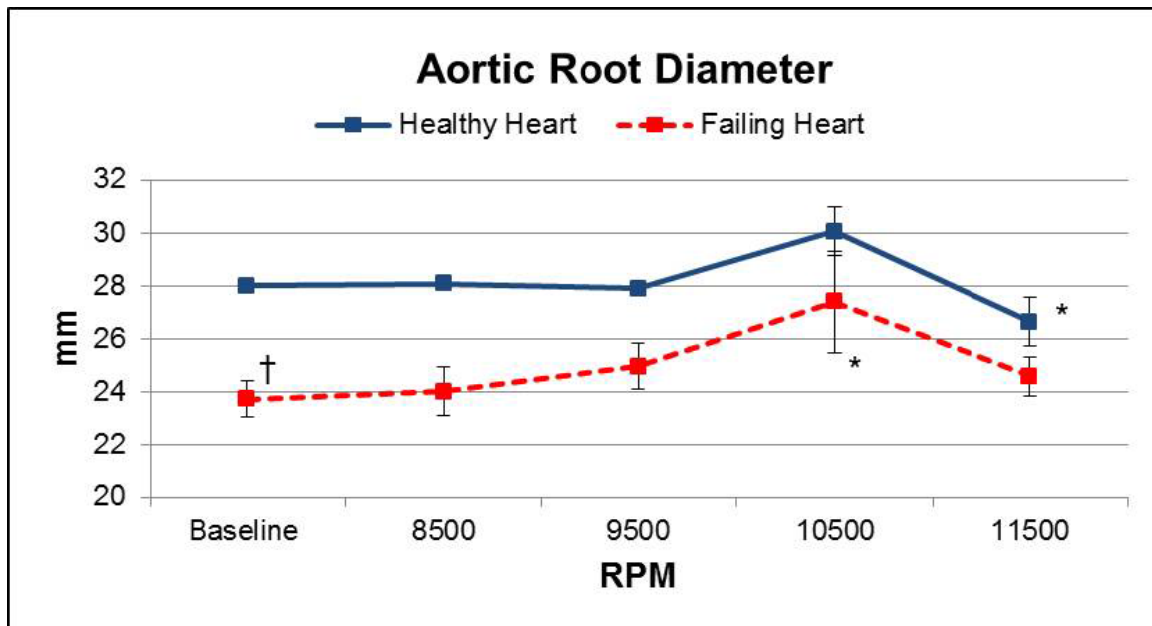


Figure 3.8: Aortic root diameter at the baseline and increasing VAD supports in healthy and failing heart modes. († $p < 0.05$ vs healthy; * $p < 0.05$ vs baseline). VAD: Ventricular assist device; RPM: Rotation per minute.

3.4.2 Hemodynamic data after VAD support in ex-vivo healthy and failing heart conditions

The mean AoP increased at increasing pump speeds with a corresponding decrease at the LVP and PP in healthy and failing hearts compared to baseline values as shown in **Figure 3.2A and 3.2B** ($p < 0.05$ for all parameters). The mean LAP gradually and significantly decreased at increasing pump speeds in healthy and failing heart conditions ($p < 0.05$ vs baseline). **Figure 3.4** shows pressure volume relations for the VAD supported heart for one of the cases, where increasing pump speed decreased the ventricular pressure as well as the ventricular volume gradually in healthy and failing heart conditions. The mean Q_{vad} significantly increased at increasing pump speeds in healthy and failing conditions ($p < 0.05$) along with a sharp decrease in Q_a flow ($p < 0.05$). The increase in the mean total cardiac output obtained at the increasing pump speeds was more pronounced in failing heart conditions compared to healthy hearts ($p < 0.05$). Depending upon the extent of LV unloading the Q_a flow gradually decreased and reversed direction at increasing VAD supports resulting aortic regurgitation at speeds exceeding 9500 rpm in both healthy and failing conditions ($p < 0.05$ vs baseline) (**Figure 3.5A and 3.5B**). The mean transvalvular pressure gradually and significantly increased from 25 ± 5 mmHg (baseline) to 67 ± 7 mmHg (11500 rpm) in healthy heart and from 10 ± 9 mmHg (baseline) to 73 ± 8 mmHg in failing heart conditions ($p < 0.05$ vs baseline) (**Figure 3.6**). There was no statistically significant difference between healthy and failing groups in terms of

transvalvular pressure ($p=0.86$) Aortic valve open time decreased from $36\pm 7\%$ of the cardiac cycle to 0% in healthy heart and from $18\pm 16\%$ of the cardiac cycle to 0% in failing heart condition as calculated by pressure signals ($p<0.05$ vs baseline) **(Figure 3.7)** There was no statistically significant difference between healthy and failing groups in terms of aortic valve open time ($p=0.45$).

Aortic root diameter increased from 28 ± 0.1 mm to 30.1 ± 0.9 mm at 10500 rpm in healthy heart mode ($p<0.05$ vs baseline). At 11500 rpm aortic root diameter decreased below the baseline level (28 ± 0.1 mm to 26.7 ± 0.9 mm, $p<0.05$ vs baseline) along with an increase in retrograde Qa flow and ventricular suction effect detected by echocardiography. Aortic root diameter increased from 23.7 ± 0.7 mm to 27.4 ± 1.9 mm at 10500 rpm ($p<0.05$ vs baseline) in failing mode followed by a reduction as detected in healthy mode (23.7 ± 0.7 mm to 24.6 ± 0.7 mm, $p=0.13$ vs baseline) **(Figure 3.8)**.

3.5 Discussion

In the ex-vivo beating heart model (PhysioHeart, HemoLab) loaded with a continuous flow VAD, we were successfully able to simulate healthy and failing heart conditions. We demonstrated that the pressure load on the aortic valve was almost 2.5 times higher than the baseline when the left ventricle was fully unloaded with a continuous flow VAD in healthy heart experiments, whereas the pressure load was 7 times higher under failing heart conditions. With increasing VAD speeds, aortic valve open time reduced to zero, aortic root diameters were increased compared to baseline measurements and aortic leaflet motions were partially or completely impaired.

The aim of our study was to explore hemodynamic and functional changes in the duration and level of the diastolic pressure load on a normally functioning aortic valve being subjected to the non- or near-physiological hydrodynamic conditions imposed by a healthy and failing heart being assisted by a continuous-flow VAD. Although we performed our preliminary studies on in-vitro mock loop models [160], we believe that a mock-loop loaded with a mechanical valve and rigid tubes wouldn't have sufficient hemodynamic similarity to a native heart valve to support our findings and to translate these into loads on a native valve. Therefore, we chose this established model of ex-vivo beating heart model to better assess the aortic valve and continuous flow VAD interaction under more realistic conditions. In this study, we demonstrated that normal cardiac hemodynamic performance was achieved both qualitatively, in terms of pulse waveforms (Aop, LVAP, LAP), and quantitatively, in terms of average cardiac output and pressures (PV loops). In all but one heart, cardiac performance was controlled and kept at normal levels for up to 4 hours, with only minor deterioration of hemodynamic performance. One heart developed early

failure possibly due to inadequate myocardial preservation. Furthermore, this model enabled us to use the epicardial echocardiography to assess the leaflet functions and flow dependent morphological changes at the leaflets and aortic root such as flow stagnation, leaflet and aortic root dilation and/or aortic regurgitation in response to VAD speed changes. Another advantage of the model is that we use fresh pig hearts acquired from a local slaughterhouse. Although different groups [49,117] have reported that prolonged warm ischemia may well be tolerated, none of their models were able to regain close to normal cardiac hemodynamics. We have experienced that it was essential to keep warm ischemic time as short as possible because of clear hemodynamic deterioration of the heart performance. The use of slaughterhouse hearts was beneficial from a time, cost and ethical perspective [88] but also allowed us to have access to a virtually unlimited supply of fresh hearts.

Aortic valve commissural fusion and resultant insufficiency have recently begun to be considered complications of the prolonged use of the pulsatile or nonpulsatile left ventricular assist devices which may cause poor patient prognosis [7,67,150]. Previous in-vitro and postmortem studies suggested that increased pressure load above the aortic valve due to increased VAD flow may result in impaired aortic valve functions and opening, and consequently may lead to aortic valve fusion, thrombosis or incompetence [56,83,160]. Under normal physiological conditions, a constant tissue renewal in aortic valve leaflets is demonstrated while altered mechanical forces (i.e.hypertension) result in changes in their structural and biological properties [126,149,172]. Our hemodynamic data is closely correlated with previous in-vitro studies which have demonstrated an increase in TVP along with a decrease in aortic valve open time and aortic blood flow at increasing VAD speeds and flows in healthy and failing heart conditions [160,178]. Nevertheless, the aortic valve is a functional assembly composed of the three cusps, corresponding sinuses, and the sinotubular junction. It is characterized not only by morphological features but also its functional properties, which together create an environment that is optimal for distribution of diastolic pressure load, and assures proper and timely valve opening and closure [113]. Therefore it is unlikely to assess precisely the complex interaction between constantly changing aortic valve geometry and continuous flow VADs in in-vitro models. The uniqueness of our study is to show the real time changes on the aortic leaflet shape and aortic root circumferential diameter along with the aortic leaflet functions under different VAD flow rates and hydrodynamic conditions with epicardial echocardiographic measurements. We have demonstrated that prior to the VAD support, failing hearts had significantly smaller aortic root diameters compared to the healthy hearts which may be explained by the decreased aortic root pressure and wall tension secondary to the left ventricular failure. The initiation of VAD support resulted in pressure overload above the aortic valve which caused

flattening of the aortic leaflets, increase in aortic root diameter during diastole and retrograde flow through aortic leaflets due to altered leaflet coaptation in both healthy and failing hearts. The aortic root diameter decreased below baseline levels when the left ventricle is over unloaded at maximum VAD speeds due to collapsed left ventricular outflow tract and increased retrograde aortic flow. Under physiological conditions, the radial length of the aortic leaflets does not change significantly during systolic aortic flow; however, when the leaflets close and coapt under increasing pressure, the radial length increases during diastole [149] but as shown in our study, altered hemodynamic changes above and below the aortic valve may result in aortic root dilation, leaflet deformation and aortic regurgitation immediately after continuous flow VAD implantation. Considering that aortic valve fusion and/or regurgitation is reported to be a time-dependent process with increasing severity over time which may be related to continued valve remodeling from altered hemodynamics causing prolonged leaflet coaptation, phenotypic remodeling of valvular endothelial cells promoting local fibrosis or inflammatory processes [11,12,16,90], our data may be valuable to show that the onset of this process is immediate in increasing pump flows/speeds. Therefore, during clinical patient follow up, we may suggest that performing regular echocardiographic assessments and keeping the pump speed at the lowest level in order to provide an optimum cardiac output without compromising the aortic leaflet functions will be a rational preventive measure to avoid valve fusion and/or regurgitation after VAD implantations.

The present study has some limitations. First, the ventricular assist devices are designed to be used in patients with end-stage cardiac failure; therefore, our present results, obtained in a healthy/failing ex-vivo heart model, may not be directly applicable to the clinical setting. Second, we examined the immediate effects of the continuous flow LVAD implantation, therefore, we cannot draw any conclusions about the long-term effects of continuous-flow LVADs on aortic valve functions and structures. This limitation might be addressed in the future by establishing chronic heart failure animal models in which the chronic effects of the continuous flow ventricular assist devices on aortic valve function and structure could be assessed. Third, our conclusions were based on a relatively small number of ex-vivo hearts; nevertheless, because this is the first and only ex-vivo study focused on this topic, we believe that the very consistent trends in even four ex-vivo hearts with healthy and failing settings are important. Fourth, it must be taken into consideration that in ex-vivo heart studies, the aortic root is completely dissected free from its surrounding structures such as pericardium and pulmonary artery which may indirectly affect the normal aortic root configuration during the cardiac cycle and may interfere with the hemodynamic and echocardiographic measurements. And finally, it must be

considered that the outflow graft anastomosis angle, location, diameter and the distance to the aortic valve may affect the hemodynamic and flow measurements. Although our 90 degree anastomotic angle is not a perfect simulation of the clinical implant scenario, we think that the distance between the outflow graft anastomosis and the aortic valve is a relatively long (15 cm) in our ex-vivo study compared to clinical cases, therefore anastomotic variables may not have a big influence in hemodynamic measurements.

3.6 Conclusion

Increasing levels of continuous flow VAD support results in an immediately increased pressure overload on the aortic valve and reduced aortic valve opening time during the cardiac cycle along with an end-diastolic aortic root dilation, leaflet flattening and central aortic regurgitation. It is likely that chronically altered aortic valve mechanics and functions may explain structural valve changes causing leaflet fusion, thrombosis and/or regurgitation reported in the clinical situation.

4

The Effect of Intermittent Low Speed Mode on Aortic Valve Opening in Calves Supported With a Jarvik 2000 Axial-Flow Device

The contents of this chapter are based on: Tuzun E, Gregoric ID, Conger JL, Golden K, Jarvik R, Frazier OH, Kadipasaoglu KA. The Effect of Intermittent Low Speed Mode on Aortic Valve Opening in Calves Supported With a Jarvik 2000 Axial-Flow Device. ASAIO J 2005;51:139-143.

4.1 Abstract

We assessed the effects of an axial-flow left ventricular assist device (LVAD) on aortic valve opening, pump outflow, and biologic and hematologic parameters when operated in intermittent low speed (ILS) mode. An ILS controller-equipped Jarvik 2000 LVAD was implanted in 6 calves. Pump speed was maintained at 10,000 rpm and pump outflow measured throughout the study period (mean \pm SD, 71 \pm 6 days). Hematologic and biochemical parameters were analyzed daily for the first 10 days, weekly for the first month, and biweekly thereafter to monitor for kidney or liver dysfunction, hemolysis, bleeding, or infection. Before study termination, esmolol hydrochloride was infused to induce low cardiac output and totally impair aortic valve opening. Radiopaque cine-aortography was performed over 30-second intervals (10 seconds before, 10 seconds during, and 10 seconds immediately after ILS controller activation) to assess the effect of ILS mode on aortic valve opening. After study termination, major end organs and the major vascular tree were removed and examined macroscopically and histologically for thrombus formation and infarction; the aortic valve was examined for thickening and fusion. All pumps were explanted and examined for thrombus formation. All 6 calves recovered without surgical or mechanical complications. Hematologic and biochemical parameters did not change significantly between baseline and study termination. The aortic valve successfully opened when ILS mode was activated, even under low cardiac output conditions. No thrombus was detected in the major end organs and vascular tree, except for some small renal infarcts in 3 calves that did not affect renal function. These results indicate that operating an axial-flow LVAD in ILS mode allows aortic valve opening and aortic root washout.

4.2 Introduction

The left ventricular assist device (LVAD) is currently used as a bridge to transplantation [33], a bridge to recovery [32], or destination therapy [31] in patients with end-stage heart failure refractory to conventional medical and surgical treatments. Despite technological advances, prolonged use of LVADs has raised concerns about their long-term effects on flow properties and end-organ physiology, such as disturbances in aortic valve motion and related complications [16,114,115]. The Jarvik 2000 FlowMaker (Jarvik Heart, Inc., New York, NY), designed for temporary or permanent circulatory support in severe heart failure, is an axial-flow LVAD that provides continuous flow from the left ventricle to the aorta [35]. Axial-flow devices operating at higher speeds may cause extensive left ventricular (LV) unloading resulting in reduced wall stresses, myocardial contractility, and cardiac

output (CO) [42,43]. The resulting reduction of forward ejection across the aortic valve and increase of aortic diastolic pressure due to increased pump outflow into the aorta may impair aortic valve opening and cause aortic flow stagnation, which may in turn cause thrombosis or fusion of the aortic valve during long-term support [35]. To prevent hemostagnation in the aortic valve, the pump speed may be lowered so as to reduce unloading and allow for some degree of valve opening to wash out the aortic root [35,95]. However, in some cases of severe heart failure, decreased native heart function results in diminished or totally impaired aortic valve ejection, even at lower pump speeds, and makes such adjustment impossible [21]. To alleviate this problem, an intermittent low speed (ILS) controller for the Jarvik 2000 has been designed and tested in a calf model. In the present study, we assessed the effects of the controller on aortic valve opening, pump outflow, biochemical and hematologic parameters, and end-organ physiology in 6 calves supported with Jarvik 2000 pumps.

4.3 Materials and Methods

4.3.1 Device

The Jarvik 2000, a 90-g, 20-cc intraventricular axial-flow pump, is capable of augmenting the flow of the natural heart by up to 6 L/min. Total cardiac output measured in the pulmonary artery reaches 8-10 L/min in some cases. When the pump is equipped with a regular controller (as opposed to the ILS controller used in the present study), the pump speed is set manually in the range of 8,000-12,000 rpm. With the natural heart contracting, the device typically produces pulsatile flow instantaneously; this flow varies by as much as 5-8 L/min over the cardiac cycle. Typically, the pulsatile pressure is approximately 15-25 mmHg but may be lower in patients with very poor natural ventricular function or in patients whose pumps operate at speeds high enough to capture the full cardiac output and prevent ejection through the aortic valve. The ILS controller, which is also set manually in the range of 8,000-12,000 rpm, is identical to the regular controller with the exception of the ILS function.

4.3.2 Animal model

Experiments were conducted on 6 Corriente crossbred calves, each weighing between 108 and 135 kg. All animals received humane care in compliance with the Principles of Laboratory Animal Care (National Society of Medical Research) and the Guide for the Care and Use of Laboratory Animals (National Institutes of Health

publication no. 85-23, revised 1996). Our institution's Animal Care and Use Committee approved all protocols used in the present study. All animals were given intravenous warfarin (5 mg/day) beginning 3 days before surgery.

4.3.3 Anesthesia and Surgical Preparation

A standard anesthesia protocol was followed. Food was withheld from each calf 12 hours before induction of anesthesia. A 12-Fr triple-lumen venous catheter was inserted percutaneously into the right external jugular vein. Anesthesia was induced with intravenous (IV) diazepam (0.1 mg/kg) and ketamine (5-10 mg/kg). A cuffed endotracheal tube and an orogastric decompression tube were inserted. General anesthesia was maintained with isoflurane (1.0-3.0%) in oxygen (40-100%). The anesthetized calf was then placed on the operating table in the right lateral decubitus position in preparation for a left thoracotomy and left neck cutdown.

4.3.4 Operative Technique

A detailed description of the surgical implantation procedure has been published elsewhere [156]. Briefly, a left thoracotomy was performed in the fifth intercostal space, and the fifth rib was removed. An arterial pressure catheter was placed into the left internal thoracic artery (LIMA). The left carotid artery and left jugular vein were exposed for cardiopulmonary bypass (CPB) cannulation. After heparinization (300 units/kg), a 16-mm Dacron outflow graft was anastomosed to the descending thoracic aorta in end-to-side fashion with a 5-0 propylene suture using a partially occluding vascular clamp. After partial CPB was initiated, a silicone/polyester sewing cuff was sewn to the LV apex with pledgeted, coated, braided 2-0 polyester mattress sutures. The LV apex of the beating heart was cored with a circular knife. The Jarvik was inserted into the LV apex and secured with cotton tape and band(s) tied around the cuff. After the pump was secured, the outflow graft was connected to the pump outflow and was secured with 2 pieces of cotton tape. The pump and graft were deaired using an 18-gauge needle, and the resulting needle hole was repaired with 5-0 propylene sutures. A 16-mm ultrasonic flow probe (Transonics Inc., Ithaca, NY) was placed on the outflow graft and tunneled out from the eighth intercostal space. After removal of the CPB cannulas, the arterial pressure catheter was removed from the LIMA and transferred to the left carotid artery for postoperative follow-up. A #40 chest tube was placed into the left pleural space, and the incisions were closed in standard fashion.

4.3.5 Postoperative Care and Follow-up

Postoperatively, each calf was transported to the recovery room and weaned from the ventilator as soon as it regained the chewing reflex. Aortic pressure (AoP), heart rate, temperature, respiration rate, appetite, and pump flow were monitored hourly. All animals received a low-dose heparin infusion (8-10 U/kg/h) for 48 hours. After removal of the chest tube and AoP line 1-3 days after surgery, the calves were examined daily by veterinarians. Intravenous (IV) antibiotic therapy (cefazolin, 3 g/day) was continued until all IV catheters were removed 7-10 days after surgery. Warfarin was administered orally to all calves until study termination to maintain an international normalized ratio (INR) between 2.0 and 4.0. The pump speed was maintained at 10,000 rpm throughout the study.

Hematological and biochemical parameters were analyzed daily for the first 10 days, weekly for the first month, and biweekly thereafter to monitor for signs of kidney or liver dysfunction, hemolysis, bleeding, or infection.

At the end of the 10th week, the calves were fully heparinized (300 units/kg), and a Swan-Ganz catheter was placed to measure cardiac output. Esmolol hydrochloride infusion was initiated to induce severe biventricular heart failure. Pump speed was then increased to 12,000 rpm to test aortic valve opening under conditions of low cardiac output and maximal continuous flow retrograde through the aortic valve. An 8-Fr introducer was inserted into the left carotid artery, and a 6-Fr pig-tail catheter was advanced into the aortic root. Radiopaque cine-aortography was performed with an OEC® 9800 Plus Cardiac C-arm fluoroscope (General Electric) over 30-second intervals (10 seconds before, 10 seconds during, and 10 seconds after ILS controller activation) to assess the effect of ILS on aortic valve opening. Then, all calves were euthanized. Complete autopsies were performed and documented photographically. The heart, brain, lungs, kidneys, liver, and spleen and the major vascular tree were removed and examined macroscopically and histologically for signs of thrombus formation and infarction; the aortic valve was examined for signs of thickening and fusion. All pumps were explanted and grossly examined for thrombus formation.

4.4 Results

The Jarvik 2000 axial-flow LVAD was successfully implanted in all 6 cases, and all calves recovered from the implantation procedure without surgical or mechanical (device) complications. The early postoperative and follow-up period (mean \pm SD, 71 \pm 6 days) was uneventful. All calves were sacrificed at study termination according to the approved protocol. The mean pump flow throughout the study was 4.1 \pm 0.2 L/min.

Hematological and biochemical parameters are shown in **Tables 4.1 and 4.2**. There was no significant change in hematological parameters from baseline to study

termination, except for an elevation in prothrombin time (PT) and INR in the first postoperative week that may have been related to the preoperative IV administration of warfarin. Levels of serum glutamic oxaloacetic transaminase (SGOT), lactate dehydrogenase (LDH), and creatine kinase (CK) increased after surgery, but returned to normal limits within 3-7 days after surgery.

Table 4.1. Preoperative (Baseline) and Postoperative Hematologic Parameters^a

	Baseline	Postoperative Day			
		1	7	28	60
WBC (x 1,000/mm ³)	11.4 ± 2.1	13.6 ± 2	9.6 ± 2.4	9.3 ± 2.5	9.8 ± 3.1
RBC (x 1,000,000/mm ³)	9.6 ± 1.2	8.5 ± 0.7	6.5 ± 0.9	7.6 ± 1	7.2 ± 1.1
Hemoglobin (gm/dl)	11.5 ± 1.1	10.7 ± 0.9	8.4 ± 1.3	10.8 ± 1.1	10.8 ± 1.4
Hematocrit (%)	33 ± 2	28 ± 2	23 ± 3	30 ± 3	31 ± 4
Platelets (x 1,000/mm ³)	413 ± 150	231 ± 70	672 ± 167	223 ± 86	249 ± 184
Neutrophils (%)	18 ± 4	55 ± 8	31 ± 12	43 ± 11	37 ± 15
Lymphocytes (%)	73 ± 13	44 ± 11	65 ± 13	53 ± 16	60 ± 17
PT (sec)	14 ± 1	24 ± 2	21 ± 2	16 ± 1	16 ± 2
INR	1.7 ± 0.3	4.9 ± 0.4	4.1 ± 0.3	2 ± 0.2	1.9 ± 0.3
PTT (sec)	32 ± 3	40 ± 4	49 ± 4	37 ± 3	44 ± 6
Fibrinogen (mg/dl)	516 ± 120	456 ± 98	672 ± 116	443 ± 99	506 ± 106
Plasma free Hgb (mg/dl)	5 ± 0.6	2.8 ± 0.1	2 ± 0.2	2.1 ± 0.3	2.1 ± 0.2

WBC, white blood cells; RBC, red blood cells; PT, prothrombin time; INR, international normalized ratio; PTT, partial thromboplastin time; Plasma free Hgb, plasma free hemoglobin.

^a Values are mean ± SD.

Table 4.2. Preoperative (Baseline) and Postoperative Biologic Parameters^a

	Baseline	Postoperative Day			
		1	7	28	60
BUN (mg/dl)	11 ± 1.6	5.4 ± 1.1	7.8 ± 3.4	10 ± 2.9	9.3 ± 3.2
Glucose (mg/dl)	105 ± 7.2	107 ± 10.7	105 ± 9.6	98 ± 8.1	94 ± 9.2
Creatinine (mg/dl)	0.8 ± 0.2	0.6 ± 0.2	0.6 ± 0.1	0.6 ± 0.1	0.7 ± 0.2
SGPT (IU/L)	18 ± 2	23 ± 4	7 ± 1	13 ± 3	13 ± 3
SGOT (IU/L)	48 ± 2	184 ± 6	199 ± 7	57 ± 3	46 ± 4
Total protein (g/dl)	6.9 ± 0.4	5.1 ± 0.3	5.9 ± 0.3	6.3 ± 0.4	6.8 ± 0.4
Albumin (g/dl)	3.7 ± 0.3	3 ± 0.2	3.1 ± 0.1	3.5 ± 0.2	3.8 ± 0.2
Direct bilirubin (mg/dl)	0.08 ± 0.01	0.14 ± 0.01	0.18 ± 0.02	0.1 ± 0.01	0.1 ± 0.02
Total bilirubin (mg/dl)	0.1 ± 0.01	0.2 ± 0.02	0.12 ± 0.01	0.1 ± 0.02	0.16 ± 0.02
GGT (IU/L)	19 ± 2	13 ± 4	14 ± 3	17 ± 3	15 ± 3
LDH (IU/L)	520 ± 26	923 ± 42	863 ± 31	740 ± 23	670 ± 19
Cholesterol (mg/dl)	100 ± 16	58 ± 21	68 ± 16	91 ± 33	104 ± 23
ALK (IU/L)	154 ± 31	105 ± 26	117 ± 19	150 ± 25	158 ± 30
CK (IU/L)	268 ± 12	2000 ± 39	156 ± 14	188 ± 31	94 ± 12

BUN, blood urea nitrogen; SGPT, serum glutamic pyruvic transaminase; SGOT, serum glutamic oxaloacetic transaminase; GGT, gamma glutamyl transferase; LDH, lactate dehydrogenase; ALK, alkaline phosphatase; CK, creatine kinase.

^a Values are mean ± SD.

Esmolol hydrochloride infusion immediately affected several hemodynamic parameters. The heart rate decreased from 75±5 bpm at baseline to 45±6 bpm. Mean AoP decreased from 103±5 mmHg at baseline to 60±5 mmHg. Mean systolic pulmonary artery pressure increased from 20±4 mmHg at baseline to 45±3 mmHg. Mean cardiac output, as measured by the Swan-Ganz catheter, decreased from 16.6±3 L/min at baseline to 8.2±2.1 L/min. The pump's contribution to native cardiac

output increased from $25\pm 5\%$ at baseline to $75\pm 8\%$ in the low cardiac-output state. The flow in the vascular bed was totally nonpulsatile, and the aortic valve remained closed in all calves. Radiopaque cine-aortography demonstrated that the aortic valve was open during ILS controller activation (10 seconds) (**Figure 4.1B**) and remained closed until the next activation (50 seconds) in all calves (**Figure 4.1A and 4.1C**).

On macroscopic examination, 2 pumps had an organized thrombus on their outer surface. In all pumps but one, small, organized, red and white thrombus rings were seen on the inflow and outflow bearings; such rings are frequently seen in both animal and clinical studies and do not negatively affect pump function or increase the risk of thromboembolism. The inner surfaces of the outflow grafts were evenly covered with glistening white neointima and had no organized thrombus formations. Aortic valve leaflet coaptation was normal, and no thrombus, thickening, or signs of regurgitation were detected. Multiple large infarcts were seen in the kidneys of 2 calves; however, renal function in these 2 cases remained normal throughout the study, and there was no gross evidence of either acute or chronic infarcts in any other explanted organs. Clinically, there was no evidence of neurologic deficit in any of the calves.

4.5 Discussion

Long-term patient outcome after conventional, pulsatile LVAD implantation is adversely affected by infection, bleeding, and thromboembolism [92]. These complications may be reduced by using smaller, more easily implantable LVADs. This led to the development and clinical testing of a new generation of continuous-flow (i.e., centrifugal or axial-flow) pumps [29,54]. The small, easily implantable, and reliable Jarvik 2000 significantly improves native heart function in patients with end-stage heart failure refractory to conventional medical and surgical treatments¹⁵ and significantly reduces the incidence of postoperative bleeding and infection [30].

As previously stated, the circulation in patients supported with an axial-flow LVAD is partially pulsatile when the pump speed setting allows flow through the native aortic valve [30]. Such partial unloading of the left ventricle may be more effective than total unloading in achieving ventricular recovery during long-term support [28,81]. As the pump speed is increased, the aortic valve remains closed, causing flow stagnation and reducing aortic washout. This, in turn, may trigger a thrombogenic state marked by platelet aggregation, hypercoagulability, and white cell adhesion [58,102,174]. Blood trauma during axial-flow pumping may accelerate this phenomenon by promoting red cell aggregation and reducing cell deformability, which lead to increased blood and plasma viscosity [161].

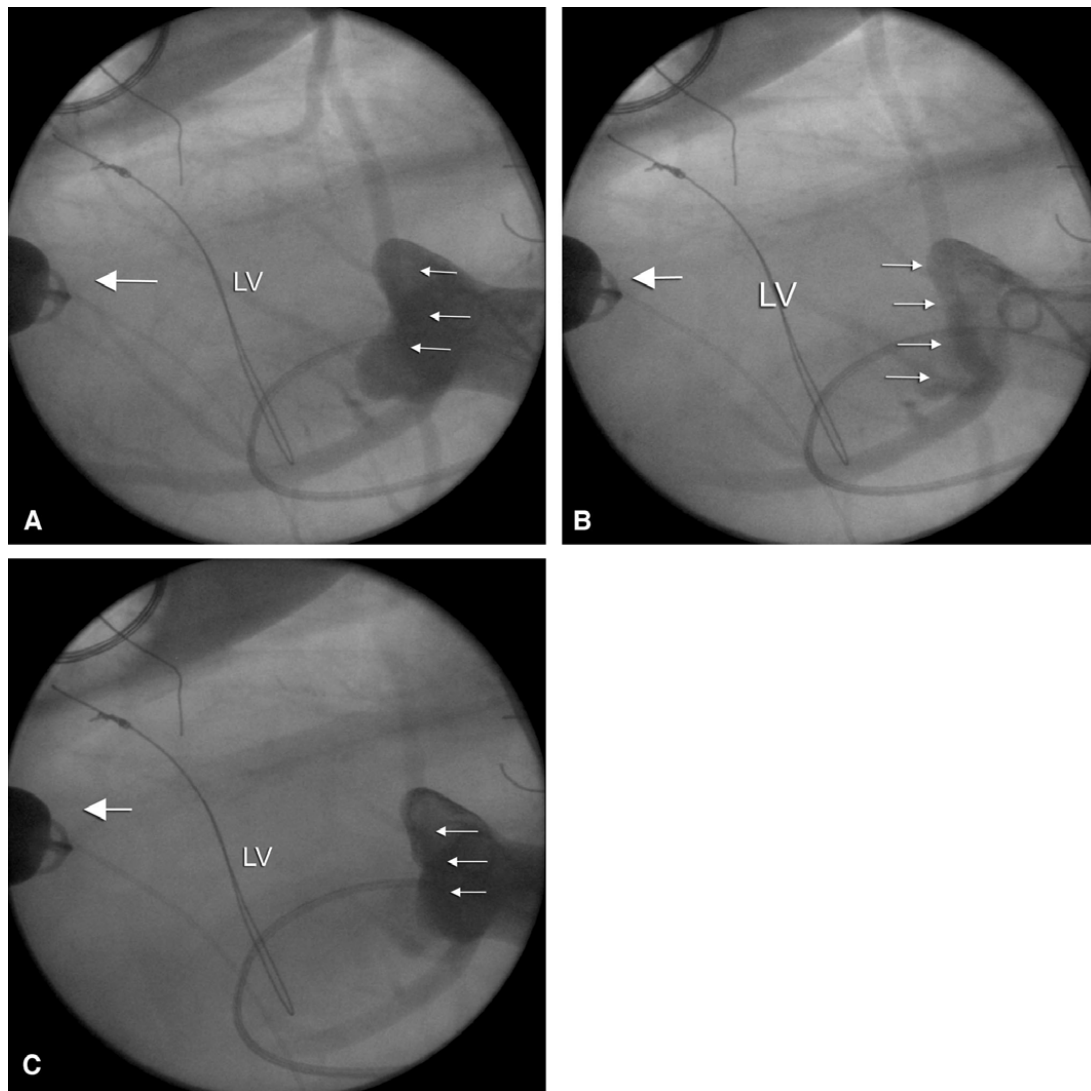


Figure 4.1A, 4.1B and 4.1C: Serial images obtained by radiopaque cine-aortography showing aortic valve totally closed when the ILS controller is not activated (A and C) and open when the controller is activated (B). Small arrows indicate Jarvik 2000 pump. LV, left ventricular cavity; ILS, intermittent low speed.

If the outflow graft of the axial-flow pump is anastomosed to the descending aorta, then there is the potential for retrograde flow, which may encourage stagnation at the aortic valve [21,30,95]. This phenomenon is not observed when the outflow graft is anastomosed to the ascending aorta, even if the native aortic valve does not open [30]. In patients with severe heart failure, several factors may affect placement of the outflow graft. These factors include previous sternotomy, patient size, LV dimension, presence and extent of coronary artery disease, and aortic calcification and/or atherosclerosis [30]. In our study, we preferred to anastomose the outflow graft to the descending aorta in order to create a worst-case scenario in which to assess the long-term effects of ILS on aortic valve opening.

We proposed alleviating hemostagnation by intermittently minimizing the pump flow to allow opening of the aortic valve. Our rationale was that the systolic ejection

time is inversely related to pump speed via decreased LV end-systolic pressure, increased aortic diastolic pressure, and increased retrograde flow, especially when the outflow graft is anastomosed to the descending aorta [28]. In such cases, even if the aortic valve were to continue to open at higher pump speeds, the reduced ejection time and decreased LV contractility might not allow for an ejection powerful enough to wash out the aortic root. This might in turn lead to stasis at the aortic root. In the present study, we demonstrated that aortic valve opening and ejection could be successfully achieved by temporarily reducing the pump speed for 10 seconds each minute (i.e., operating the pump in ILS mode), even in states of low cardiac output associated with total closure of the aortic valve. This allowed the aortic valve to open 6 times per minute during a 60-bpm cardiac cycle, thus preventing stasis-related complications (e.g., thrombosis, emboli, and/or leaflet fusion) and apparently providing enough flow to wash out the aortic root.

Large animals seem to be able to adapt to nonpulsatile circulation [39,175]. However, over long periods, the blood flow must exceed 90 mL/kg/min for normal organ function to be maintained, and the perfusion pressure must be kept within the normal range [175]. Pulsatile flow seems more likely to maintain normal organ function at reduced flow rates and pressures. The ILS mode increases the degree of pulsatility above and beyond the partial pulsatility generated by contraction of the native heart when the axial-flow pump is running at a constant speed. Taking advantage of this observation may help avoid the need for increased flow requirements, as noted above, during long-term support.

4.6 Conclusion

In conclusion, our results indicate that operating an axial-flow pump at intermittent low speeds allows the aortic valve to open and the aortic root to be washed out even in states of low cardiac output and under continuous-flow conditions, thus preventing valvular thrombosis, fusion, or both.

5

Continuous flow cardiac assist and regional myocardial perfusion interaction: An ex-vivo heart study

The contents of this chapter are based on: Tuzun E, Pennings K, van Tuijl S, de Hart J, Stijnen M, van de Vosse F, de Mol B, Rutten M. Assessment of aortic valve pressure overload and leaflet functions in an ex-vivo beating heart loaded with a continuous flow cardiac assist device.*Submitted.*

5.1 Abstract

Background: We sought to assess the complex interaction between continuous flow left ventricular assist device (CFLVAD) physiology and myocardial perfusion in an ex-vivo beating heart system.

Materials and Methods: A CFLVAD was implanted in 4 swine hearts and operated at baseline (device off) and at device speeds ranging between 7500 to 11500 rpm under healthy and failing heart conditions. At each setting, aortic and left atrial pressure signals were continuously monitored along with aortic, right and left main coronary artery flows, PV loops, and device output. Right and left ventricular regional perfusions were assessed with epicardial laser probes. Serial blood gas samples were collected to calculate intramyocardial arteriovenous oxygen difference and cell metabolism.

Results: Healthy and failing ex-vivo beating heart models were successfully created in all hearts. Right and left main coronary artery flows gradually increased at increasing pump supports in healthy and failing conditions ($p < 0.05$ vs baseline) while left and right ventricular regional myocardial perfusions remained unchanged or slightly decreased compared to baseline values. Left ventricular myocardial cell metabolism did not change in healthy and failing heart conditions. A gradual decrease in arteriovenous oxygen difference at increasing pump supports was observed in healthy and failing hearts along with a significant decrease in coronary vascular resistance and tension-time index ($p < 0.05$ vs baseline).

Conclusion: Increased coronary artery flow along with unchanged regional blood flow and cell metabolism, and decreased arteriovenous oxygen difference support occurrence of intramyocardial arteriovenous shunts at increasing CFLVAD supports.

5.2 Introduction

The terms coronary blood flow and regional myocardial perfusion are often used as synonyms, although they are not quite the same. Regional myocardial perfusion depends on coronary artery blood flow, using conductance vessels as epicardial coronary trunks, resistance vessels as coronary perforants, arterioles and capillaries. Blood volume is distributed all through myocardial wall, but is mostly present at subendocardial area, filled by approximately 80% of myocardial blood volume [38]. Eventually, the coronary blood drains through three types of channels: the subepicardial veins, the thebesian veins, and the arteriosinusoidal vessels [1]. Although, the regional myocardial perfusion partially depends on the epicardial blood flow, other factors such as epicardial coronary artery stenosis, perfusion pressure, intraventricular pressures, flow mode (pulsatile vs continuous), myocardial

geometry (wall shape and thickness) and intramural pressures (fractional shortening) may affect regional myocardial perfusion properties [38].

Continuous flow left ventricular assist devices (CFLVADs) are being used to bridge patients with end-stage heart failure to heart transplantation, by enhancing myocardial and systemic end-organ perfusion [139]. It has been demonstrated that in the lack of a donor heart, they can provide adequate systemic flow to a heart failure patient for up to 7.5 years [170]. Although, maintaining the regional myocardial perfusion is one of the essential end-points of the CFLVAD therapy, the (patho-) physiological effects of the continuous flow and reduced pulsatility on myocardial perfusion are still not well understood which is particularly important for patients supported for bridge to myocardial recovery with or without ischemic etiology. It is well known that in patients suffering from dilated cardiomyopathy, microvascular dysfunction leading to severe myocardial hypoperfusion results in left ventricular remodeling with progressive wall thinning, left ventricular dysfunction, and progression of the existing heart failure [13]

In this study, we performed an ex-vivo healthy and failing beating heart study in porcine hearts in order to investigate the effects of reduced pulsatile flow on left and right ventricular regional myocardial blood flow.

5.3 Materials and Methods

5.3.1 Animals

Four domestic Dutch landrace hybrid adult pig hearts were obtained from pigs that were slaughtered for human consumption. The protocols at the slaughterhouse and laboratory were developed in accordance with EC regulations 1774/2002 regarding the use of slaughterhouse animal material for diagnosis and research, supervised by the Dutch Government (Dutch Ministry of Agriculture, Nature and Food Quality) and approved by the associated legal authorities of animal welfare (Food and Consumer Product Safety Authority). These protocols prevent additional animal suffering and sacrifice in performing the experiments. The slaughterhouse procedures were carried out under supervision of representatives (veterinary officers) of the regulatory authorities.

5.3.2 Ex-vivo Beating Heart Preparation

A detailed description of the preparation has been published previously [20]. Briefly, following regular slaughter protocols, the chest was opened and hearts were then removed en bloc with the heart usually still beating. The heart was immediately

cooled topologically in ice slush. A liter of cardioplegic solution (4°C Modified StThomas2+5000IU Heparin) was given into the coronary arteries at a pressure of 80 mmHg and the heart was submersed in the same solution for transportation. In the laboratory, a 17 mm cannula was inserted into the aorta approximately 40 mm distal to the aortic valve annulus. A 27 mm cannula was inserted into the left atrium to allow sufficient atrial filling after resuscitation. Similarly, a 19 mm cannula was inserted into the pulmonary artery. The azygos vein, inferior and superior vena cava were ligated. Epicardial pacing wires were placed on the aorta, left atrium, and left ventricle to monitor electrical activity and to pace the heart. A Micromed DeBakey CFLVAD (MicroMed Cardiovascular Inc, Houston, TX) is used for the experiments. The inflow cannula is inserted via left ventricular apex and the outflow graft is mounted 7-9 cm distal to the aortic valve.

5.3.3 Ex-vivo Beating Heart Perfusion on the Perfusion Circuit

The perfusion circuit (PhysioHeart, HemoLab, Netherlands) (**Figure 5.1**) was primed with a normothermic (38 °C) 1:1 mixture of Krebs-Henseleit buffer (4.0 ± 0.5 L) and heparinized autologous blood (4.0 ± 0.5 L) (Hematocrit, $15\% \pm 1\%$; pH, 7.40 ± 0.05) supplemented with insulin (0.32 units/L). Each heart was suspended in an elastic sleeve, and the left side of the heart was connected to the circuit as follows. The aortic cannula was connected to the circuit to induce modified Langendorff mode. The heart was perfused retrogradely from the aorta at a coronary perfusion pressure of 70 mmHg. Following five minutes of modified Langendorff mode perfusion, regular myocardial contractile activity was reestablished, and the left atrial cannula was connected to the circuit to induce beating-ejecting mode. If needed, the heart is defibrillated with 10J. The heart was then perfused anterogradely from the left ventricle into the coronary arteries through the aorta. The heights of the preload and afterload reservoirs were adjusted to create a preload of 10 to 20 mmHg and an afterload of 100 to 120 mmHg.

5.3.4 Perfusion of Isolated Hearts on the Ex-Vivo Circuit

In beating-ejecting mode, the left ventricle ejected the perfusate into the aortic cannula, where aortic pressures (AoP) were measured. The compliance chamber, placed in series between the aorta and the afterload reservoir, partially corrected cyclic fluctuations in pump pressure. Through an overflow tube in the afterload reservoir, the perfusate was collected into a reservoir and pumped by the first roller pump into the venous reservoir, where it then passed through an arterial filter. A centrifugal pump routed the perfusate into the oxygenator which contained 95%

oxygen and 5% carbon dioxide. The oxygenator was connected to the heater-cooler, which kept the perfusate at 37 °C by recirculating heated water through the oxygenator. The heated and oxygenated perfusate was then pumped by the second roller pump back into the preload reservoir. From the preload reservoir, the left atrium was supplied with oxygenated perfusate. Coronary venous perfusate was returned to the circuit through the cannula leading from the pulmonary artery to the reservoir. The third roller pump was used to fill the afterload reservoir initially for modified Langendorff-mode perfusion. The preload reservoir could be emptied into the reservoir through an overflow tube.

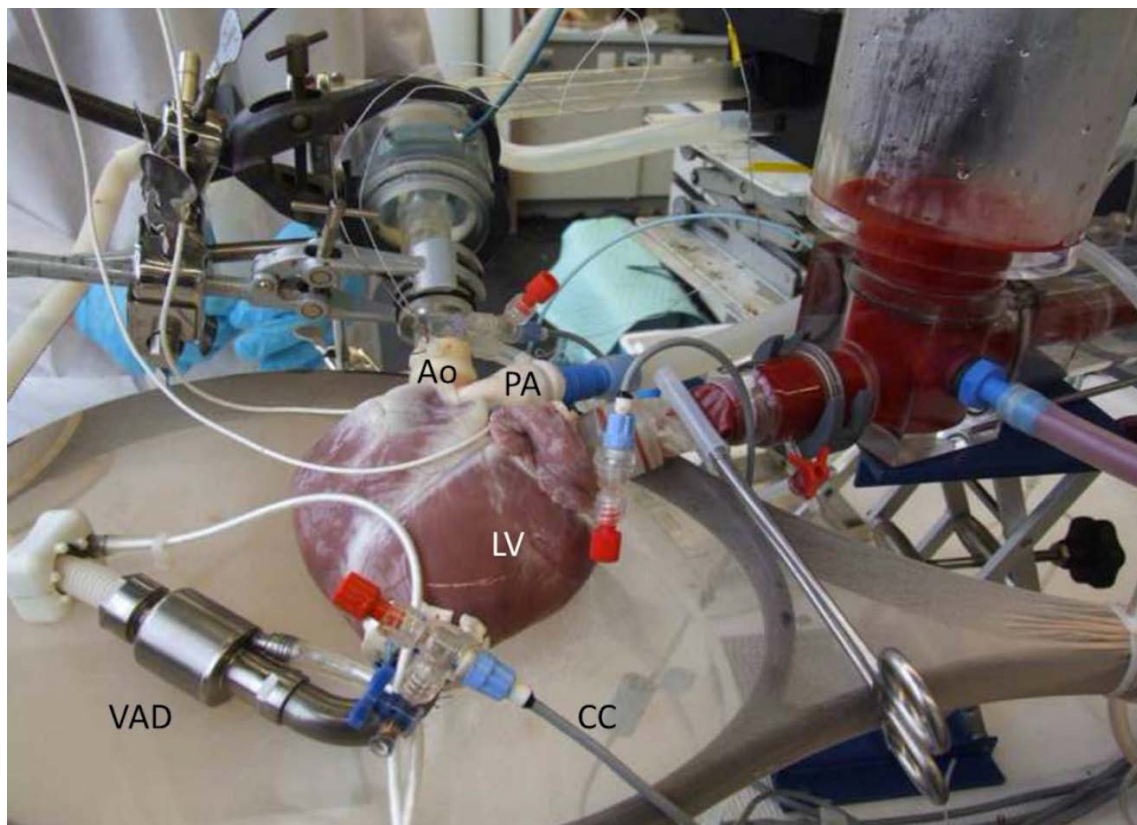


Figure 5.1: Ex-vivo beating heart perfusion circuit loaded with a left ventricular assist device. Ao: Aorta; CC: Conductance catheter; CFLVAD: Ventricular assist device; LV: Left ventricle; PA: Pulmonary artery.

5.3.5 Data Collection

The following data is collected at the baseline (CFLVAD off and outflow graft is clamped) and with the CFLVAD running at speeds from 7500, 8500, 9500, 10500 and 11500 rpm during measurements on healthy heart and failing heart, 2 minutes of interval between each speed change. Once hemodynamic steady state was reached in beating-ejecting mode, AoP, left atrial pressure (LAP) and heart rate were continuously recorded. The left ventricular pressure-volume (PV) loops were created

with a transapically inserted conductance catheter (CD Leycom, The Netherlands). Left ventricular pressures (LVP), dp/dt_{max} , left ventricular coronary vascular resistance (CVR) and tension time index (TTI) were extracted from PV loop and hemodynamic data. The CFLVAD outflow graft (Q_{vad}), aortic root (Q_a), left main coronary artery (QLC) and right coronary artery (QRC) flows were measured by ultrasonic flow sensors (Transonic Systems Inc.).

Left and right ventricular regional myocardial perfusions (LVper and RVper) were measured with a laser Doppler probe (Transonic Systems, Inc) attached to the epicardial surface of the right and left ventricle.

Arterial (aortic root) and venous (coronary sinus) blood samples were collected at baseline and each experimental setting to calculate left ventricular myocardial arteriovenous oxygen difference and CO₂ production (TCO₂) which are indirect indicators of cell metabolism. Net TCO₂ is calculated based on the formula proposed by Rozin [118]: $Net\ TCO_2 = Venous\ pCO_2 - Arterial\ pCO_2$. Increased or unchanged TCO₂ along with venous hyperoxia compared with baseline is considered a result of intramyocardial arteriovenous shunts (AVS) whereas decreased TCO₂ is considered sign of low oxygen utilization (LOU). Although both ventricles' venous blood drains into the coronary sinus, our mock-loop is a 2-chamber beating heart model and the right ventricular preload, afterload and cell metabolism are fairly constant since there is no systemic venous return to the right ventricle; therefore venous TCO₂ mainly reflects changes in left ventricular cell metabolism.

5.3.6 Induction of Ex-vivo Heart Failure

Distal left anterior descending and first circumflex obtuse margin coronary arteries were ligated and acute ischemic heart failure is successfully created as detected by PV loops.

5.3.7 Statistics

The data is expressed in mean \pm SD format. The reproducibility of the ex-vivo measurements was determined using a paired t-test, comparing the two measurements done under the same conditions. A three-way ANOVA test is performed to calculate the significance of the hemodynamic parameters between healthy and failing conditions and different levels of CFLVAD support. A p value smaller than 0.05 is considered statistically significant.

5.4 Results

5.4.1 Procedural Success

A 2-chamber ex-vivo beating heart mode was successfully created in all hearts. Data were collected at two time intervals (first healthy, then failing heart condition) for each ex-vivo experiment while the hearts were kept in a beating heart mode for up to 4 hours.

5.4.2 Baseline data in ex-vivo healthy and failing heart conditions

Comparison of PV loops and hemodynamic data recorded before (baseline) and after coronary artery ligation confirmed the efficacy of the heart failure induction protocol. **Figures 5.2A, 5.2B and 5.2C** show, respectively, the characteristic aortic, left atrial and left ventricular pressure waveforms and PV loops generated by the healthy and failing heart conditions in one experiment prior to VAD support. Mean dp/dt_{max} decreased $43\% \pm 5\%$ in failing hearts compared to healthy baseline measurements ($p < 0.05$ vs baseline) (**Figure 5.3**).

LV CVR significantly increased after hearts failure induction (**Figure 4**) along with a significant decrease in TTI (**Figure 5**) ($p < 0.05$ healthy vs failing heart).

The mean AoP and LVP and LAP achieved at the baseline healthy heart conditions were 84 ± 10 mmHg, 59 ± 9 mmHg and 18 ± 7 mmHg, respectively. These values were decreased to 65 ± 11 mmHg, 45 ± 16 mmHg and 29 ± 12 mmHg respectively, in failing heart state ($p < 0.05$ for all parameters).

The mean Q_a obtained at the baseline under healthy heart conditions were 3.7 ± 0.6 L/min. After the induction of heart failure, the mean Q_a decreased to 2.5 ± 1.5 L/min ($p < 0.05$).

Mean QLC and QRC were 73 ± 55 mL/min and 71 ± 53 mL/min in healthy heart, respectively. In failing heart conditions, QLC and QRC decreased to 45 ± 26 mL/min and 39 ± 27 mL/min, respectively ($p < 0.05$ for both parameters).

Under healthy conditions, mean LVper and RVper were 2.1 ± 0.8 mL/min/gr and 1.6 ± 0.5 mL/min/gr, respectively. LVper significantly decreased to 1.8 ± 0.1 mL/min/gr whereas RVper increased significantly to 2.1 ± 1.9 mL/min/gr after the heart failure creation ($p < 0.05$ for both parameters).

In 2 healthy heart conditions, arterial and venous blood gas samples were excluded due to a sampling error, therefore mean TCO_2 was calculated from the samples collected from 2 healthy hearts. Basic mean TCO_2 were 2.1 mmHg and 2.4 mmHg in healthy and failing hearts, respectively. Statistical analysis was not performed for this parameter according to the low sample size.

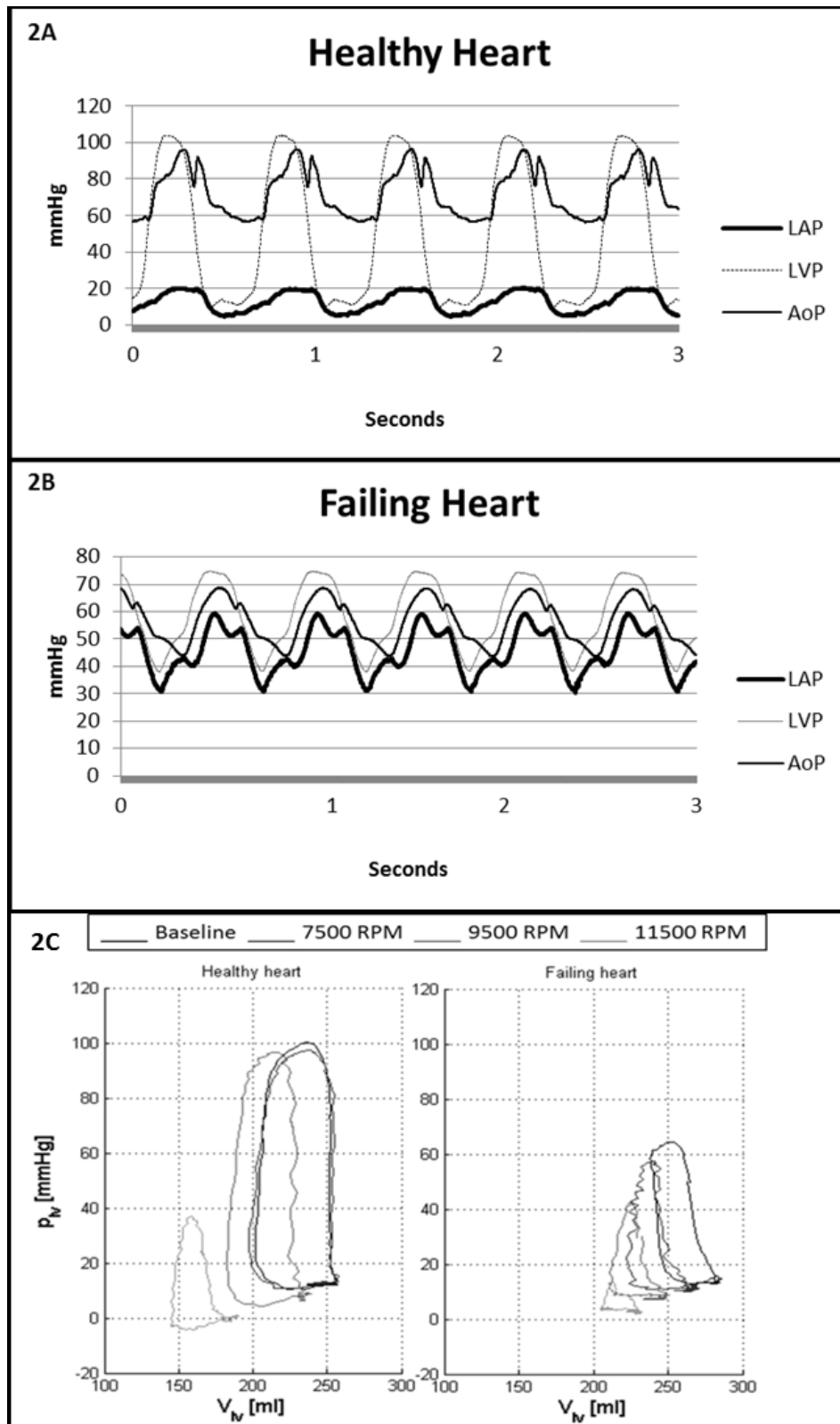


Figure 5.2A, 5.2B and 5.2C: Typical LVP, AoP and LAP waveforms on healthy (A) and failing heart (B) modes. (C) PV loops generated by the healthy (left) and failing (right) heart modes in one experiment before and after assist device support. AoP: Aortic pressure; CFLVAD: Ventricular assist device; LAP: Left atrial pressure; LVP: Left ventricular pressure; VLV: Left ventricular volume; PV: Pressure-volume; RPM: rotation per minute.

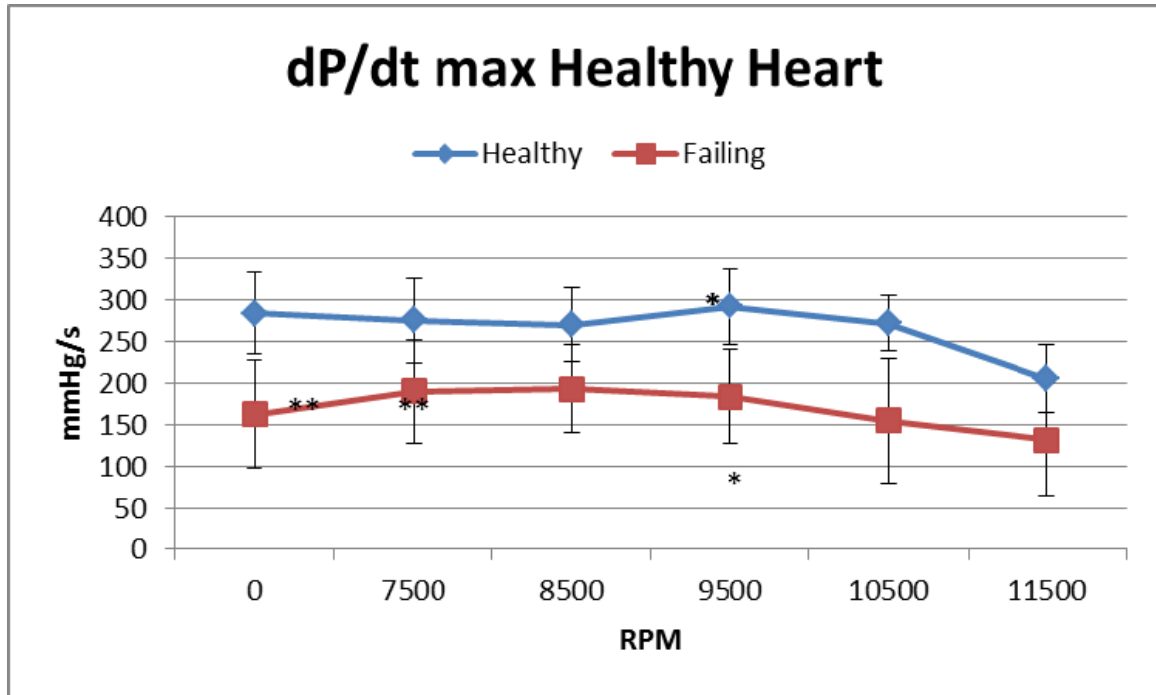


Figure 5.3: dP/dtmax in healthy and failing hearts at the baseline and increasing assist device support. RPM: Rotation per minute; *: $p < 0.01$ vs baseline; **: $p < 0.05$ vs baseline.

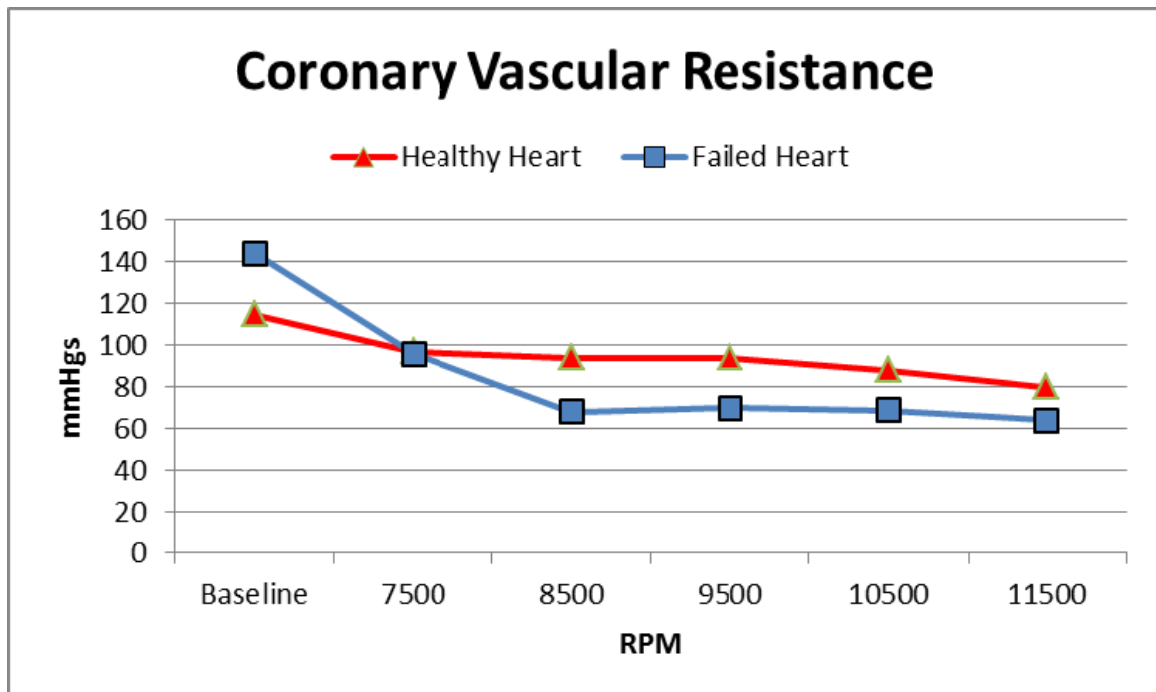


Figure 5.4: Changes in coronary vascular resistance in healthy and failing hearts under CFLVAD support. RPM: Rotation per minute; *: $p < 0.05$ vs baseline..

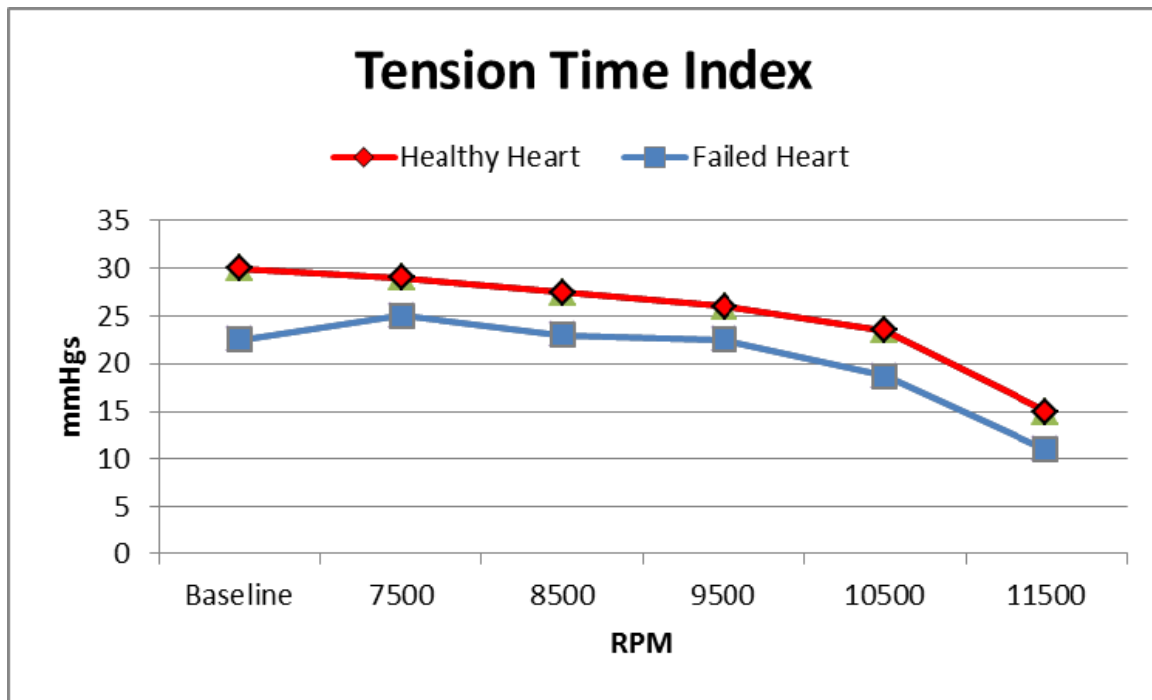


Figure 5.5: Changes in tension time index in healthy and failing hearts under CFLVAD support. RPM: Rotation per minute; *: $p < 0.05$ vs baseline.

5.4.3 Data after VAD support in ex-vivo healthy and failing heart conditions

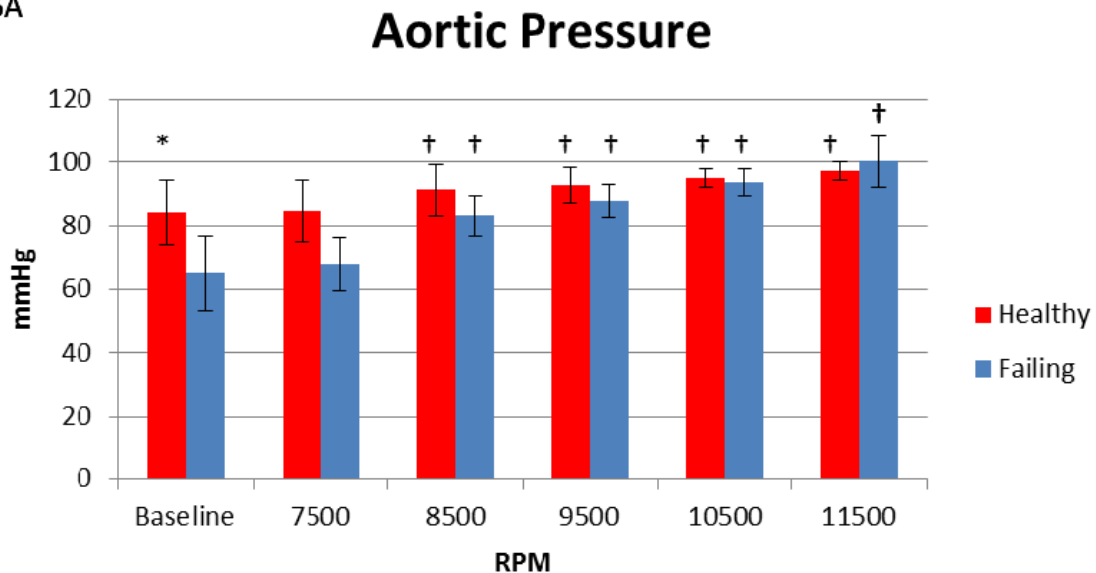
In all hearts, a gradual leftward shift of the PV loops was observed under healthy and failing heart conditions with increasing CFVAD supports. Mean dP/dt_{max} slightly decreased in healthy hearts during lower pump speeds (partial left ventricular unloading) but sharply decreased at total left ventricular unloading at 11500 rpm ($p < 0.01$ vs baseline). In failing hearts, dP/dt_{max} significantly increased at partial left ventricular unloading ($p < 0.05$ at 7500 and 8500 rpm, vs baseline) then gradually and significantly decreased at total left ventricular unloading at 11500 rpm ($p < 0.01$ vs baseline) (**Figure 5.3**). There was a gradual decrease in LV CVR in healthy hearts which became statistically significant at 10500 rpm and 11500 rpm ($p < 0.05$ vs baseline). The decrease was more steep and statistically significant in all pump speeds in failing hearts ($p < 0.05$ vs baseline) (**Figure 5.4**). TTI showed a gradual decrease which became statistically significant at 10500 rpm and 11500 rpm in both healthy and failing hearts ($p < 0.05$ vs baseline) (**Figure 5.5**).

The mean AoP gradually and significantly increased at increasing pump speeds with a corresponding decrease at the LVP, LAP and PP in healthy and failing hearts compared to baseline values as shown in **Figure 5.6A, 5.6B and 5.6C**. The mean Q_a sharply decreased at increasing pump speeds in healthy and failing conditions ($p < 0.05$ vs baseline for all speeds) along with a significant increase in Q_{vad} ($p < 0.05$ vs 7500 rpm for all speeds). Depending upon the extent of LV unloading the Q_a

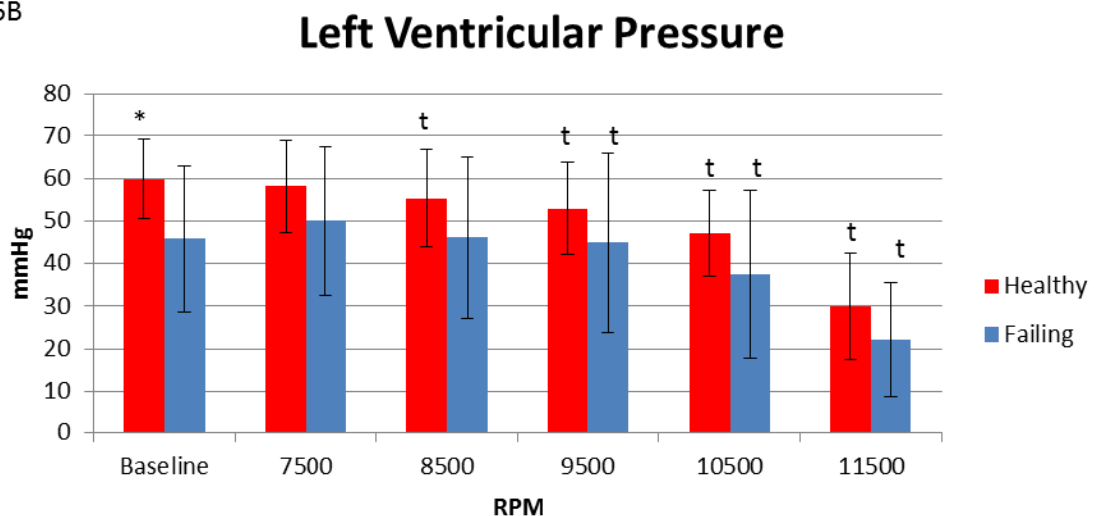
reversed direction at increasing VAD supports resulting aortic regurgitation at speeds exceeding 8500 rpm and 9500 rpm, in both healthy and failing conditions, respectively (**Figure 5.7A and 5.7B**). Mean QLC and QRC gradually increased at speeds 8500 rpm and above in healthy and failing conditions ($p < 0.05$ vs baseline) while the LVper and RVper remained unchanged or slightly decreased compared to baseline values (**Figure 5.8A- 5.8D**).

Assessment of arterial and venous blood gas samples in healthy and failed hearts revealed a gradual increase at the partial venous oxygen pressure at increasing pump speeds while the partial arterial oxygen pressure remained unchanged at all speeds. There was no significant change in TCO₂ at increasing pump supports under healthy or failing heart conditions. **Figure 5.9A and 5.9B** show the data obtained from TCO₂ and blood gas measurements at increasing pump supports.

6A



6B



6C

Left Atrial Pressure

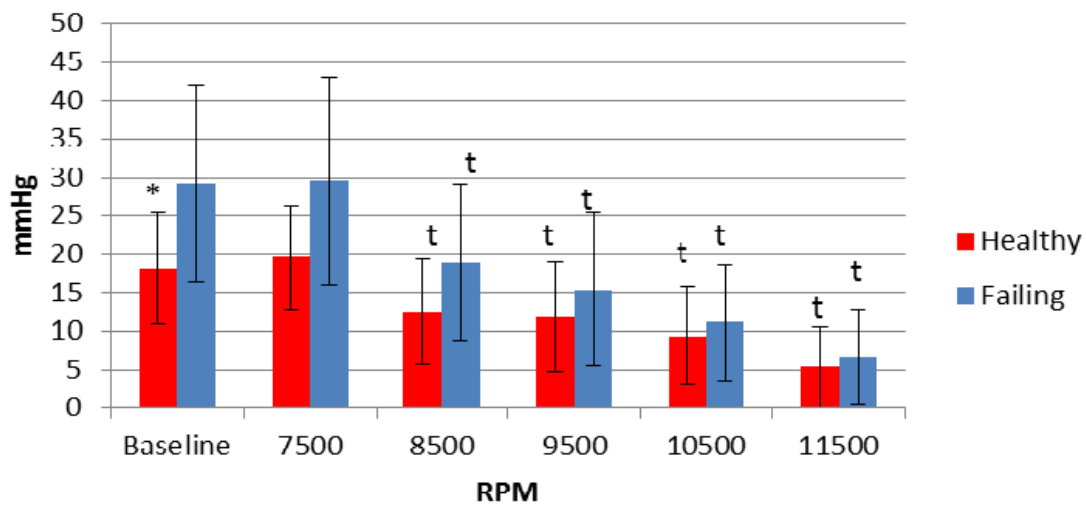
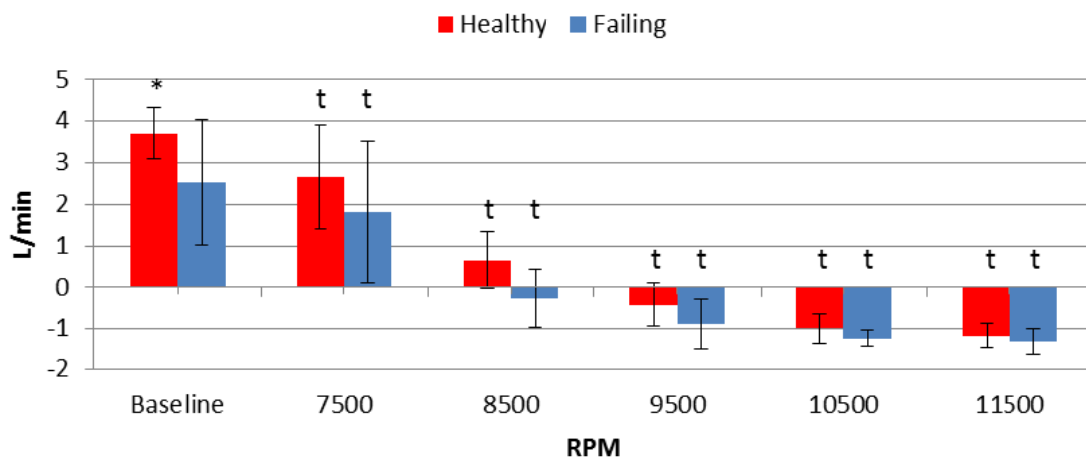


Figure 5.6A, 5.6B and 5.6C: Aortic (A), left ventricular (B) and left atrial (C) pressures at the baseline and increasing assist device support in healthy and failing heart modes. RPM: Rotation per minute; *: $p < 0.05$ healthy vs failing; †: $p < 0.05$ vs baseline.

7A

Aortic Flow



7B

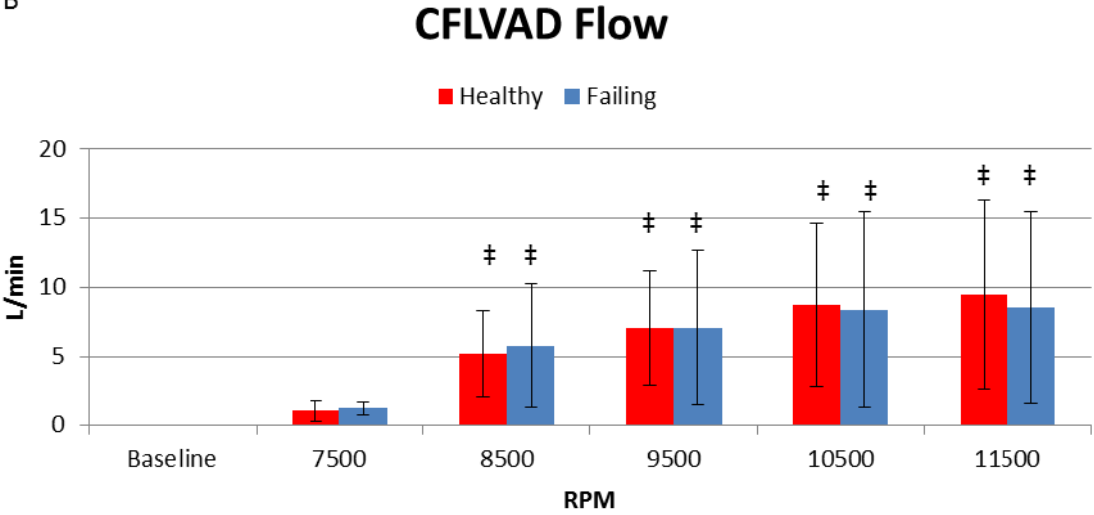
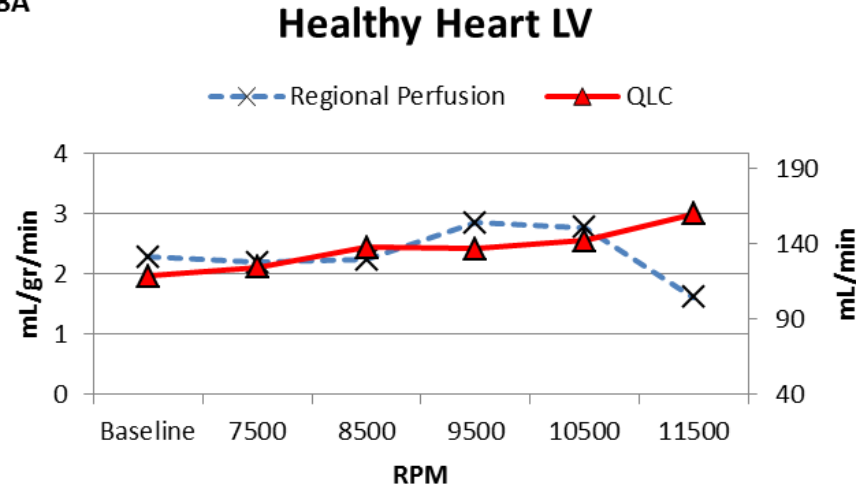
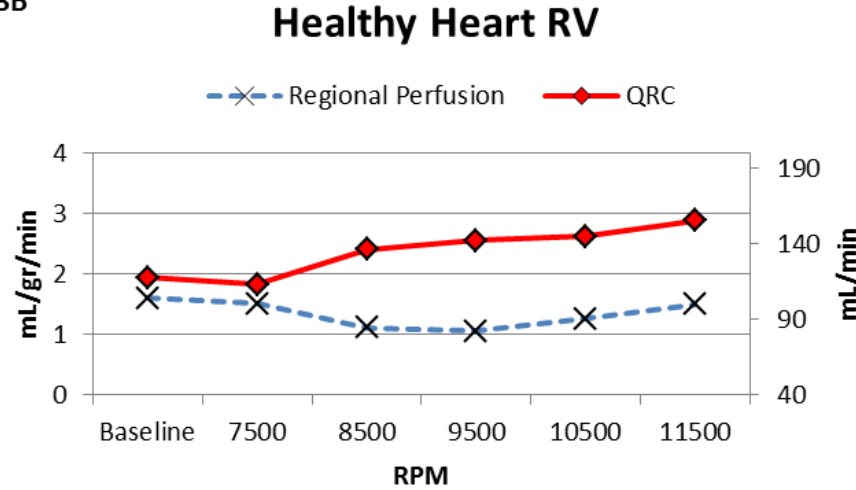


Figure 5.7A and 5.7B: Aortic (A) and CFLVAD (B) flows at the baseline and increasing assist device support in healthy and failing heart modes. CFLVAD: Ventricular assist device; RPM: Rotation per minute; *: $p < 0.05$ healthy vs failing; †: $p < 0.05$ vs baseline; ‡: $p < 0.05$ vs 7500 RPM.

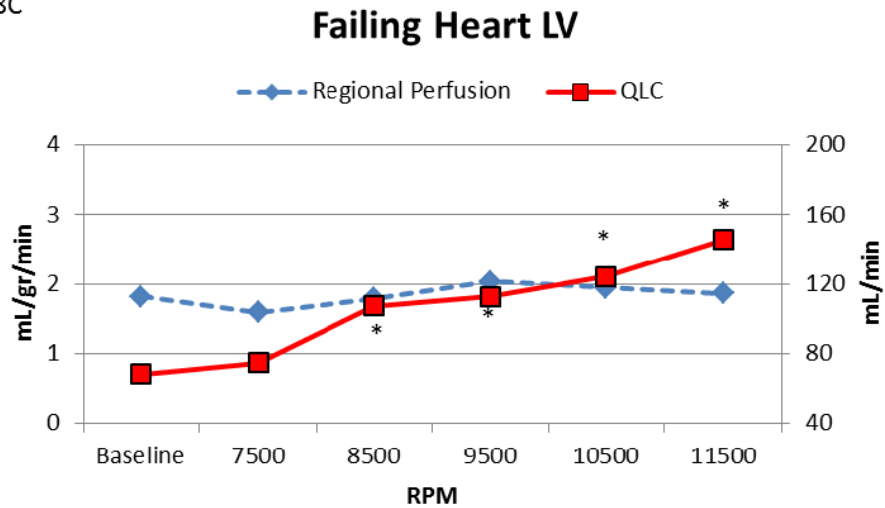
8A



8B



8C



8D

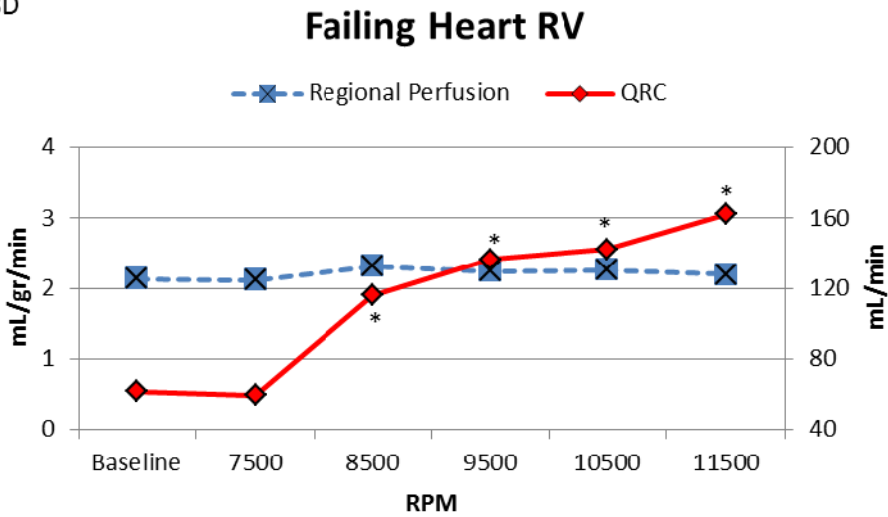
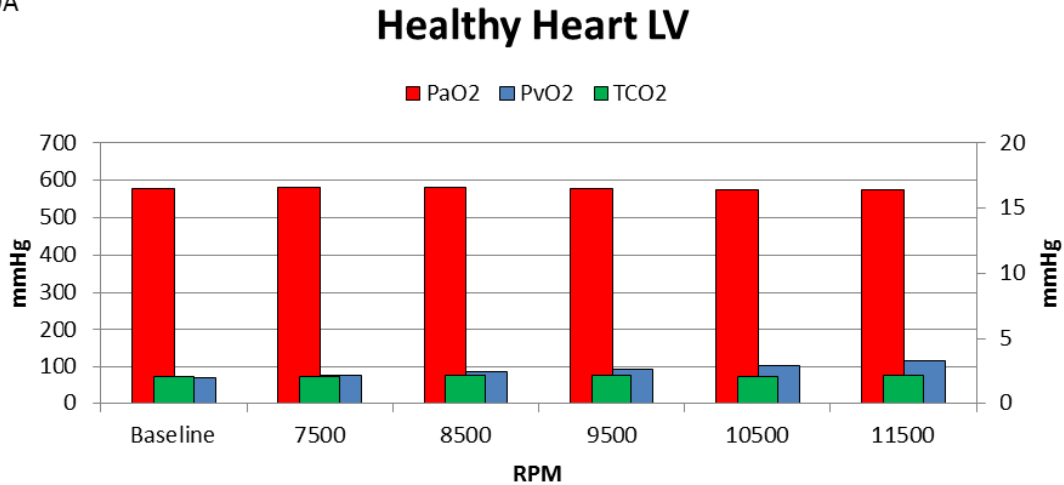


Figure 5.8A, 5.8B, 5.8C and 5.8D: LV and RV regional perfusions, QLC and QRC at the baseline and increasing assist device support in healthy (A and C) and failing heart (B and D) modes. LV: Left ventricle; QLC: Left main coronary flow; QRC: Right coronary flow; RPM: Rotation per minute; RV: Right ventricle. *: $p < 0.05$ vs

9A



9B

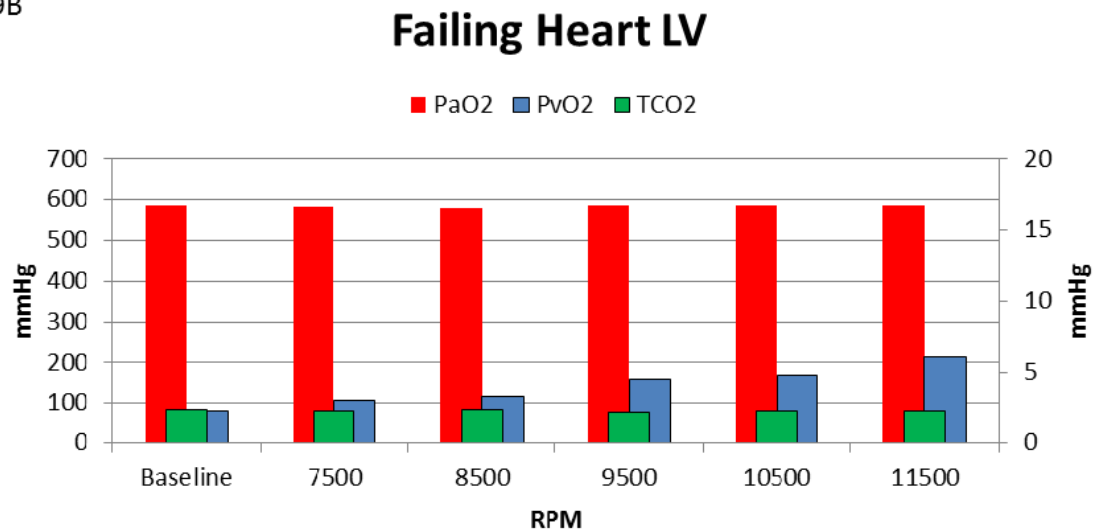


Figure 5.9A and 5.9B: PaO₂, PvO₂ and TCO₂ at the baseline and increasing assist device supports in healthy (A) and failing (B) heart modes. TCO₂: Carbondioxyde production; RPM: Rotation per minute; PaO₂: Arterial partial oxygen pressure; PvO₂: Venous partial oxygen pressure.

5.5 Discussion

Using an ex-vivo beating heart model loaded with a CFLVAD, we showed that left main (QLC) and right (QRC) coronary artery flows gradually and significantly increased at increasing LVAD flows (Q_{vad}) but the left (LV_{per}) and right (RV_{per}) ventricular regional myocardial perfusions remained unchanged or slightly decreased under healthy and failed heart simulations. There was no significant change in TCO₂ at increasing Q_{vad} in healthy and failing hearts. Arteriovenous oxygen difference gradually decreased at increasing Q_{vad} in healthy and failing heart simulations.

5.5.1 Experimental Model

The changes in coronary artery flow, regional myocardial perfusions and ventricular wall mechanics in response to increasing CFLVAD flow were partially assessed in limited number of acute healthy or failing heart models [23,84,156,158,166,167]. Although very valuable preliminary data was collected with those studies, it was not possible to quantify or isolate the effects of the anesthetics and neurohumoral autoregulatory mechanisms on myocardial perfusion which was also affected by reduced pulsatile flow physiology. In our study, we were able to demonstrate healthy and failed cardiac hemodynamic performance both qualitatively, in terms of pulse waveforms (AoP, LVAP, LAP), and quantitatively, in terms of average cardiac output and pressures (PV loops) in the same heart and to eliminate most of the uncontrollable effects on myocardial perfusion such as anesthetics, body autoregulation and/or neurohumoral mechanisms. Therefore we think that in this ex-vivo beating heart model we were able to assess purely acute mechanical effects of the reduced or non-pulsatile flow on myocardial perfusion since the hearts were totally denervated. In all hearts cardiac performance was successfully controlled and kept at normal levels for up to 4 hours, with only minor deterioration of hemodynamic performance. The mean weight increase of the ex-vivo hearts was less than 5% at the study termination, indicating only a mild level of edema. In addition, the use of fresh pig hearts acquired from a local slaughterhouse was very beneficial from a time, cost accessibility, reproducibility and ethical perspective [20].

5.5.2 Aortic and ventricular hemodynamic changes in response to cf-LVAD

In our study, we observed a gradual increase in mean AoP along with a decrease in PP with increasing pump speed in healthy and failed heart conditions. This effect, which was related to the increasingly predominant continuous flow characteristics associated with progressively reduced native cardiac pulsatility (LV unloading), was more pronounced at higher CFLVAD speeds and failed heart condition which was consistent with previous experimental and clinical observations [23,84,139,156,158,170]. Increasing CFLVAD speeds resulted in increased Q_{vad} , impaired aortic valve opening and eventually reversal of the aortic flow (regurgitation) which occurred earlier at lower speeds in failing hearts compared to healthy heart conditions. The early closure of the aortic valve and aortic regurgitation at lower CFLVAD speeds in failing hearts may be attributed to the decreased contractility of the left ventricle which resulted in decreased aortic flow, unloading most of the left ventricular volume through the CFLVAD and increased pressure overload above the aortic valve [83,160].

5.5.3 Left and right ventricular coronary flow and myocardial perfusion in response to cf-LVAD

The major determinants of myocardial oxygen demand are wall tension, contractility and heart rate [176]. The complex interaction between myocardial oxygen demand and coronary flow in healthy and failing hearts is regulated by changes in coronary vessel diameter and consequently the vascular resistance of the coronary arteries. The epicardial arteries are known to contribute to only 5% of the total coronary vascular resistance while intramyocardial coronary arterioles are responsible for 95% of the total coronary vascular resistance [60]. Since myocardial perfusion occurs mainly during diastole, any change of the myocardial contractility pattern may affect epicardial and intramyocardial coronary flows [76]. In our study, significant decrease in dP/dt_{max} at higher speeds in healthy hearts, particularly observed at extensive LV unloading has been reported previously [23,121,156] and may be attributed to delayed LV relaxation and decreased TTI secondary to extensive LV unloading. Unchanged TCO₂ despite increasing epicardial coronary flows at increasing pump supports may be attributed to decreased coronary vascular resistance and TTI resulting in intramyocardial arteriovenous shunting along with well protected myocardial cell metabolism [1,44,65,101]. In case of failing hearts, partial unloading of the LV with lower pump speeds resulted in increased contractility noted by increased dP/dt_{max} but extensive unloading resulted in delayed ventricular relaxation and decreased contractility as observed in healthy hearts. Although TCO₂ was protected at increasing pump supports, significant increase in QLC and decrease in arteriovenous oxygen difference suggested more pronounced intramyocardial arteriovenous shunting compared to healthy hearts possibly due to less stiff myocardium and lower intramyocardial pressure. Limited number of studies performed with microspheres or positron emission tomography techniques reported unchanged or decreased regional myocardial perfusion under CFLVAD support in either healthy or diseased myocardium but they were not able to outline the mechanism of this phenomenon [23,81,68,156]. Our study showed that higher CFLVAD flows result in actively changing myocardial mechanical properties and regional myocardial perfusion is closely dependent to several intrinsic and extrinsic factors such as degree of myocardial stiffness, CVR, TTI and AVS. Two conditions, AVS and LOU, may exist simultaneously as result of venous hyperoxia in the tissues; thus, there is a need to differentiate one condition from the other. It is well known that under normal tissue perfusion conditions, one O₂ molecule is utilized as one CO₂ molecule is produced; however, LOU is associated with low CO₂ production. Therefore, AVS may be associated with unchanged or increased CO₂ production. According to our data, we believe that immediate occurrence of venous hyperoxia

with unchanged myocardial cell metabolism despite increasing coronary blood flows is strong evidence of intramyocardial AVS opening under continuous flow physiology. It is noteworthy that QRC significantly increased at increasing pump supports along with a slight decrease or unchanged regional myocardial perfusion similar to the LV although the RV is not unloaded by a CFLVAD. In our two-chamber ex-vivo mock loop, the RV wall function and tension was not affected by increased systemic venous return or pulmonary vascular resistance since RV stroke volume was only limited with coronary sinus return. Moreover, the hearts we get from the slaughterhouse are not dilated, and therefore exhibit no or very little septal shifting during LV unloading at maximum rotational speeds confirmed by real time transepical echocardiography. Therefore, one might speculate that increasing mean arterial pressure as a result of increasing reduced or non-pulsatile flow is solely responsible for this phenomenon since metabolic status and mechanical wall properties of the RV has not changed compared to baseline conditions at increasing CFLVAD supports. The occurrence of the intramyocardial arteriovenous shunts under CFLVAD support and its mid or long-term effects may be particularly important in patients developing RV failure after CFLVAD implantations and this complex interaction needs further assessment. Similarly, the effects of the AVS on LV recovery and reverse remodeling need to be investigated with mid- or long-term studies.

5.5.4 Conclusion

In our ex-vivo beating heart model, increasing CFLVAD support resulted in increased RV and LV coronary blood flow but unchanged or slightly decreased regional myocardial perfusion and cell metabolism in healthy and failing heart conditions. The decrease in myocardial arteriovenous oxygen difference was more pronounced in failing hearts compared to healthy ones. Increased coronary artery flow along with unchanged regional blood flow and cell metabolism, and venous hyperoxia support occurrence of intramyocardial arteriovenous shunts at increasing CFLVAD supports.

6

Myocardial Hemodynamics, Physiology, and Perfusion with an Axial-Flow Left Ventricular Assist Device in the Calf

The contents of this chapter are based on: Tuzun E, Eya K, Chee HK, Conger JL, Bruno NK, Frazier OH, Kadipasaoglu KA. Myocardial Hemodynamics, Physiology, and Perfusion with an Axial-Flow Left Ventricular Assist Device in the Calf. ASAIO Journal 2004; 50:47–53.

6.1 Abstract

Background: The Jarvik 2000 axial-flow left ventricular assist device (LVAD) is used clinically as a bridge to transplantation or as destination therapy in end-stage heart disease. The effect of the pump's continuous flow output on myocardial and end-organ blood flow has not been studied experimentally.

Materials and Methods: To address this, the Jarvik 2000 pump was implanted in 8 calves and then operated at speeds ranging from 8000 to 12000 rpm. Micromanometry, echocardiography and blood oxygenation measurements were used to assess changes in hemodynamics, cardiac dimensions, and myocardial metabolism in this experimental model, respectively, at different speeds compared with baseline (pump off, 0 rpm). Microsphere studies were performed to assess the effects on heart, kidney, and brain perfusion at different speeds.

Results: The Jarvik 2000 pump unloaded the left ventricle and reduced end-diastolic pressures and left ventricular dimensions, particularly at higher pump speeds. The ratio of myocardial oxygen consumption to coronary blood flow and the ratio of subendocardial to subepicardial blood flow remained constant. Optimal adjustment of pump speed and volume status allowed opening of the aortic valve and contribution of the native left ventricle to cardiac output, even at the maximum pump speed. Neither brain nor kidney microcirculation was adversely affected at any pump speed.

Conclusion: We conclude that the Jarvik 2000 pump adequately unloads the left ventricle without compromising myocardial metabolism or end-organ perfusion.

6.2 Introduction

The Jarvik 2000 left ventricular assist device (LVAD) (Jarvik Heart, Inc., New York, NY) is a small, intraventricular, easily implantable axial flow pump designed be used either for bridging to transplantation or for permanent mechanical circulatory support in end-stage heart disease [17]. It is suitable for use in smaller adults and children [91]. The advantage of intraventricular placement is the elimination of problems related to inlet graft kinking, stagnation, and thrombosis. Additionally, the Jarvik 2000 pump prevents suction of the septal or left ventricular (LV) free walls, does not cause significant hemolysis, and is associated with a low risk of infection [28].

However, it is not known how the continuous flow output of the Jarvik 2000 pump may affect blood flow to the myocardium or other end organs, such as the liver, kidney, and brain. In their experimental study, Saito et al. [122] found that long-term continuous blood flow was well tolerated by healthy sheep and produced no functional or histologic changes in the myocardium, brain, kidney, or liver. In a study

by Merhige et al., changes in regional myocardial perfusion were measured with microspheres in the presence and absence of ischemia in dogs supported by a continuous flow pump, and the pump was found to increase blood flow in the ischemic myocardial region [84]. On the other hand, Sezai et al. [129] found that, compared with continuous circulation, pulsatile circulation provided enough blood to satisfy the physiologic demand to the major organs (myocardium, kidney, and liver) and better microcirculation at the cellular level in ischemic pigs. In this context of contradictory reports, we assessed the relationships between continuous pump flow and changes in LV mechanics and end-organ perfusion in an acute, non-ischemic calf model.

6.3 Materials and Methods

6.3.1 Jarvik 2000 Axial Flow Pump

The Jarvik 2000 LVAD is a compact axial-flow impeller pump that consists of a blood pump, a percutaneous power cable, a pump-speed controller, and an external direct-current power supply. The pump's design has been described in detail elsewhere [77].

6.3.2 Animal Model

Eight Corriente crossbred calves weighing 92 to 130 kg were used in the study. All calves received humane care in compliance with the Principles of Laboratory Animal Care (National Society of Medical Research) and the Guide for the Care and Use of Laboratory Animals (National Institutes of Health publication no. 85-23, revised 1996). Our institution's Institutional Animal Care and Use Committee approved all protocols used in the present study.

6.3.3 Anesthesia and Surgical Preparation

A standard anesthesia protocol was followed. Food was withheld from each calf 12 hours before induction of anesthesia. Each calf was premedicated with glycopyrrolate (0.02 mg/kg) intramuscularly (IM) and xylazine (0.2-0.7 mg/kg) IM. A 12-Fr triple-lumen venous catheter was inserted percutaneously into the right external jugular vein. Anesthesia was induced with intravenous ketamine (10-20 mg/kg). A cuffed endotracheal tube and an orogastric decompression tube were inserted. General anesthesia was maintained with isoflurane (1.0-3.0%) in oxygen (40-100%). The anesthetized calf was then placed on the operating table in the right

lateral decubitus position in preparation for a left thoracotomy and left neck cutdown. Electrocardiographic leads were connected, and a rectal temperature probe was inserted.

6.3.4 Implantation operation

The Jarvik 2000 pump was implanted through a left thoracotomy during partial cardiopulmonary bypass (CPB). The left carotid artery and jugular vein were exposed for CPB cannulation. A left thoracotomy was then performed in the fourth intercostal space. The fifth rib was removed to expose the apex of the left ventricle and the descending thoracic aorta. The pericardium was incised from the apex to the pulmonary artery, and the heart was suspended in a pericardial cradle. Heparin (3 mg/kg) was administered. Then, a 22-Fr cannula was placed in the left common carotid artery, and 28-Fr wire-reinforced venous cannula was advanced through the left external jugular vein to the right atrium. The calf's body temperature was cooled to 30°C to 32°C, and all cannulas were connected to the CPB circuit (Terumo SX-10 membrane oxygenator and Terumo roller pump; Terumo, Inc., Tokyo, Japan).

Next, the 16-mm Dacron outflow graft of the Jarvik 2000 pump was anastomosed to the descending thoracic aorta with a 4-0 propylene suture while aortic flow was temporarily impeded with a partially occluding vascular clamp. CPB was initiated, and the heart was fibrillated. A silicone/polyester sewing cuff was sewn to the ventricular apex with pledgeted, coated, braided 2-0 polyester mattress sutures. The Jarvik 2000 pump was then inserted into the ventricular apex and secured with cotton tape around the cuff and pump casing. After the pump was secured, air was removed from the left ventricle, pump, and graft. Once the calf's body temperature was normalized (37.7-38.8 °C), the heart was defibrillated and paced if necessary. The calf was then slowly weaned from CPB.

6.3.5 Intraoperative Hemodynamic Assessment

Once surgery was completed, the venous cannula was removed and an 8-Fr Swan-Ganz catheter was inserted into the pulmonary artery via the left external jugular vein. The carotid arterial cannula was removed to insert a special catheter fitted with a high-fidelity micromanometer tip (Millar Mikro-Tip Catheter; Millar Instruments, Houston, TX) into the left ventricle. A pressure catheter was inserted from the left internal thoracic artery and advanced proximally into the immediate vicinity of the aortic valve to measure arterial pressure. Four different ultrasonic flow probes (Transonics Inc., Ithaca, NY) were then placed (**Figure 6.1**): a 16-

mm flow probe on the outflow graft; a 24-mm probe 2 cm cranial from the site of anastomosis on the descending thoracic aorta; a 16-mm probe on the brachiocephalic artery 2 cm above its bifurcation from the aorta; and a 3-mm probe around the proximal left anterior descending coronary artery. Data were recorded by a 16-channel computer data acquisition system (Ponemah System version 3.3; Gould Instrument Systems Inc., Valley View, OH). Hemodynamics were assessed with the pump off and the outflow graft clamped to avoid pump regurgitation (0 rpm, baseline) and with the pump operating at various speeds (8000, 9000, 10000, 11000, and 12000 rpm) for 20 minutes at each speed. Mean heart rate (HR); systolic (AoPs), diastolic (AoPd), and mean (AoPm) aortic pressures; mean pulmonary artery pressure (PAP); pulmonary capillary wedge pressure (PCWP); central venous pressure (CVP); LV systolic pressure (LVP); LV end-diastolic pressure (LVEDP); and various flow rates were measured at increasingly higher pump speeds.

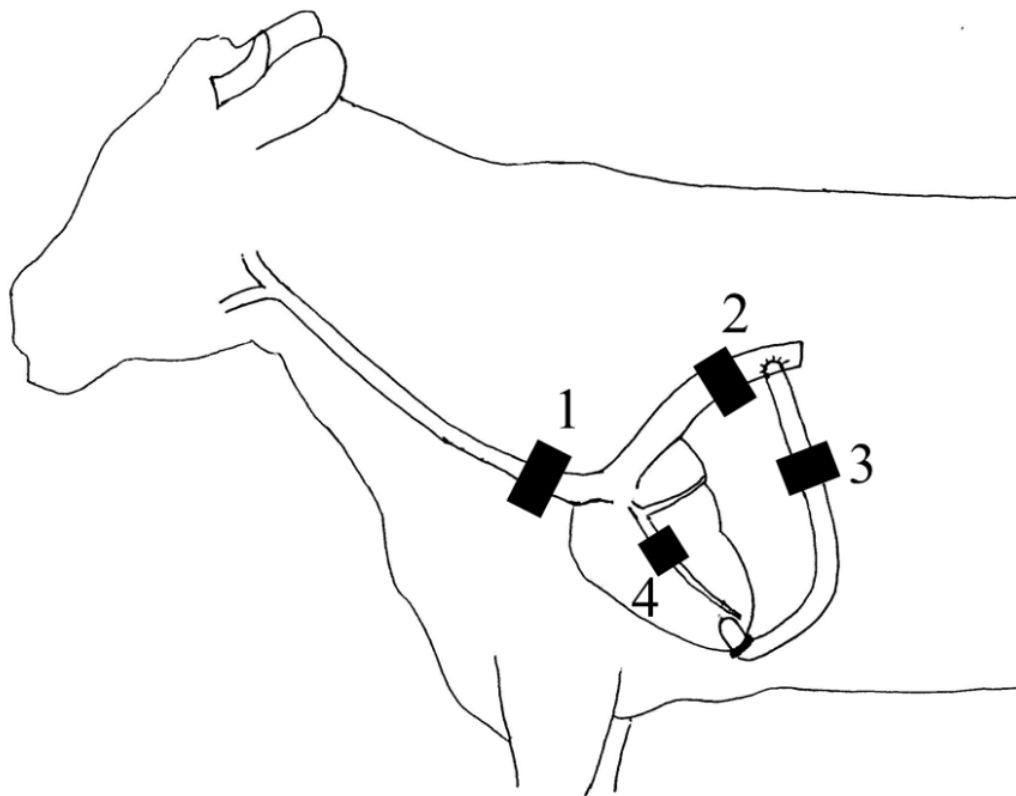


Figure 6.1: Schematic of instrumentation technique. Black bars show the placement of ultrasonic flow probes on the brachiocephalic artery (1), descending thoracic aorta (2), pump outflow graft (3), and proximal left anterior descending coronary artery (4).

6.3.6 Echocardiographic Assessment

Serial 2-dimensional transepical studies were performed at each pump speed. Echocardiographic assessment was accomplished using a Hewlett Packard Sonos

2000 ultrasound system equipped with a 2.5-MHz phased-array transducer, according to the guidelines of the American Society of Echocardiography [48]. The echocardiogram was used to measure systolic and diastolic LV internal dimensions (LVISd and LVIDd), aortic valve motion, and LV wall motion.

6.3.7 Myocardial Oxygen Consumption Assessment

An 18-gauge angiocatheter was inserted into the coronary sinus via the azygos vein to take coronary sinus blood samples. Samples were taken at each of the 6 speeds to assess myocardial oxygen consumption (MVO₂). MVO₂ was approximated as the difference between aortic (\bar{a}) and coronary sinus (v) blood oxygen content, multiplied by the left anterior descending (LAD) coronary artery blood flow rate (CBF) (i.e., $MVO_2 = CBF \cdot [\bar{a} - v]$). A Novastat Profile M blood gas analyzer (Nova Biomedical Co., Waltham, MA) was used for blood gas analysis.

6.3.8 Tissue Perfusion Assessment

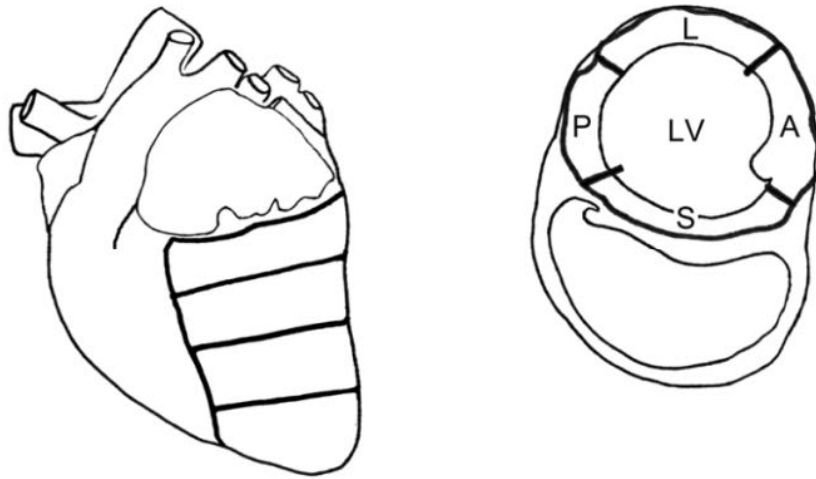
Tissue perfusion was assessed by microsphere analysis using 15- μ m, non-radioactive, stable isotope-labeled microspheres (BioPAL, Inc., Worcester, MA). The microspheres were injected, according to the manufacturer's suggested standards, into the left atrium while the pump was off or operating at 8000, 9000, 10000, 11000, and 12000 rpm. Microspheres labeled with gold appeared red; lanthanum, blue; antimony, violet; and lutetium, pink. Each labeled microsphere was used at a different pump speed.

After tissue perfusion assessment, each calf was euthanized. Then, its heart, brain and left kidney were harvested for analysis as follows. In the case of the heart, the left ventricle was isolated and divided into 4 equal transverse sections along the atrioventricular groove (**Figure 6.2**). The basal and apical sections were discarded. The more distal of the remaining 2 sections was selected and divided into 4 segments representative of the septal, anterior, lateral, and posterior walls (**Figure 6.2A**). Each segment was further divided into an epicardial and an endocardial subregion (In total 8 tissue samples from the heart). Two grams of tissue were taken from each region for microsphere analysis.

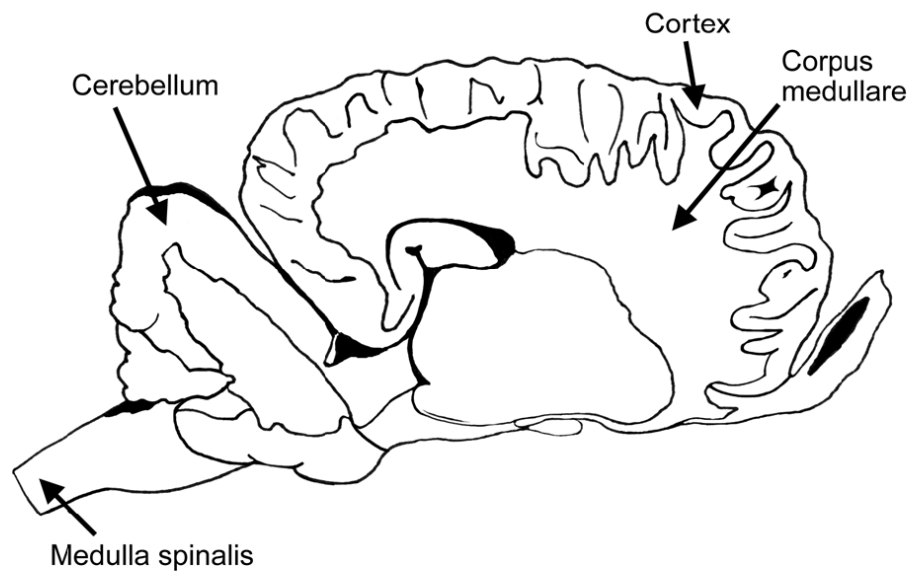
The left hemisphere of the brain, the cerebellum, and the upper 3 cm of the medulla spinalis were each divided into 3 equal parts posteroanteriorly, and the middle sections were harvested. Two grams of tissue were taken from each of the cortex, corpus medullare, cerebellum, and medulla spinalis subregions (In total 4 tissue samples from the brain) for microsphere analysis (**Figure 6.2B**).

The left kidney was divided into 3 frontal sections, and the middle section was divided into cortical, subcortical, and papillary subregion. Totally 3 tissue samples (2 grams from each subregion) were taken for microsphere analysis (**Figure 6.2C**).

A



B



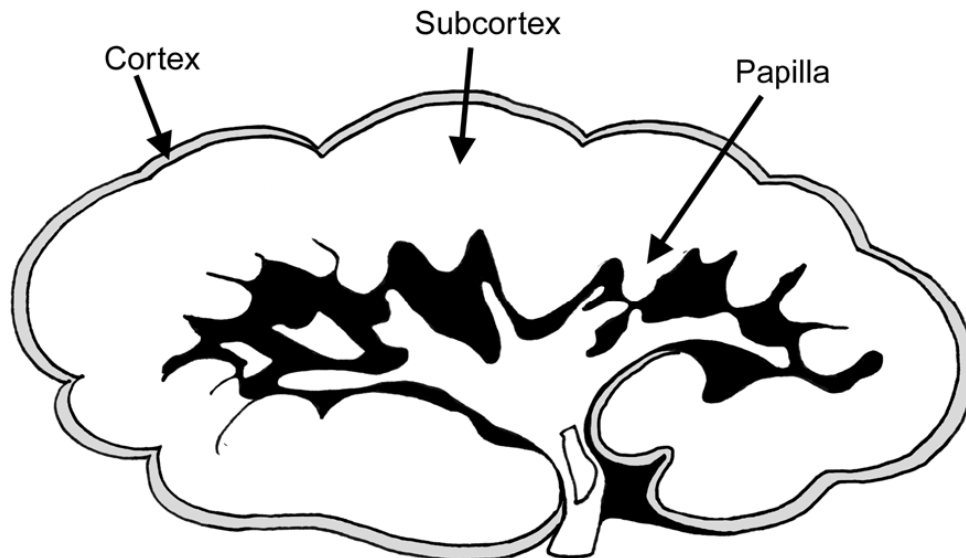
C

Figure 6.2A, 6.2 B and 6.2C: Schematics of tissue sections used in assessing perfusion in the heart (A), brain (B), and kidney (C). S, septal wall; A, anterior wall; L, lateral wall; LV, left ventricle; P, posterior wall.

All tissue samples were dried overnight at 70°C and sent out for analysis. Blood samples were obtained and used to normalize tissue sample readings. The analysis was based on an automated neutron activation system described in detail elsewhere [135,165,171].

6.3.9 Statistical Analysis

All statistical tests were performed using Microsoft Excel or SAS (SAS Institute, Inc., Cary, NC) software on a personal computer. A value of $P < 0.05$ was considered significant. The power was 80%. Student's t-test was used whenever 2 continuous variables were compared.

6.4 Results

All experiments were successfully completed without surgical or mechanical (device) complications. Mean body temperature of the animals was measured $38.2 \pm 6^\circ\text{C}$.

6.4.1 Hemodynamic Studies

Table 6.1 shows the data obtained from left and right heart catheterization. As pump speed increased above 10000 rpm, mean AoPd increased progressively but not

significantly ($P=0.07$ for 10000, 11000, and 12000 rpm vs baseline). The increases in mean AoPs and AoPm were less pronounced, and as a result, the aortic pulse pressure narrowed from 21 ± 8 mmHg at baseline to 11 ± 6 mmHg at 12000 rpm ($P=0.08$ vs baseline) (**Figure 6.3**). Mean CVP and PAP were not affected by variations in pump speed.

Table 6.1: Left and Right Heart Hemodynamic Measurements. Values are mean \pm SD. bpm indicates beats per minute; CO, cardiac output; CVP, central venous pressure; dP/dt, rate of change of LVP over time; HR, heart rate; LVEDP, left ventricular end-diastolic pressure; LVP, left ventricular systolic pressure; PCWP, pulmonary capillary wedge pressure. * $P<0.05$, † $P<0.01$, and ‡ $P<0.001$ vs baseline.

Pump speed, rpm						
	Pump off	8000	9000	10000	11000	12000
	(Baseline)					
HR, bpm	78 \pm 14	80 \pm 14	77 \pm 16	77 \pm 17	78 \pm 15	78 \pm 14
Aortic pressure, mmHg						
Systolic	80 \pm 9	83 \pm 7	84 \pm 9	84 \pm 9	85 \pm 9	85 \pm 9
Diastolic	61 \pm 12	65 \pm 8	70 \pm 10	72 \pm 9	74 \pm 12	74 \pm 13
Mean	71 \pm 9	74 \pm 8	76 \pm 10	77 \pm 9	77 \pm 11	77 \pm 13
LVP, mmHg	84 \pm 12	83 \pm 8	83 \pm 8	77 \pm 15	54 \pm 21†	42 \pm 22‡
LVEDP, mmHg	11 \pm 3	10 \pm 3	9 \pm 3	9 \pm 4	7 \pm 3*	6 \pm 5*
Maximal dP/dt	1488 \pm 638	1470 \pm 673	1372 \pm 693	1213 \pm 780	862 \pm 608	749 \pm 559*
PCWP, mmHg	12 \pm 2	11 \pm 4	11 \pm 4	10 \pm 4	9 \pm 4	8 \pm 5
CVP, mmHg	12 \pm 6	12 \pm 6	13 \pm 6	13 \pm 6	13 \pm 6	13 \pm 5
CO, L/min	7.1 \pm 0.9	6.7 \pm 1	6.3 \pm 1.1	6.3 \pm 1.2	6.3 \pm 2	6.7 \pm 1.6

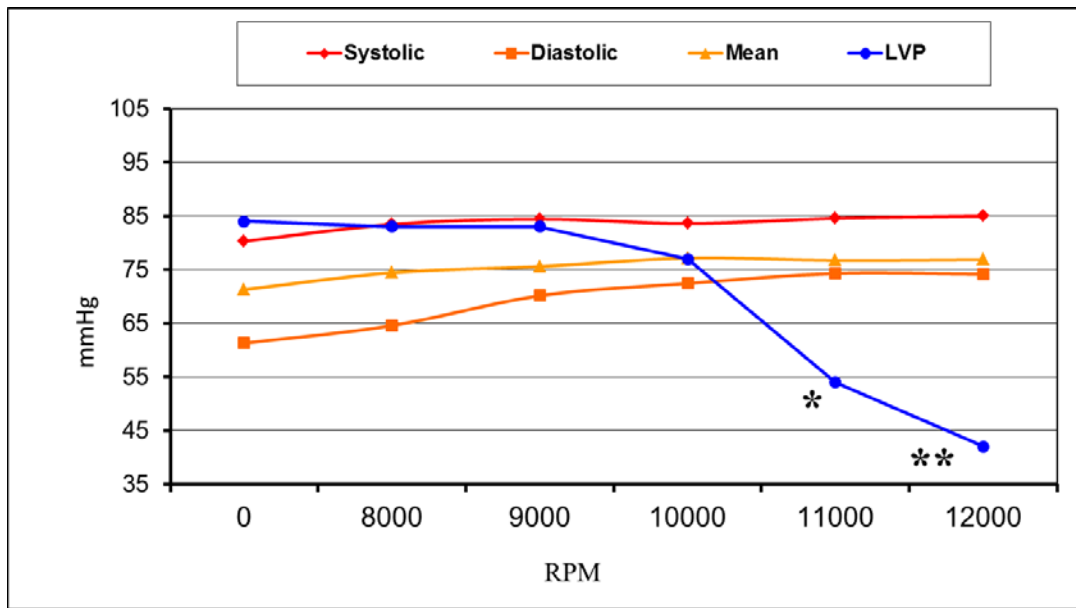


Figure 6.3: Peak aortic blood pressures and peak left ventricular pressure (LVP)

at fell sharply at 11000 rpm ($P < 0.01$ vs baseline). Depending on the extent of LV unloading, mean LVEDP and PCWP also decreased at speeds of 11000 and 12000 rpm ($P < 0.05$ for LVEDP and $P = 0.07$ for PCWP vs baseline) (**Figure 6.4**). The systolic pressure gradient between the left ventricle and the aorta (LVP – AoP) was 4 mmHg at baseline and decreased to -31 mmHg at 11000 rpm and -43 mmHg at 12000 rpm, in favor of systemic pressures.

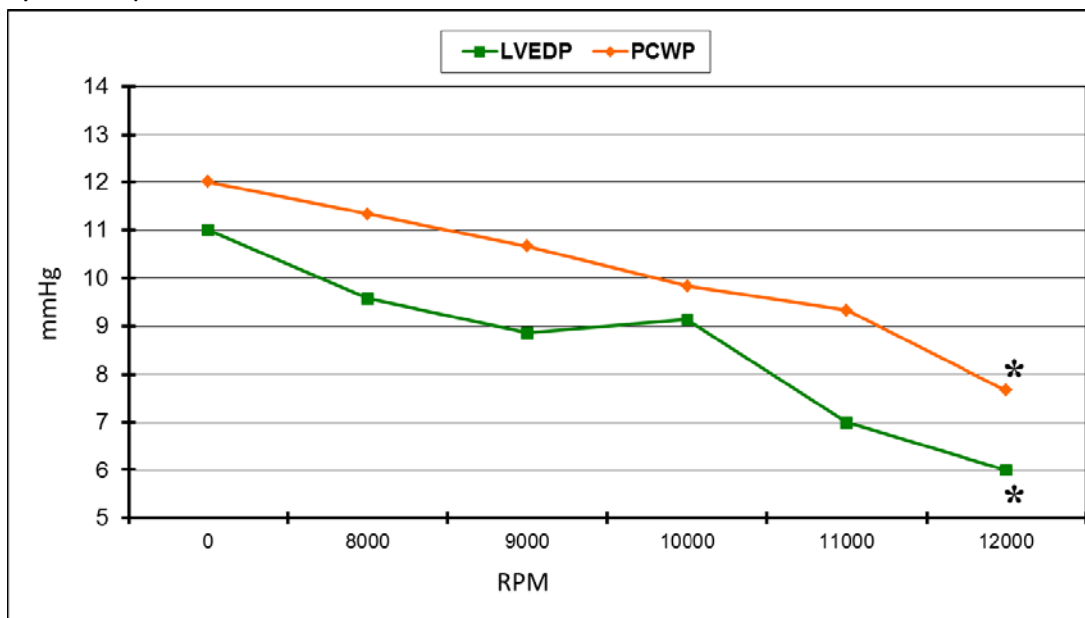


Figure 6.4: Left ventricular end-diastolic pressure (LVEDP) and pulmonary capillary wedge pressure (PCWP). * $P < 0.001$ vs baseline.)

graft clamped. After the pump was activated and the clamp released, mean pump flow gradually rose from 2.72 ± 0.33 L/min (contributing $34\% \pm 0.2\%$ of the cardiac

output) at 8000 rpm to 4.94 ± 0.77 L/min (contributing 73 ± 2 % of the cardiac output) at 12000 rpm ($P < 0.001$ for all speeds vs 8000 rpm) (**Figure 6.5**). On the other hand, the mean blood flow in the descending aorta dropped from 4.84 ± 1.7 L/min at baseline to 0.47 ± 1.83 L/min as soon as the pump began operating at 8000 rpm. At 8500 rpm, the blood flow reversed direction and began flowing from the graft anastomosis towards the aortic root at a rate of 0.55 ± 1.46 L/min. At higher pump speeds, this reversed flow gradually increased until it reached 1.56 ± 0.93 L/min at 12000 rpm ($P < 0.001$ for all speeds vs baseline). The mean brachiocephalic arterial blood flow did not vary with increasing pump speed.

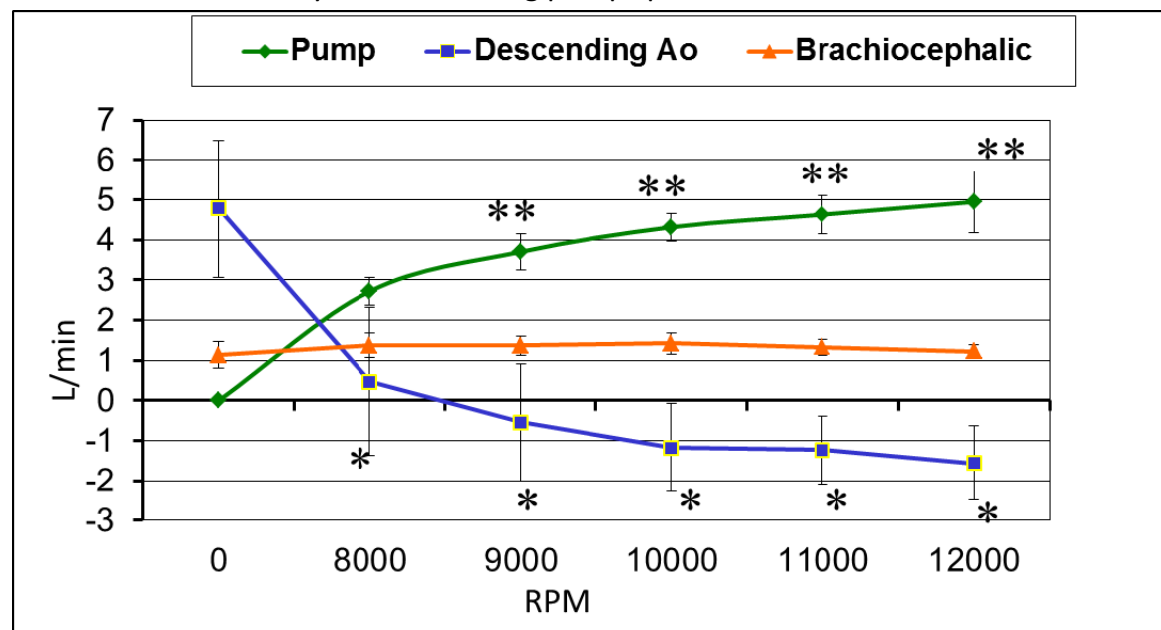


Figure 6.5: Blood flow in descending aorta, brachiocephalic artery, and pump outflow graft.

* $P < 0.001$ vs baseline; ** $P < 0.05$ vs 8000 rpm.pressure (PCWP). * $P < 0.001$ vs baseline.)

Mean CBF decreased slightly between 8000 and 10000 rpm, but then dropped significantly between 11000 and 12000 rpm ($P < 0.05$ and $P < 0.01$ vs baseline, respectively) (**Figure 6.6**). The fall in mean MVO₂ levels was consistent with and steeper than the fall in CBF, nearing statistical significance at 10000 and 11000 rpm ($P = 0.08$ and $P = 0.07$, respectively) and becoming highly significant at 12000 rpm ($P < 0.001$). Despite the decreasing CBF and MVO₂ levels at increasingly higher pump speeds, the baseline ratio of CBF to MVO₂ was well preserved at all speeds and remained between 0.19 and 0.22 throughout the study.

6.4.2 Echocardiographic Studies

Epicardial echocardiography confirmed the unloading effect of the Jarvik 2000 pump at increasingly higher speeds. At 12000 rpm, mean LVISd decreased from a baseline value of 35.1 ± 0.4 mm to 22.1 ± 2.6 mm, while mean LVIDd decreased from a baseline

value of 55.9 ± 2.8 mm to 29.5 ± 4.7 mm. Systolic and diastolic LV dimensions were significantly below baseline levels at all speeds ($P < 0.001$) (**Figure 6.7**). Aortic valve opening was impaired in 1 calf at 10000 rpm, in 2 calves at 11000 rpm, and in 4 calves at 12000 rpm. Septal and lateral wall motion was not affected by increasing pump speed, and right heart pressures remained close to baseline levels.

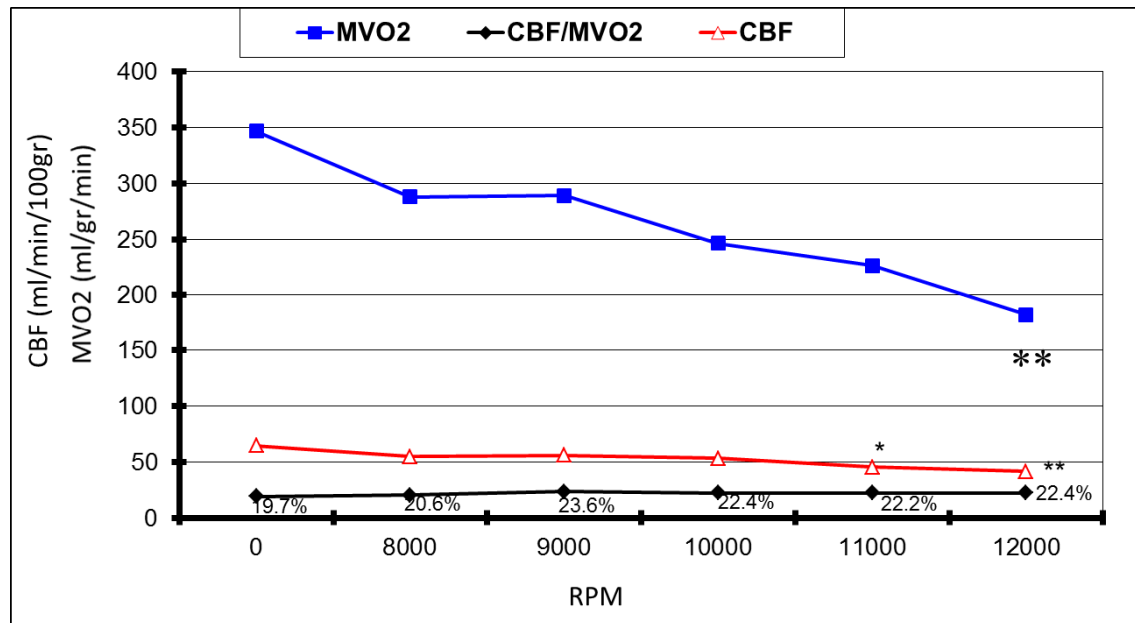


Figure 6.6: Coronary blood flow (CBF), myocardial oxygen consumption (MVO2), and CBF/MVO2 ratio. * $P < 0.05$ vs baseline; ** $P < 0.01$ vs baseline; ‡ $P < 0.001$ vs baseline.

6.4.3 Tissue Perfusion

At increasing pump speeds, blood flow in myocardial subregions (i.e., subendocardium and subepicardium) gradually decreased below baseline levels in all segments (septal, lateral, anterior, and posterior) (**Table 6.2**). Endocardial blood flow in the LV free wall, which was calculated as the sum of the anterior, lateral, and posterior endocardial blood flows, was significantly reduced below baseline at 10000 and 12000 rpm ($P < 0.05$ and $P < 0.01$, respectively). Similarly, epicardial blood flow in the LV free wall decreased at increasing pump speeds to levels that approached statistical significance at 10000 rpm ($P = 0.08$) and achieved statistical significance at 12000 rpm ($P < 0.05$). Interestingly, the subendocardial/subepicardial blood flow ratio in the LV wall, which was 1.17 ± 0.45 at baseline, remained relatively constant and unimpaired at all pump speeds (**Figure 6.8**).

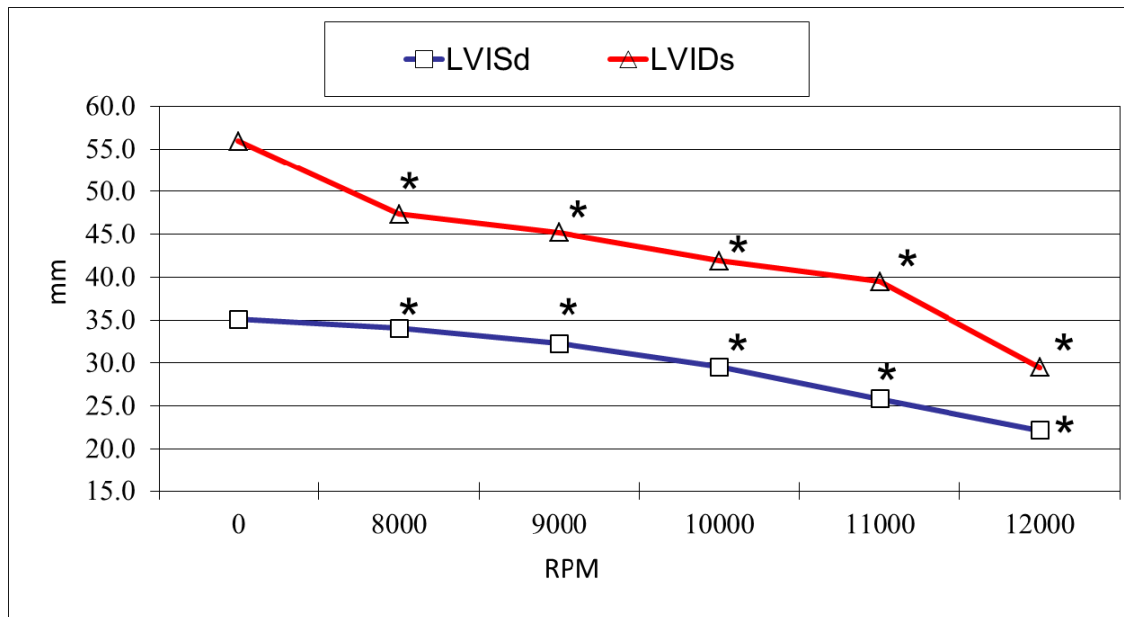


Figure 6.7: Left ventricular internal systolic dimension (LVISd) and diastolic dimension (LVIDd). * $P < 0.001$ vs baseline.

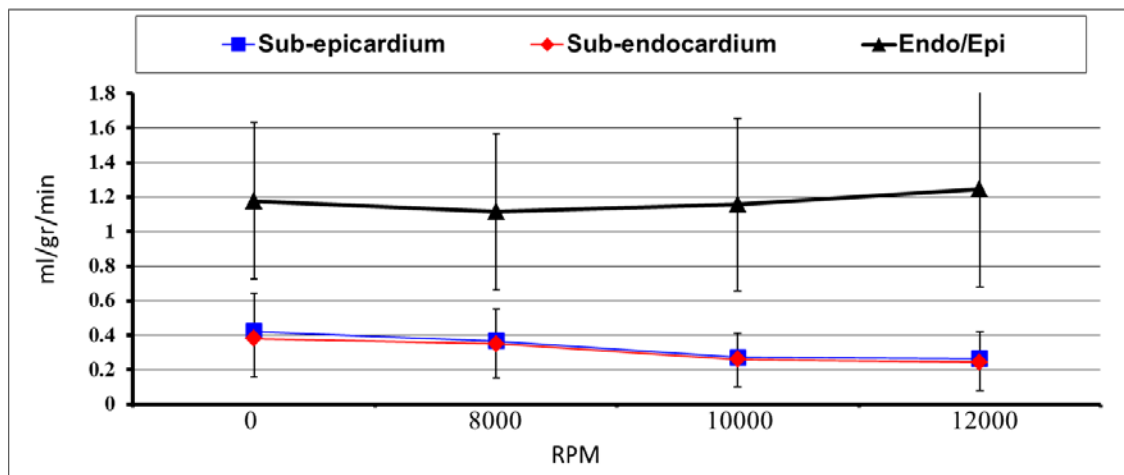


Figure 6.8: Tissue perfusion in subendocardium (Endo) and subepicardium (Epi) of left ventricular free wall.

Regional blood flow in the kidneys (cortex, subcortex, and papilla) and brain (cortex, corpus medullare, cerebellum, and medulla spinalis) also did not change significantly from baseline levels as pump speeds increased (**Table 6.3**).

Table 6.2: Myocardial Blood Flow Measurements

Pump speed, rpm				
	Pump off (Baseline)	8000	10000	12000
Septal wall				
Endocardium	0.46±0.18	0.39±0.20	0.30±0.17	0.27±0.16
Epicardium	0.38±0.19	0.36±0.20	0.34±0.18	0.28±0.15
Anterior wall				
Endocardium	0.48±0.26	0.39±0.20	0.30±0.16	0.29±0.21
Epicardium	0.38±0.23	0.35±0.23	0.25±0.16	0.25±0.15
Lateral wall				
Endocardium	0.43±0.22	0.36±0.20	0.29±0.17	0.26±0.15
Epicardium	0.39±0.29	0.34±0.19	0.28±0.18	0.23±0.20
Posterior wall				
Endocardium	0.36±0.19	0.34±0.17	0.23±0.06	0.24±0.11
Epicardium	0.37±0.17	0.37±0.21	0.27±0.15	0.22±0.15
Anterior wall + lateral wall + posterior wall				
Endocardium	0.42±0.22	0.36±0.18	0.27±0.13*	0.26±0.15†
Epicardium	0.38±0.22	0.35±0.20	0.26±0.15	0.24±0.16*

Values (mL/g/min) are mean±SD.

*P<0.05 and †P<0.01 vs baseline

Table 6.3: Tissue Perfusion Management

Pump speed, rpm				
	Pump (Baseline)	off8000	10000	12000
Kidney				
Cortex	1.8±0.7	1.5±1.2	1.7±1.4	1.6±0.8
Subcortex	1.0±0.6	0.8±0.6	0.8±0.8	0.9±0.8
Papilla	0.8±0.6	0.6±0.4	0.6±0.6	0.7±0.6
Brain				
Cortex	0.4±0.2	0.4±0.3	0.4±0.2	0.3±0.1
Corpus medullare	0.2±0.1	0.2±0.2	0.2±0.1	0.2±0.1
Cerebellum	0.4±0.3	0.4±0.4	0.4±0.3	0.3±0.1
Medulla spinalis	0.3±0.3	0.4±0.4	0.3±0.2	0.3±0.1

Values (mL/g/min) are mean±SD.

6.5 Discussion

In the present study, we observed that an increase in AoPd associated with a slight increase in AoPs and AoPm led to a narrowing of pulse pressure with increasing pump speed. This effect, which was related to the increasingly predominant continuous flow characteristics associated with progressively reduced native cardiac pulsatility (LV unloading), was more pronounced at speeds above 10000 rpm, consistent with previous experimental and clinical studies.³ One cause of the increase in AoPd was the reversal of blood flow direction, which occurred at speeds greater than 8500 rpm (Figure 5); when combined with extensive LV unloading, this reversal helped impair aortic valve opening at higher speeds (>10000 rpm). We also observed that the resulting reduction of systolic ejection caused blood to stagnate in the supra-avalvular regions, leading to diminished myocardial perfusion via the epicardial arteries. Moreover, we observed that the aortic valve stayed closed more frequently in hypovolemic calves, a problem that we found could be alleviated by fluid replacement at increasingly higher pump speeds. This observation agrees with that of Westaby et al., who found that transfusion lessened the effects of left atrial

collapse caused by extensive unloading of the left ventricle at high pump speeds [169]. Thus, achieving optimal LV filling and operating the pump at submaximal speeds appear to be essential to preserving normal aortic valve function and pulsatile blood flow. In addition, preserving normal aortic valve motion may produce the added benefit of washing out the aortic root and thus preventing thrombosis of the valve, coronary arteries, or both during pump support, as previously described by Frazier et al. [28] Several investigators have pointed out that partial unloading of the left ventricle may be more effective than total unloading [71,80], which is recommended for achieving ventricular recovery [41] but can cause myocyte atrophy during long-term support [62,125].

Continuous removal of LV blood (LV unloading) with an LVAD can decrease myocardial workload [40]. The gradual decrease in dP/dt at increasing pump assist rate may be attributed to delayed LV relaxation which is consistent with Saito et al. [121] findings. In our study, the gradual decrease in CBF and MVO₂ at increasing pump speeds seemed to be related to effective unloading of the left ventricle and reduced energy demand by the healthy myocardium secondary to decreased LV wall tension, as previously shown in several studies [8,25,32,82,132]. Moreover, the CBF/MVO₂ ratio remained almost constant at increasing pump speeds, indicating that the decreases in CBF and MVO₂ were proportional to the decreased workload of the unloaded left ventricle and did not impair LV wall function or cause iatrogenic ischemia, as confirmed by intraoperative echocardiography. Similar findings by others support these observations. In a model of ischemia produced by LAD coronary artery ligation, Nakata et al. [93] showed that LVAD support restored LAD coronary artery flow by decreasing coronary vascular resistance secondary to reduced LVEDP. In experimental studies with an axial flow pump, Merhige et al. [84] and Smalling et al. [140] showed that coronary perfusion of the non-ischemic myocardium decreased while that of the ischemic myocardium increased following ventricular unloading. Consistent with the decrease we observed in CBF was the gradual reduction of regional blood flow to the left ventricle at increasing pump speeds that we detected by colored microsphere analysis. In addition, the constant endocardial/epicardial blood flow ratio in the LV free wall, even in reduced pulsatile aortic flow states achieved at pump speeds above 10000 rpm, showed that the Jarvik 2000 pump did not adversely affect the autoregulation and transmural distribution of CBF in the normal myocardium.

Little is known about the effects of non-pulsatile blood flow on cerebral microcirculation. Significant differences in intracerebral perfusion during both pulsatile and non-pulsatile states in models of ischemia have been described [64,129]. We found that different regions of the central nervous system (and the kidney) were equally perfused at baseline (during a pulsatile state) and at higher

pump speeds (during a diminished or absent pulsatile state). Therefore, continuous flow did not appear to cause any microcirculatory shunting during end-organ perfusion in our study. This echoes the findings of Saito et al. [122] who found no functional or histologic changes in major end organs during chronic support with a non-pulsatile LVAD.

The present study has some limitations. First, Jarvik 2000 is designed to be used in end-stage cardiac failure. Therefore our results may not be directly applicable to the clinical situation and it may be beneficial to plan an ischemic model to clarify the microcirculatory effects of Jarvik 2000 on diseased myocardium. Second, this is an acute experiment and long-term effects of continuous flow to the myocardial microcirculation cannot be studied with this data due to body's autoregulation mechanisms. Third, it's not possible to quantify and standardize the effect of anesthesia and surgical trauma during pump implantation although the baseline hemodynamic values of the animals are within normal values. And finally, further studies are needed to study effect of the anastomose site of the outflow graft (ascending or descending aorta) to aortic and myocardial blood flow properties.

6.6 Conclusion

Our data suggests that the Jarvik 2000 pump may effectively unload the left ventricle and decrease MVO₂ secondary to reduced wall tension. Although the CBF decreases at increasing pump speeds as a result of reduced cardiac work, the CBF/MVO₂ ratio remains constant and does not impair normal LV function. Optimal adjustment of pump speed and LV volume allows the aortic valve to open and the native left ventricle to contribute to cardiac output even at maximum pump speed. Finally, brain and kidney microcirculation is not adversely affected at any pump speed.

Effect of Pump-Flow Mode of Novel Left Ventricular Assist Device on End-Organ Perfusion in Dogs with Doxorubicin-Induced Heart Failure

The contents of this chapter are based on: Eya K, Tuzun E, Conger JL, Chee HK, Byler D, Nojiri C, Frazier OH, Kadipasaoglu KA. Effect of Pump-Flow Mode of Novel Left Ventricular Assist Device on End-Organ Perfusion in Dogs with Doxorubicin-Induced Heart Failure. *ASAIO Journal* 2005; 51:41–49.

7.1 Abstract

Background: End-organ effects of nonpulsatile (NP) and pulsatile (P) left ventricular assist device (LVAD) flow were compared in a canine model of doxorubicin-induced heart failure.

Materials and Methods: After heart failure induction, a prototype bimodal LVAD was implanted. Hemodynamics, cardiac dimensions, and myocardial metabolism were monitored with the LVAD off (baseline) and on (in NP and P modes at 70% or 100% power). End-organ perfusion was assessed by colored microsphere analysis.

Results: Seven dogs were used: 2 died before pump implantation and were excluded from analysis; the remaining 5 survived to study termination. At 70%NP, ascending aortic flow and myocardial oxygen consumption (MVO₂) decreased significantly. At 100%NP, LV dimensions decreased; aortic systolic, pulse, and LV pressures decreased but not significantly; and ascending aorta flow reversed. At 100%NP, coronary blood flow, MVO₂, and LV free wall subepicardial and subendocardial blood flows decreased significantly. However, as NP support increased, the subepicardial/subendocardial blood flow ratio remained near baseline. At 100%NP, right ventricular perfusion decreased but not significantly, cerebral perfusion decreased significantly, and renal perfusion stayed constant. P-mode results were similar, except that ascending aorta flow decreased significantly at 100%P instead of reversing as at 100%NP.

Conclusion: These results suggest that end-organ perfusion is not differentially affected by LVAD flow mode during chronic heart failure

7.2 Introduction

Mechanical circulatory support (MCS) devices have been used successfully as bridges to transplantation [33], as bridges to myocardial recovery [32], and as permanent circulatory support [31] in patients with end-stage heart failure. These devices can be classified into 2 general categories according to the type of flow they generate: pulsatile (P) or nonpulsatile (NP). Several experimental studies have investigated the short- and long-term effects of flow mode on the microcirculation, metabolism, and physiology of end-organs (i.e., the heart, brain, kidney, and liver) [6,84,85,122], although these studies have usually been performed in healthy or acutely failing hearts. To our knowledge, no study has yet evaluated the effect of MCS flow mode on end-organs in an appropriate model of chronic dilated cardiomyopathy. In the present study, we assessed the short-term effects of P versus NP flow from a prototype left ventricular assist device (LVAD) on the microcirculation, metabolism,

and function of major end-organs including the heart in a canine model of doxorubicin-induced chronic dilated cardiomyopathy.

7.3 Materials and Methods

7.3.1 Animals

Experiments were conducted on mongrel dogs (n=7), each weighing 35–40 kg. All dogs received humane care in compliance with the Principles of Laboratory Animal Care (National Society of Medical Research) and the Guide for the Care and Use of Laboratory Animals (National Institutes of Health publication no. 85-23, revised 1996). Our institution's Animal Care and Use Committee approved all protocols used in this study.

7.3.2 Heart Failure Model

Heart failure was induced as follows. Each dog was premedicated with acepromazine and oxymorphone, placed in a supine position, and intubated for mechanical ventilation. Anesthesia was induced and maintained with isoflurane. The right femoral artery was punctured and threaded with a 6F Judkins catheter. The catheter was then advanced under fluoroscopic guidance into the left main coronary artery. Serial ventriculography and 2-dimensional echocardiography were used to evaluate left ventricular (LV) end-systolic dimension (LVSD), LV end-diastolic dimension (LVDd), and fractional shortening (FS). Doxorubicin (Adriamycin) (0.7 mg/kg) was infused rapidly into the coronary artery through the catheter. This infusion was repeated weekly for 5 consecutive weeks. Hemodynamic status was evaluated periodically. After the last infusion of doxorubicin, each dog was kept in a dedicated animal care facility for 1 week.

7.3.3 Pump Description

A prototype pump (DuraHeart; Terumo, Inc., Minneapolis, MN) was used to provide MCS. The prototype pump and its controller were customized for this particular animal experiment at our institution's request. The pump is a sterile, titanium centrifugal device containing a magnetically suspended impeller. The customized controller has two sets of analog circuitry, one for magnetic levitation of the impeller and the other for control of the motor's rotational speed. For this particular study, we utilized a laptop personal computer to control the rotational speed (revolutions per minute, or rpm) in either nonpulsatile (NP) or pulsatile (P) mode.

Pulsatile flow was based on changes in motor speed (sine wave) at a given frequency. In P mode, mean rotational speed, amplitude of pulsatility, and pulse rate can be programmed via the external personal computer to create a pulsatile flow. In this study, we programmed the computer to produce P flow at a mean rotational speed of ± 300 rpm (amplitude, 600 rpm) and a pulse rate of 80 beats per minute (bpm). The pump was operated in each mode at 70% and 100% of maximum power (70NP, 100NP, 70P, and 100P, respectively).

7.3.4 Pump Implantation

Each dog was premedicated and anesthetized as described above and then positioned for left thoracotomy. A Swan-Ganz pulmonary arterial catheter and an arterial cannula were introduced into the left jugular vein and the left common carotid artery, respectively. The chest was entered through the fifth intercostal space, the pericardium was opened, and a 3-mm perivascular ultrasonic flow probe (Transonic Systems, Ithaca, NY) was placed around the left anterior descending (LAD) coronary artery. After intravenous injection of heparin (1 mg/kg), the pump outlet graft was anastomosed end-to-side to the descending thoracic aorta, and a sewing cuff for the pump inlet was sutured around the LV apex. During pump inlet insertion, myocardial tissue samples were harvested from the LV apex with a coring knife and sent for histopathological examination. The pump was then implanted, and air was thoroughly evacuated from the system. A 16-mm ultrasonic flow probe was placed around the ascending aorta, and a 12-mm probe around the outlet graft. A microtip pressure catheter (Millar PC 500; Millar Instruments, Inc, Houston, TX) was advanced into the left ventricle through the left femoral artery. An 8-Fr Swan-Ganz catheter was inserted into the pulmonary artery via the left external jugular vein.

7.3.5 Hemodynamic Assessment

After pump implantation, hemodynamics were allowed to stabilize for 30 minutes. Hemodynamics were assessed with the pump off and the outflow graft clamped to avoid pump regurgitation (baseline) and with the pump operating at the 4 experimental settings described above (70NP, 100NP, 70P, and 100P) for 30 minutes at each setting. After each change to a new pump setting, hemodynamics were allowed to stabilize for 10 minutes before collecting hemodynamic data. Heart rate (HR), aortic systolic pressure (AoPs), aortic diastolic pressure (AoPd), mean aortic pressure (AoPm), LV systolic pressure (LVP), LV end-diastolic pressure (LVEDP), mean pulmonary artery pressure (PAP), central venous pressure (CVP), and cardiac output

(CO) were measured at each setting. Data from 10-20 consecutive beats were averaged and used to derive steady-state parameters.

7.3.6 Echocardiographic Assessment

Serial 2-dimensional transepical studies were performed at each pump setting. Echocardiographic assessment was accomplished using a Hewlett Packard Sonos 2000 ultrasound system equipped with a 2.5-MHz phased-array transducer, according to the guidelines of the American Society of Echocardiography [48]. The echocardiogram was used to measure systolic and diastolic LV internal dimensions (LVDs and LVDd); LV, RV, and septal wall motion; and aortic valve motion.

7.3.7 Myocardial Oxygen Consumption Assessment

An 18-gauge angiocatheter was inserted into the coronary sinus to take blood samples at baseline and each experimental setting. These samples were used to assess myocardial oxygen consumption (MVO₂), calculated as $MVO_2 = CBF \cdot [\bar{a} - \bar{v}]$, where \bar{a} and \bar{v} are aortic and coronary sinus blood oxygen content, respectively, and CBF is the left anterior descending (LAD) coronary artery blood flow rate. A Novastat Profile M blood gas analyzer (Nova Biomedical Co., Waltham, MA) was used for blood gas analysis.

7.3.8 Regional Blood Flow Distribution Assessment

Regional blood flow distribution to end organs of interest (heart, brain, and kidney) was evaluated by microsphere analysis using 15- μ m, nonradioactive, stable isotope-labeled microspheres (BioPAL, Worcester, MA), as described in detail elsewhere [135,165]. The microspheres were injected into the left atrium (LA) immediately before pump implantation (baseline) and 10 minutes after pump operation at each experimental setting (70NP, 100NP, 70P, and 100P). Microspheres labeled with samarium appeared black; gold, red; iridium, yellow; lutetium, pink; rhenium, orange; and antimony, violet. Each labeled microsphere was used at a different pump setting. Arterial reference blood samples were taken from the left common carotid artery after LA injections and used to normalize tissue sample readings.

A neutron activation technique was used to detect microspheres in tissue samples. Neutron activation is capable of detecting a single microsphere in an intact myocardial sample while providing simultaneous quantitative measurements of multiple isotope labels. This high sensitivity and capability for measuring perfusion in intact tissue are advantages over other techniques, such as optical detection of

microspheres. Neutron activation is also an effective technique for reducing the production of low-level radioactive waste generated during biomedical research. The principle involved in neutron activation analysis consists of first irradiating a sample with neutrons in a nuclear reactor to produce specific radionuclides. After the irradiation, the characteristic gamma rays emitted by the decaying radionuclides are quantitatively measured by gamma spectroscopy, where the gamma rays detected at a particular energy are indicative of a specific radionuclide's presence. Data reduction of gamma ray spectra then yields the concentrations of various elements in the samples being studied [109].

At study termination, dogs were euthanized with an intravenous bolus of potassium chloride while still under general anesthesia. The heart, brain, and kidney were then harvested for further analysis of regional blood flow. In the case of the heart, both ventricles were isolated, and both were divided into 4 equal transverse sections along the atrioventricular groove. Basal and apical sections were discarded. The more distal of the remaining 2 sections was selected. The LV section was then divided into 2 segments representative of the anterolateral and posterior walls. Then, each segment was further subdivided into an epicardial and an endocardial subregion. Two grams of tissue were taken from each region (a total of 4 tissue samples) for microsphere analysis. RV blood flow was assessed in 3 total-thickness tissue samples weighing 2 g each.

The left hemisphere of the brain was divided into 3 equal parts posteroanteriorly, and the middle sections were harvested for microsphere analysis. Two grams of tissue were taken from the cortex and corpus medullare (a total of 2 samples) for microsphere analysis.

The left kidney was divided into 3 frontal sections, and the middle section was divided into cortical and medullar subregions. Two grams of tissue were taken from each subregion (a total of 2 kidney tissue samples) for microsphere analysis.

All tissue samples were dried overnight at 70°C and sent out for analysis.

7.3.9 Statistical Analysis

All statistical tests were performed using Microsoft Excel software on a personal computer. A single-tailed Student t-test or analysis of variance (ANOVA) was used to compare continuous variables. $P < 0.05$ was considered significant.

7.4 Results

7.4.1 Procedural Success

Five of 7 dogs underwent successful pump implantation, experienced no surgical complications or mechanical (device) failures, and survived to study termination. Two dogs experienced complications and died before study termination: one died of an air embolus in the coronary artery during the second doxorubicin infusion; the other died of ventricular fibrillation intraoperatively during pump implantation.

7.4.2 Heart Failure Induction

Comparison of echocardiographic and hemodynamic data recorded before the first intracoronary doxorubicin injection and immediately before pump implantation confirmed the efficacy of the heart failure induction protocol (**Table 7.1**). There was a statistically significant increase in LVDs and LVDd (from 21.9 ± 1.4 mm to 31.5 ± 2.6 mm and from 34 ± 2.0 mm to 40.4 ± 3.0 mm, respectively; $P < 0.05$) and a decline in fractional shortening (FS) (from $35.5 \pm 1.5\%$ to $22.0 \pm 2.3\%$; $P < 0.05$). Right ventricular dimensions and function were normal and remained close to baseline levels. Heart rate and LVEDP significantly increased (from 99 ± 3 bpm to 115 ± 10 bpm and from 6.4 ± 1.8 mmHg to 13.6 ± 2.1 mmHg, respectively; $P < 0.05$).

Table 7.1 Echocardiographic and Hemodynamic Measurements Before and After Heart Failure Induction by Doxorubicin Infusion

	Before (Baseline)	First Infusion	After Last Infusion (Before Pump Implantation)	<i>P</i>
LVDs (mm)	21.9 ± 1.4		31.5 ± 2.6	0.05
LVDd (mm)	34 ± 2.0		40.4 ± 3.0	0.05
FS (%)	35.5 ± 1.5		22.0 ± 2.3	0.05
HR (bpm)	99 ± 3		115 ± 10	0.05
LVEDP(mmHg)	6.4 ± 1.8		13.6 ± 2.1	0.05
dp/dt(mmHg/sec)	2355 ± 95		2485 ± 238	NS
PAP (mmHg)	24.6 ± 1.5		23.2 ± 0.8	NS
CVP (mmHg)	4.6 ± 0.9		5.2 ± 0.8	NS
CO (L/min)	4.49 ± 0.45		4.17 ± 0.7	NS

Values shown are mean \pm SD. CO, cardiac output; CVP, central venous pressure; dp/dt, rate of change in left ventricular pressure over time; FS, fractional shortening; HR, heart rate; LVDd, left ventricular end-diastolic dimension; LVDs, left ventricular end-systolic dimension; NS, not significant; PAP, pulmonary artery pressure.

Electron microscopic evaluation of myocardial tissue showed degenerative changes including loss of myofibrils and cytoplasmic vacuolization, as well as atypical myocyte arrangement without signs of disarray (**Figure 7.1**).

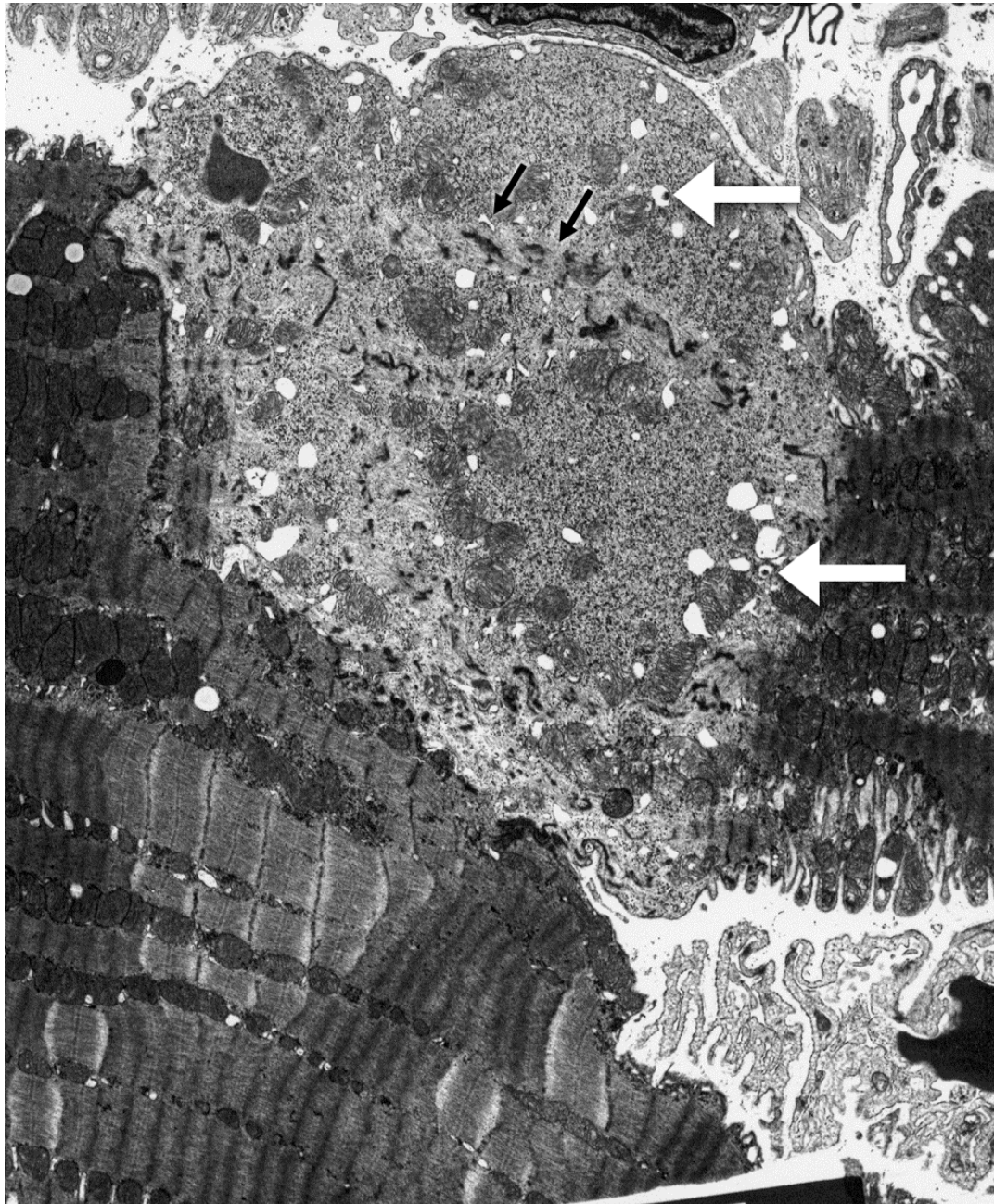


Figure 7.1: Electron micrograph showing degeneration of isolated cardiac myocytes 4 weeks after fifth and final doxorubicin infusion. Signs of degeneration include myofibril loss, intracytoplasmic vacuoles (some containing membrane whorls) (black arrows), and Z-band widening and splitting (white arrows). Magnification = 2500 \times .

Hemodynamic data are summarized in **Table 7.2**.

Table 7.2 Echocardiographic, Hemodynamic, and Perfusion Data During Pump Support

	Pump Setting (% Support)				
	Pump Off	70NP	100NP	70P	100P
LVDs (mm)	31.5 ± 2.6	22.7 ± 3.6*	20.8 ± 6.5*	23.2 ± 5.1*	20.2 ± 5.3*
LVDd (mm)	40.4 ± 3.0	31.3 ± 2.9*	25.8 ± 6.7*	31.8 ± 4.2*	26.2 ± 4.9*
FS (%)	22.0 ± 2.3	27.8 ± 5.6	20.5 ± 4.9	27.56 ± 8.5	23.4 ± 6.7
HR (bpm)	115 ± 10	108 ± 14	108 ± 13	109 ± 4	109 ± 17
Aortic pressure (mm Hg)					
Systolic	98 ± 11	90 ± 8	75 ± 9*	86 ± 10	78 ± 15*
Diastolic	57 ± 8	64 ± 6	65 ± 8	61 ± 6	55 ± 9
Mean	69 ± 8	73 ± 7	69 ± 9	70 ± 7	64 ± 10
Pulse pressure (mm Hg)	41 ± 16	27 ± 6	10 ± 5*	27 ± 10	21 ± 14
LVP (mm Hg)	94 ± 8	85 ± 10	54 ± 18*	82 ± 11	52 ± 12*
dp/dt _{max} (mm Hg/sec)	2,485 ± 238	2,281 ± 329	1,576 ± 285*	2,293 ± 115	1,531 ± 410*
LVEDP (mm Hg)	13.6 ± 2.1	12 ± 2.7	11.8 ± 2.6	12.2 ± 2.4	11.8 ± 2.2
CO (L/min)	4.17 ± 0.7	3.85 ± 0.7	3.80 ± 0.4	4.10 ± 0.2	3.71 ± 0.4
Pump flow (L/min)	0	2.23 ± 0.36	3.37 ± 0.43**	2.31 ± 0.14	3.47 ± 0.38**
Asc Ao flow (L/min)	3.44 ± 0.3	0.98 ± 0.16*	-0.14 ± 0.3*	0.94 ± 0.11*	-0.24 ± 0.33*
CBF (mL/min)	64 ± 9	51 ± 9	41 ± 12*	56 ± 7.1	44 ± 11*
MVO ₂	317 ± 51	221 ± 69*	153 ± 31*	224 ± 25*	137 ± 45*
CBF/MVO ₂	0.21 ± 0.04	0.24 ± 0.06	0.27 ± 0.05	0.25 ± 0.03	0.33 ± 0.07*
PAP (mm Hg)	23.2 ± 0.8	23.1 ± 0.6	22.4 ± 0.6	22.9 ± 0.6	22.6 ± 0.5
CVP (mm Hg)	5.2 ± 0.8	5.0 ± 0.6	5.3 ± 0.4	5.1 ± 0.7	5.2 ± 0.7

Values are mean ± SD. Asc Ao, ascending aorta; CBF, coronary blood flow; CO, cardiac output; CVP, central venous pressure; dp/dt, rate of change of left ventricular pressure over time; FS, fractional shortening; HR, heart rate; LVDd indicates left ventricular end-diastolic dimension; LVDs, left ventricular end systolic dimension; LVEDP, left ventricle end diastolic pressure; LVP, left ventricle systolic pressure; MVO₂, myocardial oxygen consumption; NP, nonpulsatile; P, pulsatile; PAP, pulmonary artery pressure.

* $p < 0.05$ vs. pump off.

** $p < 0.05$ vs. 70 NP or 70 P.

The interaction between CO, pump flow, and ascending aortic flow is shown in **Figure 7.2**. Changes in CBF and MVO₂ are shown in **Figure 7.3**.

At 70NP, no statistically significant changes were observed in aortic pressures, pulse pressure, LVP, dp/dt_{max}, LVEDP, or CO. The mean pump flow was 2.23±0.36 L/min. The mean contribution of the pump to CO was 54±11%. Compared with baseline (pump-off) values, ascending aortic flow and MVO₂ decreased significantly ($P<0.05$); CBF also decreased but not significantly. The CBF/MVO₂ ratio was not affected. PAP and CVP remained close to baseline levels.

At 100NP, mean AoPs declined progressively from baseline levels (from 98±11 mmHg to 75±9 mmHg; $P<0.05$). Mean AoPd and AoPm also decreased, although the declines were less pronounced and were not statistically significant. Mean aortic pulse pressure decreased significantly from 41±16 mmHg to 10±5 mmHg ($P<0.05$), as did LVP and dp/dt_{max} ($P<0.05$).

Mean LVEDP and CO values slightly decreased but not significantly. Mean pump flow rose gradually from 2.23±0.36 L/min to 3.37± 0.43 L/min ($P<0.05$, vs 70NP). The mean contribution of the pump to CO at 100 NP was 86%±6%. The mean blood flow in the ascending aorta dropped significantly from 3.44±0.3 L/min to -0.14±0.3 L/min ($P<0.05$, vs pump-off) and reversed direction toward the aortic valve. Mean CBF decreased from 64±9 mL/min to 41±12 mL/min ($P<0.05$, vs pump-off). The reduction

in mean MVO₂ levels (from 317±51 mL/min/kg to 153±31 mL/min/kg) was consistent with the fall in CBF ($P<0.05$, vs pump-off). The ratio of CBF to MVO₂ was well preserved at 100NP. PAP and CVP remained near baseline (pump-off) levels.

At 70P, aortic pressures remained close to baseline (pump-off) values and pulse pressure slightly decreased. LVP, dp/dt_{max}, LVEDP, CO, and pump flow measurements did not change significantly. The mean contribution of the pump to CO was 56±6%. The mean blood flow in the ascending aorta diminished from 3.44±0.3 L/min to 0.94±0.11 L/min ($P<0.05$, vs pump-off). The mean CBF decreased slightly, while the mean MVO₂ significantly decreased from 317±51 mL/min/kg to 224±25 mL/min/kg ($P<0.05$, vs pump-off). Nevertheless, the CBF/MVO₂ ratio was not adversely affected. Again, PAP and CVP remained near baseline (pump-off) levels.

At 100P, mean AoPs decreased significantly (from 98±11 mmHg to 78±15 mmHg; $P<0.05$, vs pump-off). Mean AoPd and AoPm also decreased, but not significantly. Unlike at 100NP, pulse pressure did not significantly decrease at 100P. Mean LVP and dp/dt_{max} both decreased significantly from baseline levels (from 94±8 mmHg to 52±12 mmHg and from 2485±238 mmHg/sec to 1531±410 mmHg/sec, respectively; $P<0.05$). Mean pump flow increased significantly from 2.31±0.14 L/min to 3.47±0.38 L/min ($P<0.05$, vs 70P). The mean contribution of the pump to CO was 93%±1%. Blood flow in the ascending aorta reversed direction toward the aortic valve at a rate of -0.24±0.33 L/min ($P<0.05$, vs pump-off). CBF and MVO₂ decreased sharply (from 64±9 mL/min to 44±11 mL/min and from 317±51 mL/min/kg to 137±45 mL/min/kg, respectively; $P<0.05$). Although mean CBF and MVO₂ both decreased gradually, the CBF/MVO₂ ratio significantly increased (from 0.21±0.04 to 0.33±0.07; $P<0.05$, vs pump-off). Again, PAP and CVP remained near baseline (pump-off) levels.

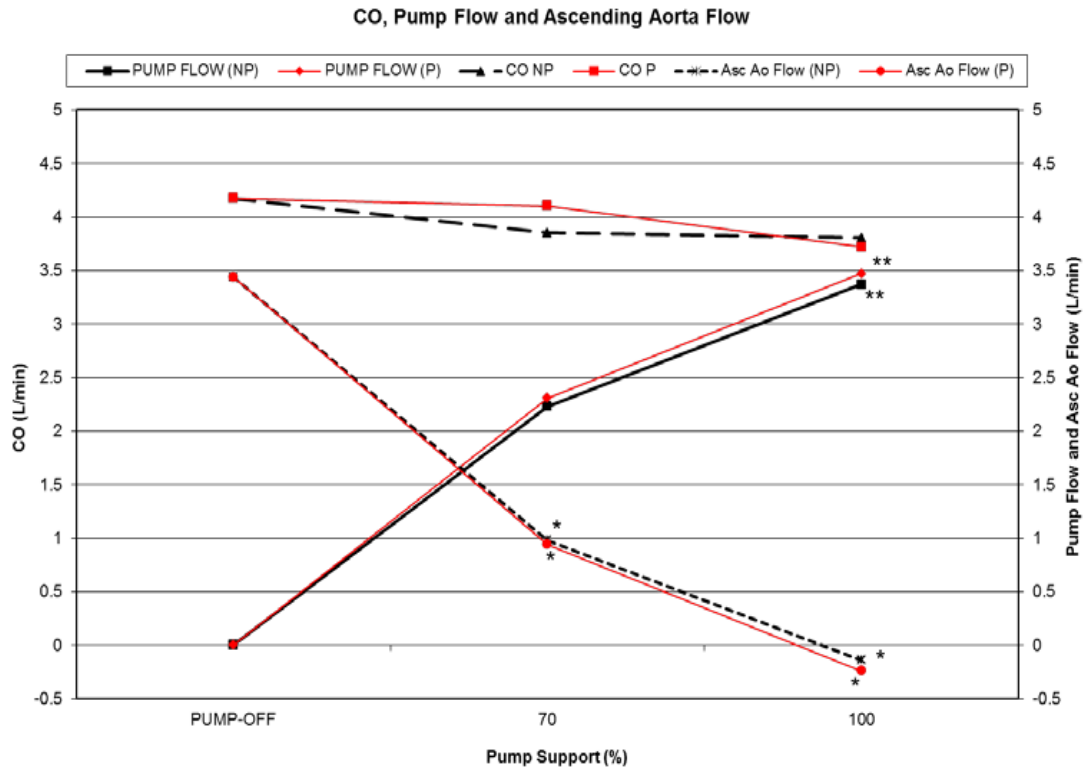


Figure 7.2: Cardiac output (CO), pump flow, and ascending aorta flow (Asc Ao Flow) during pump support. NP, nonpulsatile; P, pulsatile. * $P < 0.05$, vs pump-off; ** $P < 0.05$, vs 70NP or 70P.

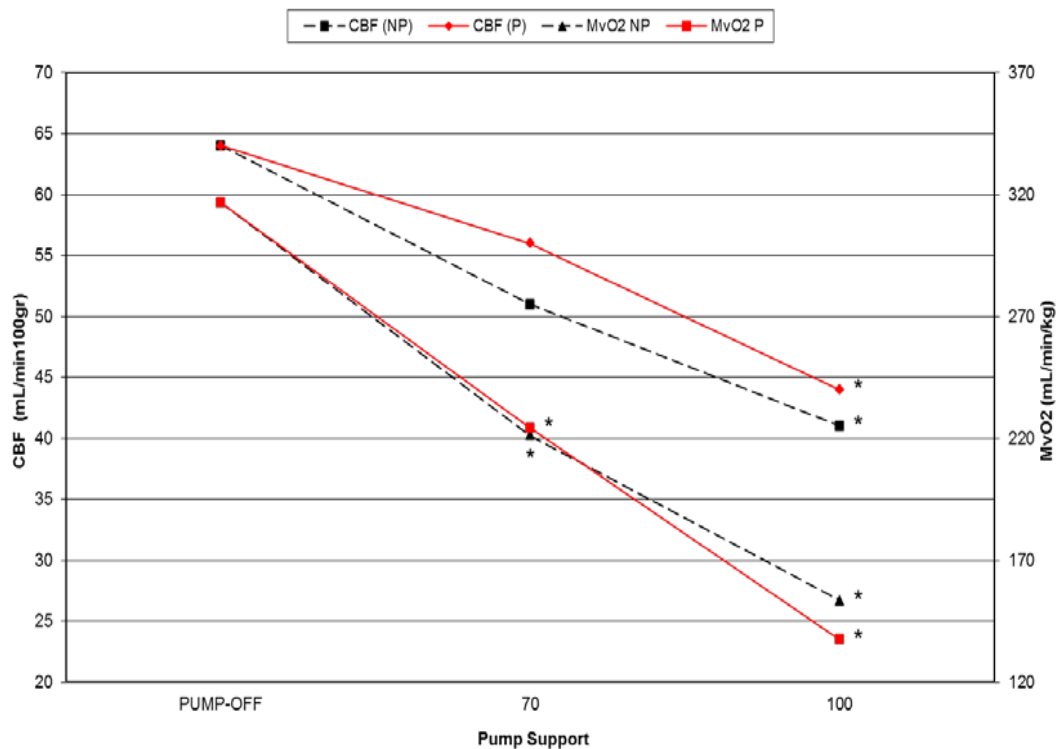


Figure 7.3: Coronary blood flow (CBF) and myocardial oxygen consumption (MVO2) during pump support. NP, nonpulsatile; P, pulsatile. * $P < 0.05$, vs pump-off.

At 70NP, LVDs and LVDd were significantly reduced compared to the pump-off values (Table 2; $P < 0.05$, for both). At 100NP, LVDs and LVDd further decreased (Table 2; $P < 0.05$, vs pump-off). Similarly, at 70P, LVDs and LVDd significantly decreased (Table 2; $P < 0.05$, vs pump-off). At 100P, LVDs and LVDd decreased even further ($P < 0.05$, vs pump-off). When compared with baseline values, FS, RV dimensions, and wall motion did not change at any experimental setting.

7.4.5 Microsphere Analysis of End-Organ Perfusion

The results of microsphere analysis of end-organ perfusion are summarized in **Table 7.3**.

Table 7.3 End-organ Perfusion

	Pump Setting (% Support)				
	Pump Off	70NP	100NP	70P	100P
Left ventricle					
Anterolateral wall					
Epicardium	1.3 ± 0.5	0.9 ± 0.3	$0.4 \pm 0.2^*$	0.8 ± 0.1	$0.5 \pm 0.1^*$
Endocardium	1.4 ± 0.8	1.1 ± 0.2	$0.5 \pm 0.2^*$	0.9 ± 0.2	$0.5 \pm 0.3^*$
Posterior wall					
Epicardium	1.3 ± 0.7	1.0 ± 0.3	$0.5 \pm 0.2^*$	0.9 ± 0.2	0.5 ± 0.2
Endocardium	1.6 ± 0.9	1.2 ± 0.3	0.5 ± 0.3	1.0 ± 0.2	0.6 ± 0.4
Free wall					
Epicardium	1.2 ± 0.6	0.9 ± 0.6	$0.4 \pm 0.2^*$	0.8 ± 0.1	$0.5 \pm 0.2^*$
Endocardium	1.5 ± 0.8	1.1 ± 0.2	$0.5 \pm 0.2^*$	1.0 ± 0.2	$0.6 \pm 0.3^*$
Right ventricle	0.9 ± 0.4	0.8 ± 0.3	0.4 ± 0.2	0.7 ± 0.1	0.5 ± 0.2
Brain					
Cortex	0.4 ± 0.2	0.4 ± 0.1	$0.3 \pm 0.1^*$	0.4 ± 0.1	0.3 ± 0.1
Medulla	0.3 ± 0.1	0.3 ± 0.1	0.2 ± 0.1	0.3 ± 0.1	0.2 ± 0.1
Kidney					
Cortex	5.0 ± 1.8	4.8 ± 2.6	2.9 ± 1.3	4.5 ± 2.2	3.4 ± 1.8
Medulla	6.9 ± 3.1	5.7 ± 0.4	3.9 ± 1.9	5.7 ± 1.5	4.2 ± 2.3

Values (mL/min/g) are mean \pm SD. NP, nonpulsatile; P, pulsatile.

* $p < 0.05$ vs. pump off.

In the left ventricle, blood flow remained near baseline levels at 70NP or 70P. At 100NP, however, blood flow decreased significantly below baseline levels in the posterior and anterolateral epicardial segments; in the anterolateral endocardial segment; and in the subendocardium and subepicardium of the LV free wall, which were calculated as the means of anterolateral and posterior subendocardial and subepicardial blood flow, respectively (**Figure 7.4**). At 100P, blood flow decreased significantly in the anterolateral epicardium and endocardium and in the

subepicardium of the LV free wall (Figure 4). In the right ventricle, transmural blood flow decreased gradually, but not significantly, from baseline levels at increasing NP and P settings (**Figure 7.5**).

In the brain, cortical blood flow at 70NP decreased, but not significantly, from baseline levels. At 100P, this decrease became statistically significant. At 70P and 100P, the blood flow reduction was less pronounced and not statistically significant. In the corpus medullare, blood flow decreased slightly from baseline levels at increasing NP and P settings.

In the kidneys, blood flow in the renal cortex and medulla gradually decreased, but not significantly, at increasing NP and P settings.

7.5 Discussion

Using a prototype LVAD capable of producing both NP and P flow in a canine model of doxorubicin-induced heart failure, we showed that flow mode did not significantly affect either hemodynamics or end-organ perfusion in the short term.

Our decision to use a model in which dilated cardiomyopathy is induced by intracoronary doxorubicin infusion offered several experimental advantages. First, this model not only mimicked the altered end-organ perfusion seen clinically before pump implantation, but it also controlled for the influence of the native healthy heart on pump performance. Thus, we were able to assess more precisely the microcirculatory effects of MCS on poorly perfused end-organs (heart, brain, and kidney). Second, intracoronary delivery of doxorubicin allowed us to avoid systemic side effects such as myelosuppression [42,152], avoid complex surgical interventions including thoracotomy and ligation of coronary arteries [3,78,87], and selectively depress LV wall function without severely impairing RV function [153]. Intracoronary delivery also gave us a superior alternative to coronary embolization, which may induce chronic ischemic cardiomyopathy and consequently result in higher mortality rates related to myocardial infarction-induced arrhythmias [120]. Third, this model produced hemodynamic and neurohumoral changes that are similar to those seen clinically in patients with heart failure [70]. One disadvantage of the model, however, was its possibility of inducing irreversible myocardial damage, which would have precluded any experimental assessment of myocardial recovery [179].

In light of our present results, we believe that our model and its simple and minimally invasive protocol for inducing heart failure by doxorubicin infusion can be safely used to evaluate experimentally the short- and long-term end-organ effects of LVADs. Indeed, only 2 dogs died before study termination, one of a coronary air embolism during the doxorubicin induction period and the other of ventricular

fibrillation during surgical pump implantation; the 5 remaining dogs all underwent pump implantation surgery as scheduled. Moreover, as shown by echocardiographic

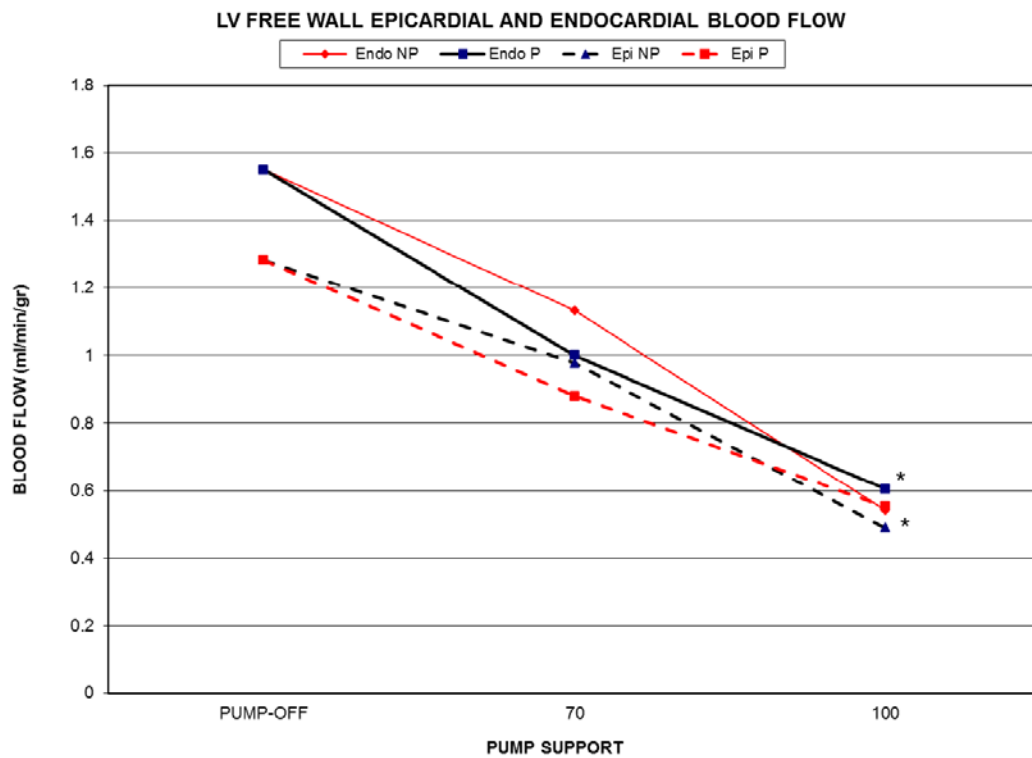


Figure 7.4: Epicardial (Epi) and endocardial (Endo) blood flow in left ventricular free wall. NP, nonpulsatile; P, pulsatile. * $P < 0.05$, vs pump-off.

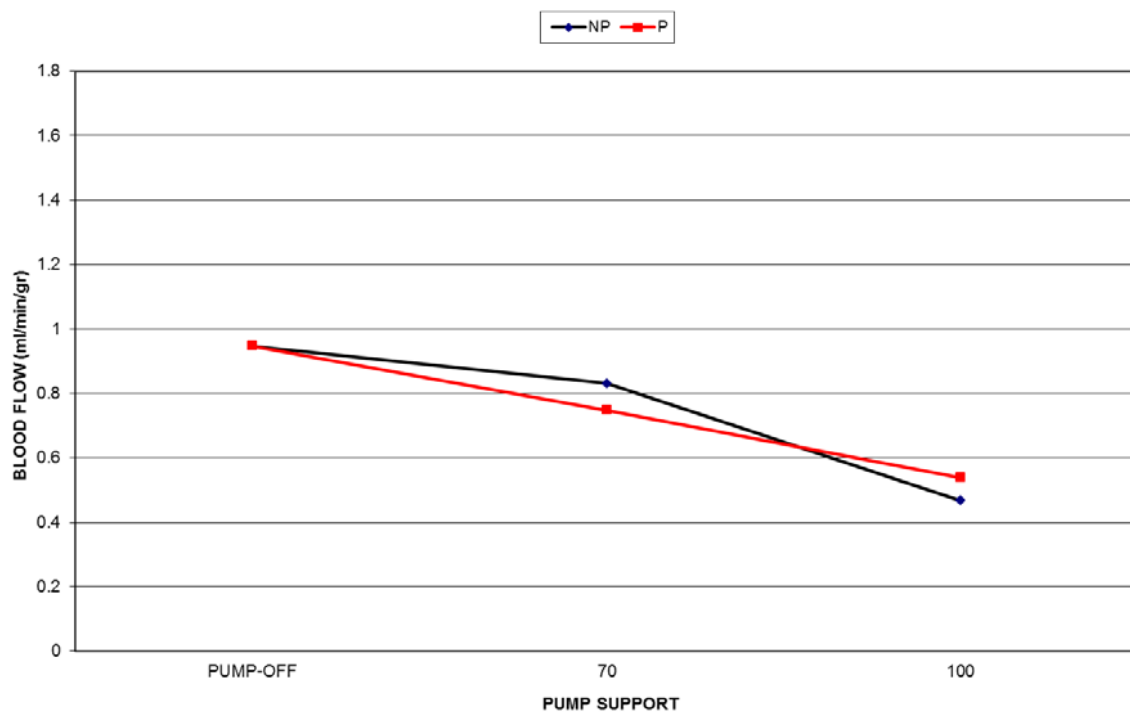


Figure 7.5: Myocardial (full-thickness) blood flow in right ventricle. NP, nonpulsatile; P, pulsatile.

examination of the left ventricle before and after doxorubicin induction, heart failure was successfully induced (**Table 7.1**).

In contrast to reports of improved FS in normal healthy hearts during long-term LVAD support [94], our present results suggest that no improvement in FS should be expected immediately after pump implantation in a chronic cardiomyopathy model. In our study, FS remained unchanged even after pump implantation and operation at all experimental settings. However, LVDd and LVDs improved, most likely as a result of effective unloading of the left ventricle [121,156,168].

The effect of NP versus P flow on LV function is controversial. Several previous studies suggest that flow with no- or reduced pulsatility during acute or chronic NP support does not adversely affect LV function [26,31,106], whereas other studies with CPB machine or VADs suggest that P support is superior to NP support in preserving major end-organ perfusion and metabolism [37,131,147,151]. Our present results have shed some light on these 2 issues. For instance, even though pulse pressure at 70P was 35% lower than at baseline in our study, there was no significant difference between the functional effects of 70P and 70NP flow (**Table 7.2**). This may have been related to partial unloading of the left ventricle that allowed blood to eject through the aortic valve, thus preserving aortic pulsatility. Nor was there any significant decrease in pulse pressure at 100P. At 100NP, however, the pulse pressure significantly narrowed, presumably as a result of extensive unloading of the left ventricle and impaired aortic valve opening [156].

Although blood flow through the pump is continuous throughout the cardiac cycle, aortic blood flow remains partially pulsatile. This is because of the contribution of left ventricular contractions, which increases the inlet pressure of the pump during systole (**Figure 7.6A and 7.6B**). On the other hand, the aortic pressure and pump flow waveforms observed during pulsatile pump support were irregular and different from those of the natural heart (**Figure 7.6C and 7.6D**). This phenomenon was probably related to the independent pulse rate of the pump, which was not ECG-triggered, and one might even speculate that some degree of negative interference may have affected cardiac hemodynamics and end-organ microcirculation.

The gradual decrease in dp/dt_{max} that we observed at increasing levels of pump support has been noted before [121,156] and may be attributed to delayed LV relaxation secondary to extensive LV unloading, particularly at 100% of pump support. In fact, the gradual decrease in LVP with increasing pump support, whether NP or P, may lead to a decrease in myocardial work [133].

Even though the decrease in CBF that we observed was more pronounced in NP mode than in P mode, this did not adversely affect the MVO₂ of the left ventricle (**Figure 3**). In fact, the continuous decrease in CBF (i.e., myocardial perfusion) at increasing levels of pump support (i.e., increasing levels of LV unloading) and in

different flow modes paralleled the continuous decrease in the reduced energy demand of the myocardium (MVO₂) secondary to decreased myocardial work and LV wall tension. This was consistent with the finding of previous studies [33,40,64]. Moreover, the increase in CBF/MVO₂ ratio at increasing levels of pump support suggested that the pump did not cause any iatrogenic ischemia of the left ventricle when operating in either NP or P mode.

The gradual decrease in total subendocardial and subepicardial blood flow in the LV free wall that we observed at increasing levels of pump support was consistent with the decrease in CBF and myocardial energy demand. Importantly, the Endo/Epi ratio remained constant as pump support increased, and there was no marked difference in regional perfusion patterns between NP or P flow modes. Yet, even though LV hemodynamics were not altered during our 4-hour study period, longer-term studies are needed to assess the recovery potential of myocytes and the adaptive response of the myocardium to chronically reduced perfusion conditions during prolonged periods of LVAD support.

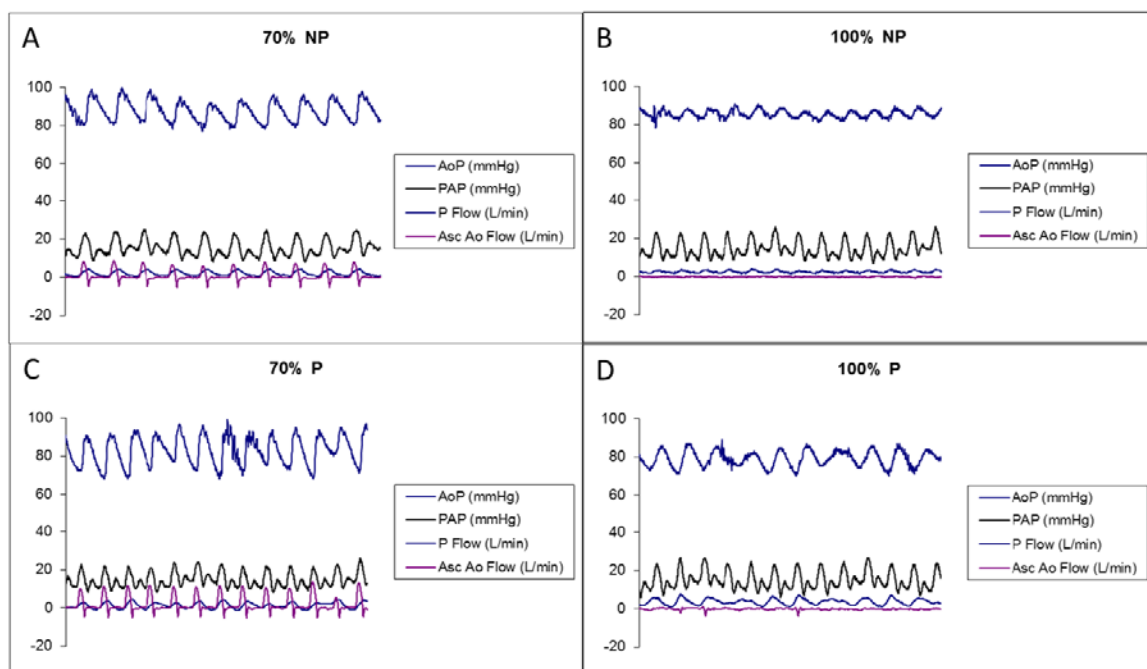


Figure 7.6A-7.6D: Waveforms of aortic pressure (AoP), pulmonary artery pressure (PAP), pump flow (P Flow), and ascending aortic flow (Asc Ao Flow) during pump support. NP, nonpulsatile; P, pulsatile.

The effects of P and NP flow on cerebral perfusion have been studied previously. A number of groups have used hypothermic cardiopulmonary bypass models but produced inconsistent results [49,75,123,124]. Others have shown cerebral circulation not to be adversely affected by continuous (i.e., NP) pump flow in either acute [59] or chronic [122] settings and cerebral autoregulation to be well

maintained in both. In the present study, however, we found that regional perfusion of the cerebral cortex and medulla gradually decreased with increasing pump support, until the decrease finally became significant in the cerebral cortex at 100NP. Interestingly, these findings are inconsistent with several previously published reports [97,129,154]. This inconsistency may be related to differences in measurement techniques (microsphere analysis [85] versus tissue flow meters [129] or behavioral observation [122]), model (chronic dilated cardiomyopathy [153] versus acute cardiogenic shock [84]), or device (a single bimodal pump implanted in the same animal [97] versus different pumps with different flow modes implanted in different animals [84,122]). It may even be related to anesthesia-induced alterations in the cerebral autoregulatory system.

There have been many studies of kidney perfusion during circulatory support. In an ovine model of acute myocardial ischemia, Meyns et al. [85] observed an insignificant decrease in cortical and medullar perfusion during both P and NP support. In another experimental study, Saito et al. [122] showed that chronic NP circulatory support induced no functional or histologic changes in the kidneys. Many other experimental studies have shown the superiority of P over NP support [93,129,130]. Most of those studies, however, were performed in acute cardiogenic shock models, in which the renal autoregulatory (neurohumoral) mechanisms may have differed from those that would be seen in comparable chronic heart failure models [14,104,108]. In the present study, both NP and P support in our animal model of chronic heart failure reduced kidney perfusion to similar extents in the short term. It remains to be seen whether the long-term adaptive responses to P and NP circulatory support in these 2 types of models differ substantially from the short-term responses. Furthermore, it is impossible to extrapolate these animal findings to the human patient with chronic heart failure and its multiple variables. For instance, the chronic pulmonary hypertension that accompanies chronic heart failure in humans is not reproduced in this or any other experimental animal model.

Others have reported that, under NP flow conditions, the velocity of erythrocytes in capillaries and the number of perfused capillaries decrease in direct proportion to the impairment in basal and flow-stimulated release of nitric oxide from the microvascular endothelium [4]. In our study, we did not observe any significant difference in end-organ regional perfusion between the flow modes; however, we do note here that the NP and P modes at different pump support levels were maintained for only 10 minutes before measurements were taken. Perhaps, the 10-minute time period has not been long enough to allow the pump flow mode to affect erythrocyte flow patterns and microsphere distribution in the end-organs. Therefore, further studies are needed to clarify the short- and long-term effects of NP and P flow on cerebral and other end-organ microcirculation.

The effects of mechanical LV support on the unassisted right ventricle have not been fully documented. Several investigators have argued that ventricular septal shifting and/or increased venous return that reportedly occurs during LVAD support may detrimentally affect RV function [24,52,89]. Others have suggested that LVAD support may exacerbate a preexisting state of RV ischemia or induce it [134]. In general, experimental studies have not shown any effect of LVAD support on the function of a nonischemic right ventricle [15,134]. In an experimental study using healthy pig hearts supported by a pulsatile LVAD operating in synchronous (EKG-triggered) and asynchronous (volume-triggered) modes, Hendry et al. [47] observed a gradient of regional blood flow within the right ventricle along the right coronary artery in both modes. They also observed that this gradient did not cause RV dysfunction and that perfusion throughout the LV septum and free wall remained almost constant. In our present study, we observed that RV myocardial perfusion was adversely affected at increasing levels of pump support, regardless of flow mode, but we could not say whether this was due to the pump's flow properties. Consequently, the potential effects of long-term P and NP pump support on RV perfusion, with or without increased venous return and/or septal shift, should be tested in larger numbers of animal subjects in appropriate nonischemic and ischemic models.

Our study did have some limitations. Although performed in a doxorubicin-induced chronic dilated cardiomyopathy model, it did not produce findings on which we could base any definitive conclusions about the long-term effects of continuous or pulsatile flow on the end-organ (heart, kidney and brain) microcirculation. Instead, our findings reflected the acute setting changes that were made when autoregulatory mechanisms were at work. Moreover, it was not possible to quantify or standardize the effects of the anesthesia performed and surgical trauma incurred during pump implantation, although the baseline hemodynamics immediately after pump implantation were normal. It is also not clear what effect, if any, the choice of graft anastomosis site (i.e., ascending vs. descending aorta) had on aortic and myocardial blood flow properties. Further studies in this regard are warranted.

7.6 Conclusion

The present results suggest that hemodynamics and end-organ function are not differentially affected by LVAD flow mode in a canine model of doxorubicin-induced congestive heart failure. Larger, longer-term studies are warranted to confirm the validity of these findings in chronic circulatory assist and to establish the utility of this animal model.

8

Ventricular Assist Device Outflow-Graft Site: Effect on Myocardial Blood Flow

The contents of this chapter are based on: Tuzun E, Narin C, Gregoric ID, Cohn WE, Frazier OH. Ventricular Assist Device Outflow-Graft Site: Effect on Myocardial Blood Flow. Journal of Surgical Research 2011 Nov;171(1):71-5.

8.1 Abstract

Background: Recent advances in left ventricular assist device (LVAD) technology have resulted in small, durable, energy-efficient, continuous-flow blood pumps that can support patients with end-stage heart failure. However, the effects of reduced or nonpulsatile flow on end-organ function are unclear. We performed a pilot study in calves with a continuous-flow LVAD to assess the effects of the pump's outflow-graft location (ascending versus descending aorta) on myocardial blood flow.

Materials and Methods: In 8 healthy calves, we implanted the Jarvik 2000 LVAD in the left ventricular apex without the use of cardiopulmonary bypass. We anastomosed the outflow graft to either the ascending aorta (group 1; n=4) or the descending aorta (group 2; n=4). Hemodynamic parameters, myocardial oxygen consumption, and regional myocardial blood flow (analyzed with colored microspheres) were assessed at baseline (pump off) and during pump operation at 8000, 10,000, and 12,000 rpm.

Results: No intergroup differences were found in the aortic pressure, heart rate, central venous pressure, pump-flow to total-cardiac-flow ratio, or blood flow in the left anterior descending and right posterior descending coronary arteries at increasing pump speeds. Neither myocardial oxygen consumption nor myocardial tissue perfusion differed significantly between the 2 groups.

Conclusion: Regardless of the outflow-graft location (ascending versus descending aorta), the continuous-flow LVAD unloaded the left ventricle and did not adversely affect myocardial perfusion in either the right or left ventricle. Owing to the small number of animals studied, however, the most we can conclude is that neither outflow-graft location appeared to be inferior to the other.

8.2 Introduction

In the last decade, we have witnessed the development and clinical application of several new continuous-flow blood pumps, which provide long-term support for the failing left ventricle. Compared to their pulsatile predecessors, these pumps have a reduced mechanical complexity that makes them more durable, reliable, and energy efficient. Previous studies of continuous-flow blood pumps implanted in various animal models have yielded contradictory findings: some researchers found that the devices were well tolerated and increased regional myocardial blood flow [22,156]; other researchers concluded that pulsatile circulation was more beneficial to the microcirculation [61].

Because of these contradictory reports, we conducted a series of experiments in which continuous-flow left ventricular assist devices (LVADs) were implanted in a canine model of doxorubicin-induced heart failure [30] and in a healthy bovine model [157]. In those experiments, we assessed the relationship between continuous pump flow and acute changes in left ventricular (LV) and right ventricular (RV) mechanics, myocardial oxygen consumption (MVO₂), and regional myocardial, renal, and cerebral blood flow. According to our data, perfusion of various regions of the central nervous system and the kidney was equal at baseline (characterized by normal, pulsatile physiology) and at increasing pump rotational speeds (which gradually diminish pulsatility by decreasing the pulse pressure). However, endocardial and epicardial myocardial blood flow in the left ventricle gradually but significantly decreased in all regions at increasing pump speeds, concomitant with a decrease in coronary artery blood flow (CBF) in the left anterior descending artery (LAD). Because these experiments all involved a descending aortic outflow-graft anastomosis, it was not clear whether the graft-anastomosis site would affect regional myocardial blood flow. Consequently, we undertook the present short-term study to assess the effects of outflow-graft location (ascending versus descending aorta) on regional myocardial blood flow in calves with a continuous-flow blood pump.

8.3 Materials and Methods

8.3.1 Animals

Eight calves weighing 80 to 100 kg (mean, 92 ± 7 kg) were used in the study. All calves received humane care in compliance with the Principles of Laboratory Animal Care (National Society of Medical Research) and the Guide for the Care and Use of Laboratory Animals (National Institutes of Health publication no. 85-23, revised 1996). Our Institutional Animal Care and Use Committee approved all protocols used in the present study.

8.3.2 Pump Description

The Jarvik 2000 LVAD (Jarvik Heart, Inc., New York, New York) is an intraventricular axial-flow blood pump that comprises the pump itself, a percutaneous power cable, a pump-speed controller, and an external direct-current power supply. The pump speed is set manually in the range of 8000 to 12,000 rpm. With the natural heart contracting, the device typically produces pulsatile flow instantaneously; this flow varies by as much as 5 to 8 L/min over the cardiac cycle [157]. Owing to its relatively

simple design, the device can be inserted without the use of cardiopulmonary bypass (CPB) [36,128]. For this study, we used the standard controller, not the intermittent low speed (ILS) controller, which is now routinely used in all cases [157].

8.3.3 Anesthesia and Surgical Preparation

Each calf was premedicated with intramuscular glycopyrrolate (0.02 mg/kg) and xylazine (0.2-0.7 mg/kg). A 12-French triple-lumen venous catheter was inserted percutaneously into the right external jugular vein. Anesthesia was induced with intravenous ketamine (10-20 mg/kg). After orotracheal intubation was achieved, anesthesia was maintained with isoflurane (1.0-3.0%) in oxygen (40-100%). The anesthetized calf was then placed on the operating table in the right lateral decubitus position in preparation for a left thoracotomy.

8.3.4 Operative Technique

A left thoracotomy was performed in the fifth intercostal space. The left carotid artery was cannulated with a fluid-filled catheter, which was advanced proximally into the immediate vicinity of the aortic valve to monitor arterial pressure and to sample blood. The pericardium was incised from the apex to the pulmonary artery, and the heart was suspended in a pericardial cradle. The ascending or descending aorta was exposed, and heparin (3 mg/kg) was administered. The 16-mm Dacron outflow graft of the Jarvik 2000 pump was anastomosed to either the ascending (group 1; n=4) or the descending (group 2; n=4) thoracic aorta with a 4-0 polypropylene suture and the aid of a partially occluding vascular clamp. A silicone/polyester sewing cuff was sewn to the ventricular apex with pledgeted, coated, braided 2-0 polyester mattress sutures. After LV apical coring was performed, the pump was inserted into the ventricular cavity of the beating heart without the use of CPB and was secured with cotton tape. The air was removed from the left ventricle, pump, and graft.

8.3.5 Assessment of Hemodynamic Parameters

The right carotid artery was exposed so that a special catheter fitted with a high-fidelity micromanometer tip (Millar Mikro-Tip Catheter; Millar Instruments, Houston, Texas) could be inserted into the left ventricle. Four different ultrasonic flow probes (Transonics Inc., Ithaca, New York) were then placed: a 16-mm flow probe on the outflow graft, a 24-mm probe on the ascending aorta, a 3-mm probe around the proximal LAD, and a 3-mm probe around the right posterior descending coronary

artery (RC-PDA). Data were recorded with a 16-channel computer data-acquisition system (Ponemah System, Version 3.3; Gould Instrument Systems Inc., Valley View, Ohio). Hemodynamic parameters were assessed while the pump was off and the outflow graft was clamped to avoid pump regurgitation (0 rpm, baseline). The pump was then operated at various speeds (8000, 10,000, and 12,000 rpm) for 20 minutes at each speed.

The heart rate, aortic pressure (AoP), central venous pressure (CVP), cardiac output, and pump flow rates were measured at baseline and at each of the 3 pump speeds.

8.3.6 Assessment of Myocardial Oxygen Consumption

Left ventricular and RV myocardial oxygen consumption (MVO₂) was assessed selectively at baseline and at each of the 3 pump speeds. Twenty-two-gauge angi catheters were inserted into the anterior interventricular vein and middle cardiac vein to take selective coronary venous blood samples. Selective LV and RV MVO₂ values were calculated as the difference between the aortic (\bar{a}) and coronary venous (v) blood oxygen content (in either the interventricular or middle cardiac vein), multiplied by the right or left CBF according to the following formula: $MVO_2 = CBF \cdot [\bar{a} - v]$. A Novostat Profile M blood gas analyzer (Nova Biomedical Co., Waltham, Massachusetts) was used for blood-gas analysis.

8.3.7 Assessment of Regional Myocardial Blood Flow

Myocardial tissue perfusion was assessed with 15- μ m, nonradioactive, stable isotope-labeled microspheres (BioPAL, Inc., Worcester, Massachusetts). The microspheres were injected into the left atrium under 4 test conditions: while the pump was off (baseline), or while it was operating at 8000, 10,000, or 12,000 rpm according to the manufacturer's suggested standards. Each type of labeled microsphere was used under a different test condition: microspheres labeled with gold appeared red (pump off), those labeled with lanthanum appeared blue (8000 rpm), those labeled with antimony appeared violet (10,000 rpm), and those labeled with lutetium appeared pink (12,000 rpm).

After tissue perfusion was assessed, each calf was euthanized. The heart was then harvested for analysis by isolating and dividing the left ventricle into 4 equal transverse sections along the atrioventricular groove [23,156]. The basal and apical sections were discarded. The remaining 2 distal sections were selected and divided into 4 segments representing the septal, anterior, lateral, and posterior walls (**Figure 8.1**). Each segment was further divided into epicardial and endocardial subregions. Two grams of tissue were taken from each region (yielding a total of 8 tissue samples

from the left ventricle) for microsphere analysis. The right ventricle was also isolated and divided into 2 segments representing the anterior and posterior walls. All tissue samples were dried overnight at 70°C and sent out for analysis. Blood samples were obtained and used to normalize tissue-sample readings. The analysis of labeled microspheres was based on an automated neutron-activation system described in detail elsewhere [135].

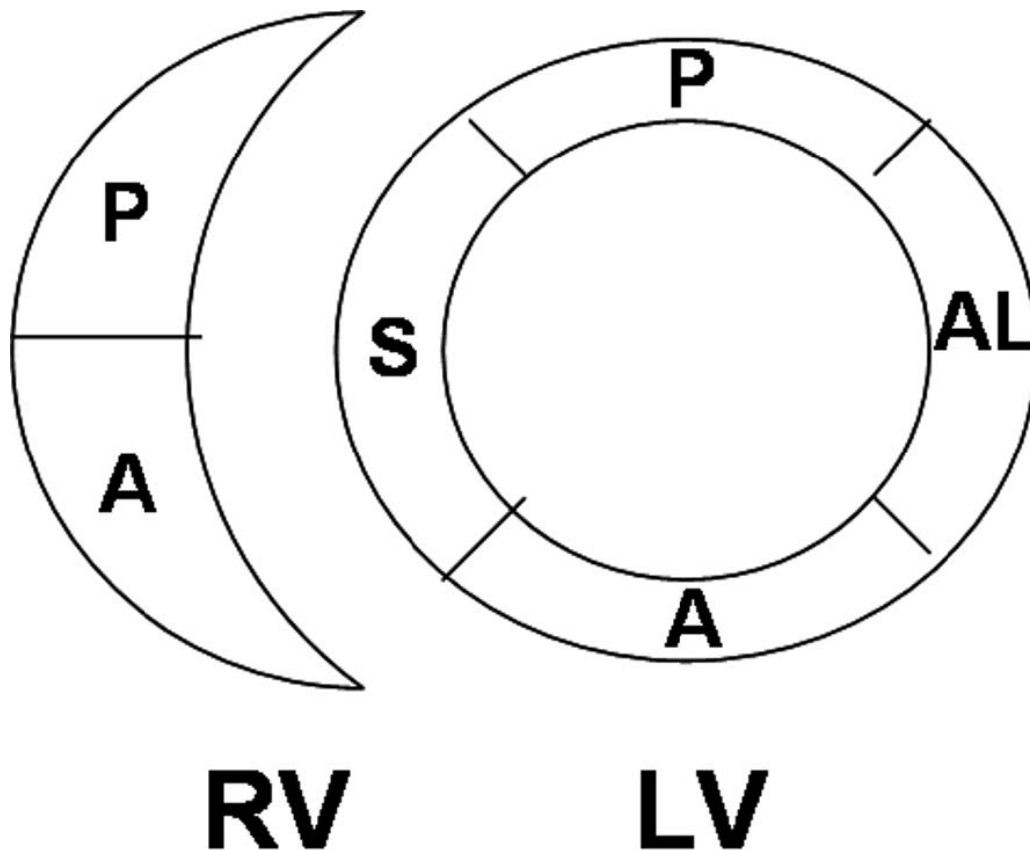


Figure 8.1: Diagram showing how the left and right ventricles were sectioned to assess regional blood flow. RV, right ventricle; LV, left ventricle; S, septal wall; A, anterior wall; AL, anterolateral wall; P, posterior wall.

8.3.8 Statistical Analysis

All statistical tests were performed with Microsoft Excel or Statistical Analysis Software (SAS Institute, Inc., Cary, North Carolina). $P < 0.05$ was considered significant. Analysis of variance (ANOVA) was used for comparing multi-group variables.

8.4 Results

All experiments were successfully completed without surgical or device-related complications.

8.4.1 Hemodynamic Parameters

In both groups, the mean diastolic AoP, mean systolic AoP, mean AoP, and heart rate gradually increased with increasing pump speeds, but these changes were not significant compared to baseline levels (**Table 8.1**).

Table 8.1. Hemodynamic Parameters Assessed at Baseline (Pump Off) and at Increasing Pump Speeds in Calves with a Continuous-Flow Left Ventricular Assist Device

	Pump Speeds (rpm)			
	Baseline (PumpOff)	8000	10,000	12,000
Heart rate (bpm)	88±4/90±5	89±3/91±3	91±5/93±2	91±6/94±4
AoP (mmHg)				
Systolic	105±11/102±9	108±9/104±4	110±8/109±6	110±9/110±7
Diastolic	65±4/68±3	69±5/70±4	74±6/73±3	77±5/76±5
Mean	79±4/81±2	81±5/82±2	82±4/83±4	84±6/85±5
CVP (mmHg)	9±2/7±2	9±1/7±2	8±2/7±3	8±2/8±1

Values are presented as mean ± standard deviation (Group 1/Group 2). Abbreviations: rpm, revolutions per minute; bpm, beats per minute; AoP, aortic pressure; CVP, central venous pressure

The mean CVP was not affected by variations in pump speed. In both groups, the pump-flow to total-cardiac-output ratio was significantly higher than the baseline value at all speeds ($P<0.05$) (**Figure 8.2**). In addition, LAD and RC-PDA blood flow decreased with increasing pump speeds in both groups, but the decrease was not significant compared to baseline levels. We observed no significant intergroup differences in the hemodynamic parameters.

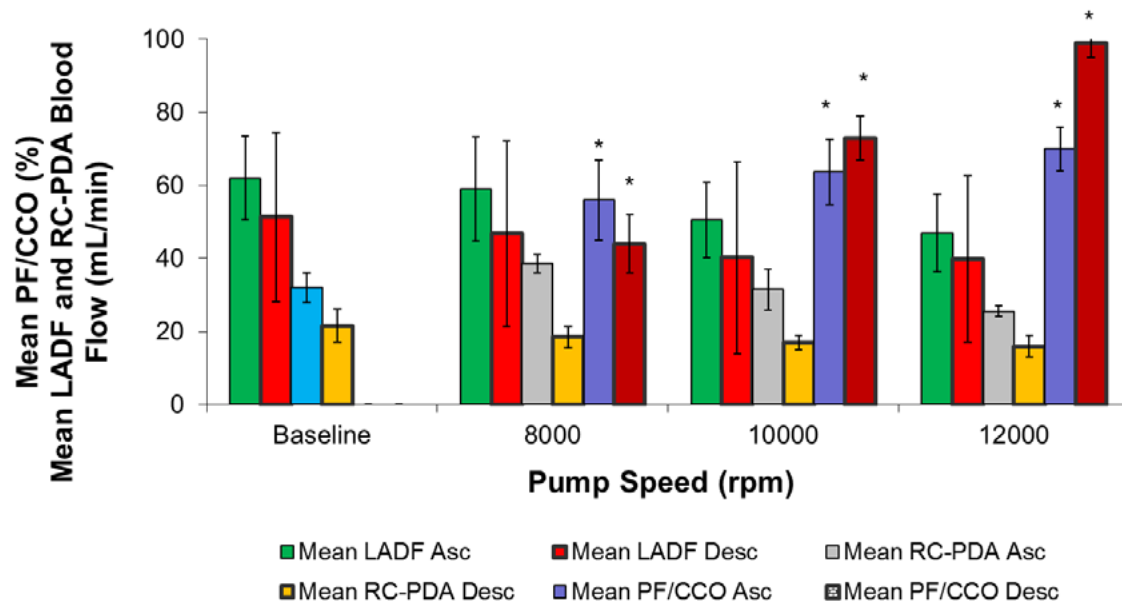


Figure 8.2: Pump-flow to total cardiac output ratio (PF/CCO), left anterior descending artery blood flow (LADF), and right posterior descending coronary artery blood flow (RC-PDA) in calves with an ascending (Asc) versus a descending (Desc) aortic anastomosis. The parameters were assessed at baseline and at increasing pump speeds.

8.4.2 Myocardial Oxygen Consumption

Left ventricular MVO₂ decreased significantly with increasing pump speeds in both groups ($P < 0.05$ vs baseline) (**Figure 8.3**). Right ventricular MVO₂ decreased significantly at 12,000 rpm in both groups ($P < 0.05$ vs baseline). Baseline LV MVO₂ was significantly higher in group 1 (ascending aortic anastomosis) than in group 2 (descending aortic anastomosis) ($P < 0.05$); however, we observed no other significant intergroup differences.

8.4.3 Myocardial Tissue Perfusion

In group 1, regional myocardial blood flow in the RV and LV segments (left ventricle: septal, lateral, anterior, posterior; right ventricle: anterior, posterior) was not significantly changed at increasing pump speeds compared to baseline levels (**Figure 8.4**). In group 2, regional myocardial blood flow in all the evaluated LV and RV segments decreased slightly below baseline levels with increasing pump speeds, but this change was not significant. Therefore, we observed no significant intergroup differences in myocardial tissue perfusion.

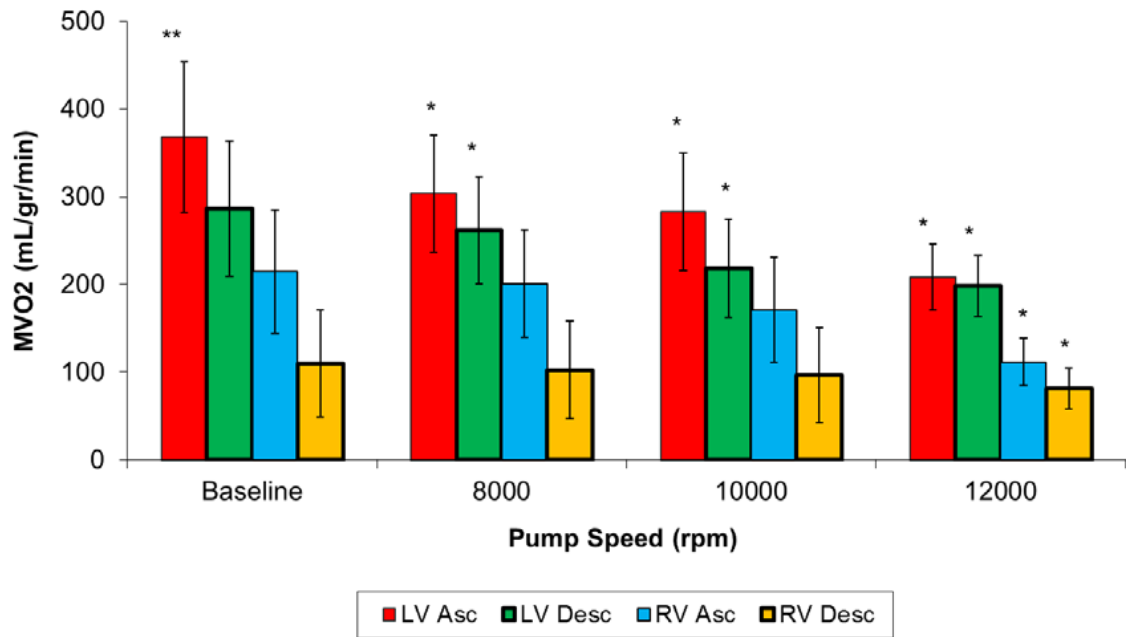


Figure 8.3: Left ventricular (LV) and right ventricular (RV) myocardial oxygen consumption (MVO2) for calves with an ascending (Asc) aortic anastomosis (group 1) versus a descending (Desc) aortic anastomosis (group 2). The MVO2 was assessed at baseline and at increasing pump speeds.

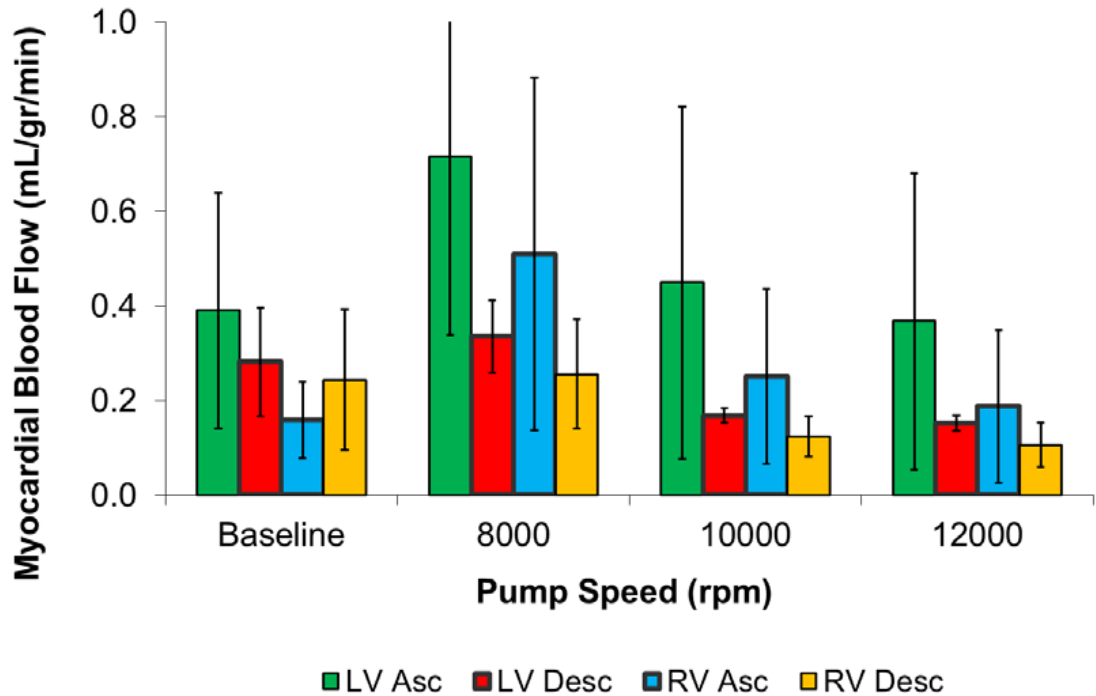


Figure 8.4: Left ventricular (LV) and right ventricular (RV) myocardial blood flow for calves with an ascending (Asc) aortic anastomosis (group 1) versus a descending (Desc) aortic anastomosis (group 2). Myocardial blood flow was assessed at baseline and at increasing pump speeds.

8.5 Discussion

The results of this small pilot study suggest that the location of the continuous-flow LVAD outflow graft (ascending versus descending aorta) does not affect coronary and regional myocardial blood flow in the right and left ventricles. In both groups of calves, LV MVO₂ significantly decreased with increasing pump speeds, and RV MVO₂ significantly decreased at 12,000 rpm. Owing to the small number of animals studied, however, the most we can conclude is that neither outflow-graft location appeared to be inferior to the other with respect to overall results.

Because of their small, compact design, continuous-flow LVADs are optimal for minimally invasive and reoperative cardiac procedures because they can be implanted with a descending or an abdominal aortic anastomosis through a small incision [27,43,51,103,128]. The descending aortic anastomosis also preserves the sternum for subsequent cardiac transplantation or other cardiac procedures that require a median sternotomy. So far, however, controversial results from some animal and in vitro studies have precluded wide use of this method, even for primary LVAD implantations [57,61,73]. Kar and colleagues [57] reported that LVADs implanted with an outflow-graft anastomosis to the descending aorta have potential drawbacks such as aortic valve fusion and aortic-root flow stagnation that may alter myocardial perfusion. Similarly, in their experimental study, Litwak and colleagues [72] reported that the mean aortic-arch blood flow decreased when the LVAD outflow-graft anastomosis site was the descending aorta versus the ascending aorta. They also reported that, although mean aortic-root and carotid-artery flow are independent of the LVAD outflow-graft location, competitive flow between the native heart and the LVAD may result in turbulent mixing or stagnation in the aortic arch if the LVAD outflow-graft anastomosis is located in the descending aorta [72]. Therefore, they suggested that anastomosis of the outflow-graft to the ascending aorta may be optimal for a continuous-flow LVAD. However, none of these investigators addressed the effect of stagnation on regional myocardial perfusion. Because of these controversies, the descending anastomosis is mostly performed as an alternative approach in patients who have undergone a previous sternotomy, coronary artery bypass patients with vein grafts, and patients with atherosclerotic disease of the ascending aorta [57].

In previous experimental studies [23,156], we demonstrated that LVAD support with a descending aortic anastomosis successfully unloads the left ventricle and decreases MVO₂ without adversely affecting regional myocardial perfusion. We attributed these results to unloading of the left ventricle and to the reduced energy demand of both ventricles. In those studies, we also showed that cerebral blood flow was not adversely affected after LVAD implantation. In our present study, we found that

regional myocardial blood flow was similarly protected in both anastomotic locations (the ascending or descending aorta) with no significant intergroup difference.

8.6 Limitations

This study was limited by the following factors: 1) All experiments were conducted in calves with healthy hearts. Because the Jarvik 2000 LVAD is designed to be used in patients with end-stage cardiac failure, our results may not be directly applicable in the clinical setting. 2) We examined the short-term effects of experimental LVAD implantation. Therefore, we cannot draw any conclusions about the long-term effects of continuous-flow LVADs on myocardial perfusion, which may be affected by neurohormonal compensatory mechanisms. 3) Because this was a pilot study, our conclusions were based on a relatively small number of calves; it is possible that a larger study, involving more than 8 animals, would have shown significant differences between the 2 groups. Unfortunately, financial restrictions prevented us from performing these expensive tests in more than 8 animals. Nevertheless, because this is the first and] only study focused on this topic, we believe that the intergroup trends in even 8 animals are important. 4) It was not possible to quantify or standardize the effects of anesthesia and surgical trauma on the hemodynamic parameters during pump implantation. The calves' baseline hemodynamic parameters were normal at that time. 5) The aortic anatomy is different in the calf than in the human. The ascending aorta bifurcates within 1 to 2 cm of the aortic valve in the calf, so performing a complete ascending aortic anastomosis at that site is impossible. Therefore, ascending-aortic anastomosis is usually performed at the brachiocephalic trunk, as close to the aortic bifurcation as possible, and this was done in our calves. Consequently, with regard to the location of the ascending aortic anastomosis, the present animal model might not precisely duplicate LVAD-related physiology in humans.

8.7 Conclusion

Our data suggest that regional myocardial blood flow was not adversely affected by the location of the outflow-graft anastomosis (ascending versus descending aorta) in healthy calves implanted with a continuous-flow LVAD. By increasing the pump flow, we successfully reduced MVO₂ in the right and left ventricles independently of the outflow-graft location. Owing to the small number of animals studied, however, the most we can conclude is that neither outflow-graft location appeared to be inferior to the other with respect to overall results.

9

Modification of a volume-overload heart failure model to track myocardial remodeling and device-related reverse remodeling

The contents of this chapter are based on: Tuzun E, Bick R, Kadipasaoglu C, Conger JL, Poindexter BJ, Gregoric ID, Frazier OH, Towbin JA, Radovancevic B. Modification of a volume-overload heart failure model to track myocardial remodeling and device-related reverse remodeling. ISRN Cardiol. 2011;2011:831062.

9.1 Abstract

Background: To provide an ovine model of ventricular remodeling and reverse remodeling by creating congestive heart failure (CHF) and then treating it by implanting a left ventricular assist device (LVAD).

Materials and Methods: We induced volume-overload heart failure in 2 sheep; 20 weeks later, we implanted an LVAD and assessed recovery 11 weeks thereafter. We examined changes in histologic and hemodynamic data and levels of cellular markers of CHF.

Results: After CHF induction, we found increases in LV end- diastolic pressure, LV systolic and diastolic dimensions, wall thickness, left atrial diameter, and atrial natriuretic protein (ANP) and endothelin-1 (ET-1) levels; β -adrenergic receptor (BAR) and dystrophin expression decreased markedly. Biopsies confirmed LV remodeling. After LVAD support, LV systolic and diastolic dimensions, wall thickness, and mass, and ANP and ET-1 levels decreased. Histopathologic and hemodynamic markers improved, and BAR and dystrophin expression normalized.

Conclusions: Myocardial remodeling secondary to experimental volume overload heart failure followed by reverse remodeling related to CFLVAD support was successfully created.

9.2 Introduction

Congestive heart failure (CHF) is characterized by an initial cardiac insult, followed by a compensatory response that results in ventricular remodeling. At the cellular level, CHF involves myocyte hypertrophy, cell death, and replacement fibrosis. At the subcellular level, the disease causes loss of myofilaments, alterations in cytoskeletal proteins, and adrenergic desensitization.

For the past 2 decades, the diagnosis of heart failure has relied on noninvasive methods (physical examination, chest roentgenography, electrocardiography, and echocardiography) and invasive tests [53]. Various biomarkers have also been used to diagnose heart failure with marginal clinical utility. In patients with ischemic heart disease and myocardial infarction, the following biomarkers have shown varying levels of sensitivity in detecting heart failure: lactic dehydrogenase, creatine kinase myocardial band (CKMB), troponins T and I, C-reactive protein, norepinephrine, endothelin-1 (ET-1), interleukin-6, tumor necrosis factor- α (TNF- α), atrial natriuretic protein (ANP), B-type natriuretic peptide, beta-adrenergic receptors (BARs), and angiotensin II [9,10,45,96,107,110,111,112,141,146,173]. Another cellular marker of heart failure is dystrophin, a protein that connects the extracellular matrix with the sarcomere via actin. Dystrophin abnormalities have been associated with heart

failure caused by genetic susceptibility and viral infection [79]. Treatment of CHF with left ventricular assist devices (LVADs) can reverse the ventricular remodeling associated with heart failure, and this reversal is correlated with normalization of cellular markers in myocytes [163,164]. The present pilot study was undertaken to provide an ovine experimental model for creating CHF, then reversing this condition by implanting an LVAD. We assessed the changes in immunohistochemical, histopathologic, and hemodynamic parameters to verify the occurrence and extent of the remodeling events in heart failure development (remodeling) and subsequent LVAD-assisted recovery (reverse remodeling).

9.3 Materials and Methods

9.3.1 Animal Model.

Two male Rambouillet sheep (54 ± 4 kg) were used in this study. The animals received humane care in compliance with the Principles of Laboratory Animal Care (National Society of Medical Research) and the Guide for the Care and Use of Laboratory Animals (National Institutes of Health Publication no. 85-23, revised 1996). Our Institutional Animal Care and Use Committee approved the protocol in advance.

To accurately mimic the clinical scenario of ventricular remodeling in heart failure, we created a volume-overload heart-failure model by destroying the chordae tendineae of each sheep's mitral valve. After 20 weeks, we implanted a Levitronix CentriMag (Levitronix LLC, Waltham, Mass) (1st case) and a HeartWare LVAD (HeartWare International, Inc., Framingham, Massachusetts) (2nd case) to support the animals. After 11 weeks of LVAD support, the sheep were reexamined for evidence of myocardial recovery.

9.3.2 Operative Procedures

9.3.2.1 Anesthesia

We followed a standard institutional anesthesia protocol that has previously been described in detail [35]. Each sheep was premedicated with glycopyrrolate (0.02 mg/kg) and xylazine (0.2–0.7 mg/kg); both drugs were administered intramuscularly. Intravenous ketamine (10–20 mg/kg) was administered to induce anesthesia. General anesthesia was maintained with isoflurane (1–3%) in oxygen (40–100%).

9.3.2.2 1st Operation: Creation of Mitral Regurgitation (Baseline).

Transthoracic echocardiography was performed to obtain baseline measurements of the left and right ventricular dimensions, left ventricular mass, ventricular wall thickness, and valve function. The baseline left ventricular end-diastolic pressure (LVEDP) was measured with a micromanometer-tip pigtail catheter (Millar Mikro-Tip Catheter; Millar Instruments, Houston, Tex) inserted via the left carotid artery. After baseline hemodynamic measurements were made, baseline endomyocardial biopsy specimens were taken from the left ventricle via a transaortic route. With the sheep in stable condition, a baseline left ventriculogram was performed to assess mitral valve function. The pigtail catheter was removed, and a reusable biopsy and retrieval forceps (Cook Urological Inc., Spencer, Idaho) were introduced into the left ventricle. Under fluoroscopic guidance, this forceps was used to grasp and cut 1 or more chordae tendineae upon forceful withdrawal, creating severe MR (3+ to 4+ Seller's grade [127]) (**Figures 9.1A and 9.1B**). This condition was defined by a high degree of opacification of the left atrium 2 beats after left ventricular contrast injection. After creation of the MR, the left carotid artery was repaired, and the sheep was allowed to recover. This procedure has previously been described elsewhere [155]. During the follow-up period, the sheep underwent echocardiography every 2 weeks to detect volume-overload heart failure.

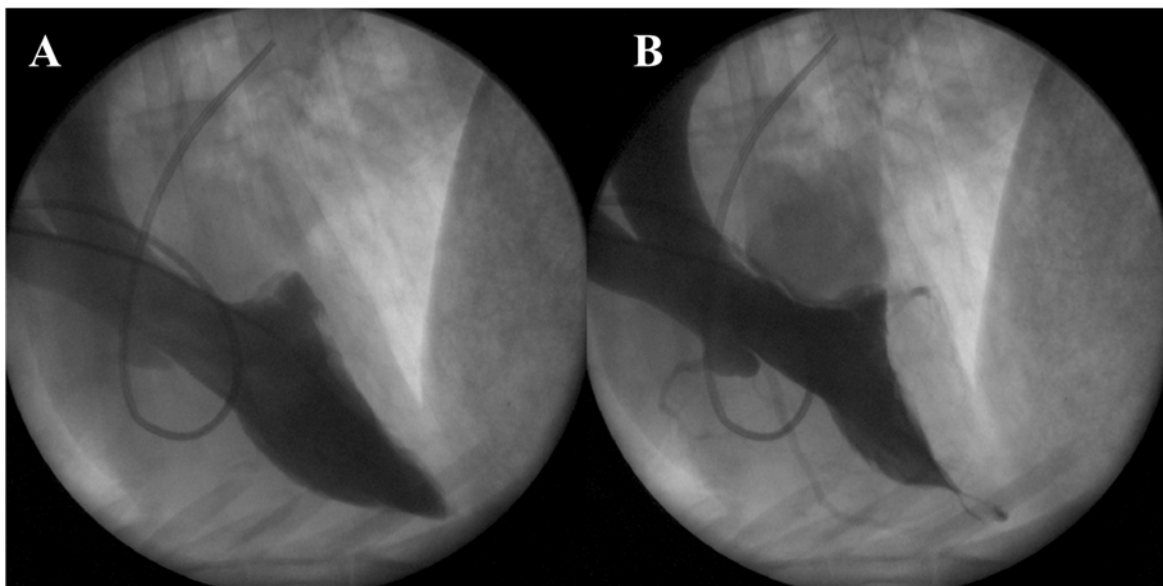


Figure 9.1A and 9.1B: (A) Normal ventriculogram obtained before creation of mitral regurgitation (MR). (B) After chordal disruption, the ventriculogram shows 2nd- to 3rd-degree MR.

9.3.2.3 2nd Operation: Implantation of an LVAD (20th Week)

Levitronix CentriMag LVAD. The Levitronix CentriMag LVAD is a sterile, single-use, disposable, and centrifugal pump. The pump's 32-mL priming volume minimizes the wetted surface area and helps to limit the need for intravenous fluids during surgery. The pump inlet is on the rotational axis of the rotor; the pump outlet is perpendicular to the inlet and tangential to the outer diameter. Both the inlet and outlet ports are standardized 3/8-inch barbed connectors for easy application to standard medical-grade 3/8-inch tubing. The blood pump design is based on magnetic-levitation motor-bearing technology that allows pumping without mechanical bearings and seals. The pump's rotor "floats" in a rotating magnetic field without mechanical contact, and an external compact digital signal processor system allows precise regulation of the rotor's speed. The pump is designed to provide flow in the range of 0.5 to 9.9 L/min.

The drive console is a microprocessor-based system that includes user interface keys which provide convenient management points for pump operation; a 4-line alphanumeric display for showing the system status; alert and alarm information; 27-segment digital displays that show the pump speed and blood flow rate.

9.3.2.4 HeartWare LVAD

The HeartWare LVAD is described in detail elsewhere [159]. Briefly, the HeartWare LVAD is a small, wearless, and centrifugal blood pump. It has a displaced volume of just 45 cc, weighs 145 g, and can deliver flows of up to 10 L/min.

9.3.2.5 Implantation Technique

For implantation of the CentriMag LVAD, anesthesia was induced routinely, and hemodynamic, echocardiographic, and fluoroscopic measurements were repeated as were the endomyocardial biopsies. A left thoracotomy was then performed in the 5th intercostal space, and the left ventricular apex and descending aorta were exposed for inflow and outflow cannula placement, respectively. After 2 pledgeted, 2-0 braided polyester pursestring sutures were placed on the left ventricular apex and descending aorta, 32F inflow and 20F outflow cannulas were inserted into these 2 structures, respectively. The procedures were done on the beating heart without cardiopulmonary bypass. After the cannulas were tunneled outside the chest wall, they were connected to a centrifugal CentriMag extracorporeal LVAD, and flow was initiated at 4 L/min. Pump flow was measured throughout the study with a 10-mm flow probe (Transonic Systems Inc., Ithaca, New York) on the outflow graft cannula, and unloading of the left ventricle was adjusted according to that chamber's size. Device flow was maintained between 5 and 7 L/min. The LVAD was secured to each

sheep's body with a girth strap. Postoperatively, the animals were treated the same as after the initial operation. Adjunctive esmolol infusion and diuretics were used to control tachycardia and peripheral vascular resistance/urine output, respectively. The animals were given warfarin to keep the international normalized ratio between 2.5 and 3.5.

The same anesthesia and postoperative protocols were used for HeartWare implantation, which has been detailed elsewhere [159].

9.3.2.6 3rd Operation. Hemodynamic, Echocardiographic, and Fluoroscopic Studies after 11 Weeks of LVAD Support (31st Week).

Eleven weeks after placing the LVAD, we remeasured the hemodynamic, echocardiographic, and fluoroscopic variables and repeated the endomyocardial biopsies with the sheep under general anesthesia.

9.3.3 Echocardiographic Assessment

Echocardiographic assessment was performed according to the guidelines of the American Society of Echocardiography [48] by an echocardiologist using a Sonos 2000 ultrasound system (Hewlett-Packard Co., Palo Alto, Calif) equipped with a 2.5-MHz phased-array transducer.

9.3.4 Histopathologic Evaluation

Endomyocardial biopsies were performed before MR creation (baseline), during the 2nd operation (week 20), and during the 3rd operation (week 31) and were evaluated with transmission electron microscopy. Macroscopic postexplant analyses of the pump were also done after termination of the study.

9.3.5 Immunohistochemical Staining

β -adrenergic receptor, ANP, and ET-1 levels were selected as markers of heart failure and were fluorescently labeled. Fluorescence was quantified as pixel densities of specific colors in split color images, using Corel Draw (Corel Corporation, Ottawa, ON, Canada) and Sigma Scan Pro software (Aspire Software International, Leesburg, Va).

9.3.6 Quantification of Dystrophin in Ventricular Biopsy Specimens

Expression of dystrophin was quantified by Western blotting of whole tissue lysates prepared from biopsy tissues. Consequently, confocal immunofluorescence was used to obtain robust quantitative information about the number of immunoreactive signals at discrete sites within the cell.

9.4 Results

9.4.1 Induction (Remodeling Phase) and Treatment (Reverse Remodeling Phase) of Heart Failure

In both cases, comparison of hemodynamic, fluoroscopic, echocardiographic, histopathologic, and immunohistochemical data recorded (1) during the 1st operation and (2) immediately before pump implantation confirmed the effectiveness of the heart failure induction protocol.

After the 2nd operation, both sheep recovered from anesthesia without complications and were extubated within the 1st postoperative hour. Eleven weeks after LVAD implantation, they reached the scheduled endpoint without experiencing anorexia, infection, or a neurologic disorder.

9.4.2 Device Examination and Animal Necropsy

The explanted pumps' interior, inflow cannula, and outflow cannula were completely free of thrombus. There was no evidence of ischemia or infarction in any of the peripheral end organs (brain, liver, spleen, and kidneys).

9.4.3 Hemodynamic Data

The mean LVEDP, which was 8 ± 2 mmHg at baseline, increased to 16 ± 2 mmHg immediately after chordal disruption and to 27 ± 4 mmHg during the 2nd operation. After 11 weeks of LVAD support, the mean LVEDP measured 14 ± 2 mmHg.

9.4.4 Fluoroscopic Data

After the mitral chordae tendineae were disrupted, left ventriculography confirmed the presence of 2nd- to 3rd-degree MR (**Figures 9.1A and 9.1B**). During the 2nd operation, repeat ventriculography showed 4th-degree MR and a dilated left atrium. After 11 weeks of LVAD support, ventriculography revealed 4th-degree MR and a dilated left atrium at a pump flow of 5 L/min in both sheep.

9.4.5 Echocardiographic Data

Table 9.1 shows the mean echo- car diographic results obtained during the 1st operation (after mitral chordal disruption), 2nd operation (LVAD implantation), and 3rd operation (after 11 weeks of LVAD support). The echocardiographic data demonstrate that volume-overload heart failure was successfully created in both animals, with a resulting increase in the left ventricular diastolic dimension (LVDD), left ventricular systolic dimension (LVSD), and left ventricular mass. After LVAD support, the echocardiographic measurements improved, with a substantial decrease in the LVDD, LVSD, and left ventricular mass.

Table 9.1 Mean echocardiographic measurements obtained in each individual sheep during the 1st operation (after mitral chordal disruption), 2nd operation (left ventricular assist device (LVAD) implantation), and 3rd operation (after 11 weeks of LVAD support).

Time	LVDD(mm)	LVSD (mm)	IVS (mm)	PW	RVDD(mm)	LA (mm)	EF	LV mass (g)
Sheep 1								
1 st operation	32	22	7	7	19	32	55	201
2 nd operation	59	44	11	9	26	48	44	570
3rd operation	41	26	11	10	29	48	56	210
Sheep 2								
1st operation	36	26	9	9	25	36	65	233
2 nd operation	68	50	13	11	30	56	50	610
3rd operation	45	30	13	12	35	56	64	236

EF: ejection fraction; IVS: interventricular septal thickness; LA: left atrial dimension; LV: left ventricular; LVDD: left ventricular diastolic dimension; LVSD: left ventricular systolic dimension; PW: posterior wall thickness; RVDD: right ventricular diastolic dimension.

9.4.6 Histopathologic Data

Transmission electron microscopy of the myocardial biopsy specimens obtained during LVAD placement (2nd operation) showed a $58 \pm 5\%$ loss of myofilaments in the perinuclear region; the presence of cytoplasmic vacuoles $>1.5 \mu\text{m}$ in diameter decreased by $33 \pm 4\%$ compared to baseline biopsy findings (**Figure 9.2A**). After 11 weeks of LVAD unloading, the percentage of cells with moderate to severe myofilament loss decreased from $58 \pm 5\%$ (at LVAD implantation) to $18 \pm 3\%$. The percentage of cells with cytoplasmic vacuoles $>1.5 \mu\text{m}$ in diameter decreased from $33 \pm 4\%$ to $5 \pm 2\%$. Cardiac myocytes showed an increase in the number and size of their mitochondria (**Figure 9.2B**).

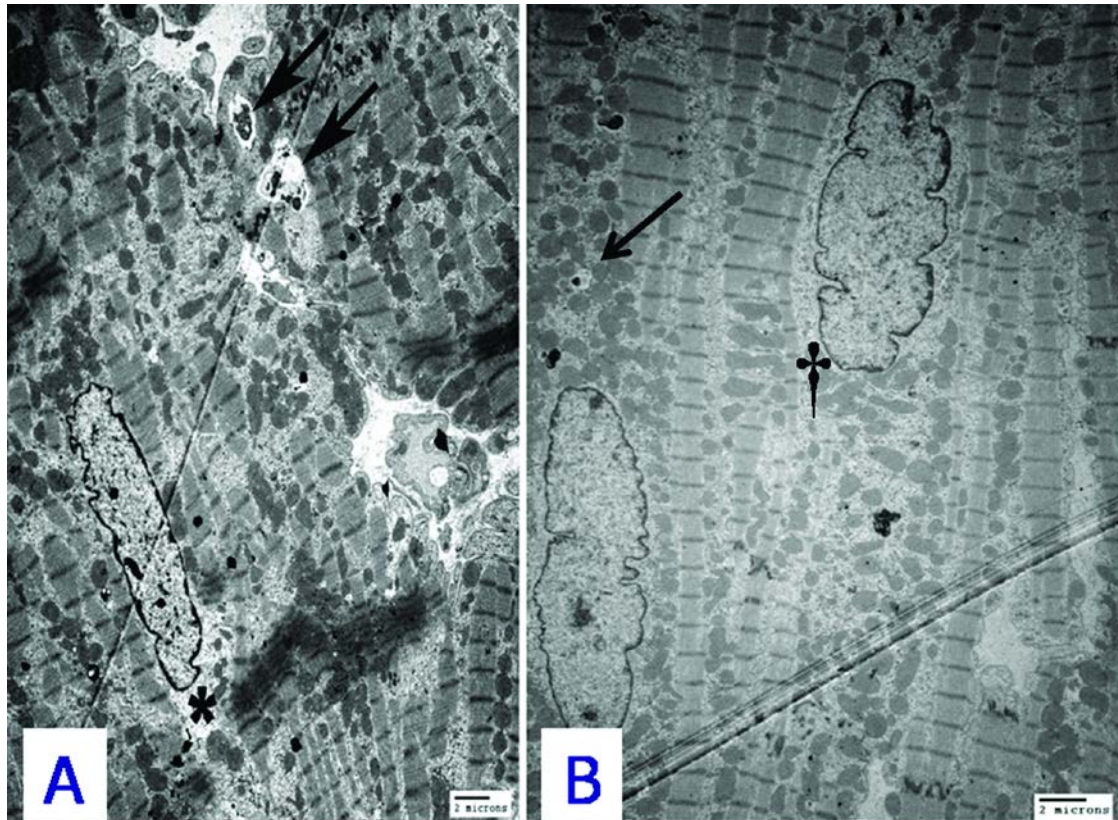


Figure 9.2A and 9.2B: (A) Biopsy specimen obtained at left ventricular assist device (LVAD) implantation, showing a loss of myofilaments in the perinuclear region (asterisk) and the presence of cytoplasmic vacuoles (arrows). (B) Biopsy specimen obtained after 11 weeks of LVAD unloading, showing a reduced loss of myofilaments, with fewer and smaller cytoplasmic vacuoles (arrow) and more and larger mitochondria (dagger). Magnification $\times 2500$; scale bar 2 μM .

Compared to baseline values, there was a marked increase in the fluorescence pixel density for ANP and ET-1 along with a reduction in BAR and dystrophin density (**Figure 9.3**), which is evidence of volume- overload heart failure.

After 11 weeks of LVAD support, biopsy samples showed a marked decrease in fluorescence pixel density for ANP and ET-1, along with an increase in BAR and dystrophin density (**Figure 9.3**) which may be considered a sign of myocardial reverse remodeling.

In our pilot study, the left ventricular diastolic and systolic dimensions increased with heart failure and decreased after LVAD support, although baseline levels were not regained after 11 weeks of LVAD support. The cardiac index and left ventricular mass were elevated during heart failure and returned to near baseline levels after 11 weeks of LVAD support. Together, these results indicated the successful development of heart failure in sheep after chordal disruption, followed by recovery after LVAD support, as determined by physical measurements and hemodynamic data.

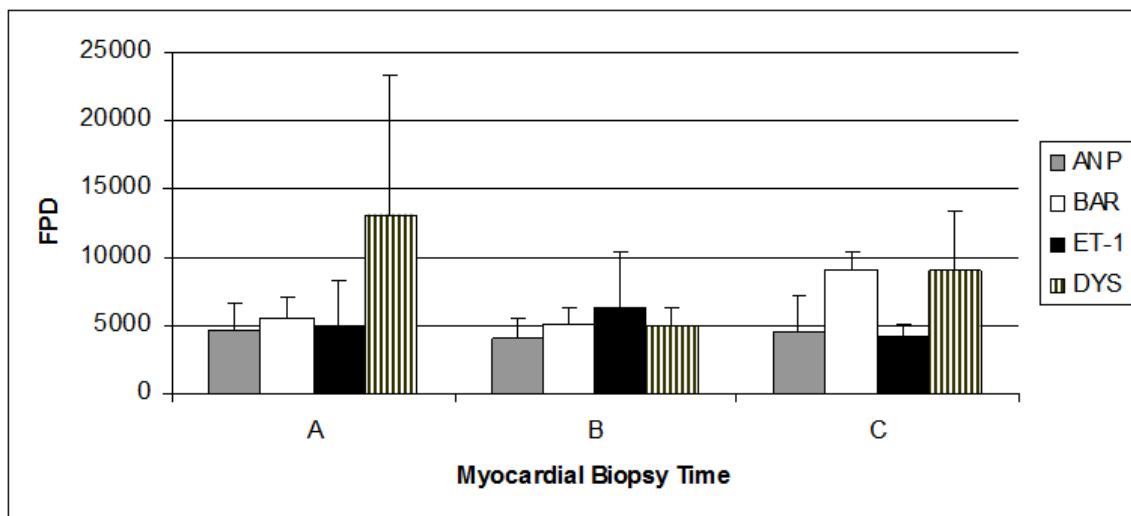


Figure 9.3: Identification of markers in heart failure and recovery. The results are expressed as the mean and standard error for each time point: before induction of heart failure (A), after induction of heart failure (B), and after 11 weeks of LVAD support (C). ANP: atrial natriuretic protein; BAR: β -adrenergic receptors; ET-1: endothelin-1; DYS: dystrophin; FPD: fluorescence pixel density.

We used an adult sheep model, primarily because of the ease with which heart failure can be induced and subsequent LVAD therapy can be applied in this model. Other fundamental advantages of the sheep are the animal's size (which allows placement of a human-sized LVAD), minimal growth rate, ease of management, and hemodynamic similarities to humans. Moreover, the ability to perform sequential biopsies allowed us to monitor the progress of heart failure and to correlate the extent of remodeling and its reversal with ANP, ET-1, BAR, and dystrophin levels. Because our volume-overload heart failure ovine model was not a previously established one, biopsies to detect heart failure creation (remodeling) and postimplant recovery timing (reverse remodeling) were scheduled and performed according to the guiding results of the echocardiographic follow-up data. The echocardiographic findings of volume-overload heart failure (such as ejection fraction, left atrial diameter, left ventricular end-systolic and end-diastolic dimensions, ventricular mass and thickness, etc.) and LVAD recovery correlated well with the animal's clinical picture and hemodynamics, so we also scheduled LVAD implantation and support times according to these echocardiographic results. The changes in dystrophin expression in our pilot study were consistent with the development of heart failure and subsequent recovery after LVAD placement in humans [163]. Because dystrophin has been demonstrated to play a key role in linking the actin cytoskeletal networks and the sarcolemmal dystrophin-associated protein complex, the lack of dystrophin is associated with altered structure and

mechanical adherence of costameres to the underlying cytoskeletal actin network, resulting in cardiomyopathy [164]. Therefore, the possible fragility (disruption) of the dystrophin-actin bonds may be important for tracking early myocardial structural changes in remodeling and reverse remodeling and for developing a more precise animal model of heart failure to test the efficacy of short- or long-term LVAD support. One of our study's limitations was the lack of plasma profiles of dystrophin levels, which may be used as a predictive/clinical biomarker for left ventricular remodeling related to LVAD use. Such plasma profiles will be a main focus of our future studies involving a larger number of animals. Moreover, the location of the outflow-graft anastomosis may be considered another study limitation, as it may not be the anastomotic site currently preferred for most fully implantable LVAD outflow grafts.

9.6 Conclusion

In this pilot experimental study, we have demonstrated an experimental animal model in which we created CHF in 2 adult sheep and subsequently reversed this condition by implanting 2 different centrifugal LVADs (1 device in each animal). The degree of remodeling was indicated by the disruption of dystrophin expression, as well as hemodynamic, echocardiographic, histologic, molecular, and clinical signs of heart failure. The reversal of heart failure (myocardial recovery), by means of mechanical circulatory assistance, was indicated by the normalization of dystrophin expression and integrity. We believe that this technique for creating and subsequently treating CHF with LVAD therapy may be useful in future studies investigating the diagnosis and prevention of CHF.

10

The Effects of Continuous and Intermittent Reduced Speed Modes on Renal and Intestinal Perfusion in an Ovine Model

The contents of this chapter are based on: Tuzun E, Chorpenning K, Liu MQ, Bonugli K, Tamez D, Lenox M, Miller MW, Fossum WF, Rutten M, Dat M, Van de Vosse F, Kadipasaoglu C, de Mol B. The Effects of Continuous and Intermittent Reduced Speed Modes on Renal and Intestinal Perfusion in an Ovine Model. ASAIO J. 2014 Jan-Feb;60(1):19-24.

10.1 Abstract

The effects of the continuous flow output on renal and intestinal microcirculation has not been extensively studied. In order to address this, the Heartware HVAD pump loaded with continuous and intermittent reduced speed (IRS) modes was implanted in four sheep and then operated at low and high speeds to mimic partial and complete unloading of the left ventricle. Then microsphere and positron emission tomography (PET/CT) studies were used to assess renal and intestinal tissue perfusion at various pump speeds and flow modes as compared with baseline (pump off). Arterial and venous oxygen (TO₂) and carbondioxyde (TCO₂) contents were measured to assess changes in intestinal metabolism. Renal and intestinal regional blood flows did not produce any significant changes compared to baseline values in either continuous or IRS modes and speeds. The venous TO₂ and TCO₂ significantly increased in continuous and IRS modes and speeds compared to baseline. Our data suggested that renal and intestinal tissue perfusions were not adversely affected by continuous and IRS modes either in partial or complete unloading. Intestinal venous hyperoxia and increased TCO₂ may be evidence of intestinal arteriovenous shunting along with increased intestinal tissue metabolism. Longer term studies are warranted in chronic heart failure models.

10.2 Introduction

Mechanical circulatory support using an implantable ventricular assist device (VAD) is applied routinely in patients needing temporary circulatory assistance while awaiting cardiac transplantation or to provide permanent support for patients with end-stage heart failure who are not candidates for heart transplantation [31]. While pulsatile flow conditions are considered the most physiologic, continuous-flow VADs (CFVADs) are also being developed to reduce complications associated with pulsatile technology. Some common complications being addressed are infection, thromboembolic events, device failure, and the needs of patients who are too small to be fitted with current pulsatile VADs [55]. LVAD recipients had 1- and 2-year survivals that were 2 to 3 times greater than patients treated with medical therapy alone [116]. Additional studies have demonstrated similar efficacy for LVAD use as a bridge-to-transplant in patients awaiting a donor heart [136]. Early follow-up of CFVAD recipients demonstrated improved functional status and quality of life 3 months after implantation, with a 6-month survival of 75% [86]. Long-term follow-up of patients with CFVADs demonstrated not only preservation of, but also improvement in, hepatic and renal function [119]. Some organs, however, may be very sensitive to non-pulsatile (or reduced-pulsatile) blood flow. Gastrointestinal (GI)

bleeding occurs in 15-30% of patients implanted with a CFVAD and is 10 times more frequent in patients supported with CFVADs than in patients with pulsatile pumps [19,69]. This bleeding appears to be directly associated with reduced-pulsatile blood flow, as similar bleeding is not seen in patients with mechanical valves and comparable levels of anticoagulation [138]. Unfortunately, the mechanisms underlying GI bleeding are not well outlined and need to be understood in order to improve the treatment of patients with congestive heart failure (CHF) needing mechanical circulatory support. Several explanations for the association between GI bleeding and CFVAD interaction have been proposed and include: 1) acquired von Willebrand's disease due to shear stress in CFVAD-implanted patients 2) increased intraluminal pressure coupled with muscular contraction which may result in dilated mucosal veins and the development of arteriovenous communications, 3) neurovascular etiology in which increased sympathetic tone results in smooth muscle relaxation and a subsequent propensity for angiodysplasia or hypoperfusion of the intestines, and 4) lowered pulse pressure which leads to intestinal hypoxia, vascular dilation, and angiodysplasia [145]. Whether the cause of GI bleeding is related to one or a combination of these factors, GI perfusion assessment is crucial to understand the complex interaction between GI bleeding and CFVAD physiology, and to improve device design to prevent or reduce this serious complication.

The primary purpose of our study was to investigate renal and intestinal perfusion changes in response to continuous and intermittent reduced speed modes using microsphere and positron emission tomography/computed tomography (PET/CT) techniques in an acute ovine model implanted with a CFVAD.

10.3 Materials and Methods

10.3.1 HeartWare HVAD

The HeartWare HVAD® Pump (Miami Lakes, FL) is a continuous flow, centrifugal ventricular assist device (VAD). The pump's design has been described elsewhere [66]. For this study, an intermittent reduced speed (IRS) algorithm was implemented using a custom software application developed on a Labview platform (National Instruments, Austin, TX). The IRS algorithm reduced the rotational speed by 20% of the set speed for 5 seconds with a 10 second offset in between each cycle. In this study, we tested 2 continuous modes (low and high flow) and 2 IRS modes (low and high flow). Low continuous (LC) and low IRS (LIRS) modes targeted partial left ventricular unloading with a flow ranging between 2.4 to 3.5 L/min. High continuous (HC) and high IRS (HIRS) modes aimed to fully unload the left ventricle which was possible with flows higher than 3.5 L/min depending on the size of the animal.

During high flow modes the aortic valve was closed and there was some degree of ventricular suction without any premature ventricular contractions confirmed through pressure, flow and EKG signals.

10.3.2 Animal model

Experiments were conducted in healthy Suffolk Cross sheep (n=4), each weighing 68±15 kg. Animals received humane care in compliance with the “Principles of Laboratory Animal Care,” formulated by the National Society for Medical Research, and the “Guide for the Care and Use of Laboratory Animals” (NIH Publication). Our Institute performed the study in accordance with the Animal and Plant Health Inspection Service, United States Department of Agriculture, Animal Welfare Act, 9 CFR, Parts 1, 2, and 3 as applicable; and according to an Animal Use Protocol (AUP) approved by the University’s Institutional Animal Care and Use Committee (IACUC).

10.3.3 Anesthesia and surgical preparation

After the endotracheal intubation, general anesthesia was maintained with Isoflurane (0.5-4.0%) in oxygen (100%). Lactated Ringers solution for fluid support was given IV at a rate of 5-20 ml/kg/h via the venous catheter.

10.3.4 Surgical procedure

The HeartWare HVAD pump was implanted through a left thoracotomy without the use of cardiopulmonary bypass (CPB). The left carotid artery and jugular vein were exposed for monitoring of arterial and venous pressures. Once the heparin (250 IU/kg) was administered, the HeartWare HVAD pump outflow graft was anastomosed to the descending thoracic aorta. A titanium/polyester sewing cuff was sewn to the ventricular apex. Then the HeartWare HVAD pump was inserted into the ventricular apex and secured to the sewing ring. After de-airing the graft, a 10 mm ultrasonic flow probe (Transonics Inc., Ithaca, NY) was attached to the outflow graft for flow measurement. The graft was clamped to avoid retrograde flow into the left ventricle until data collection began. A fluid-filled catheter was inserted into the left ventricle for left ventricular pressure monitoring.

Via a left flank incision to the abdomen, 14 gauge catheter was inserted into the cranial mesenteric vein to selectively capture intestinal venous drainage and for serial venous blood gas measurements to calculate intestinal metabolism. The catheter end was tunneled through the skin. The chest and abdomen were closed in

single layer with a #1 nylon suture to avoid exposure to room air. The animal was then transported to the PET/CT suite.

10.3.5 Hemodynamic Assessments

After pump implantation, hemodynamics were allowed to stabilize for 60 minutes. Hemodynamics were assessed at the baseline and with the pump operating at the four experimental settings described previously (LC, HC, LIRS, HIRS modes). After each change to a new pump setting, hemodynamics were allowed to stabilize for 30-45 minutes before collecting hemodynamic data. Microsphere injections were performed concomitantly, immediately followed by Cu62 injections. Heart rate (HR), systolic aortic pressure (AoPs), diastolic aortic pressure (AoPd), mean aortic pressure (AoPm), pulse pressure (PP), central venous pressure (CVP), LV systolic pressure (LVP), and pump flow (PF) were measured at each setting.

Pressure and flow data were continuously recorded with a computer data acquisition system (ADInstruments Power Lab ML880, LabChart Pro, Colorado Springs, CO)

10.3.6 Intestinal and renal blood perfusion assessment with microspheres

Regional blood flow (RBF) distribution to the proximal jejunum, distal ileum and right renal cortex was evaluated by microsphere analysis using 15µm nonradioactive microspheres (BioPAL, Worcester, MA), as described in detail elsewhere [109]. Briefly, the labeled microspheres (gold, samarium, ytterbium, europium, terbium) were injected into the left atrium at the baseline and at each experimental pump setting (LC, HC, LIRS, HIRS modes). Arterial reference blood samples were taken from the left common carotid artery and used for normalizing tissue sample readings. At study termination, target abdominal organs were harvested and two grams of tissue were taken from each for microsphere analysis. A neutron activation technique was used to detect microspheres in tissue samples.

10.3.7 Intestinal and renal blood perfusion assessment with PET/CT

The animal was transported to the PET/CT suite (Siemens 128 slice Biograph mCT PET/CT, Siemens Molecular Imaging, Knoxville, TN) and secured to the CT table in right lateral recumbency. A baseline CT study was obtained to provide anatomic reference and attenuation correction. Omnipaque 350 (1±0.1 mL/kg IV) was infused at a rate of 4 mL/sec during CT scans to highlight the blood pool. Abdominal PET perfusion studies were performed for baseline as well as for each pump setting. ⁶²Cu-PTSM (⁶²Cu-labeled pyruvaldehyde bis (N-4-methylthiosemicarbazone)

copper), a freely diffusible, metabolically trapped perfusion tracer, was infused IV at a dose of 5-10 mCi/animal/study, during each PET study. All studies were compensated for body mass and the actual amount of tracer injected. Scans were started 10 seconds prior to infusion to obtain baseline activity information, and data were acquired listmode for 600 seconds total duration. Image data were re-framed at 3 sec/fr for the first 20 frames to accurately define the input bolus, followed by 1 min/fr to obtain the final disposition. All intestinal and renal perfusion images were reconstructed iteratively with Ordered Subsets Expectation Maximization (OSEM), scatter and attenuation correction applied. Approximately 30-45 minutes of interval was given for ^{62}Cu decay (9.67 min half-life) and hemodynamic adjustment to the new speed change. The arterial input function (AIF) was extracted from the time sequence images using automated methods (U.S. Patent Application 61/736,242) and applied to the remainder of the regions of interest to generate parametric images of tissue perfusion. This automated approach allowed the selection an AIF from the entire 3-D volume at one time, which increased the quantitative measurement efficiency and inter-operator consistency.

10.3.8 Intestinal arterio-venous oxygen difference assessment

Immediately prior to each microsphere injection, arterial and venous blood samples were concomitantly withdrawn from the carotid artery and cranial mesenteric vein catheters. This occurred at baseline and at each subsequent speed setting to calculate intestinal arteriovenous oxygen difference and CO_2 production (TCO_2) changes which are indirect indicators of arteriovenous shunting (AVS) or low oxygen utilization (LOU) and cell metabolism. The differentiation between AVS and LOU is based on the formula proposed by Rozin et al.: ($\text{Venous TCO}_2 - \text{Arterial TCO}_2$) [118]. Increased or unchanged CO_2 production along with venous hyperoxia compared to baseline is considered a result of AVS whereas decreased CO_2 production is considered sign of LOU.

10.3.9 Statistical analysis

All statistical tests were performed using Microsoft Office Excel software (Microsoft Corp., Redmond, WA). Analysis of variance (ANOVA) was used to compare continuous variables. P values of < 0.05 were considered significant.

10.4 Results

All sheep (n=4) underwent successful pump implantation, experienced no surgical complications or mechanical device failures, and survived to study termination.

10.4.1 Hemodynamic assessments

Hemodynamic data and LVAD related parameters are summarized in **Table 10.1**. The interactions between AoPs, AoPm, AoPd, PP and CVP at baseline and the different pump settings are shown in **Figure 10.1**. Changes in LVP at different pump settings are shown in **Figure 10.2**.

HR, AoPs and AoPm were not significantly affected compared with baseline values at different pump settings. AoPd increased significantly at HC and LIRS settings ($p < 0.05$ vs baseline) whereas no significant changes were observed in LC and HIRS modes despite higher AoPd values compared with baseline settings. PP was maintained close to baseline values at CL setting, whereas significant decreases were observed at CH, LIRS and HIRS settings. LIRS and HIRS settings had higher PP compared with CH but the difference was not statistically significant. CVP remained near baseline values at all speed changes. At LC and LIRS settings, LVP remained close to baseline values without significant statistical changes. LVP decreased significantly at HC and HIRS settings compared with baseline, LC and LIRS levels, respectively ($p < 0.05$).

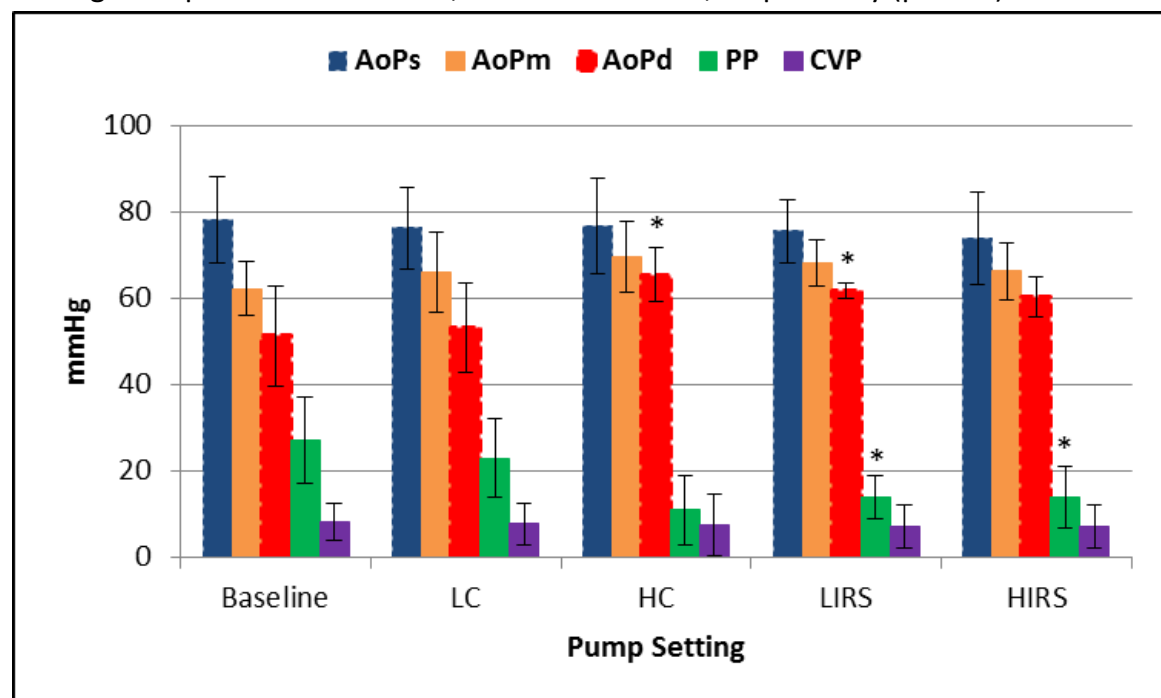


Figure 10.1. Aortic, pulse and central venous pressures before and during pump support. LC, low speed continuous flow mode; HC, high speed continuous flow mode; LIRS, low intermittent reduced speed mode; HIRS, high intermittent reduced speed mode; AoPs, systolic aortic pressure; AoPm, mean aortic pressure; AoPd, diastolic aortic pressure; PP, pulse pressure; CVP, central venous pressure. *, $p < 0.05$ vs baseline.

Table 10.1. Hemodynamic and assist device related data

	Baseline	LC	HC	LIRS	HIRS
HR (bpm)	82±11	80±12	81±8	83±8	82±10
AoPs (mmHg)	78±10	76±9	77±11	76±7	74±11
AoPm (mmHg)	62±6	66±9	70±8	68±5	66±7
AoPd (mmHg)	51±11	53±10	66±6*	62±2*	60±5
PP (mmHg)	27±10	23±9	11±8*	14±5*	14±7*
CVP (mmHg)	8±4	8±5	8±7	7±5	7±5
LVP (mmHg) Set/ Reduced Speed	24±8	24±6/NA	4±11* [‡] /NA	18±3/30±6	12±7/9±4* [†]
Pump RPM at Set/ Reduced Speed	-	1925±150/NA	2825±450/NA	2350±100/ 1880±80	2800±200/ 2240±160
LVAD Flow (L/min) at Set/ Reduced Speed	-	2.4±0.2/NA	3.8±1.4 [‡] /NA	3.3±1.2/ 1.9±0.7	3.6±1.5/ 2.7±1.3 [†]

Values are ± SD. LC, low speed continuous flow mode; HC, high speed continuous flow mode; LIRS, low intermittent reduced speed mode; HIRS, high intermittent reduced speed mode; HR, heart rate; AoPs, systolic aortic pressure; AoPm, mean aortic pressure; AoPd, diastolic aortic pressure; PP, pulse pressure; CVP, central venous pressure; LVP, left ventricular pressure; RPM, rotation per minute; LVAD, left ventricular assist device.

*, p<0.05 vs baseline, ‡, p<0.05 vs LC, †, p<0.05 vs LIRS

10.4.2 Intestinal and renal blood perfusion assessment with microspheres and PET/CT

The results of microsphere and PET/CT analysis of renal and gastrointestinal perfusion are summarized in **Table 10.2**.

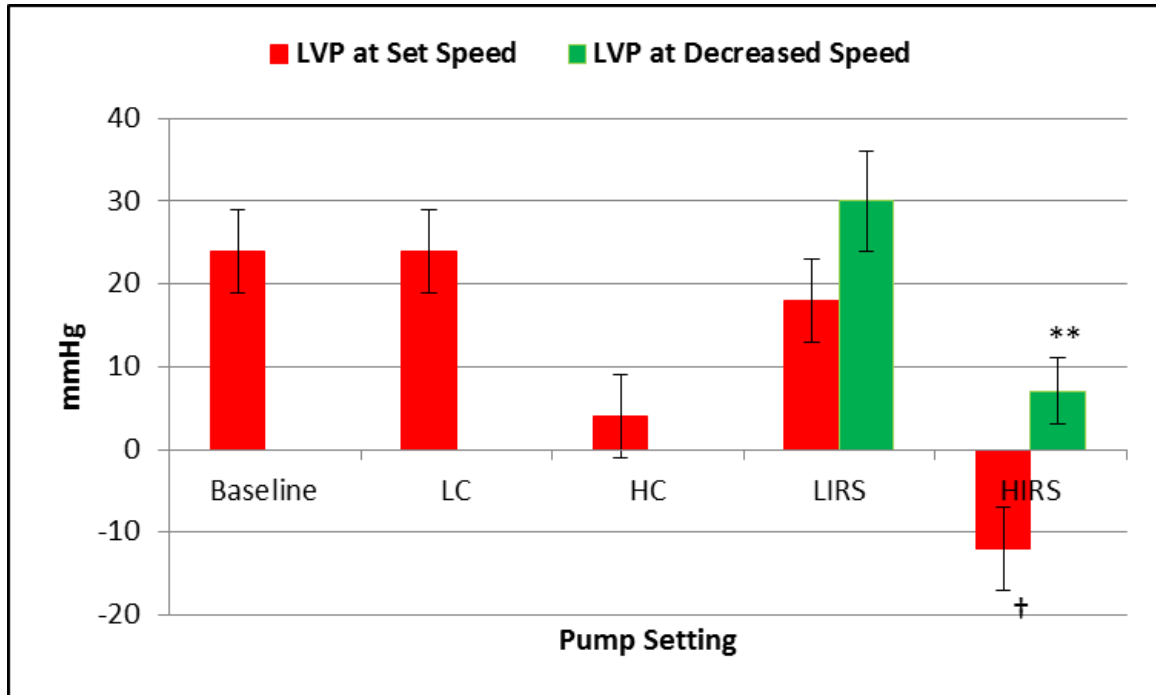


Figure 10.2. Left ventricular pressures before and during pump support. LVP, left ventricular pressure; LC, low speed continuous flow mode; HC, high speed continuous flow mode; LIRS, low intermittent reduced speed mode; HIRS, high intermittent reduced speed mode. *, $p < 0.05$ vs baseline, ‡, $p < 0.05$ vs LC, †, $p < 0.05$ vs LIRS

Table 10.2. RBF analysis with microspheres (upper rows) and PET/CT (lower rows)

	Baseline	CL	CH	LIRS	HIRS
Right renal cortex (mL/min/gr)	3.5±0.8	5.1±1.3	4.7±0.2	4.4±2	4.3±0.5
	5.9±0.7	6.9±0.7	5.8±0.8	6.3±0.7	6.9±1
Proximal Jejunum (mL/min/gr)	1.5±0.8	2.3±0.3	2.2±0.2	2±0.1	2.4±1.6
	1.8±0.4	2.2±0.5	1.7±0.4	1.9±0.4	2.4±0.6
Distal Ileum (mL/min/gr)	0.5±0.1	0.5±0.2	0.6±0.2	1±0.6	0.8±0.4
	0.4±0.1	0.4±0.1	0.4±0.1	0.4±0.1	0.6±0.2

Values are \pm SD. LC, low speed continuous flow mode; HC, high speed continuous flow mode; LIRS, low intermittent reduced speed mode; HIRS, high intermittent reduced speed mode.

As shown in **Figure 10.3A and 10.3B**, kidney, proximal jejunum and distal ileum regional perfusions measured with microspheres increased in all pump settings except the CL mode compared to baseline levels where the increase was not statistically significant. PET/CT data revealed similar trends of increased perfusion in the kidney and proximal jejunum in CL, LIRS and HIRS modes while distal ileum perfusion remained close to the baseline values and showed non-significant perfusion increases at HIRS mode only.

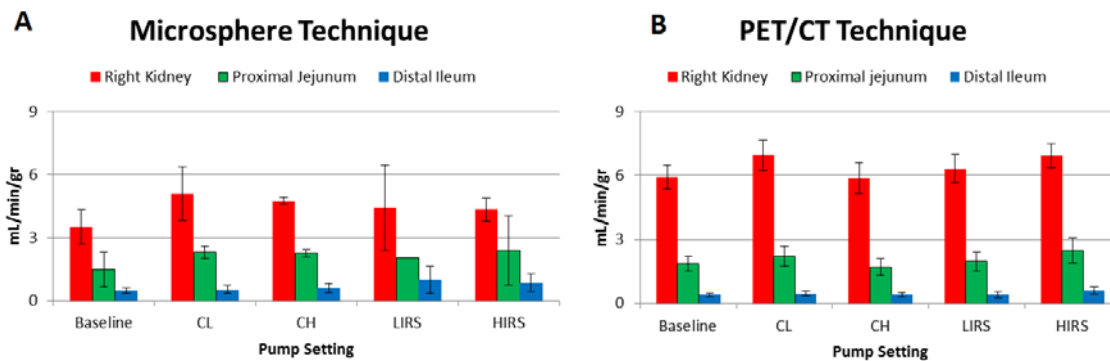


Figure 10.3A and 10.3B. Right kidney, proximal jejunum and distal ileum regional perfusions measured with microsphere (A) and PET/CT (B) techniques. PET/CT, positron emission tomography/computed tomography; LC, low speed continuous flow mode; HC, high speed continuous flow mode; LIRS, low intermittent reduced speed mode; HIRS, high

Serial aortic and cranial mesenteric vein blood gas analysis revealed significant increases in venous partial oxygen pressures at the intestinal level compared to baseline values in all pump flow modes (**Figure 10.4**). Intestinal arteriovenous CO₂ production (TCO₂) significantly increased in all pump settings compared to baseline levels ($p < 0.05$) except LIRS mode ($p = 0.07$) (**Figure 10.5**). There was no statistical significance between various pump settings.

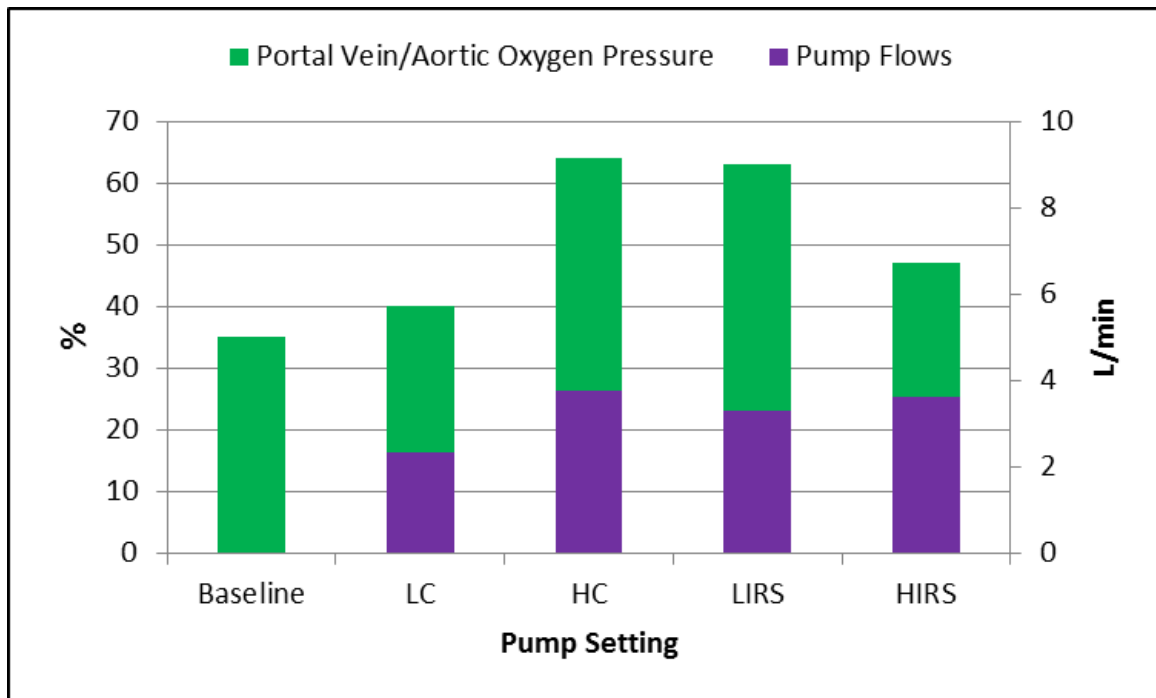


Figure 10.4. Cranial mesenteric vein/aorta partial oxygen pressure ratio and pump flow before and during pump support reduced speed mode. LC, low speed continuous flow mode; HC, high speed continuous flow mode; LIRS, low intermittent reduced speed mode. HIRS, high intermittent reduced speed mode.

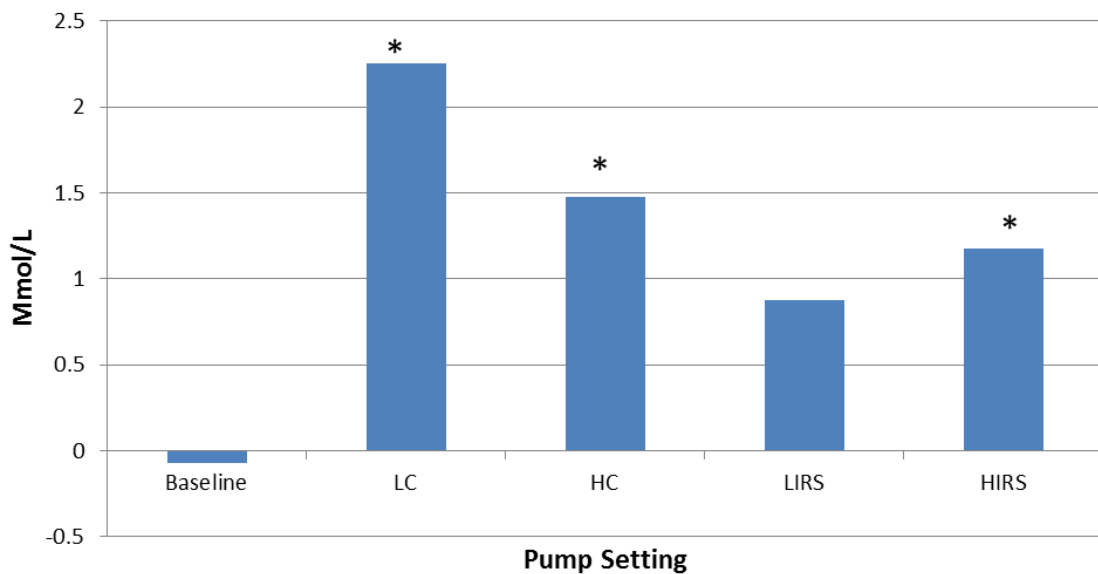


Figure 10.5. Intestinal arteriovenous CO₂ production before and during pump support HIRS, high intermittent reduced speed mode. *, $p < 0.05$ vs baseline

10.5 Discussion

Using an LVAD (Heartware HVAD pump) capable of producing both continuous and intermittent reduced speed flow modes in a healthy ovine model, we have shown that renal, proximal jejunal, and distal ileal regional blood flows measured with

microsphere and PET/CT techniques did not produce any significant over- or under-perfusion changes compared to baseline values in either continuous or reduced pulsatile modes. Although there were fundamental differences between the region-of-interest (ROI) measurements provided with ^{62}Cu PTSM/PET/CT and microspheres techniques, the trends closely matched. The microsphere technique used a very small amount of tissue sample (2-3 gr) to measure the regional blood flow with a high degree of accuracy and relies on capillary size to trap the material, while PTSM is a fully diffusible small molecule that is metabolically bound in place. Nearly all microspheres are lodged in the first pass, while it takes several passes for PTSM to bind. PET/CT provides uniform sampling throughout the field of view, enabling measurement over a large volume of tissue as opposed to microspheres. For example, perfusion over the entire right kidney and gastrointestinal tract was measured with PET/CT versus only 2 grams of tissue samples collected from the right kidney and the first and last 10 cm of small intestine for microspheres. Therefore, since only a small sample was taken for microsphere analysis, small regional differences that can bias a microsphere measurement are evened out statistically by selecting a larger ROI with PET. Although the microsphere technique is widely accepted as a “gold standard” in perfusion assessment studies, our study showed that the PET/CT technique with ^{62}Cu PTSM is equally reliable in renal and gastrointestinal regional perfusion measurements.

The second important observation of our study was a significant increase in cranial mesenteric vein partial oxygen pressures in both continuous and reduced speed flow modes. Selective cannulation of this vein allowed us to measure changes in partial oxygen pressures specific to the small and large intestines. Considering that this is a healthy heart model, under partial (CL, LIRS modes) or full (HC, HIRS modes) ventricular unloading simulations, the total cardiac output and blood flow to the intestines theoretically should not change, nor should intestinal tissue perfusion, which was proven with microsphere and PET/CT measurements. Therefore, the only variable which may cause immediate venous hyperoxia is the effect of the continuous flow physiology. Two conditions, AVS and LOU, may exist simultaneously as result of venous hyperoxia in the tissues; thus, there is a need to differentiate one condition from the other. It is well known that under normal tissue perfusion conditions, one O_2 molecule is utilized as one CO_2 molecule is produced; however, LOU is associated with low CO_2 production. Therefore, AVS may be associated with relatively high O_2 utilization from the capillary vessels and increased CO_2 production. Our studies revealed a significant increase in TCO_2 production at the intestinal region in both continuous or reduced speed modes as calculated by the formula proposed by Rozin et al. [118]. We believe that this is strong evidence of immediate intestinal AVS opening under continuous flow physiology without intestinal tissue perfusion

defect as proved by microsphere and PET/CT measurement. Although one may speculate that the immediate occurrence of AVS at the gastrointestinal level may be linked to the development of intestinal arteriovenous malformations and intestinal bleeding complication, we refrain from making such predictions without chronic in-vivo studies.

Favorable outcomes of the continuous-flow technology are mostly attributed to device-related benefits such as smaller pump size, ease of implantation, reduced infection and postoperative bleeding rates, rather than the flow pattern itself. Therefore, there is a growing interest to provide more induced pulsatility to the circulatory system of the patients supported by continuous flow pumps in order to provide better unloading without left ventricular suction, aortic valve opening, pulse transmission and end-organ perfusion [2,105]. In our study, the perfusion trends in target organs (renal and gastrointestinal system) were similar in both continuous and intermittent reduced speed modes which are similar to one of our earlier studies comparing the effects of continuous flow and induced pulse modes on renal perfusion [23]. Nevertheless, it must be considered that in our current experiments only one asynchronous intermittent reduced speed mode under low and high pump flow conditions was used. Additional studies are needed in order to investigate the effects of the EKG triggered and/or other artificially induced pulse modes on various end-organs. To our knowledge, there are no previous studies investigating the acute or chronic effects of pure continuous or induced pulse flow physiology on gastrointestinal perfusion and AVS formation provided by a continuous flow ventricular assist device. Our acute study is the first and only in-vivo study focused on this topic.

Our study did possess some limitations. First, this is a healthy and anesthetized animal model which does not directly simulate the real chronic heart failure and awake patient clinical scenario. Second, our study used relatively small animal numbers but we believe that the consistency of our preliminary results in these four animals are important and may shed some light toward future studies focused on this topic. Third, the sheep is an herbivore with four stomachs that have nearly a 20-30 liter capacity. Their small intestine is 7 times longer than that of humans and does not precisely simulate human omnivore histology and physiology. Nevertheless, considering the relatively minimal limitations of using animal models for assist device testing, we believe that our results provide some insight into unknown complex device-intestine interaction.

10.6 Conclusion

Results of the present study suggest that renal and intestinal tissue perfusion is not adversely and differentially affected by a cardiac assist device loaded with continuous and intermittent reduced speed modes. Immediate cranial mesenteric venous hyperoxia and increased CO₂ production occurred during all pump modes and may be evidence of intestinal arteriovenous shunting. Longer term studies are warranted to test the validity of these findings in chronic heart failure models.

11

Discussion

11.1 Main findings

11.1.1 Continuous flow cardiac assist adversely alters aortic valve functions in a mock-loop circulation

This study was performed in collaboration with Technical University of Eindhoven (TUE), HemoLab and Texas Heart Institute Cardiovascular Surgical Research Laboratories (THI-CVRL) with the involvement of master and PhD students, cardiovascular surgeons and engineers. The validity of the mock circulatory system was initially confirmed by our ability to produce physiologic pressure and flow waveforms for normal heart function with no functioning LVAD support. Once the system was validated, we incorporated CFLVAD function into the model at increasing pump speeds, which correlated with clinically used pump settings. In this mock-loop system integrated with an LVAD, we were able to simulate healthy and failing heart clinical scenarios, to show the increasing pressure overload above the aortic valve and impaired leaflet opening at increasing CFLVAD supports which may be a link between aortic leaflet fusion or regurgitation in CFLVAD implanted patients. Since the aortic valve used in this study was a mechanical valve, we were unable to assess the acute effects of the CFLVAD physiology on aortic root and leaflets structure and we decided to perform an ex-vivo study for further investigation.

11.1.2 Continuous flow cardiac assist adversely alters aortic valve functions and root structure in a swine ex-vivo beating heart model

Although we performed our preliminary studies on in-vitro mock loop models, we believe that a mock-loop loaded with a mechanical valve and rigid tubes wouldn't have sufficient hemodynamic and structural similarity to a native heart valve to support our findings and to translate these into loads on a native valve. Therefore, we chose this established model of ex-vivo beating heart model to better assess the aortic valve and continuous flow VAD interaction under more realistic conditions. In this study, we demonstrated that normal cardiac hemodynamic performance was achieved both qualitatively, in terms of pulse waveforms (Aop, LVAP, LAP), and quantitatively, in terms of average cardiac output and pressures (PV loops). In most of the studies cardiac performance was controlled and kept at normal levels for up to 4 hours, with only minor deterioration of hemodynamic performance with the collaborative work of cardiovascular surgeons, engineers, scientists, master and PhD students. Furthermore, this model enabled us to use the epicardial echocardiography to assess the leaflet functions and flow dependent morphological changes at the leaflets and aortic root such as flow stagnation, leaflet and aortic root dilation and/or

aortic regurgitation in response to CFLVAD speed changes. Another advantage of the model is that we used fresh pig hearts acquired from a local slaughterhouse which was beneficial from a time, cost and ethical perspective but also allowing us to have access to a virtually unlimited supply of fresh hearts. Our ex-vivo beating heart model created by multidisciplinary approach successfully showed the acute deformation and the impaired opening of the aortic leaflets as well as the aortic root dilatation secondary to increasing CFLVAD supports. We believe that this study confirmed the accuracy of our previous data with mock-loop and provided further solid scientific information to the medical community in order to understand the pathophysiology of the aortic leaflet fusion and/or regurgitation in CFLVAD implanted patients.

11.1.3 The Effect of Intermittent Low Speed Mode on Aortic Valve Opening in Calves Supported With a Jarvik 2000 Axial-Flow Device

This study demonstrated that intermittent low speed mode successfully allowed the aortic valve to open under continuous flow conditions. This is particularly important to avoid aortic valve fusion and/or regurgitation in clinical settings. We believe that this study will give some insight to the biomedical community to further improve continuous flow pump design.

11.1.4 Continuous flow cardiac assist causes opening of intramyocardial arteriovenous shunts in a swine ex-vivo beating heart model

Using the same ex-vivo beating heart model loaded with a CFLVAD, our team demonstrated several indirect evidences of intramyocardial arteriovenous shunt occurrence on both right and left ventricles along with protected myocardial cell metabolism in increasing CFLVAD supports. Since our model allowed us to eliminate most of the uncontrollable effects on myocardial perfusion such as anesthetics, body autoregulation and/or neurohumoral mechanisms, we were able to assess purely acute mechanical effects of the reduced or non-pulsatile flow on myocardial perfusion since the hearts were totally denervated. We believe that the occurrence of the intramyocardial arteriovenous shunts under CFLVAD support may be particularly important in patients developing RV failure after CFLVAD implantations as well as in patients supported for bridge to recovery. The preliminary data collected from this acute multidisciplinary and translational research may shed some light on this complex interaction and may give some insight for the future studies.

11.1.5 Continuous flow cardiac assist changes myocardial hemodynamics, physiology and perfusion in a healthy bovine model but did not adversely affect brain and kidney perfusions

Although we were able to collect valuable preliminary data from our in-vitro and ex-vivo our studies, we decided to perform an in-vivo study to validate and improve our existing data in a more clinically relevant model. In this experimental study, our team which was built from cardiovascular surgeons, engineers, scientists and students investigated myocardial, renal and cerebral perfusion changes under continuous or reduced flow physiology in 8 healthy calves implanted with an axial flow pump. Our new data supported the accuracy of our preliminary studies and proved the importance of the in-vitro and ex-vivo work on the road from bench to clinical testing and development. Nevertheless, since our new in-vivo studies were performed on a healthy bovine model, we decided to move forward and create a heart failure model in order to better simulate the clinical scenario.

11.1.6 Continuous or induced pulse flow modes did not differentially affect cardiac (right and left ventricular), renal or cerebral perfusion in a canine model of doxorubicin-induced heart failure

In this study, we, cardiac surgeons, cardiologists, engineers, veterinarians, pathologists and industry partners, created a doxorubicin induced chronic selective left heart failure in canine model implanted with a centrifugal cardiac assist device which was loaded with a custom made induced pulse mode. Therefore, we were able to assess not only the effects of the continuous flow physiology on myocardium (right and left ventricles), kidneys and brain in a failing heart model, but the effects of the induced pulsatile physiology as well. This was the first publication in this field reporting that continuous or induced pulse modes do not differentially affect end-organ perfusions. Moreover, we were also able to introduce a reproducible modified model of heart failure to the mechanical assist device community which can be used in chronic studies for device testing, development and/or end-organ interaction assessments.

11.1.7 The location of the outflow graft anastomosis (ascending vs descending aorta) does not adversely and differentially affect right and left ventricular perfusion in healthy bovine implanted with continuous flow cardiac assist device.

In clinical practice, ascending aorta location is preferred to descending one for CFLVAD outflow graft anastomosis since it provides a better aortic root washout. However, the effects ventricular assist device outflow-graft site (ascending vs descending aorta) on myocardial perfusion has never been studied. In this acute in-vivo study, despite anatomic limitations of the very short bovine ascending aorta, we managed to perform the ascending aortic anastomosis without the use of cardiopulmonary bypass and mimic the human anatomy to a great extent. At the end of the study, we were able to show that myocardial perfusions were not differentially affected by the outflow graft location. This was the first and only report in the literature comparing the effect of the outflow graft locations on myocardial perfusion.

11.1.8 Continuous flow cardiac assist provides myocardial reverse remodeling in an experimentally created volume overload ovine heart failure model

In this chronic experimental study (approximately 5 months of duration), we have demonstrated an experimental animal model in which we created volume overload heart failure in 2 adult sheep and subsequently reversed this condition by implanting 2 different centrifugal CFLVADs. The degree of remodeling was indicated by the disruption of dystrophin expression, as well as hemodynamic, echocardiographic, histologic, molecular, and clinical signs of heart failure. The reversal of heart failure (myocardial recovery), by means of mechanical circulatory assistance, was indicated by the normalization of dystrophin expression and integrity. Our team formed from cardiovascular surgeons, cardiologists, engineers, pathologists, immunologists and students believe that this technique for creating and subsequently treating heart failure with CFLVAD therapy may be useful in future studies investigating the diagnosis and prevention of heart failure.

11.1.9 Continuous flow or induced pulse mode cardiac assistance does not adversely and differentially affect renal or intestinal perfusion but causes indirect evidences of intestinal arteriovenous shunting in healthy ovine model

Using a continuous flow cardiac assist device capable of producing both continuous and induced pulse flow modes, we have shown that renal, proximal jejunal, and distal ileal regional blood flows measured with microsphere and PET/CT techniques did not produce any significant over- or under-perfusion changes compared to baseline values in either continuous or reduced pulsatile modes. Nevertheless, we also observed that there was an immediate and significant increase in cranial mesenteric vein partial oxygen pressures (hyperoxia) and venous carbondioxide

production after the initiation of both continuous and induced pulse flow modes which may be an indirect evidence of intestinal arteriovenous shunting. This is the first experimental work in this field reporting the potential link between gastrointestinal bleeding complications and arteriovenous shunt formation with advanced imaging and microsphere techniques, as well as a comparison between continuous flow and induced pulse physiology at the gastrointestinal and renal system.

11.2 Wrap-up and conclusions

In our in-vitro, ex-vivo and in-vivo studies we were able to demonstrate that the aortic valve opening is reduced or eliminated due to increased pressure overload during continuous flow cardiac assist device support. However the long term effects of that increased tensile and decreased shear loading on side-specific changes in aortic leaflet cell behavior are still unknown and need to be investigated in chronic experimental heart failure models, as well as in bioreactor and cell culture studies. The information gained from these studies will not only be very helpful in understanding the mechanism and the time course of aortic insufficiency or fusion after the continuous flow cardiac assist device implantation, but will also help to develop a definitive preventive strategy by investigating the effects of the induced pulse modes on aortic valve mechanics and structure, and by improving the pump designs in order to work better with the native cardiac physiology. Moreover, an improved device design may help to reduce or prevent potential intramyocardial or gastrointestinal arteriovenous shunts and provide better functional and structural left and right ventricular recovery and reverse remodeling, as well as to reduce gastrointestinal bleeding complications.

We successfully used mock-loop and ex-vivo beating heart models to mimic the real clinical scenarios and test our hypothesis, and then develop or modify acute and/or chronic healthy and failing heart animal models in order to validate our preliminary data. This methodological approach from bench (in-vitro) to clinic (in-vivo) allowed us to demonstrate the necessity, importance and accuracy of these models in understanding device/end-organ interactions.

References

1. Addetia AM, Callaghan JC. Intramyocardial arteriovenous shunting of blood with nonpulsatile perfusion. *J Thorac Cardiovasc Surg* 1981;81(2):219-26.
2. Ando M, Nishimura T, Takewa Y, Yamazaki K, Kyo S, Ono M, Tsukiya T, Mizuno T, Taenaka Y, Tatsumi E. Electrocardiogram-synchronized rotational speed change mode in rotary pumps could improve pulsatility. *Artif Organs* 2011;35(10):941-7.
3. Armstrong PW, Stopps TP, Ford SE, de Bold AJ: Rapid ventricular pacing in the dog: pathophysiologic studies of heart failure. *Circulation* 1986;74: 1075-1084.
4. Baba A, Dobsak P, Saito I, et al: Microcirculation of the bulbar conjunctiva in the goat implanted with a total artificial heart: effects of pulsatile and nonpulsatile flow. *ASAIO J* 2004;50(4): 321-327.
5. Balachandran K, Sucosky P, Jo H, et al. Elevated cyclic stretch alters matrix remodeling in aortic valve cusps: Implications for degenerative aortic valve disease. *Am J Physiol Heart Circ Physiol* 2009;296:H756.
6. Baldwin RT, Radovancevic B, Conger JL, et al: Peripheral organ perfusion augmentation during left ventricular failure: a controlled bovine comparison between the intraaortic balloon pump and the Hemopump. *Tex Heart Inst J* 1993;20: 275-280.
7. Baradaran S, Dembitsky WP, Jaski B, et al. Left ventricular outflow tract obstruction associated with chronic ventricular assist device support. *ASAIO J* 2002;48(6):665-7.
8. Beloni FL: The local control of coronary blood flow. *Cardiovasc Res* 13: 63–85, 1979.
9. Bristow MR. β -Adrenergic receptor blockade in chronic heart failure. *Circulation*, 2000;5:558–569.
10. Brutsaert DL. Cardiac endothelial-myocardial signaling: its role in cardiac growth, contractile performance, and rhythmicity. *Physiological Reviews* 2003;83(1):59–115.
11. Butcher JT, Nerem RM. Valvular endothelial cells and the mechanoregulation of valvular pathology. *Philos Trans R Soc Lond B Biol Sci* 2007;29;362(1484):1445-57.
12. Butcher JT, Penrod AM, Garcia AJ, Nerem RM. Unique morphology and focal adhesion development of valvular endothelial cells in static and fluid flow environments. *Arterioscler Thromb Vasc Biol* 2004;24(8):1429–34.
13. Cecchi F, Sgalambro A, Baldi M et al. Microvascular dysfunction, myocardial ischemia, and progression to heart failure in patients with hypertrophic cardiomyopathy. *J Cardiovasc Transl Res* 2009;2(4):452-61.

14. Charloux A, Piquard F, Doutreleau S, Brandenberger G, Geny B: Mechanisms of renal hyposponsiveness to ANP in heart failure. *Eur J Clin Invest* 2003;33: 769-778.
15. Chow E, Brown CD, Farrar DJ: Effects of left ventricular pressure unloading during LVAD support on right ventricular contractility. *ASAIO J* 1992;38: M473-M476.
16. Connelly JH, Abrams J, Klima T, Vaughn WK, Frazier OH. Acquired commissural fusion of aortic valves in patients with left ventricular assist devices. *J Heart Lung Transplant* 2003;22(12):1291-5.
17. Cooley DA: Initial clinical experience with the Jarvik 2000 implantable axial-flow left ventricular assist system. *Circulation* 2002;105: 2808-2809.
18. Cowger J, Pagani FD, Haft JW, Romano MA, Aaronson KD, Kolias TJ. The development of aortic insufficiency in LVAD-supported patients. *Circulation Heart Failure* 2010;3:668-674.
19. Crow S, John R, Boyle A et al. Gastrointestinal bleeding rates in recipients of nonpulsatile and pulsatile left ventricular assist devices. *J Thorac Cardiovasc Surg.* 2009;137(1):208-15.
20. de Hart J, de Weger A, van Tuijl S, Stijnen JM, van den Broek CN, Rutten MC, de Mol BA. An ex vivo platform to simulate cardiac physiology: a new dimension for therapy development and assessment. *Int J Artif Organs* 2011;34(6):495-505.
21. DiGiorgi PL, Smith DL, Naka Y, Oz MC. In vitro characterization of aortic retrograde and antegrade flow from pulsatile and non-pulsatile ventricular assist devices. *J Heart Lung Transplant* 2004;23: 186-192.
22. Drews T, Jurmann M, Michael D, et al. Differences in pulsatile and non-pulsatile mechanical circulatory support in long-term use. *J Heart Lung Transplant* 2008;27:1096.
23. Eya K, Tuzun E, Conger JL et al. Effect of pump-flow mode of novel left ventricular assist device on end-organ perfusion in dogs with Doxorubicin-induced heart failure. *ASAIO J* 2005;51:41-9.
24. Farrar DJ, Compton PG, Hershon JJ, Fonger JD, Hill JD: Right heart interaction with the mechanically assisted left heart. *World J Surg* 1985;9: 89-102.
25. Feigl EO, Neat GW, Huang AH: Interrelations between coronary artery pressure, myocardial metabolism and coronary blood flow. *J Mol Cell Cardiol* 1990;22: 375-390.
26. Finlayson DC: Con: nonpulsatile flow is preferable to pulsatile flow during cardiopulmonary bypass. *J Cardiothorac Anesth* 1987;1: 169-170.

27. Frazier OH, Gregoric ID, Cohn WE. Initial experience with non-thoracic, extraperitoneal, off-pump insertion of the Jarvik 2000 Heart in patients with previous median sternotomy. *J Heart Lung Transplant* 2006;25:499.
28. Frazier OH, Myers TJ, Gregoric ID, Khan T, Delgado R, Croitoru M, Miller K, Jarvik R, Westaby S. Initial clinical experience with the Jarvik 2000 implantable axial-flow left ventricular assist system. *Circulation* 2002;18;105(24):2855-60.
29. Frazier OH, Myers TJ, Jarvik RK, et al. Research and development of an implantable, axial-flow left ventricular assist device: the Jarvik 2000 Heart. *Ann Thorac Surg* 2001;71(3 Suppl): S125-S132.
30. Frazier OH, Myers TJ, Westaby S, Gregoric ID. Clinical experience with an implantable, intracardiac, continuous flow circulatory support device: physiologic implications and their relationship to patient selection. *Ann Thorac Surg* 2004;77: 133-142.
31. Frazier OH, Myers TJ, Westaby S, Gregoric ID: Use of the Jarvik 2000 left ventricular assist system as a bridge to heart transplantation or as destination therapy for patients with chronic heart failure. *Ann Surg* 2003; 237(5): 631–637.
32. Frazier OH, Myers TJ. Left ventricular assist system as a bridge to myocardial recovery. *Ann Thorac Surg* 1999;68: 734-741.
33. Frazier OH, Rose EA, Oz MC, Dembitsky W, McCarthy P, Radovancevic B, Poirier VL, Dasse KA; Multicenter clinical evaluation of the HeartMate vented electric left ventricular assist system in patients awaiting heart transplantation. HeartMate LVAS Investigators. Left Ventricular Assist System. *J Thorac Cardiovasc Surg* 2001;122(6):1186-95.
34. Frazier OH, Shah NA, Myers TJ, Robertson KD, Gregoric ID, Delgado R. Use of the Flowmaker (Jarvik 2000) left ventricular assist device for destination therapy and bridging to transplantation. *Cardiology* 2004;101: 111-116.
35. Frazier OH, Tuzun E, Cohn W, Tamez D, Kadipasaoglu KA, Mallia M. Total heart replacement with dual centrifugal ventricular assist devices. *ASAIO J* 2005; 51, 224–229.
36. Frazier OH. Implantation of the Jarvik 2000 left ventricular assist device without the use of cardiopulmonary bypass. *Ann Thorac Surg* 2003;75:1028.
37. Fukae K, Tominaga R, Tokunaga S, Kawachi Y, Imaizumi T, Yasui H: *The effects of pulsatile and nonpulsatile systemic perfusion on renal sympathetic nerve activity in anesthetized dogs.* *J Thorac Cardiovasc Surg* 1996;111: 478-484.
38. Gewirtz H. Regulating myocardial blood flow in health and disease. *Curr Cardiol Rep* 2009;11:117-124.
39. Golding LR, Murakami G, Harasaki H, et al: Chronic nonpulsatile blood flow. *Trans Am Soc Artif Intern Organs* 1982; 28: 81– 85.

40. Goldstein AH, Pacella JJ, Clark RE: Predictable reduction in left ventricular stroke work and oxygen utilization with an implantable centrifugal pump. *Ann Thorac Surg* 1994;58: 1018–1024.
41. Goldstein D, Oz M, Rose E: Implantable left ventricle assist devices. *N Engl J Med* 1998; 339: 1522–1533.
42. Gralla EJ, Fleischman RW, Luthra YK, Stadnicki SW: The dosing schedule dependent toxicities of adriamycin in beagle dogs and rhesus monkeys. *Toxicology* 1979;13: 263-273.
43. Gregoric ID, La Francesca S, Myers T, et al. A less invasive approach to axial flow pump insertion. *J Heart Lung Transplant* 2008;27:423.
44. Griffith LD, Shoor PM, Dilley RB, Bernstein EF. Beneficial effects of nonpulsatile left ventricular bypass on myocardial energy utilization: interaction of oxygen demand and supply. *Trans Am Soc Artif Intern Organs* 1978;24:298-304.
45. Hama N, Itoh H, Shirakami G et al. Rapid ventricular induction of brain natriuretic peptide gene expression in experimental acute myocardial infarction. *Circulation* 1995;9(6):1558–1564.
46. Heart disease and stroke statistics: 2005 update. Dallas: American Heart Association; 2005.
47. Hendry PJ, Nathan H, Rajagopalan K: Right ventricular blood flow during left ventricular support in an experimental porcine model. *Ann Thorac Surg* 1996;61: 1199-1204.
48. Henry WL, DeMaria A, Gramiak R, et al: Report of the American Society of Echocardiography Committee on Nomenclature and Standards in Two-dimensional Echocardiography. *Circulation* 1980;62: 212–217.
49. Henze E, Schoser K, Lietzenmayer R, Schnur G, Sauer M, Kunz R, Clauser M, Adam WE. Studies of myocardial metabolism using P-31-NMR spectroscopy and a simple heart perfusion model of slaughtered animals--an approach to avoiding in vivo animal experiments. *Z Kardiol* 1989 Sep;78(9):553-60.
50. Henze T, Stephan H, Sonntag H: Cerebral dysfunction following extracorporeal circulation for aortocoronary bypass surgery: no differences in neuropsychological outcome after pulsatile versus nonpulsatile flow. *Thorac Cardiovasc Surg* 1990;38: 65-68.
51. Hetzer R, Potapov EV, Weng Y, et al. Implantation of MicroMed DeBakey VAD through left thoracotomy after previous median sternotomy operations. *Ann Thorac Surg* 2004;77:347.
52. Holman WL, Bourge RC, Fan P, Kirklin JK, Pacifico AD, Nanda NC: Influence of left ventricular assist on valvular regurgitation. *Circulation* 1993;88(5 Pt 2): II309-II318.

53. Hunt SA, Baker DW, Chin MH et al. ACC/AHA guidelines for the evaluation and management of chronic heart failure in the adult: executive summary. A report of the American College of Cardiology/American Heart Association task force on practice guidelines (committee to revise the 1995 guidelines for the evaluation and management of heart failure). *Circulation* 2001;104(24):2996–3007.
54. Jarvik R, Westaby S, Katsumata T, Pigott D, Evans RD. LVAD power delivery: a percutaneous approach to avoid infection. *Ann Thorac Surg* 1998;65: 470-473.
55. John R, Kamdar F, Liao K, Colvin-Adams M, Boyle A, Joyce L. Improved survival and decreasing incidence of adverse events with the HeartMate II left ventricular assist device as bridge-to-transplant therapy. *Ann Thorac Surg* 2008 Oct;86(4):1227-34.
56. John R, Mantz K, Eckman P, Rose A, May-Newman K. Aortic valve pathophysiology during left ventricular assist device support. *J Heart Lung Transplant* 2010 Dec;29(12):1321-9.
57. Kar B, Delgado RM, 3rd, Frazier OH, et al. The effect of LVAD aortic outflow-graft placement on hemodynamics and flow: Implantation technique and computer flow modeling. *Tex Heart Inst J* 2005;32:294.
58. Karino T, Goldsmith HL: Role of blood cell-wall interactions in thrombogenesis and atherogenesis: A microrheological study. *Biorheology* 1984;21: 587– 601.
59. Kashiwazaki S: Effects of artificial circulation by pulsatile and non-pulsatile flow on brain tissues. *Ann Thorac Cardiovasc Surg* 2000;6: 389-396.
60. Kelley KO, Feigl EO. Segmental alpha-receptor-mediated vasoconstriction in the canine coronary circulation. *Circ Res.* 1978;43(6):908-17.
61. Kim HK, Son HS, Fang YH, et al. The effects of pulsatile flow upon renal tissue perfusion during cardiopulmonary bypass: a comparative study of pulsatile and nonpulsatile flow. *ASAIO J* 2005;51:30.
62. Kinoshita M, Takano H, Takaichi S, Taenaka Y, Nakatani T. Influence of prolonged ventricular assistance on myocardial histopathology in intact heart. *Ann Thorac Surg* 1996; 61: 640–645.
63. Kono M, Orita H, Shimanuki T, Fukasawa M, Inui K, Wasio M: A clinical study of cerebral perfusion during pulsatile and nonpulsatile cardiopulmonary bypass. *Nippon Geka Gakkai Zasshi* 1990;91: 1016–1022.
64. Kono S, Nishimura K, Nishina T, et al: Autosynchronized systolic unloading during left ventricular assist with a centrifugal pump. *J Thorac Cardiovasc Surg* 2003;125: 353-360.
65. Laas J, Campbell CD, Takanashi Y, Replogle RL. Oxygen consumption of the left ventricle during transapical left ventricular bypass. *J Thorac Cardiovasc Surg* 1980;80(2):280-8.

66. Larose JA, Tamez D, Ashenuga M, Reyes C. Design concepts and principle of operation of the HeartWare ventricular assist system. *ASAIO J*. 2010;56(4):285-9.
67. Letsou GV, Connelly JH, Delgado RM III, et al. Is native aortic valve commissural fusion in patients with long-term left ventricular assist devices associated with clinically important aortic insufficiency? *J Heart Lung Transplant* 2006;25:395.
68. Letsou GV, Sdringola S, Gregoric ID et al. Myocardial perfusion as assessed by positron emission tomography during long-term mechanical circulatory support. *Congest Heart Fail* 2006;12(2):69-74.
69. Letsou GV, Shah N, Gregoric ID, Myers TJ, Delgado R, Frazier OH. Gastrointestinal bleeding from arteriovenous malformations in patients supported by the Jarvik 2000 axial-flow left ventricular assist device. *J Heart Lung Transplant*. 2005; 24:105-9.
70. Levine TB, Francis GS, Goldsmith SR, Simon AB, Cohn JN: Activity of the sympathetic nervous system and renin-angiotensin system assessed by plasma hormone levels and their relation to hemodynamic abnormalities in congestive heart failure. *Am J Cardiol* 1982;49: 1659-1666.
71. Lisy O, Redfield MM, Jovanovic S, et al: Mechanical unloading versus neurohumoral stimulation on myocardial structure and endocrine function in vivo. *Circulation* 2000;102: 338–343.
72. Litwak KN, Koenig SC, Cheng RC, et al. Ascending aorta outflow graft location and pulsatile ventricular assist provide optimal hemodynamic support in an adult mock circulation. *Artif Organs* 2005;29:629.
73. Litwak KN, Koenig SC, Tsukui H, et al. Effects of left ventricular assist device support and outflow graft location upon aortic blood flow. *ASAIO J* 2004;50:432.
74. Liu AC, Joag VR, Gotlieb AI. The emerging role of valve interstitial cell phenotypes in regulating heart valve pathobiology. *Am J Pathol* 2007;171:1407.
75. Lodge AJ, Undar A, Daggett CW, Runge TM, Calhoon JH, Ungerleider RM: Regional blood flow during pulsatile cardiopulmonary bypass and after circulatory arrest in an infant model. *Ann Thorac Surg* 1997;63: 1243-1250.
76. Losert U, Glogar D, Mayr H et al. Regional myocardial blood flow during nonpulsatile left ventricular bypass in calves. *Trans Am Soc Artif Intern Organs* 1982;28:86-92.
77. Macris MP, Parnis SM, Frazier OH, Fuqua JM, Jarvik RK: Development of an implantable ventricular assist system. *Ann Thorac Surg* 1997;63: 367–370.

78. Magovern JA, Christlieb IY, Badylak SF, Lantz GC, Kao RL: A model of left ventricular dysfunction caused by intracoronary adriamycin. *Ann Thorac Surg* 1992; 53: 861-863.
79. Manolio TA, Baughman KL, Rodeheffer R et al. Prevalence and etiology of idiopathic dilated cardiomyopathy. Summary of a National Heart, Lung and Blood Institute Workshop. *American Journal of Cardiology* 1992;69(17):1458–1466.
80. Maybaum S, Beniaminovitz A, Oz M, Di Tullio M, Savin S, Mancini D: Resting left ventricular size predicts improved native cardiac output during exercise and the ability to exercise with the device weaned in patients with the TCI HeartMate left ventricular assist device [abstract]. *J Heart Lung Transplant* 1999;18: 44.
81. Maybaum S, Epstein S, Beniaminovitz A, et al: Partial loading of the left ventricle during mechanical assist device support is associated with improved myocardial function, blood flow and metabolism and increased exercise capacity. *J Heart Lung Transplant* 2002;21: 446 – 454.
82. Maybaum S, Epstein S, Beniaminovitz A, Oz M, Bergman S, Mancini D: Resting myocardial blood flow and metabolism predicts improved native cardiac output and the ability to exercise with weaning in patients with the TCI HeartMate left ventricular assist device. *J Am Coll Cardiol* 1999;33 (2 Suppl 1): 219A.
83. May-Newman K, Enriquez-Almaguer L, Posuwattanakul P, Dembitsky W. Biomechanics of the aortic valve in the continuous flow VAD-assisted heart. *ASAIO J* 2010 Jul-Aug;56(4):301-8.
84. Merhige ME, Smalling RW, Cassidy D et al. Effect of the hemopump left ventricular assist device on regional myocardial perfusion and function: Reduction of ischemia during coronary occlusion. *Circulation* 1989;80(5 Pt 2):III158–66.
85. Meyns B, Nishimura Y, Racz R, Jashari R, Flameng W: Organ perfusion with Hemopump device assistance with and without intraaortic balloon pumping. *J Thorac Cardiovasc Surg* 1997;114: 243-253.
86. Miller LW, Pagani FD, Russell SD et al. Use of a continuous-flow device in patients awaiting heart transplantation. *N Engl J Med*. 2007;357:885–896.
87. Millner RW, Mann JM, Pearson I, Pepper JR: Experimental model of left ventricular failure. *Ann Thorac Surg* 1991;52: 78-83.
88. Modersohn D, Eddicks S, Grosse-Siestrup C, Ast I, Holinski S, Konertz W. Isolated hemoperfused heart model of slaughterhouse pigs. *Int J Artif Organs* 2001 April;24(4):215-21.

89. Moon MR, Castro LJ, DeAnda A, et al: Right ventricular dynamics during left ventricular assistance in closed-chest dogs. *Ann Thorac Surg* 1993;56: 54-66.
90. Mudd JO, Cuda JD, Halushka M, Soderlund KA, Conte JV, Russell SD. Fusion of aortic valve commissures in patients supported by a continuous axial flow left ventricular assist device. *J Heart Lung Transplant*. 2008 Dec;27(12):1269-74
91. Muller J, Wallukat G, Weng YG, et al: Weaning from mechanical cardiac support in patients with idiopathic dilated cardiomyopathy. *Circulation* 1997;96: 542–549.
92. Myers TJ, Khan T, Frazier OH. Infectious complications associated with ventricular assist systems. *ASAIO J* 2000; 46: S28-S36.
93. Nakata K, Shiona M, Orime Y, et al: Effect of pulsatile and nonpulsatile assist on heart and kidney microcirculation with cardiogenic shock. *Artif Organs* 1996;20: 681–684.
94. Nasu M, Okada Y, Fujiwara H, et al: Transesophageal echocardiographic findings of intracardiac events during cardiac assist. *Artif Organs* 1990;14: 377-381.
95. Nicolson DG, Porto I, Westaby S, Boardman P, Banning AP. Spontaneous echocardiographic contrast in the ascending aorta mimicking the appearance of aortic dissection in a patient with a left ventricular assist device. *Echocardiography* 2004;21: 193-195.
96. Niebauer J. Inflammatory mediators in heart failure. *International Journal of Cardiology* 2000;72(3):209–213.
97. Nishinaka T, Tatsumi E, Nishimura T, Taenaka Y, Imada K, Takano H, Koyanagi H. Effects of reduced pulse pressure to the cerebral metabolism during prolonged nonpulsatile left heart bypass. *Artif Organs* 2000 Aug;24(8):676-9.
98. Noon GP, Morley DL, Irwin S, Abdelsayed SV, Benkowski RJ, Lynch BE. Clinical experience with the MicroMed DeBakey ventricular assist device. *Ann Thorac Surg* 2001 Mar; 71(3 Suppl): S133–8.
99. Otto CM. Calcific aortic stenosis—time to look more closely at the valve. *N Engl J Med* 2008;359:1395.
100. Park SJ, Milano CA, Tatroles AJ, Rogers JG, Adamson RM, Steidley DE, Ewald GA, Sundareswaran KS, Farrar DJ, Slaughter MS; HeartMate II Clinical Investigators. Outcomes in advanced heart failure patients with left ventricular assist devices for destination therapy. *Circ Heart Fail*. 2012 Mar 1;5(2):241-8.
101. Pennock JL, Pierce WS, Prophet GA, Waldhausen JA. Myocardial oxygen utilization during left heart bypass; effect of varying percentage of bypass flow rate. *Arch Surg* 1974;109(5):635-41.

102. Petschek H, Adamis D, Kantrowitz AR: Stagnation flow thrombus formation. *Trans Am Soc Artif Intern Organs* 1968;14: 256–260.
103. Pierson RN, 3rd, Howser R, Donaldson T, et al. Left ventricular assist device implantation via left thoracotomy: alternative to repeat sternotomy. *Ann Thorac Surg* 2002;73:997.
104. Pinto YM, de Smet BG, van Gilst WH, et al: Selective and time related activation of the cardiac renin-angiotensin system after experimental heart failure: relation to ventricular function and morphology. *Cardiovasc Res* 1993;27: 1933-1938.
105. Pirbodaghi T, Axiak S, Weber A, Gempp T, Vandenberghe S. Pulsatile control of rotary blood pumps: Does the modulation waveform matter? *Thorac Cardiovasc Surg*. 2012 Oct;144(4):970-7.
106. Potapov EV, Loebe M, Nasser BA, et al: Pulsatile flow in patients with a novel nonpulsatile implantable ventricular assist device. *Circulation* 2000;102(19 Suppl 3): III183-III187.
107. Raymond RJ, Dehmer GJ, Theoharides TC, Deliargyris EN. Elevated interleukin-6 levels in patients with asymptomatic left ventricular systolic dysfunction. *American Heart Journal* 2001;141(3):435–438.
108. Redfield MM, Edwards BS, Heublein DM, Burnett JC Jr: Restoration of renal response to atrial natriuretic factor in experimental low-output heart failure. *Am J Physiol* 1989;257(4 Pt 2): R917-R923.
109. Reinhardt CP, Dalhberg S, Tries MA, Marcel R, Leppo JA. Stable labeled microspheres to measure perfusion: validation of a neutron activation assay technique. *Am J Physiol Heart Circ Physiol* 2001;280(1): H108-H116.
110. Ridker PM, Hennekens CH, Buring JE, Rifai N. C-reactive protein and other markers of inflammation in the prediction of cardiovascular disease in women. *New England Journal of Medicine* 2000;342(12):836–843.
111. Ridker PM, Rifai N, Stampfer MJ, Hennekens CH. Plasma concentration of interleukin-6 and the risk of future myocardial infarction among apparently healthy men. *Circulation* 2000;101(, no. 15, pp. 1767–1772.
112. Roberts WL, Sedrick R, Moulton L, Spencer A, Rifai N. Evaluation of four automated high-sensitivity C-reactive protein methods: implications for clinical and epidemiological applications. *Clinical Chemistry* 2000;46(4):461–468.
113. Robicsek F, Thubrikar MJ. Etiology of degenerative disease of the tri-leaflet aortic valve: a simple explanation for a complex problem. *Z Kardiol* 2001;90 Suppl 6:35-8.
114. Rose AG, Connelly JH, Park SJ, Frazier OH, Miller LW, Ormaza S. Total left ventricular outflow tract obstruction due to left ventricular assist device-

- induced sub-aortic thrombosis in 2 patients with aortic valve bioprosthesis. *J Heart Lung Transplant* 2003;22: 594-599.
115. Rose AG, Park SJ, Bank AJ, Miller LW. Partial aortic valve fusion induced by left ventricular assist device. *Ann Thorac Surg* 2000;70: 1270-1274.
 116. Rose EA, Gelijns AC, Moskowitz AJ et al. Long-term use of a left ventricular assist device for end-stage heart failure. *N Engl J Med*. 2001;345(20):1435-43.
 117. Rosenstrauch D, Akay HM, Bolukoglu H, Behrens L, Bryant L, Herrera P, Eya K, Tuzun E, Clubb FJ Jr, Radovancevic B, Hrazier OH, Kadipasaoglu K.. Ex vivo resuscitation of adult pig hearts. *Tex Heart Inst J* 2003;30(2):121-7.
 118. Rozin AP, Attias J, Presser D, Rosenberg H, Moscovitz M, Bentur Y. Alcohol poisoning and venous hyperoxia. *Toxicol Mechan Method* 2008; 745-750.
 119. Russell SD, Roger JG, Milano CA, et al: Renal and hepatic function improve in advanced heart failure patients during continuous flow support with the HeartMate II left ventricular assist device. *Circulation* 2009;120(23):2352-2357.
 120. Sabbah HN, Stein PD, Kono T, et al: A canine model of chronic heart failure produced by multiple sequential coronary microembolizations. *Am J Physiol* 1991; 260(4 Pt 2): H1379-H1384.
 121. Saito A, Shiono M, Orime Y, et al. Effects of left ventricular assist device on cardiac function: experimental study of relationship between pump flow and left ventricular diastolic function. *Artif Organs* 2001;25: 728-732.
 122. Saito S, Westaby S, Piggot D, et al: End-organ function during chronic nonpulsatile circulation. *Ann Thorac Surg* 2002;74: 1080– 1085.
 123. Sanderson JM, Wright G, Sims FW: Brain damage in dogs immediately following pulsatile and non-pulsatile blood flow in extracorporeal circulation. *Thorax* 1972; 27: 275-286.
 124. Sapire KJ, Gopinath SP, Farhat G, et al: Cerebral oxygenation during warming after cardiopulmonary bypass. *Crit Care Med* 1997;25: 1655-1662.
 125. Scheinin SA, Capek P, Radovancevic B, Duncan J, McAllister HA Jr., Frazier OH: The effect of prolonged left ventricular assist device support on myocardial histopathology in patients with end-stage cardiomyopathy. *ASAIO J* 1992;38: M271–M274.
 126. Schneider PJ, Deck JD. Tissue and cell renewal in the natural aortic valve of rats: an autoradiographic study. *Cardiovasc. Res* 1981; 15(4):181–9.
 127. Sellers RD, Levy MJ, Amplatz K, Lillehei CW. Left retrograde cardioangiography in acquired cardiac disease. Technique, indications and interpretations in 700 cases, *The American Journal of Cardiology* 1964;14(4):437–447.
 128. Selzman CH, Sheridan BC. Off-pump insertion of continuous flow left ventricular assist devices. *J Card Surg* 2007;22:320.

129. Sezai A, Shiono M, Orime Y, et al: Major organ function under mechanical support: comparative studies of pulsatile and nonpulsatile circulation. *Artif Organs* 1999;23: 280–285.
130. Sezai A, Shiono M, Orime Y, et al: Microcirculation of kidney and skin during left ventricular assisted circulation: comparative studies of pulsatile and nonpulsatile assists. *Jpn J Thorac Cardiovasc Surg* 1998;46: 1239-1246.
131. Shevde K, DeBois W: Pro: pulsatile flow is preferable to nonpulsatile flow during cardiopulmonary bypass. *J Cardiothorac Anesth* 1987;1: 165-168.
132. Shiiya N, Zelinsky R, Deleuze PH, Loisanse DY: Changes in hemodynamics and coronary blood flow during left ventricular assistance with the Hemopump. *Ann Thorac Surg* 1992;53: 1074– 1079.
133. Shiiya N, Zelinsky R, Deleuze PH, Loisanse DY: Effects of Hemopump support on left ventricular unloading and coronary blood flow. *ASAIO Tran* 1991;37: M361-M362.
134. Shuman TA, Palazzo RS, Jaquiss RB, et al: A model of right ventricular failure after global myocardial ischemia and mechanical left ventricular support. *ASAIO Trans* 1991;37: M212-M213.
135. Sidi A, Rush W: An alternative to radioactive microspheres for measuring regional myocardial blood flow, Part 1: colored microspheres. *J Cardiothorac Vasc Anesth* 1996;10: 368–373.
136. Slaughter MS, Rogers JG, Milano CA et al. Advanced heart failure treated with continuous-flow left ventricular assist device. *N Engl J Med.* 2009 Dec 3;361(23):2241-51.
137. Slaughter MS, Singh R. The Role of Ventricular Assist Devices in Advanced Heart Failure. *Rev Esp Cardiol.* 2012;65:982-5.
138. Slaughter MS. Hematologic effects of continuous flow left ventricular assist devices. *J Cardiovasc Transl Res.* 2010; 6(8):815-818.
139. Slaughter MS. Long-Term Continuous Flow Left Ventricular Assist Device Support and End-Organ Function: Prospects for Destination Therapy. *J Card Surg* 2010;25:490-494.
140. Smalling RW, Cassidy DB, Barrett R, Lachterman B, Felli P, Amirian J: Improved regional myocardial blood flow, left ventricular unloading, and infarct salvage using an axial-flow, transvalvular left ventricular assist device: a comparison with intra-aortic balloon counterpulsation and reperfusion alone in a canine infarction model. *Circulation* 1992;85: 1152–1159.
141. Sodian R, Loebe M, Schmitt C et al. Decreased plasma concentration of brain natriuretic peptide as a potential indicator of cardiac recovery in patients supported by mechanical circulatory assist systems. *Journal of the American College of Cardiology* 2001;38(7):1942–1949.

142. Soucy KG, Koenig SC, Giridharan GA, Sobieski MA, Slaughter MS. Rotary pumps and diminished pulsatility: do we need a pulse? *ASAIO J* 2013 Jul-Aug;59(4):355-66.
143. Stewart GC, Givertz MM. Mechanical circulatory support for advanced heart failure: Patients and technology in evolution. *Circulation* 2012;125:1304-1315.
144. Strueber M, O'Driscoll G, Jansz P, Khaghani A, Levy WC, Wieselthaler GM, et al. Multicenter evaluation of an intrapericardial left ventricular assist system. *J Am Coll Cardiol*. 2011;57:1375-82.
145. Suarez J, Patel CB, Felker GM, Becker R, Hernandez AF, Rogers JG. Mechanisms of bleeding and approach to patients with axial-flow left ventricular assist devices. *Circ Heart Fail*. 2011;4(6):779-84.
146. Sugawara A, Nakao K, Mor N II et al. Synthesis of atrial natriuretic polypeptide in human failing hearts. Evidence for altered processing of atrial natriuretic polypeptide precursor and augmented synthesis of β -human ANP. *Journal of Clinical Investigation* 1988;81(6):1962–1970.
147. Taylor KM, Bain WH, Davidson KG, Turner MA: Comparative clinical study of pulsatile and non-pulsatile perfusion in 350 consecutive patients. *Thorax* 1982; 37: 324-330.
148. Thubrikar M. The aortic valve. Boca Raton, Florida: CRC Press, 1990; 221.
149. Thubrikar MJ, Aouad J, Nolan SP. Comparison of the in vivo and in vitro mechanical properties of aortic valve leaflets. *J Thorac Cardiovasc Surg* 1986;92(1):29-36.
150. Toda K, Fujita T, Domae K, Shimahara Y, Kobayashi J, Nakatani T. Late aortic insufficiency related to poor prognosis during left ventricular assist device support. *Ann Thorac Surg*. 2011 Sep;92(3):929-34.
151. Toda K, Tatsumi E, Taenaka Y, Masuzawa T, Takano H: Impact of systemic depulsation on tissue perfusion and sympathetic nerve activity. *Ann Thorac Surg* 1996;62: 1737-1742.
152. Tomlinson CW, McGrath GM, McNeill JH: Adriamycin cardiomyopathy: pathological and membrane functional changes in a canine model with mild impairment of left ventricular function. *Can J Cardiol* 1986;2: 368-374.
153. Toyoda Y, Okada M, Kashem MA: A canine model of dilated cardiomyopathy induced by repetitive intracoronary doxorubicin administration. *J Thorac Cardiovasc Surg* 1998;115: 1367-1373.
154. Tsutsui T, Sutton C, Harasaki H, Jacobs G, Golding L, Nose Y: Idioperipheral pulsation during nonpulsatile biventricular bypass experiments. *ASAIO Trans* 1986;32: 263-268.

155. Tuzun E, Conger J, Gregoric ID et al. Evaluation of a new cardiac recovery system in a bovine model of volume overload heart failure," *ASAIO Journal* 2004;50(6):557–562.
156. Tuzun E, Eya K, Chee HK, et al. Myocardial hemodynamics, physiology, and perfusion with an axial flow left ventricular assist device in the calf. *ASAIO J* 2004;50: 47-53.
157. Tuzun E, Gregoric ID, Conger JL, et al. The effect of intermittent low speed mode upon aortic valve opening in calves supported with a Jarvik 2000 axial flow device. *ASAIO J* 2005;51:139.
158. Tuzun E, Narin C, Gregoric ID, Cohn WE, Frazier OH. Ventricular Assist Device Outflow-Graft Site: Effect on Myocardial Blood Flow. *J Surg Res* 2011;171(1):71-5.
159. Tuzun E, Roberts K, Cohn WE et al., "In vivo evaluation of the HeartWare centrifugal ventricular assist device. *Texas Heart Institute Journal* 2007;34(4):406–411.
160. Tuzun E, Rutten M, Dat M, van de Vosse F, Kadipasaoglu C, de Mol B. Continuous-flow cardiac assistance: effects on aortic valve function in a mock loop. *J Surg Res* 2011 Dec; 171(2): 443-7.
161. Undar A, Henderson N, Thurston GB, et al: The effects of pulsatile versus nonpulsatile perfusion on blood viscoelasticity before and after deep hypothermic circulatory arrest in a neonatal piglet model. *Artif Organs* 1999;23: 717–721.
162. United network for organ sharing: Transplants in the United States; <http://www.optn.org/latestData/rptData.asp>;2006.
163. Vatta M, Stetson SJ, Perez-Verdia A et al. Molecular remodelling of dystrophin in patients with end-stage cardiomyopathies and reversal in patients on assistance-device therapy. *Lancet* 2002;359(9310):936–941.
164. Vatta M, Stetson SJ, Jimenez S et al. Molecular normalization of dystrophin in the failing left and right ventricle of patients treated with either pulsatile or continuous flow-type ventricular assist devices. *Journal of the American College of Cardiology* 2004;43(5):811–817.
165. Versieck J, Vanballenberghe L: Determination of tin in human blood serum by radiochemical neutron activation analysis. *Anal Chem* 1991;63: 1143–1146.
166. Voiti P, Vollkron M, Bergmeister H, Wieselthaler G, Schima H. Coronary hemodynamics and myocardial oxygen consumption during support with rotary blood pumps. *Artif Organs* 2009;33(1):77-80.
167. Watanabe K, Kabei N, McRea J, Peters J. Continuous measurement of myocardial oxygen consumption (MVO₂) and hemodynamic response during

- transapical left ventricular bypass (TALVB). *Trans Am Soc Artif Intern Organs*. 1975;21:566-72.
168. Westaby S, Jin XY, Katsumata T, Taggart DP, Coats AJ, Frazier OH: Mechanical support in dilated cardiomyopathy: signs of early left ventricular recovery. *Ann Thorac Surg* 1007;64: 1303-1308.
 169. Westaby S, Katsumata T, Houel R, et al: Jarvik 2000 Heart: potential bridge to myocyte recovery. *Circulation* 1998;98: 1568–1574.
 170. Westaby S, Siegenthaler M, Beyersdorf F et al. Destination therapy with a rotary blood pump and novel power delivery. *Eur J Cardiothorac Surg* 2010;37(2):350-6.
 171. Wester PO: Concentration of 24 trace elements in human heart tissue determined by neutron activation analysis. *Scand J Clin Lab Invest* 17: 357–370, 1965.
 172. Weston MW, Yoganathan AP. Biosynthetic activity in heart valve leaflets in response to in vitro flow environments. *Ann Biomed Eng* 2001;29(9):752-63.
 173. Whicher J, Rifai N, Biasucci LM. Markers of the acute phase response in cardiovascular disease: an update. *Clinical Chemistry and Laboratory Medicine* 2001;39(11):1054– 1064.
 174. Wurzinger LJ, Blasberg P, Schmid-Schonbein H: Towards a concept of thrombosis in accelerated flow: Rheology, fluid dynamics, and biochemistry. *Biorheology* 1985;22: 437– 450.
 175. Yada I, Golding LR, Harasaki H, et al: Physiopathological studies flow in chronic models. *Trans Am Soc Artif Intern Organs* 1983;29: 520 –525.
 176. Yang SS, Bentivoglio LG, Maranhao V, Goldberg H. Assessment of ventricular function. In: Yang SS, ed. *From Cardiac Catheterization Data to Hemodynamic Parameters*. 3rd ed. Philadelphia: F.A. Davis Company;1988:207-208.
 177. Yoganathan AP, Eberhardt CE, Walker PG. Hydrodynamic performance of the Medtronic Freestyle Aortic Root Bioprosthesis. *J Heart Valve Dis* 1994;3:571.
 178. Zamarrripa-Garcia MA, Enriquez LA, Dembitsky W, May-Newman K. The effect of aortic valve incompetence on the hemodynamics of a continuous flow ventricular assist device in a mock circulation. *ASAIO J* 2008;54(3):237-44.
 179. Zhou S, Starkov A, Froberg MK, Leino RL, Wallace KB: Cumulative and irreversible cardiac mitochondrial dysfunction induced by doxorubicin. *Cancer Res* 2001;61: 771-777.

Acknowledgements

This thesis would never have come together without the guidance and support of my valuable mentors prof. dr. Bas de Mol, prof. dr. Frans van de Vosse and dr. Marcel Rutten. I would like to express my deep gratitude to each of them who made this work possible.

Dear Bas, thank you very much for your patience, confidence, advices and valuable ideas which you've generously offered me during my PhD work. You were not only a mentor to me, but you've treated me as a member of your lovely family and it was an honor for me to have you in my life as a colleague and as a friend.

Dear Frans, I would like to thank you as well for giving me the opportunity to work at the Technical University of Eindhoven, Biomedical Engineering Department. Your and your brilliant team's contributions and support will not be forgotten.

And Dear Marcel, my mentor, scientific partner and brother, I enjoyed every moment of our work together. You've been always very kind, patient, friendly and open minded to me. Your enthusiasm and relations with your students always impressed me. I feel very lucky to work with a brilliant mentor like you. Chapeau mon cher ami!

I also would like to thank valuable members of Life Tech Group, dr. Jurgen de Hart, dr. Marco Stijnen and Sjoerd van Tuijl who made my life easier during our ex-vivo heart experiments. This work became real and successful with your expertise and dedication.

Moreover, I would like to acknowledge specifically the directors of the Texas A&M University, Institute for Preclinical Studies (TIPS) drs. Terry Fossum, Matthew Miller and Joe Kornegay who were always supportive to me during my PhD work.

And finally, I express my gratitude to my mom, dad and daughters Zeynep and Asli for their encouragement in entire of my life and PhD work.

Egemen Tuzun

Eindhoven, November 2014

Curriculum Vitae

Egemen Tuzun was born on 01/01/1963 in Izmir-Turkey. After finishing Medical School in 1986 at Ege University in Izmir-Turkey, he studied Cardiovascular Surgery at Dokuz Eylul University in Izmir-Turkey. He graduated in November, 1995. In 2004, he started a PhD project at the Technical University of Eindhoven at Eindhoven, The Netherlands, the results of which are presented in this dissertation. Since July, 2010 he is employed at the Texas A&M University, Institute for Preclinical Studies.

Between 1987 and 1991, he did his military service as Lieutenant in the Turkish Army at Istanbul, Turkey. He worked as medical practitioner in Kulp Health Center, Diyarbakir, Turkey (1988-1990). From 1996 to 1997 he worked as visiting surgeon at the Texas Heart Institute, Houston, Texas, USA.

From 1995 to 2003 he worked as Assistant and Associate Professor at the Cardiovascular Surgery, Faculty of Medicine, Celal Bayar University, Manisa, Turkey. Between 2001 and 2010 he was the assistant director, research surgeon and scientist at the Cardiovascular Surgical Labs, Texas Heart Institute, Houston, Texas, USA. He currently holds an Adjunct Associate Professor position at the Cullen College of Engineering, University of Houston, Texas, USA, Visiting Associate Professor position at the Department of Cardiothoracic Surgery at the Academic Medical Center in Amsterdam, Netherlands, Industrial Advisory Board Member position at the University of Houston, Biomedical Engineering Dept. Houston, Texas, USA. He is also Special Consultant to LifeTec Group B.V., Eindhoven, the Netherlands and Scientific Consultant to Micromed, Houston, Texas, USA.

In 2004, he was awarded with the best poster presentation award at the 50th American Society of Artificial Internal Organs (ASAIO) Meeting (2004). He received H. Koyanagi, Young Investigator Award, at the International Society of Rotary Blood Pumps (ISRBP) Meeting in 2004. He is a member of the peer review committee of the American Heart Association (AHA), Western Review Consortium. He is a Board member of the American Society of Artificial Internal Organs Society. He is a member of the International Society of Rotary Blood Pumps. He is an Editorial Board Member and reviewer of the American Society for Artificial Internal Organs Journal, reviewer for the Asian Cardiovascular & Thoracic Annals, Artificial Organs, Texas Heart Institute Journal and IEEE Engineering in Medicine and Biology Magazine. He was an Organizing Committee Member

